investigation of Electronic Corrosion Mechanisms

Minzari, Daniel; Møller, Per; Ambat, Rajan

Publication date:
2010

Document Version
Publisher's PDF, also known as Version of record

Investigation of Electronic Corrosion Mechanisms

PhD Thesis

Daniel Minzari
Department of Mechanical Engineering
Technical University of Denmark

Investigation of Electronic Corrosion Mechanisms

PhD Thesis

June 2010

by

Daniel Minzari

Section for Materials and Surface Engineering
Department of Mechanical Engineering
Technical University of Denmark (DTU)
DK- 2800 – Kgs. Lyngby

PREFACE

The present thesis is submitted in candidacy for a PhD degree from the Technical University of Denmark. The work presented has been carried out under supervision of Associate Professor Rajan Ambat and co-supervision of Professor Per Møller during the period April 2007 – June 2010 at the Section for Materials Science and Engineering.

Current research has been conducted as part of the CELCORR consortium, which was funded by the Danish Ministry of Science, Technology and Innovation.

Daniel Minzari, Lyngby, June 25th 2010

ACKNOWLEDGEMENTS

First of all, my supervisor Rajan Ambat and co-supervisor Per Møller are acknowledged for their supervision of this project. Words are poor when it comes to describing the gratitude I feel for their continued support, enthusiasm, guidance and the deep insight that they have put into this work. Also my co-workers in the CELCORR group Morten Jellesen and Umadevi Rathinavelu and master students Peter Westermann and Marianna Johnsen are acknowledged for all their help, friendship and for their excellent team sprit during this project.

All of the CELCORR partners (Danfoss A/S, Grundfos A/S, Vestas Wind Systems A/S, GPV Chemitallic A/S, PRI-DANA Elektronik A/S, IPU and the Danish Technological Institute) are greatly acknowledged for their commitment, resources and expertise that has been put into this project. Special thanks to Kirsten Stentoft, Marie-Louise Pedersen, Annemette Riis, John B. Jacobsen, Lars Rimestad, Jens Peter Krog, Niels Martin Henriksen, Henrik Jensen, Henrik Sørensen, Rasmus Enemærke, Leif Højslet Christensen, Pia Wahlberg and Anette Alsted.

The Tribology Centre of the Danish Technological Institute is acknowledged for DLC and CrN surface coating of the probes for the SCECM setup. Kathrine Bjørneboe from the Danish Technological Institute is acknowledged for SEM and FIB work. Lene Hubert from DTU-Nanotech is acknowledged for XPS measurements. Flemming Grumsen from DTU Mechanical Engineering is acknowledged for TEM work. Lars Pedersen and John Troelsen from the workshop at DTU Mechanical Engineering are acknowledged for their skills and precision in the manufacturing of the SCECM, and CELCORR TestPCB setups. Danfoss Drives A/S (K. Stentoft, K. Blohm, B. Kroman, J. H. Eriksen, T. Nielsen, P. Skjold) are greatly acknowledged for their participation in the development of the CELCORR Test PCB. Christian Ravn from IPU is especially acknowledged for providing exceptional guidance within all aspects regarding electrical engineering in this project and especially for his aid in the development of the CELCORR TestPCB.

ABSTRACT

The current PhD work is carried out under the Centre for Electronic Corrosion (CELCORR, www.celcorr.com) at DTU, an integrated project on the corrosion reliability of electronics motivated by the increasing reliability threats that the electronics industries are facing today. As the use of electronics is becoming even more wide spread, and structural dimensions of electronic components gets smaller due to the drive for miniaturization, the risk of environmental interaction and the risk of corrosion increases. The Printed Circuit Board Assembly (PCBA), which is the heart of the electronic device, contains a number of corrosion susceptible materials, which makes a dangerous combination with applied potential bias and humidity/environment. The result can be a number of corrosion types, such as electrochemical migration, gaseous and galvanic corrosion, fretting etc. to name a few. The major focus of the present thesis is the "Electrochemical migration of tin (ECM)", however, part of the thesis is also dedicated to the investigation of "corrosion of silver parts in sulphur containing environments". Electrochemical migration is the growth of a metal dendrite between two closely spaced biased points on a PCBA connected by a condensed layer of water, by the dissolution of metal ions at the anode and subsequent deposition at the cathode. The mechanisms of electronic corrosion are different from that of conventional corrosion types due to the micro-volumes of electrolytes, overlapping of diffusion layers at the closely spaced electrodes, and electrode potentials that are much higher than in conventional electrochemistry. Several gases such as sulphur dioxide can cause severe corrosion on a PCBA, especially if silver parts are involved. This process is assisted by the humidity and potential bias as shown in the present thesis.

Followed by an introduction, literature survey, and methodology, the results of this PhD investigation are presented in the thesis as research papers, published or intended for individual publications. Papers 1-5 arranged as chapters 5-9 discuss the electrochemical migration of tin in detail. Paper 1 describes a setup for electrochemical migration studies on individual electronic components, and

presents results on how bias voltage and chloride contamination affects the electrochemical migration of tin on ceramic chip components. Paper 2 provides a detailed investigation of microstructure of the dendrites formed in a low chloride environment. Paper 3 describes the effect of process and service related contamination on the electrochemical migration of tin, while an in-depth discussion of the mechanisms leading to migration are proposed in paper 4. The development of a new setup for PCB level testing of electrochemical migration is described in paper 5 and results are presented. Finally, paper 6 presents a detailed failure analysis of silver sulphide corrosion on a hybrid circuit.

The results from the current thesis showed that the electrochemical migration is highly dependent on the thermodynamic stability of the tin species formed in the micro-volume electrolyte. Strong pH gradients develop due to electrochemical reactions at the electrodes, which rapidly interact due to convection in the electrolytes and tin reduction in alkaline environment is most likely to be the main mechanism for tin dendrite formation. Dendrites were found to consist of metallic tin with hydrated tin oxides embedded, and the structure was found to depend on the electric field, tin ion concentration in solution and the pH conditions during growth. Silver sulphide corrosion on the hybrid circuit was influenced by the permeation of the sulphur containing gases through the silicone coating, presence of humidity, AC potential bias, and multi-material combinations.

RESUME (IN DANISH)

Denne ph.d. afhandling er udført under Center for Korrosion i Elektronik (CELCORR) konsortiet på DTU som er et integreret projekt om pålidelighed i elektronik, motiveret af de voksende udfordringer som producenter af elektronik står over for. I takt med at de elektriske kredsløb bliver mindre og mere avancerede, samtidigt med at vi medbringer elektronik flere steder i vores hverdag øges risikoen for at de forbindes af selv meget små mængder fugt fra omgivelserne. Elektriske kredsløb indeholder en mængde materialer som kan korrodere og kombinationen af disse, sammen med en pålagt elektrisk spænding og fugt / aggressive omgivelser korrosion til en væsentlig risiko. Resultatet kan være en række korrosions former, så som blandt andet elektrokemisk migration (ECM), gas fase korrosion og galvanisk korrosion. Størst fokus i denne afhandling er lagt på elektrokemisk migration af tin, men en del af afhandlingen beskriver også et eksempel på korrosion af sølv ved tilstedeværelsen af svovlholdige gasser.

Når to lederbaner med et elektrisk potentiale forbindes af fugt, sker elektrokemiske reaktioner, der er væsentligt forskellige fra dem som forekommer i de makro-volumener, der kendes fra den gængse elektrokemi. Vores viden på dette område er meget begrænset, og i takt med at mikroelektronik anvendes flere steder i samfundet, øges konsekvenserne af fejl, f.eks. i sikkerhedsudstyr. ECM er en særlig farlig form for korrosion i elektronik, som optræder hvis fugt forbinder to metal lederbaner som har en elektrisk spænding over sig. Metal ioner opløses på den ene leder, og kan, hvis de rigtige forhold er til stede, deponeres de på den anden og vokser som en tynd metallisk bro der er ca. 100 nm i diameter, og som kortslutter de to ledere. Dette kan forårsage at elektronikken fejler i løbet af få sekunder eller få minutter, og fejlen er ofte midlertidig, idet metal-broen brænder over når fugten forsvinder, og er derfor utrolig svær at finde ved efterfølgende fejlanalyse. Reaktive gasser som f.eks. svovl dioxid kan forårsage korrosionsskader på elektronik, særligt hvis der findes eksponerede sølvoverflader.

Efter en introduktion, litteratur studie og metode afsnit vil resultaterne i denne afhandling blive præsenteret som individuelle artikler, der er blevet eller vil blive publiceret i videnskabelige tidsskrifter. Artikel 1-5 i kapitel 5-9 angår detaljerede studier af elektrokemisk migration af tin. Artikel 1 beskriver en forsøgsopstilling hvor ECM forsøg kan udføres på enkelte chip komponenter og viser resultater for effekten af spænding og klorid koncentration. Artikel 2 viser en detaljeret analyse af mikrostrukturen af tin dendritter som er dannet i svage opløsninger med klorid. Artikel 3 beskriver effekten af udvalgte proces og service relaterede forureninger på ECM af tin og artikel 4 opsummerer observationer fra en række studier, og giver en diskussion af mekanismerne bag ECM af tin. Udviklingen af en ny eksperimentel opstilling for test af ECM på PCB niveau er beskrevet i artikel 5 med resultater. Endelig viser artikel 6 en detaljeret fejlanalyse af sølvsulfid korrosion på et hybridkredsløb.

Dette forskningsprojekt har kortlagt de parametre der påvirker ECM og viser at migrations mekanismer er stærkt afhængige af den termodynamiske stabilitet af tin specier i de små mikro-volumener af elektrolyt som findes på elektronik. Stærke pH gradienter dannes pga. elektrokemiske reaktioner ved elektroderne som interagerer grundet konvektion fra gasudvikling og vandring af ioner, og tin reduktion i basisk miljø er højst sandsynligt den fremtrædende mekanisme ved ECM. Dendritterne består af metallisk tin omgivet af hydrerede oxider, og strukturen er influeret af det elektriske felt, koncentrationen af tin ioner som kan reduceres og lokal pH ved dendrittens spids under væksten. Sølvsulfid korrosion på hybridkredsløbet er influeret af permeation af svovlgasser gennem silikone coatingen, tilstedeværelsen af små mængder fugt, AC elektrisk felt og kombinationen af metaller a ulige ædelhed.

LIST OF ABBREVIATIONS:

PCB	Printed Circuit Board
PCBA	Printed Circuit Board Assembly
MLCC	Multilayer Ceramic Capacitor
SM	Surface Mount
TH	Through Hole
SEM	Scanning Electron Microscope
TEM	Transmission Electron Microscope
ECM	Electrochemical Migration
SCECM	Single Component Electrochemical Migration
SIR	Surface Insulation Resistance
RH	Relative Humidity
CV	Cyclic Voltammetry
DI	Deionized
CD	Current Density
ENIG	Electroless Nickel Immersion Gold

Unless otherwise stated throughout the thesis, use of word 'migration' refers to "Electrochemical migration".

LIST OF PUBLICATIONS

APPENDED PAPERS

[1] D. Minzari, M.S. Jellesen, P. Møller, P. Wahlberg, and R. Ambat, "*Electrochemical migration on electronic chip resistors in chloride environments*," IEEE Transactions on Device and Materials Reliability, vol. 9, 2009, pp. 392–402.

[2] D. Minzari, F. B. Grumsen, M. Jellesen, P. Møller, R. Ambat, "Investigation of the Microstructure of Tin Dendrites by Electron Microscopy" Submitted to Corrosion Science, May 2010

[3] R. Ambat, M.S. Jellesen, D. Minzari, U. Rathinavelu, M.A. K. Johnsen, P. Westermann, and P. Møller, *"Solder flux residues and electrochemical migration failures of electronic devices"*, Proc. of Eurocorr 2009, Nice, France, 6-10 September 2009.

[4] D. Minzari, M. S. Jellesen, P. Møller, R. Ambat "On the electrochemical migration mechanism of tin in electronics", To be submitted to Journal of the Electrochemical Society, 2010

[5] D. Minzari, C. Ravn, K. Stentoft, M. S. Jellesen, P. Møller, R. Ambat "PCB level Testing of Electrochemical Migration on Surface Mount Components", To be submitted to IEEE Transactions on Device and Materials Reliability, 2010

[6] D. Minzari, M. S. Jellesen, P. Møller, R. Ambat, "Morphological study of silver corrosion in sulfur environments", Microelectronics Reliability, Submitted, Nov. 2009

OTHER PUBLICATIONS

[1] D. Minzari, E. Ottesen-Hansen, P. Møller, N. G. Sarius, P. Leisner, H. Ljungcrantz, R. Ambat, "Corrosion of MAX-Phase Ti3SiC2 compound and Ti-Si-C nanocomposite coatings for Electronic Contacts" Under preparation, to be submitted to Corrosion Science, 2010

[2] M.S. Jellesen, D. Minzari, U. Rathinavelu, P. Møller, and R. Ambat, "Corrosion failure due to flux residues in an electronic add-on device," Engineering Failure Analysis, vol. 17, Sep. 2010, pp. 1263-1272

[3] M.S. Jellesen, D. Minzari, U. Rathinavelu, P. Møller, and R. Ambat, *"Corrosion in Electronics at Device Level*", ECS Transactions Volume 25, Vienna, Austria, October 7th 2009

[4] M.S. Jellesen, P. Westermann, D. Minzari, P. Møller, and R. Ambat, *"Corrosion in Electronics"*, Corrosion Management 85, 17, 2008.

[5] D. Minzari, P. Møller, P. Kingshott, L.H. Christensen and R. Ambat, "*Surface oxide formation during corona discharge treatment of AA 1050 aluminium surfaces*," Corrosion Science, vol. 50, 2008, pp. 1321–1330.

[6] D Minzari, M Jellesen, P Møller, R Ambat, *"Study of electrochemical induced migration on electronic chip resistors by use of novel electrochemical cell set-up",* Proceedings of the European corrosion congress; EUROCORR 2008, Edinburgh, UK, September 9th 2008

[7] M. S. Jellesen, D. Minzari, P. Møller, R. Ambat, *"Corrosion in electronics",* Proceedings of the European corrosion congress; EUROCORR 2008, Edinburgh, UK, September 9th 2008

[8] R. Ambat, D. Minzari and P. Westermann, "*Intergranular Corrosion Susceptibility of aluminium-magnesium alloys*", ATB Metallurgie (2006)

PATENTS

[1] *Patent Application Relating to a Tool for Improving Electronic Device Reliability,* D. Minzari, M. Jellesen, P. Westermann, P. Møller and R. Ambat

[2] *An Electrolytic CIP-Cleaning Process For Removing Impurities From The Inner Surface Of A Metallic Container,* P. Møller, J.S. Hansen, and D. Minzari, Patent Cooperation Treaty Application, patno:WO081105872008, September 2008

TABLE OF CONTENTS

1 INTRODUCTION

1.1 BACKGROUND

The current doctoral thesis is motivated by the increasing corrosion reliability threats on electronic devices today, and lack of detailed and mechanistic understanding of the corrosion processes under humid and condensing environments.

During the past couple of decades, use of electronic devices has increased in gigantic proportions and revolutionized society, especially in the communication sector. Mobile phones are obvious examples of how devices integrate more and more complex functions, such as camera, GPS and several wireless communication technologies. The integrated device is expected to be cheap, while the applications necessitate it to be robust, durable, and reliable in all environments that one encounters in everyday life, including severe conditions such as close to sea, high humidity, varying temperatures etc. However, consumer electronics is only a fraction of the total electronics market. Industrial electronics is another sector where electronic control boxes and other devices are used irrespective of the type of industries and environmental conditions. As an example, modern wind turbine nacelle consists of a number of electronic systems, and is expected to be used in all climatic conditions around the world, in land, close to the sea or offshore. Vast majority of these electronics systems are not hermetically sealed so that they are susceptible to humidity absorption and condensation causing corrosion problems by a number of susceptible material combinations existing on the Printed Circuit Board Assembly (PCBA). Failure of the electronic devices related to these applications are disastrous both from an economic point of view costing huge amount money today and safety point of view as it can cause catastrophic failures. Miniaturization and intend for high packing density of electronic components are some other reasons for increased corrosion reliability problems for electronic devices. In order to provide additional functionalities and increasing the number of components per unit area on a PCBA, the number of conduction layers on a PCB has increased over the years (it is common to see

multilayer PCB consisting of 8-12 layers), while the line width, distances, and sizes of the components are reduced exponentially. All of these factors decrease the distance for a required electrolytic bridging of two oppositely biased conductors in the electronic circuit, and therefore the risk of failure due to corrosion.

The X-ray image of a section of a PCBA in Figure 1.1 gives an illustration of the complexity of modern electronics, where multiple layers of conductors are revealed which are connected through via holes, and various surface mount components and integrated circuits are seen on the top layer.

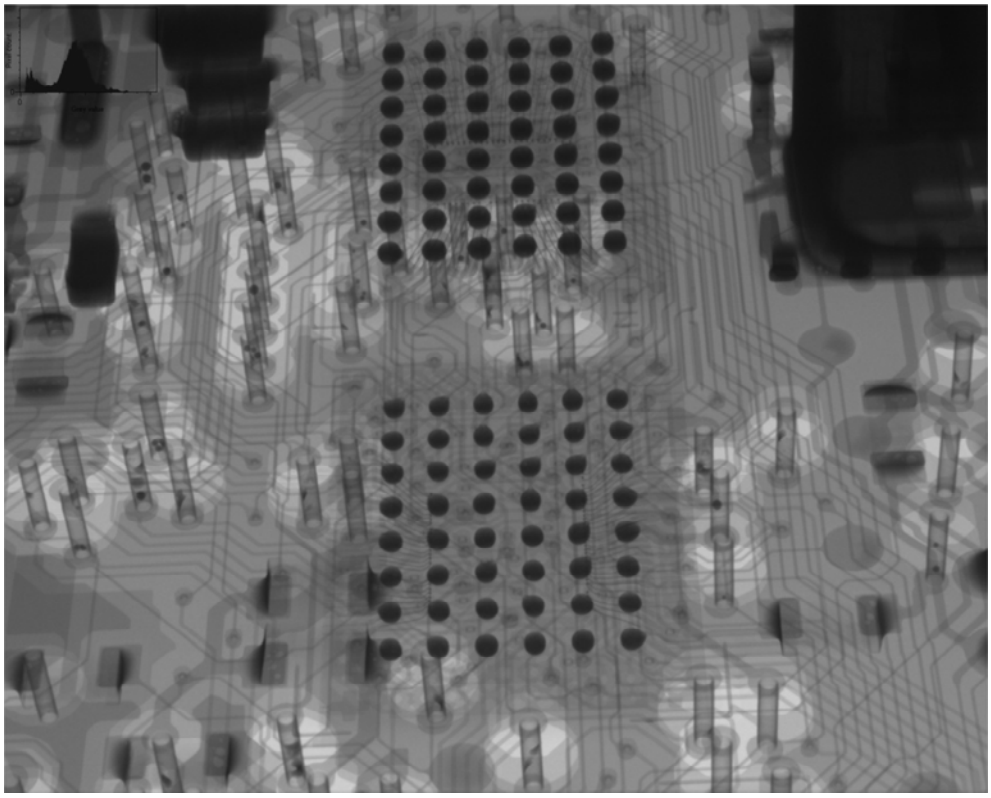

Figure 1.1: X-ray image of a PCBA revealing the multiple layers of conducting lines, vias and various components.

Reduced distances on a PCBA make it easy for humidity to condense locally on the PCBA to form a micro-droplet or thin water layer, while the electric field through the solution is enhanced due to close spacing. Above factors clearly increases the risk for the electrochemical cell to form on a PCBA either due to the potential bias

between the two closely spaced points connected by a water layer (electrolytic cell) or between two dissimilar metals/alloys leading to galvanic cell formation. For the latter it is important to understand that a PCBA consists of several metals/alloys with large difference in electrochemical potentials (typical e.g. is Copper-Nickel-Gold couple in an Electroless Nickel-Gold (ENIG) contact, see examples in Figure 1.2). Further, the sophisticated electronic circuits are becoming more sensitive to unintended stray currents on the circuit board that, in example, might alter the oscillation frequency of an incoming signal to an Integrated Circuit (IC).

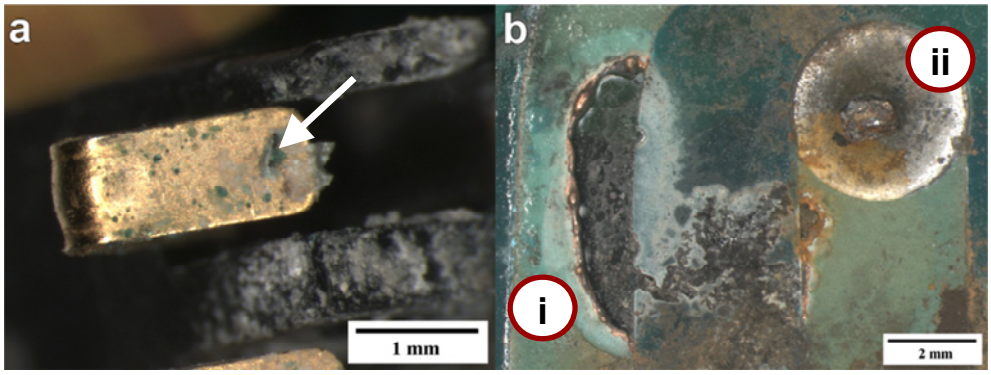

Figure 1.2: a) Example of corrosion of Ni underlayer on an ENIG contact due to galvanic cell formation between Ni anode and Au cathode. Green Ni corrosion products can be seen protruding from the gold layer, as indicated by the arrow. b) Electrolytic corrosion between Cu conducting line which is coated by soldermask (i) and Sn soldered through hole component (ii) on a PCB due to humidity ingress through soldermask coating. Both failures are from testing in harsh environment.

If the condensed water layer on the PCBA remains pure, it will seldom create any problem due to the low conductivity of pure water. However, corrosion will usually occur even if pure water is added to the surface, as dissolved CO_2 from the atmosphere causes increased conductivity, and in most cases there will also be enough process related contamination and additional service related contamination present to enhance conductivity and also to provide aggressive ions for the corrosion attack. Process related residues are an important issue today due to the use of so called 'no-clean' flux, which are not intended to be cleaned after the production process. Although, the idea of the 'no-clean' flux composition is to provide a minimal overall amount of residues, uneven distribution of residues can result in local areas on the PCBA having very high residue concentrations due to variation in temperature across the PCBA surface. For wave soldered PCBAs,

temperature differences also exist between top and bottom of the PCBA. No cleaning is advantageous to reduce the cost of production, however, it results in PCBAs that are vulnerable to corrosion attack and even pose problems for the corrosion protective measures such as the use of conformal coatings. Overall, the question here is “how clean is clean enough” for a PCBA to avoid corrosion attack and thereby the failures due to corrosion. This needs fundamental understanding of the various factors affecting the corrosion in electronics, materials involved, design of PCBA and components, types of corrosion, role of bias voltage, contamination, humidity and related mechanisms.

This is the content of the present PhD thesis; however, emphasis is placed on one of the key corrosion issue specific for electronics namely electrochemical migration and an investigation on gaseous corrosion of silver conductors.

1.2 Relevance of electronic corrosion

Corrosion of electronics can be divided into two major categories: (i) electrochemical corrosion in aqueous environment and (ii) gaseous corrosion caused by corrosive gases. Other factors such as wear and vibration can superimpose on corrosion causing tribo-corrosion types such as fretting. Gaseous corrosion at room temperature or slightly elevated temperatures can also be assisted by aqueous conditions, and therefore it is difficult to differentiate between electrochemical corrosion and gaseous corrosion similar to the work on sulphur corrosion of silver components discussed in this thesis.

Figure 1.3 summarizes the various types of corrosion encountered in electronics assisted by aqueous environment. The figure does not provide a comprehensive list and it is focused on corrosion related to the open surface of the PCBA, therefore the Conductive Anodic Filament (CAF) type of attack found inside the multi-layer PCB is not described. The common denominator for all the types of corrosion is the humidity to generate local aqueous environment and ionic contamination to enhance the conductivity of the medium.

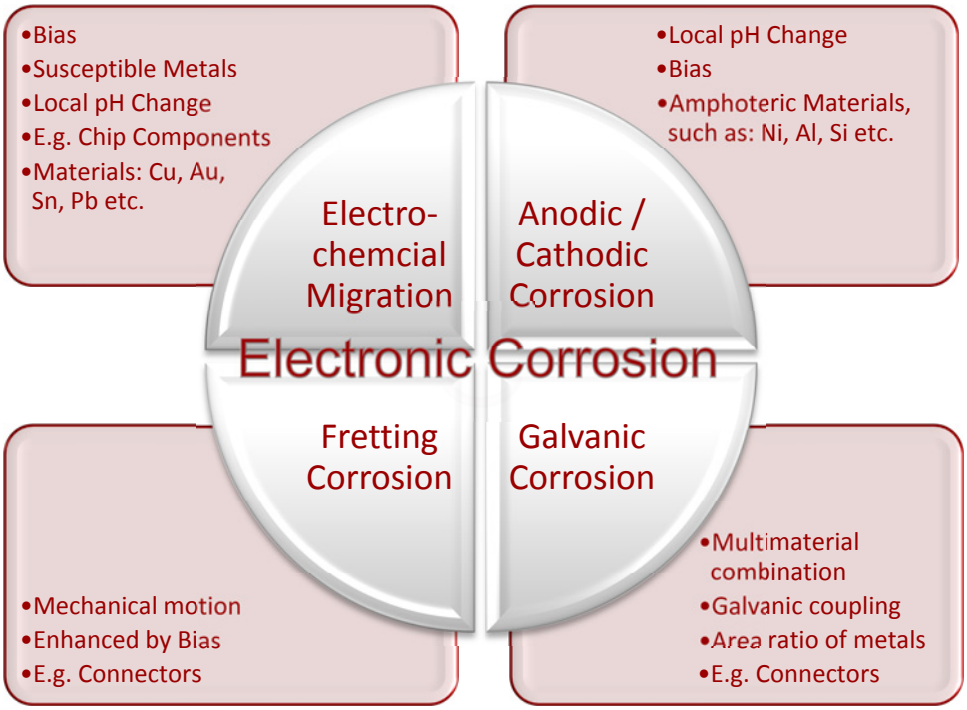

Figure 1.3: Summary of some of the corrosion mechanisms of high importance to electronic corrosion. Important parameters are shown for each case.

The electrochemical corrosion of electronics occurs in a locally formed aqueous environment on a PCBA due to the co-existence of three factors namely: (i) potential bias, (ii) metals/alloys, and (iii) humid environment. Together these form the corrosion triangle as illustrated in Figure 1.4. The exposure to water can either be through direct exposure to humid air or from the diffusion of water through a polymer coating if conformal coatings are used.

Doctoral Thesis, Daniel Minzari 2010, Technical University of Denmark, 2010

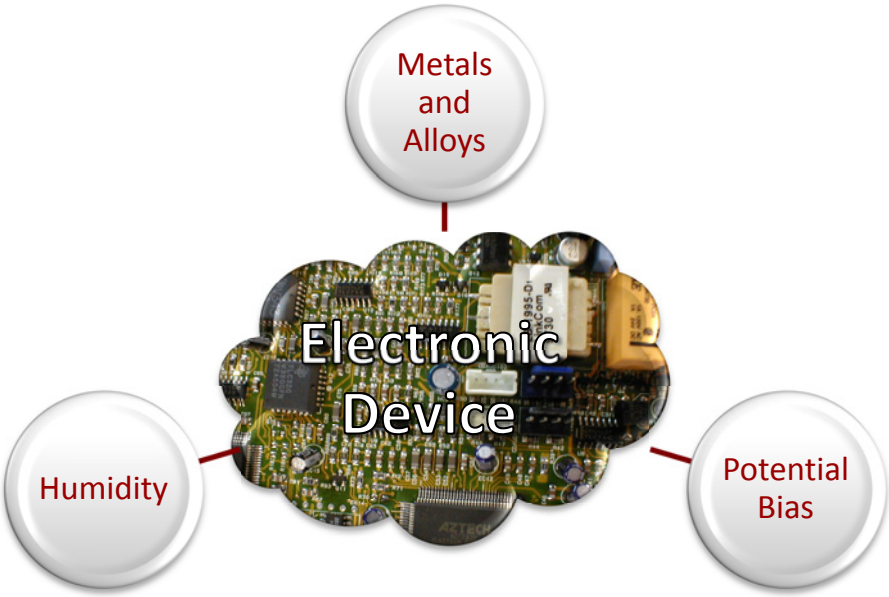

Figure 1.4: The three corrosion promoting parameters co-existing on a PCB making it a substrate of high risk for electrochemical cell formation.

The potential bias is either obtained by galvanic coupling of metals having dissimilar electrochemical equilibrium potentials, or it is delivered from the power supply of the electronic device. The former creates a galvanic cell and latter an electrolytic cell as illustrated in Figure 1.5 a and b respectively.

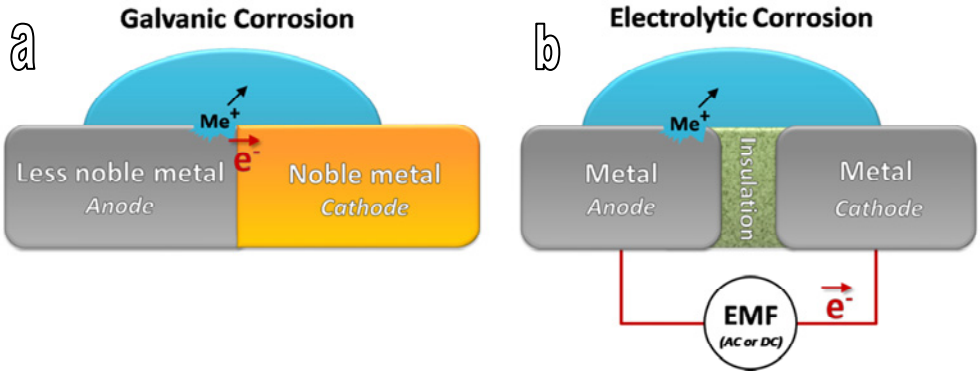

Figure 1.5: Schematic of the possibility of a) Galvanic cell and b) Electrolytic cell formation on a PCBA during local condensation. For both examples, charge balance is obtained by reduction reactions which are occurring at the cathode which is not shown on the illustration for simplicity.

The metals/alloys used in electronics are usually chosen for their cost, processing factors and physical properties such as melting point, mechanical strength, and electrical properties, while the electrochemical and corrosion properties are seldom considered. A number of metals/alloys exist on a PCBA, also as multilayer structures. The most common metals include Sn, Cu, Ni, Fe, Co, Ag, Au, Pb and Al[1]. However, if different metals are in contact and are exposed to an electrolyte, the difference in the equilibrium potentials of the metals is the thermodynamic driving force for oxidation (dissolution) of the metal having the lowest (less noble, more active) potential. When metal surfaces are exposed to humid air, a thin layer of water molecules is adsorbed to the surface. In normal conditions (ambient temperatures and low relative humidity (RH), below ~60%), a layer of 1-3 molecules of water are adsorbed on the surface of a solid substance [1,2]. At humidity lower than ~60% galvanic corrosion is usually not an issue, while higher humidity are normally enough to drive galvanic corrosion if unsuitable material combinations exist on the PCBA surface [3]. In this case, the mechanism of corrosion is similar to typical galvanic corrosion at miniaturized levels, but mostly with high cathode to anode area ratio, such as for multi-layer structures like ENIG (Electroless Nickel on Immersion Gold) contacts where porosities in the gold layer expose the underlying nickel (see example in Figure 1.2a).

On the other hand, if an electrolytic cell forms as in Figure 1.5b, the electrode with positive bias will act as anode, while the one with negative bias will be the cathode. The process is in principle similar to galvanic corrosion, however here the difference in thermodynamic activity of the two electrodes is due to the applied potential bias from the device and the potential difference is not fixed as it varies from point to point on the PCBA.

The formation of an electrolytic cell as described in Figure 1.5b gives rise to several possibilities for corrosion depending on the electrode material, as shown in Figure 1.3. Among these, electrochemical migration is of high importance, as this corrosion failure can introduce an electric short between points on the PCBA if they

[1] *No preference given to the order of the listing*

are connected by a water layer, thereby causing intermittent or permanent fault. The time constant associated with this failure mechanism is very short (few seconds) if co-existence of conditions promote migration. More detailed discussion on ECM is available in Section 3.

As the resistance through the adsorbed water layer between two points on a PCBA at atmospheric humidity is very high, electrolytic corrosion will not usually be a problem at ambient conditions and low relative humidity. However, electrochemical reactions due to electrolytic corrosion are commonly found in failed electronics. The main conditions leading to formation of an electrolytic cell in electronics are:

- Adsorbed layer increases at high humidity conditions (magnitude of 20-50 molecules [1])
- Thermal cycling leads to formation of a visually observable condensed water.
- Hygroscopic species such as salts or flux residues attract humidity from the air to form a condensed phase at humidity levels below 100%RH [1,4].

If any of these conditions are encountered, electrolytic corrosion is possible. The thickness of the adsorbed water layer on metallic surfaces is highly dependent on temperature and relative humidity, and especially the combination of high temperature and high humidity will dramatically increase corrosion speeds [1,2,5,6].

As the distances on the electronic circuits decrease, the risk of experiencing an electrolytic bridging between two points on a PCBA increases. Figure 1.6 shows comparison between the size and design of a through hole resistor and three surface mount resistors of various sizes (more details about electronic components and mounting techniques will be given in section 2).

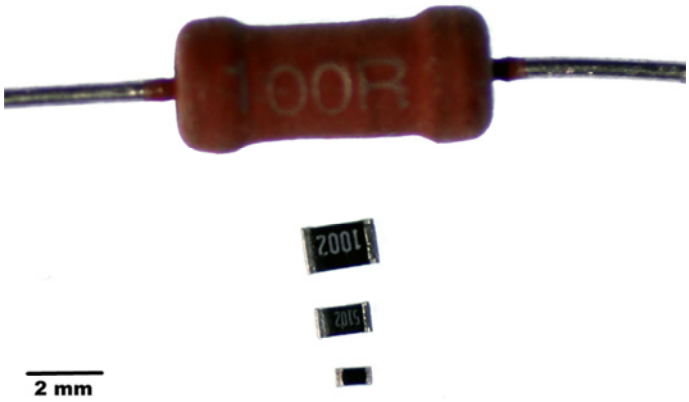

Figure 1.6: Comparison of component designs for a through hole resistor and three surface mount resistors of sizes 0805, 0603 and 0402 where 0805 is the largest housing and 0402 is the smallest.

Lastly, the conductivity for the water layer is often provided by contamination arising from production process and service conditions. Examples of contaminations often found in electronics are:

- Solder flux residues
- Remnants from plating baths from PCB manufacturing
- Human handling (fingerprints)
- De-gassing from polymer laminate or encapsulation materials
- Chlorides and other corrosive gases
- Dust particles, even in tiny quantities

Unlike conventional corrosion of big structures, electronic corrosion needs only dissolution in the order of nano to micrograms of material to cause failures. Figure 1.7 visualizes some common contaminants that can influence the corrosion of an electronic device. Especially dust and fingerprints often contain ionic species such as halides which are known to dramatically increase corrosion speeds, and corrosive gasses such as H_2S, SO_2 or NH_3 will dissolve in a water layer to form corrosive ionic species.

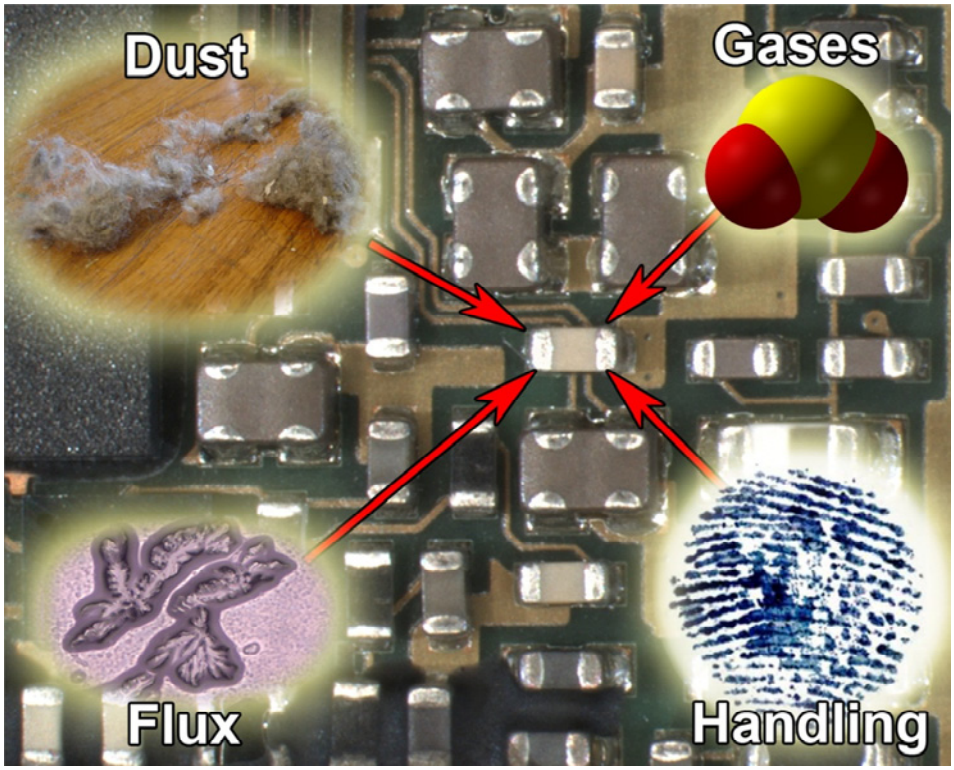

Figure 1.7: Illustration of some common contaminants that could influence corrosion properties of electronics.

Many ionic contaminants are also often hygroscopic and help forming a condensed water layer at lower humidity levels.

Increased focus on health and environmental hazards from electronics has resulted in the regulations on the materials and chemicals used in production of the electronic circuits. In the European Union, strict regulations have been implemented on devices that are produced or intend to be used in EU. These are subjected to the Restriction of Hazardous Substances Directive (RoHS) and Waste Electrical and Electronic Equipment Directives (WEEE), which went into force in July 2006. This has led to changes in many of the materials and processes used for manufacturing electronics, and the need for a thorough understanding of the mechanisms and influencing parameters for electronic corrosion is therefore more relevant than ever.

1.3 OBJECTIVES OF THE PRESENT STUDY

This PhD thesis is part of the work carried out under the Centre for Electronic Corrosion (CELCORR) research programme at DTU. Overall aim of the CELCORR is to understand electronic corrosion failures in detail, elucidate mechanisms and influencing factors, and develop control strategies. The primary objective of this thesis under the CELCORR programme is to investigate in detail the influencing factors and mechanisms related to Electrochemical Migration (ECM) in particular and develop test methods for component level and PCB level testing of electronic corrosion in general and ECM in particular. Part of the PhD work is also focused on the corrosion of silver under the influence of sulphur containing gases in the presence of humidity in connection with a power module failure. Electrochemical migration is selected as the focal point of the investigations due to the fact it is a corrosion phenomenon specifically related to electronics, and the influencing parameters and mechanisms are very little understood. Further, analysis of a large number of corrosion failures found in the electronic industries showed that the ECM is a common failure mode, and its typical characteristics resulted in intermittent and permanent failures within a short span of time, which is not the case with other corrosion forms. Electronic components focussed in the present investigation are mainly surface mount chip capacitors and resistors as the design and materials of these makes them favourable sites for nucleation of a condensed liquid, which makes these components especially susceptible towards ECM. Therefore, the materials investigated are limited to mainly Sn but also Sn-Pb, and Sn-Cu-Ag (lead free solder alloy) due to their importance in connection with PCBA surface.

The overall objectives of this thesis can be summarized to:

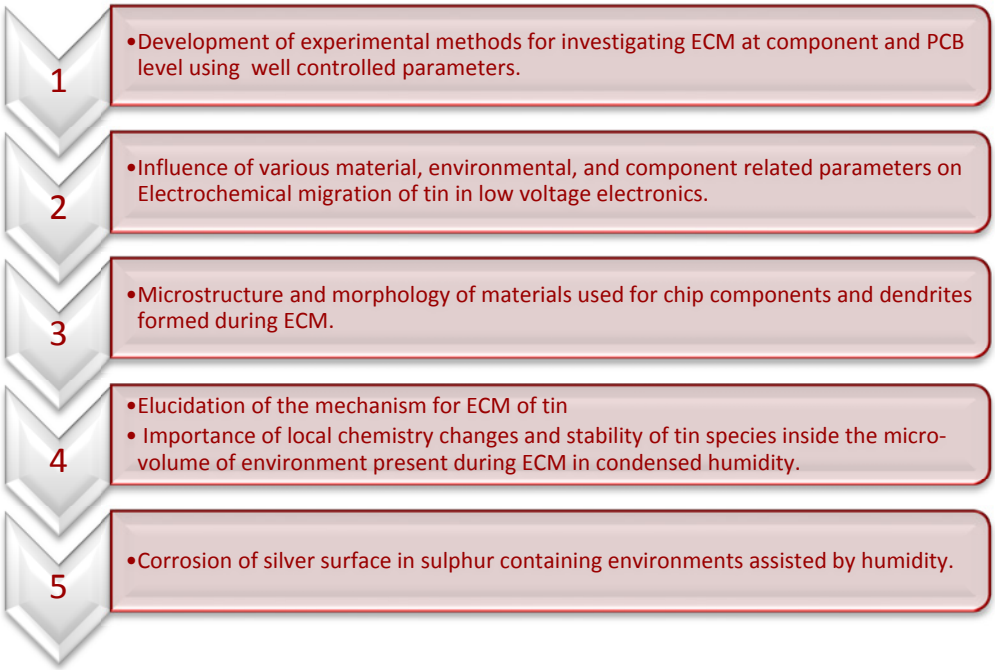

1.4 STRUCTURE OF THE THESIS

Chapter 1 of this thesis is intended to provide an overview of the relevance, magnitude, complexity, and importance of electronic corrosion, as well as describing corrosion types, terminologies, and objectives of the present thesis. As electronic corrosion is a highly interdisciplinary subject, a short introduction to the basics of electronics, components, and manufacturing processes is provided in chapter 2. The problem of electrochemical migration is discussed in detail in chapter 3, which includes an attempt to provide a proper classification and terminologies, description of the thermodynamics and electrochemistry of tin, and detailed summary of available literature on electrochemical migration in general and of tin in particular.

A substantial part of the work in the current thesis has been in the development of reliable test methods for studying electrochemical migration. The novel test methods developed are therefore described in detail in chapter 4.

The results and discussion on various investigations carried out in this PhD work is structured in this thesis as a compilation of separate technical papers already published or intended for individual publication. For this reason, some repetition is unavoidable, especially with regard to introductions and experimental procedures. In order to ensure an easily readable layout for the thesis, all papers have been formatted in the same manner, and so the layout might be different than that found in the journal paper in which it is published or communicated. However, no content has been edited in the papers that have been published or submitted for review.

The thesis consists of 6 technical papers, of which 5 are first-authored by the candidate. One paper which is co-authored by the candidate is included, as it is based on a substantial amount of results (more than 60%) that have produced by him, and as the subject is of very high relevance to the current thesis. Five of the first author papers are published or intended for publication in international journals, and the co-authored paper is published in a conference proceedings. Chapters 5-8 in the current thesis describe the investigation of electrochemical migration on un-mounted chip components, where parameters from assembly and soldering processes are excluded. Paper 1 (chapter 5) describes the effect of low concentrations of chloride on the electrochemical migration of tin, followed by paper 2 (chapter 6) on detailed microstructural characterization of tin dendrites by electron microscopy. The effect of process related residues on electrochemical migration of tin were reported in paper 3 (chapter 7) and based on the overall findings, an in-depth discussion on the mechanisms of ECM of tin was proposed in paper 4 (chapter 8). The development of a new test setup for PCB level testing of electrochemical migration and PCB level investigation on the effect of various PCB level parameters on ECM of tin is presented in paper 5 (chapter 9). Finally, a detailed investigation on the field failure due to silver sulphide corrosion on a hybrid circuit, which was coated by a silicone conformal coating, is the content for paper 6 (chapter 10).

Overall discussion of the findings from the current thesis are given in chapter 11 with some suggestions for future work and overall conclusion are presented in chapter 12

A list of appended papers and other papers by the candidate is included at the beginning of the thesis.

2 ELECTRONIC COMPONENTS AND MATERIALS

Corrosion of electronics is a multidisciplinary subject involving electrochemistry, corrosion, chemistry, materials engineering, electronics, and electrical engineering. In order to get a clear understanding of the materials, components, and terminologies involved in a PCBA for a corrosion and materials scientist, following sections are included to provide an overview of the various parts of an electronic device.

However, only topics of high importance to the current thesis are described, which includes:

- Printed circuit boards
- Important active and passive components
  - Integrated circuits
  - Hybrid circuits
  - Capacitors
  - Resistors
- Component mounting and soldering

Readers who wish for more extensive literature on the subject are referred to the following recommended literature: Coombs Jr. [7] (on printed circuits), Sangwine [8] (on electronic components) or Prasad [9] (on surface mount technology).

2.1 PRINTED CIRCUIT BOARDS

A Printed Circuit Board (PCB) is also known as Printed Wiring Board (PWB) and is the main building block of the electronic device. A PCB is used as the substrate for mounting various components and as the connection medium between components using embedded conduction lines. A PCB which has been assembled with components is usually called PCB assembly (PCBA) or PWB assembly (PWBA).

A PCB typically consists of metal patterns of conduction lines (usually made from copper) embedded on a dielectric medium which is mostly a polymer (usually epoxy, but also polyester and phenolic resins are used [7], but for special

applications ceramic substrates may be used). In order to avoid debonding of the conducting lines due to differences in the thermal expansion between the polymer and metal, the polymer matrix is usually reinforced by glass fibres. In order to reduce the risk of fire hazards, flame retardants such as e.g. Tetrabromobisphenol-A (TBBA) are also added to the PCB [10].

A PCB can be single or double sided meaning that the components can be mounted on one or two sides respectively, but often consists of several layers (multi-layer PCB as shown in Figure 2.1) to increase the density of components mounted on one side or both sides of the board. Most PCBs consist of 2-6 layers though the number of PCBs having more than 6 layers has grown rapidly over the past decade [11]. The number of layers that can be stacked depends on how thick the PCB can be, though the complexity of the board increases dramatically when many layers are used. Today boards can be produced with up to ~20 layers, but such boards are still quite rare [11].

Each layer on the multi-layer PCB consists of a pattern of conductive lines (usually made of copper), which are then stacked together. In order to make connection between the layers, plated via holes are used (see illustration in Figure 2.1). The metallic surface on the outer layer is commonly top-coated using a solder mask, which is an organic coating that covers all surfaces except contact areas or solder pads. The remaining surfaces are then coated by a variety of metal finishes depending on the application, but most commonly used are immersion tin, hot levelled solder alloy, immersion silver, or electroless nickel- immersion gold (ENIG).

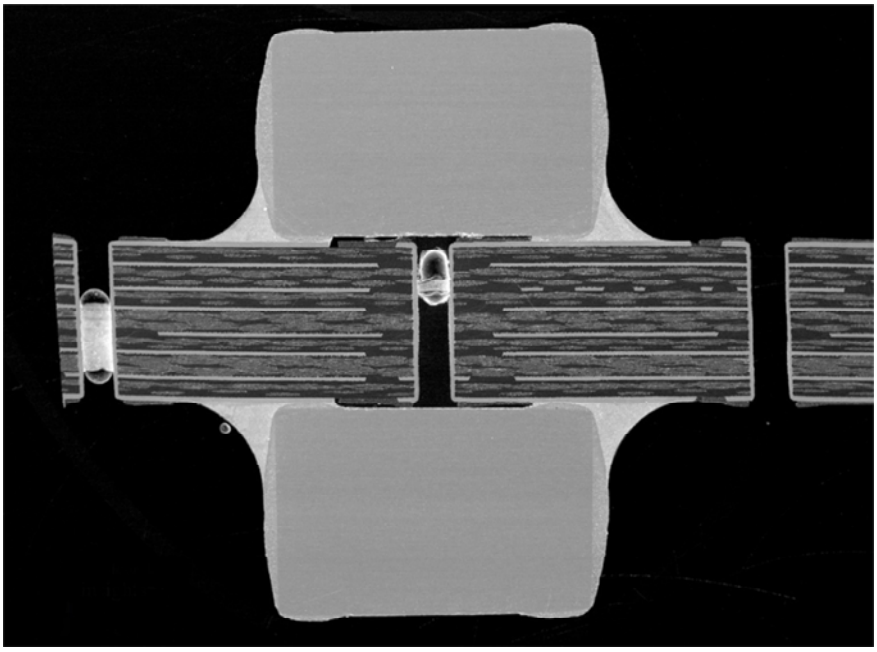

Figure 2.1: Cross-section through a multilayer PCB with 2 surface mount capacitors on either side. The capacitors are approximately 2.5mm wide and connected with a plated through hole to various layers as required (Reprinted with permission from United Business Media LLC, USA).

2.2 IMPORTANT ACTIVE AND PASSIVE COMPONENTS

The types of components found on a PCBA are numerous, as illustrated by the examples in Figure 2.2. The electronic components on a PCBA are generally divided into active and passive components.

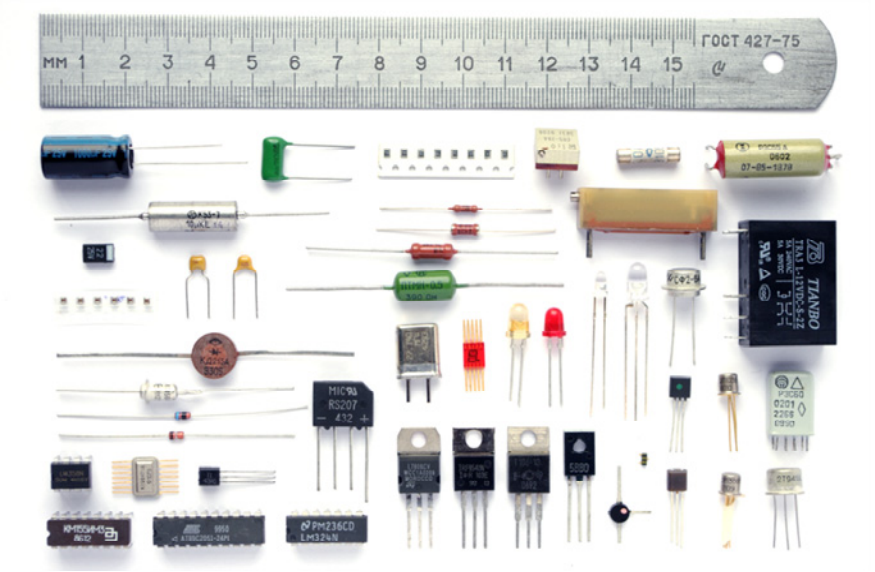

Figure 2.2: Example of electronic components. Uncopyrighted image adapted from Wikipedia.org

Passive components are components that do not have a gain to the current passing [12].

Examples of these include resistors, capacitors, inductors, diodes, and piezoelectric devices.

Active components are components that give a gain to the current. An active component will often consist of several components which are integrated to function as one single component, and an active component can therefore contain passive components.

Examples of these are transistors, amplifiers, and integrated circuits.

In each of these categories there is a large variety of different types and designs. In the following, a short explanation of selected components that are of relevance to the current thesis will be given.

2.2.1 INTEGRATED CIRCUITS

Integrated circuits (ICs), are as the name suggests consisting of several components which are integrated into one single device which is usually encapsulated, sometimes hermetically. ICs can to some extent be regarded as the brain of an electronic circuit. It is here that millions (or even billions) of transistors make the calculations and data processing, which provide the advanced features of many electronic devices. In the present thesis, corrosion reliability of IC's has not been discussed or investigated, as it would be a whole area of research by itself. However, due to their high importance to electronics, a basic explanation of what an integrated circuit consists of will be discussed from the materials and corrosion point of view.

The ICs consist of semiconductor devices such as transistors and amplifiers which are mostly made from a silicon mono-crystal and in some applications GaAs [13]. The actual IC is commonly termed the "die", but due to its small size and complexity, it is often placed on a lead frame which can be soldered on to the PCB. The die is connected to the legs of the lead frame by thin gold wires of approximately ~25µm (see Figure 2.3). The external lead frame is often made from Cu/Zn37, CuFe2, FeNi42 (alloy 42) or CuNiZn (Vacon) alloys [14] or from multiple metallic layers [15]. Apart from providing electrical connection to the PCB, the lead frame dissipates the heat from the IC; due to this reason Cu based materials are popular [16]. In most applications, the die is encapsulated in a moulded polymer, such as epoxy.

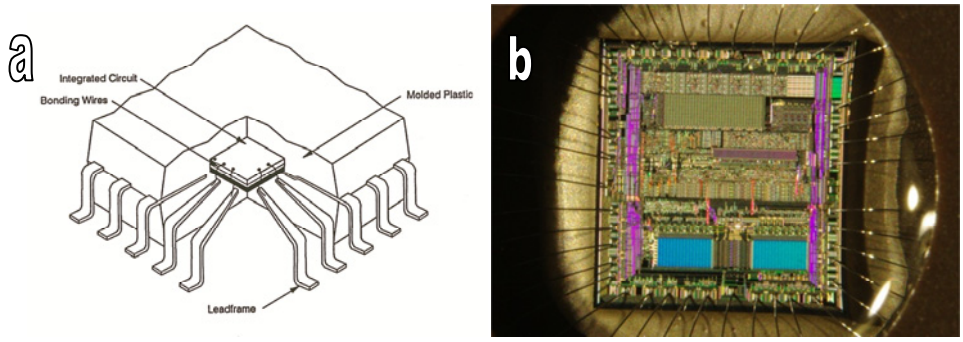

Figure 2.3: a) Schematic of an integrated circuit. The actual IC inside the encapsulation is also termed the "die". b) Image of a die. (Image a) is reprinted with permission from [7] and image b) is adapted from "yellowcloud" at flickr.com under the Creative Commons Share Alike License [17])

Connector lines on the IC are typically made from aluminium which is doped with few per cent of Cu, Ti or W to reduce the risk of electromigration [18,19] and a thin layer of silicon dioxide is used as a top protection layer. The width of the conduction lines have been dramatically reduced during the past couple of decades, as illustrated by Figure 2.4. This has increased the sensitivity to water ingress, as aluminium conduction lines under a potential bias will readily corrode in the presence of water. Corrosion of oppositely biased aluminium conduction lines on the IC results in both anodic and cathodic corrosion due to the amphoteric nature of aluminium, which means that it can dissolve electrochemically at both electrodes due to the production of local acidity at the anode and alkalinity at the cathode. Due to the sensitive nature of the ICs, high performance requirements, complicated technology and the high cost price, the ICs are usually encapsulated in epoxy. The epoxy encapsulated ICs are susceptible to corrosion issues due to penetration of water through the polymer if poor sealing technology has been used. Other possibilities for corrosion of ICs are the galvanic corrosion between coupled materials and ECM between closely spaced leads (usually coated with solder alloy) or bond pads (made of solder alloy) which are open the atmosphere surrounding the PCBA.

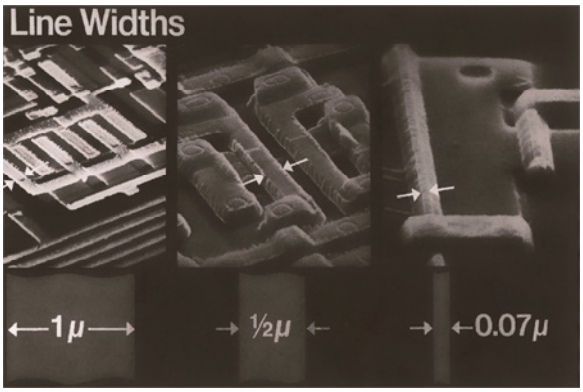

Figure 2.4: Illustration of the miniaturization of line widths of Al conductors in integrated circuits over the past decades. Reprinted with permission from [20].

2.2.2 HYBRID CIRCUITS

Hybrid circuits are called *"hybrid"* because they combine the various technologies used in electronics, such as the semiconductor technology with the batch fabricated passive components like resistors and capacitors. They are made on an electrically insulating substrate which is usually made from alumina substrate or a similar ceramic on which conductors, resistors, and simple capacitors are added by vapour deposition or screen printing process followed by sintering [21,22]. An example of a hybrid circuit is presented in Figure 2.5. Discrete components such as resistors and capacitors, and IC packages are added to the substrate by soldering, using techniques similar to that of the manufacturing of a PCBA, while some semiconductor devices are wire bonded to contact pads on the substrate. The hybrid circuits are often encapsulated in a polymer, and serves as one component on a printed circuit board in a way similar to that of an IC. In the future, hybrid circuits might take over the place of PCBA so that a number of components can be directly printed on the ceramic substrate.

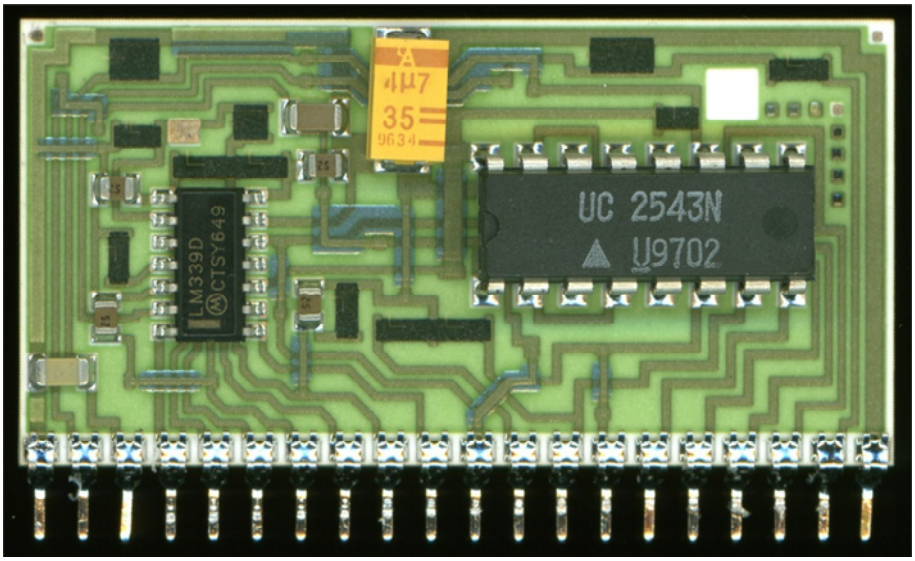

Figure 2.5: Example of a hybrid circuit on a ceramic substrate showing IC's, surface mount capacitors and the black areas are printed resistors. The resistors can be precisely tuned during calibration process by laser cutting the resistive layer. Interconnects are seen to be of multiple layers and where they cross, blue areas are used to insulate between the layers. (Image is adapted from "Nightflyer" at Wikipedia.de under the GNU Free Documentation License [23]).

2.2.3 CAPACITORS

Capacitors are bi-polar components consisting of two electrodes which are separated by a dielectric material. As the potential is applied to the electrodes, the electric field will build up charge on the two electrodes. The capacitance of a capacitor is defined by the relation C=Q/V, where C is the capacitance (measured in Farads, F), Q is the charge and V is the applied potential.

Capacitors are used to store energy[2], as the charge that is built up on the electrodes can be released after the potential has been removed. Under a DC voltage, a charged capacitor will act as an open circuit, while in an AC voltage a capacitor will allow the current to flow with a phase shift of 90 degrees (ideally) to the current. On an electronic circuit, capacitors are used to filter the DC signals from an AC source, to smoothen the noise from AC signals, in combination with the crystal oscillators, and for a variety of other applications. However, the open circuit

[2] *A charged capacitor in an open circuit can in theory hold its charge infinitely. However, in practice no dielectric is completely insulating, and the capacitor will, depending on the materials of the component, slowly discharge.*

nature of a capacitor also makes it very sensitive to leakage currents[3] (e.g. if a condensed layer of water bridges the two electrodes). As the stored electrical energy can be released from the capacitor even after the external potential bias has been switched off, a capacitor can cause corrosion failures after the electronic device has been switched off due to the remaining polarity.

The design and materials used for capacitors vary a great deal from one application to the other, and a small selection of the various types of capacitors is shown in Figure 2.6. The surface mount capacitors are marked by the red arrow, as they are very hard to see on the image due to their small size.

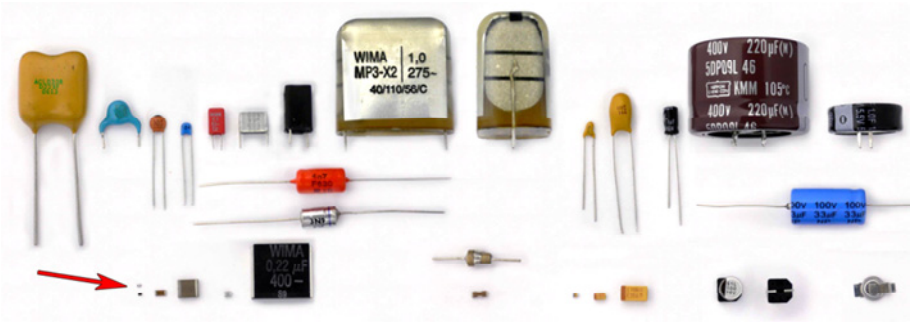

Figure 2.6: Example of a few surface mount and through hole types of capacitors. Red arrow shows the SM ceramic chip capacitors. (Image adapted from Wikipedia.de under the Creative Commons Share Alike License [17]).

Most capacitors have multiple electrodes aligned in parallel in a comb pattern (parallel plate model) [8] which is an efficient way of obtaining a large surface area in a small volume of space. In this case, the capacitance will depend on the area of the electrodes, A, the distance between them, d, and by the permittivity of the dielectric material, ε (also termed dielectric constant), by the relation $C=\varepsilon A/d$. This means that in order to obtain as large a capacitance on as little space as possible, a large electrode area and short inter-electrode distance is required. As the capacitance is also directly proportional to the permittivity of the dielectric used, a big variety of materials are used depending on the applications, including vacuum, paper, mica, polymer, ceramic, and electrolytic types [24].

[3] *Leakage currents are unintended currents between biased conductors that are intended to be isolated from each other.*

An example of the cross section of a surface mount capacitor is given in the SEM picture in Figure 2.7. Ceramic capacitors are classified by a code such as NP0 or XR7, which denotes the category of temperature stability of the dielectric constant. The ceramics are commonly based on titanium dioxide or barium titanate ($BaTiO_3$), with small additions of other elements to increase the dielectric constant. The electrodes of the comb pattern are made from nickel or silver-palladium [25].

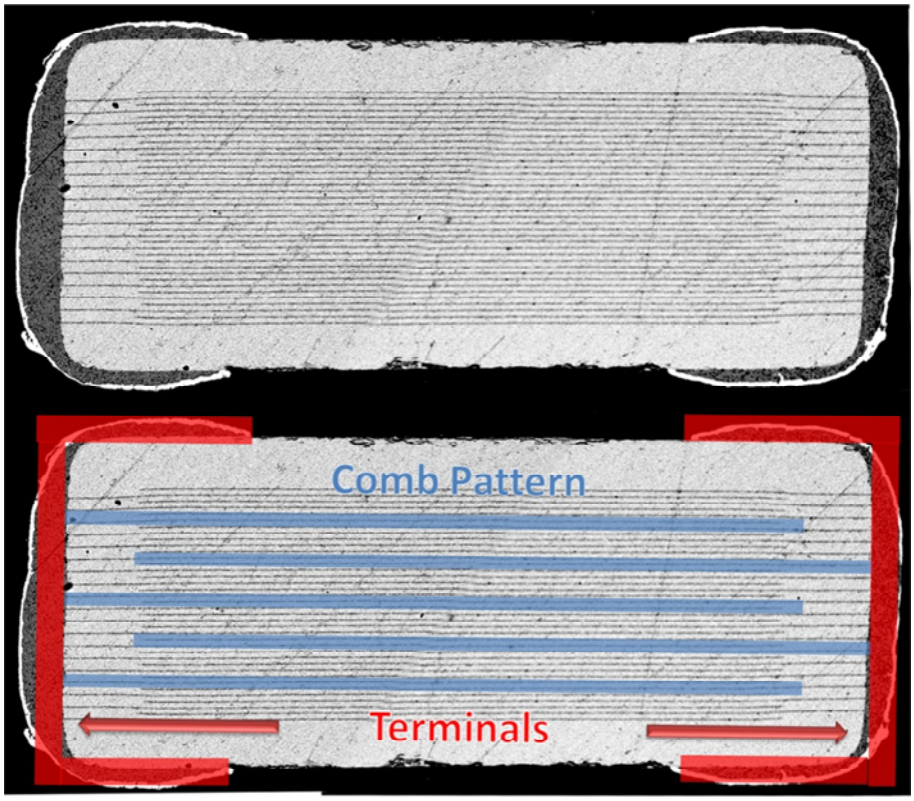

Figure 2.7: Cross section of SM capacitor and illustration of the comb pattern design.

The parts of an SM capacitor are manufactured by a sintering process, where sheets made of the ceramic substrate (green body) and the electrodes for the comb pattern are printed on to the sheet from metal powder or metal ink (see Figure 2.8).

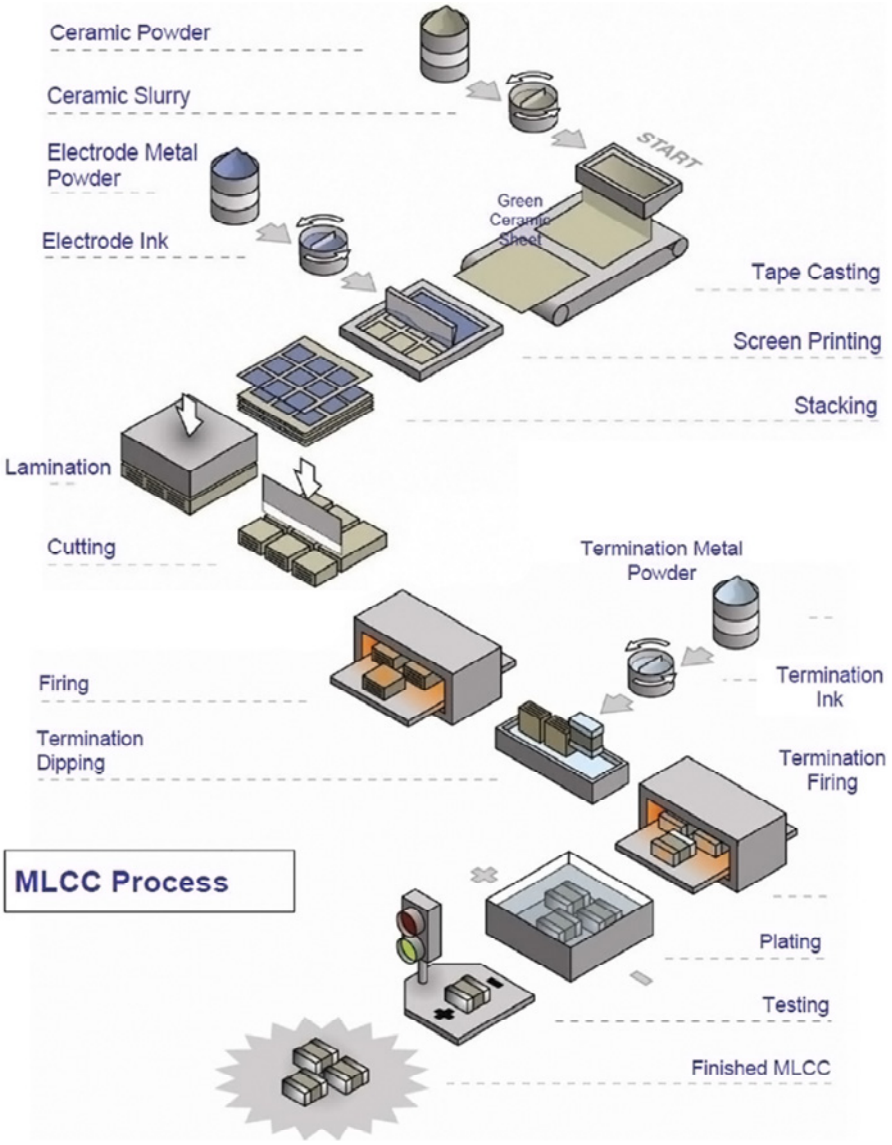

Figure 2.8: Example of the manufacturing process for multilayer ceramic chip capacitors (MLCC) (Reprinted with permission from Johanson Dielectrics, CA, USA)

The sheets are then stacked and laminated, from which the individual components are cut. The components are then fired in order to obtain dense ceramic structures with the metal electrode pattern inside. Terminations are made by dipping the ends of the components in metal powder or metal ink which is then fired again and additional metal over layers to the terminations can now be added by electroplating

process, such as barrel plating. This outer layer usually made of tin and has very rough surface morphology due to the barrel plating process.

For more details on the manufacturing of multilayer ceramic chip capacitors the reader is referred to Kahn et al. [25].

Importance of chip capacitors from corrosion reliability point of view:
The bi-polar nature of the chip capacitors with closely spaced electrodes makes them vulnerable to the formation of condensed water layer, acting as tiny electrolytic cells. Usually the surface morphology and integrity of the top tin layer is important from the corrosion point of view as this is the layer that is exposed to the corrosive environment on a PCBA. Any damage to the top tin layer will result in galvanic coupling between buried layers (e.g. Ni and Cu). Electrochemical migration is the predominant corrosion type observed on capacitors, which leads to an electric short of the component. However, severe electrode corrosion without migration is also possible, which will eventually lead to lack of electrical connection either between electrodes and capacitor plates or between electrodes and PCB solder pad. Another corrosion possibility related to capacitors is the internal ECM between parallel plates or electrodes and plates if there is damage in the ceramic layer for humidity to enter.

2.2.4 RESISTORS

Electrical resistors are used to modulate the potential, therefore a potential drop will occur on the electrodes of a resistor by the Ohms law relation of U=RI, where U is the potential drop, R is the resistance and I is the current.

There are several types of resistors, including:

Through hole (TH) resistors
Wire-bound resistors
Integrated resistors
Surface mount (SM) resistors

TH resistors were widely used in the past due to their robustness and as they are easier to hand solder. Today, they are still used in some applications, but the

majority of the resistors used are SM resistors. SM resistors are cheap to produce, they can be made smaller than TH resistors (see comparison in Figure 1.6) and easier to pick and place in an automated component assembly line. Also, the trend is to integrate resistors directly on hybrid circuits or IC's by thick film techniques, and the number of resistor components found on a PCBA is therefore decreasing.

As SM resistors have been of special focus for corrosion investigation in this PhD project together with SM capacitors, therefore the materials content and process aspects are discussed below.

The manufacturing of SM resistors is somewhat similar to that of ceramic capacitors, though no electrodes exist inside the ceramic body. The ceramic body is commonly made from Al_2O_3 which acts as a support for the component (see Figure 2.9). On the top of the component, a resistive element is applied by thick film technique which is commonly made from metal oxides or ceramic/metallic composites (cermet) [9]. Silver thick film is commonly used for connection between the resistive element and the end terminals, which are used for mounting the component to the PCB. The end terminals usually consist of multiple metallic layers where the outer layer is usually electroplated tin or tin-lead alloy on top of electroplated nickel [26]. The resistive element is protected by a glass layer, and finally a laser is used to calibrate the resistance to the desired value.

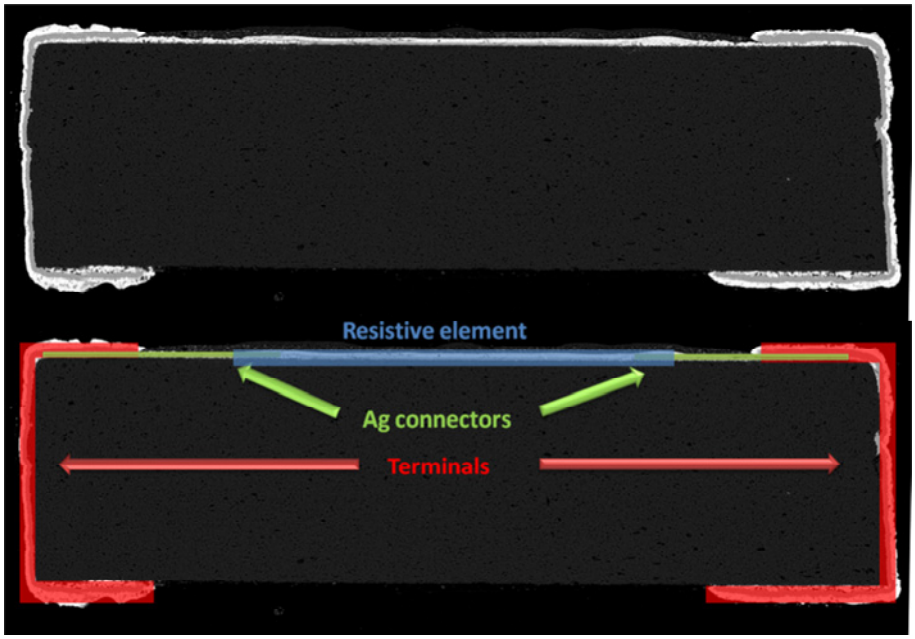

Figure 2.9: SEM image of the cross section of SM resistor. Image below shows explanation for the various features of the resistor. The resistive element is covered by a glass layer, which is difficult to see on the images due to low contrast.

Importance of resistors from a corrosion reliability point of view:

SM Resistors are bi-polar components similar to capacitors and therefore form tiny electrolytic cells if both sides of the electrodes are connected by a condensed water layer. If the water layer on the resistor is conductive enough (due to contamination on the PCB), corrosion can take place on the positive electrode and the predominant form of corrosion observed is ECM. If the inner layers are exposed, corrosion of nickel and silver is also possible and galvanic coupling can occur between tin, nickel and silver, even in the absence of potential bias. Corrosion of exposed silver under layers due to sulphur containing gasses has been reported which can eventually result in open circuit of the resistor [27].

However, from the reliability point of view, resistors in general are regarded as less susceptible to aqueous corrosion due to the generation of heat in the resistive layer, which will tend to result in a dry surface compared to other components e.g. SM capacitors.

The size of the chip resistor is another factor increasing corrosion. With reduction in size, a higher electric field will exist between the electrodes which will increase corrosion. This is also true for SM capacitors.

2.3 COMPONENT MOUNTING

Two techniques are commonly used for mounting the components to the PCB, namely through hole (TH) and surface mount technology (SMT) [28]. Illustrations of the basic design concepts of the two techniques are presented in Figure 2.10.

2.3.1 THROUGH HOLE TECHNOLOGY

TH technique has the advantage that it is easy to manually remove or add components by hand soldering and this technology has been dominant in the past. However, the increased automation and reduced size of the electronic components have made the SMT technique extremely popular in automated systems. Some of the basic advantage and disadvantages of the TH technique are [29]:

- ✓ Manual repair is easy
- ✓ Robustness of components
- ✓ Mechanical stability of large components
- ✘ Increased cost of producing through holes on PCB (drilling, plating)
- ✘ Large component size (low packing density)
- ✘ Difficulties in automated placement process
- ✘ Disadvantages of using wave soldering technique (see section 2.4 on soldering)

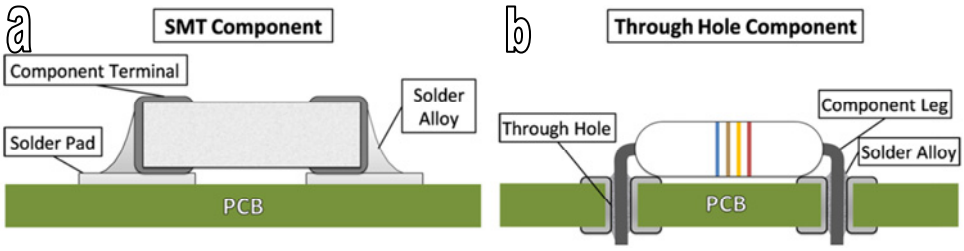

Figure 2.10:Illustration of a) SMT component and b) through hole component soldered on to a PCB

In the manufacturing of PCB's, the mechanical drilling process is time consuming and requires extreme precision. This makes the drilling process an expensive process step, and the number of holes to be made are therefore sought to kept as low as possible [11,30].

When automatically assembling a PCBA with TH components, a robotic arm places the components onto the PCB. The components are usually stored in rolls, where they are aligned on a polymer tape. The robot then picks the component from the tape, and then it has to bend the component leads to a certain angle (typically 90 degrees) and insert the leads through the holes on the PCB [30] (see Figure 2.10b). This process requires extreme mechanical precision, as a small mismatch in the distance between the bended leads and distance between the holes will make the automated insertion difficult. As TH components are often of different sizes, the robotic arm will often require several tools for different components, and the change between tools makes the placement process slower.

2.3.2 SURFACE MOUNT TECHNOLOGY

In the surface mount technique, components are placed onto solder pads on surface of the PCB (see section 2.1). The robot placing the components can typically hold several components which makes the placement process faster and with a higher precision tolerance as compared to the TH placement process.

There exists a large variety of designs for SM components including chip components (as the example shown in Figure 2.10b), ball grid array (BGA) or leads (see Figure 2.11).

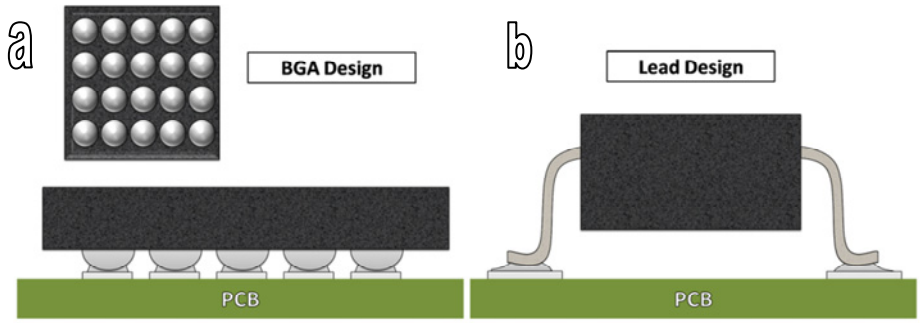

Figure 2.11: Examples of SMT designs, a) BGA design (bottom and side view of the component) and b) example of a component design with leads.

One of the drawbacks in the surface mount technology is that the manual soldering of components can be extremely difficult. As an example, if an IC module having a BGA design mounting needs to be replaced, a manual solder iron cannot reach the electrodes under the component. However, the overall benefits of SMT have made

this technology extremely popular and it is considered today as the main component assembling technique.

2.4 SOLDERING PROCESSES

When mounting components on to a PCB, solder alloys are used in order to attach the components and to provide electrical connectivity. The temperature at which the solder melts must comply with the temperature stability of the polymers on the PCB, while the solder joints must have appropriate mechanical strength to endure service life. Tin alloys are extremely suitable for this application as they combine low melting points with good mechanical strength. Tin-lead solders have historically dominated for electronic applications, but due to the environmental concerns regarding the use of lead and other heavy metals, alternative solder alloys are gaining popularity. Lead free solders are commonly based on tin ternary eutectics containing Ag and Cu (Commonly named SAC solder) or on Sn-Cu-Ni systems. Other alloy compositions include Sn-Zn or Sn-Bi. One of the key issues of shifting to lead free technologies is the increased melting temperature of these alloys. Thermal profiles, solder flux compositions (see section on Solder flux), and possibly flame retardant chemistry therefore needs to be adapted to this process change. The increased peak process temperature can reach up to 250-255°C, and degassing from flame retardants and other chemicals from the PCB laminate are suspected of having an influence on corrosion reliability. Work is currently on-going on this aspect in our laboratory, which will be published at a later stage.

2.4.1 SOLDER FLUX

For all soldering process there exists a common problem, which is the oxide layer that rapidly builds up on the metallic surface that needs to be soldered. Solder will have poor wetting on the metal oxides (see illustration in Figure 2.12) resulting in solder joints having poor mechanical properties due to the lack of adhesion. For good solder wetting on a metallic surface, the oxide layer needs to be removed immediately prior to the soldering process. This is achieved by the use of solder flux at elevated temperatures. A flux contains active components, a solvent, small amount of surfactants, and a carrier. The active components (commonly organic

acids) will etch away the oxide layer as they are activated by heat during the soldering process, while the carrier and the solvent are used to disperse the flux uniformly across the PCB surface.

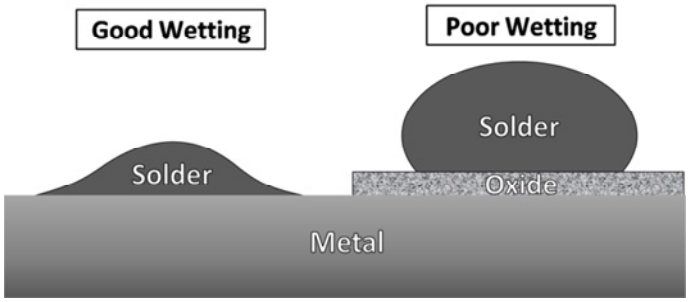

Figure 2.12: Illustration of good and poor wetting of solder on a metallic surface. .

Solder fluxes are roughly divided into:

- Rosin based flux
- Water soluble flux
- No-clean flux

Rosin based fluxes:

Rosin is an organic compound consisting mainly of colophony, a complex chemical found in the pine trees. Active agents in rosin based flux generally are abietic and plicatic acids. Additional chemicals usually consist of organic fatty acids [31]. Residues are left behind after soldering process, and a cleaning step is therefore required.

Water soluble fluxes:

Main constituents are carboxylic acids as the activator along with a surfactant and water [31]. Fluxes are designed to wash away from the board and components using plain water. However residues are very corrosive, if not completely removed by the cleaning. Occasionally, saponifiers are added to ease the cleaning, but these are alkaline and may be corrosive themselves if not completely removed.

"No-Clean" fluxes:

Widely available since the 1990s and the process has been driven for environmental considerations. Fluxes are based on a wide range of chemistries, and expected to leave only a minimal amount of residue after the soldering process, which theoretically does not need to be removed from the finished electronic assembly, as the active agents should "ideally" decompose under the influence of heat. Emphasis has here been put on "ideally", as no-clean fluxes can leave considerable quantity of residues that in reality are not as harmless as manufacturers claim [32]. Much no-clean flux chemistry contains alcohol and a low solid content, though some water-based no-clean fluxes have been developed. The solids in solder paste flux chemistry are comprised of the resin, gelling agents, wetting agents, and activators/acid components. These ingredients will remain as part of the flux residue after soldering, while the activator may remain in its reacted form and some of it will have volatized [33]. In many no-clean fluxes, adipic acid is the main component of the activator [32], while other formulations include glutaric and succinic acid [34].

Of the above mentioned flux types, no-clean flux is by far mostly used today, (excluding military and aerospace applications where more strict regulations are used for cleanliness). As an example, the distribution of no-clean flux use in North America (based on values from 2001) is presented in the diagram shown in Figure 2.13:

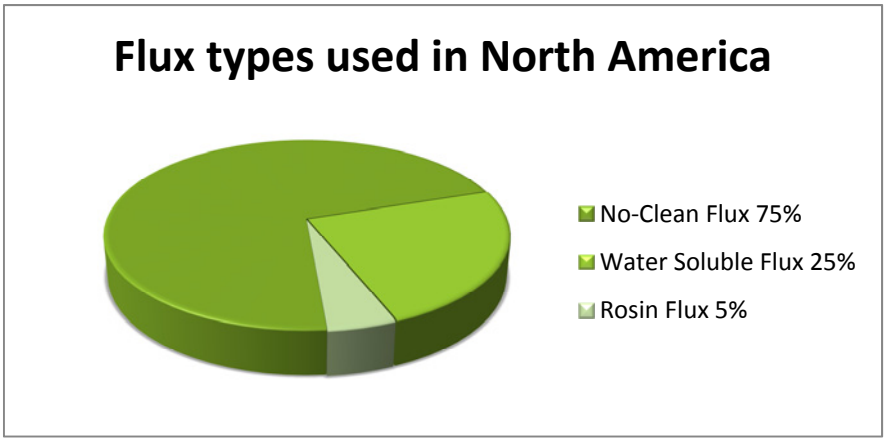

Figure 2.13: Diagram showing the distribution of the use of no-clean, water soluble, and rosin flux [33] (based on 2001 data)

The main soldering techniques used today are:

- Hand soldering
- Reflow soldering
- Wave soldering

Production of a PCBA can consist of several soldering processes depending on the types of components mounted (TH, SM), e.g. a reflow solder process, followed by a wave solder process and then hand soldering of non-standard components, which cannot be automatically soldered. However, the number of process steps are sought to be kept at a minimum due to increased cost for each process and as the amount of residues is increased by each process step.

Hand soldering is mainly used for repairs and prototyping. The solder is commonly supplied in wire form, often with flux incorporated into the wire and a solder iron having various designs is used to melt the solder. Usually, hand soldering leaves more residues due to excess flux usage for better soldering and also depends on the skills of the technical personnel.

2.4.2 *Reflow soldering*

Reflow soldering is the most common soldering technique for SM components. In reflow soldering, the solder is supplied as a paste containing a mixture of the solder

alloy in powder form and the solder flux. The main process steps of the reflow soldering process are illustrated in Figure 2.14. First a stencil is mounted on top of the bare PCB (image b). The stencil has openings at the places where solder paste is to be applied to the PCB. The solder paste is then squeezed or scraped over the stencil in a manner so that the solder paste is inserted into the openings of the stencil (image C). The stencil is then removed and SM components are mounted on top of the solder paste (image d). The solder paste act as glue and holds the components in place. The PCB assembly is then exposed to heat (image e), which melts the solder paste and activates the flux, thereby achieving the solder joint (image f).

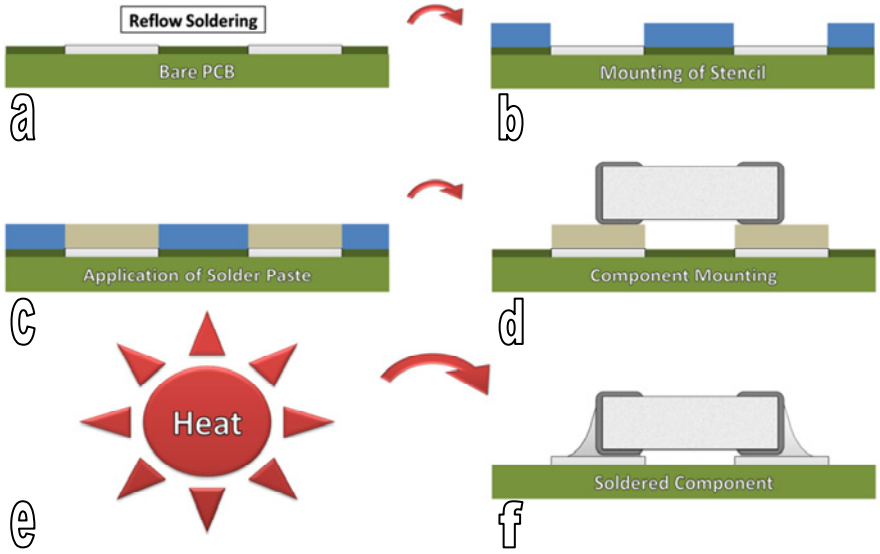

Figure 2.14: Illustration of the main process steps in reflow soldering.

The heat exposure is extremely important for the quality of the soldering. It consists of several stages [35,36], which is illustrated by the temperature profile in Figure 2.15.

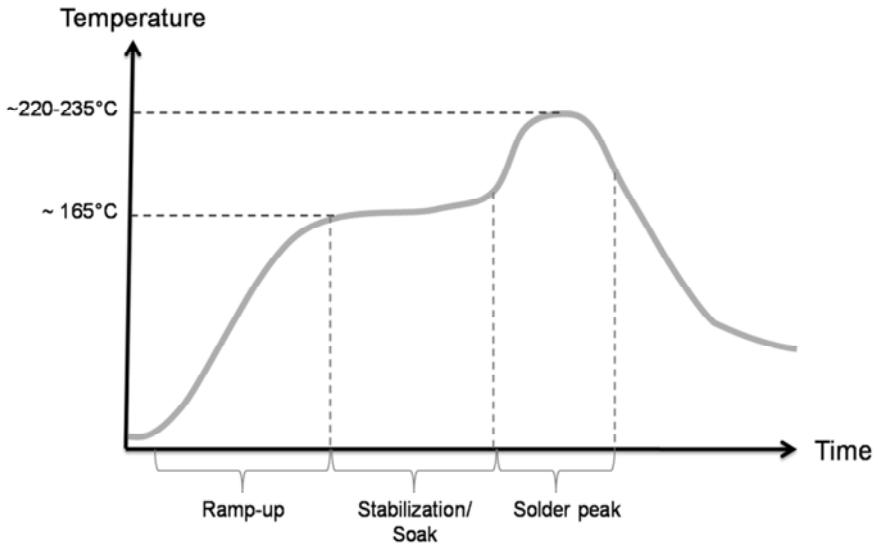

Figure 2.15: Example of temperature profile for reflow soldering.

The ramp-up stage should not be too fast in order to avoid thermal gradients due to differences in heat capacity of the materials involved. The stabilization/soak stage activates the solder flux and etches away the surface oxide film. Finally the temperature is rapidly ramped up over the liquidus temperature of the solder alloy, reaching temperatures of 220-235°C for lead containing solders and up to ~255°C for lead free solders [9,30,35-37]. Decomposition products and amount of residue created from the no-clean flux depend on the maximum temperature it experiences and rate of change of temperature. Overall time for the temperature profile shown in Figure 2.15 is about 45 seconds and our investigation using thermogravimetry has shown that it is too fast to avoid any residues [38]. With the ramping rate in Figure 2.15, (carboxylic) acid residues from the activator can be expected until the temperature 300°C, which is way above the peak temperature [38].

2.4.3 WAVE SOLDERING

The wave soldering process is used for TH components and the main process steps are illustrated in Figure 2.16. After the component mounting process (image a, see section 2.3.1 on component mounting techniques), flux is applied. This can be done by a spray process, sponge or foam applications depending on the preferences of the manufacturer and the PCBA design [36]. The PCBA is exposed to a pre-heating, similar to the ramp-up and stabilization steps of the reflow soldering process in order to activate the flux (not shown on Figure 2.16, but occurs between images b and c).

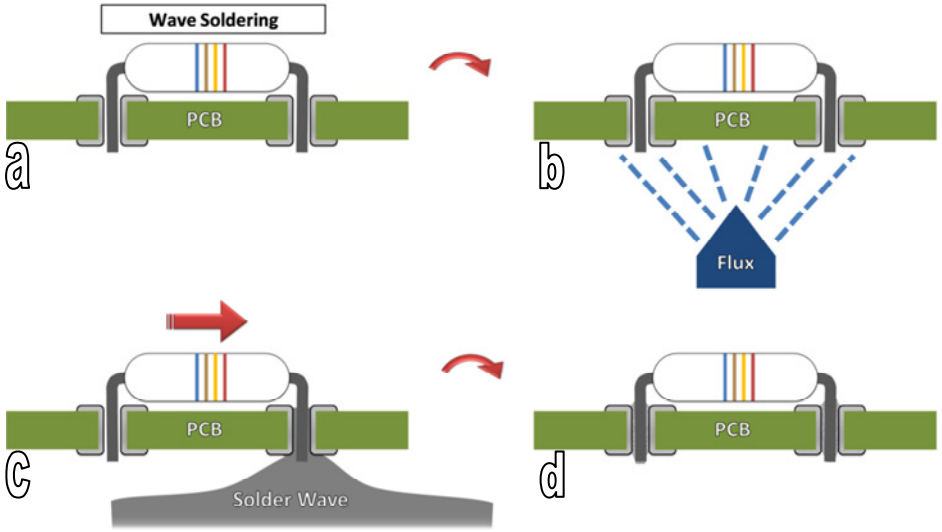

Figure 2.16: Illustration of the main process steps in wave soldering. A preheating step exists after the application of flux (between image b and c) which is not shown in the figure.

The PCBA is then transported over a wave of liquid solder which just comes in contact with the surface of the PCB (image c). The capilary forces attract the solder into the through holes, and a solder joint is achieved (image d). Due to the contact between the PCB and the solder wave, no reflowed components can be placed on the bottom side of the PCB as these would get unmounted by the wave. However, SM components can (and are often) be soldered to the top side of the PCB where there is no contact to the solder wave. Similar to re-flow soldering, wave soldering generate some residues on the bottom surface of the board where it comes in contact with solder wave. However, a more important issue related to wave-

soldering is the no-clean flux on the top part of the PCBA either from the spraying proces or rising through the through hole if other techniques are employed. No-clean flux existing on the top part will only be partially decomposed or evaporated as it is only subjected to a lower temperature of ~170°C.

3 ELECTROCHEMICAL MIGRATION OF TIN AND RELEVANT LITERATURE

This section is intended to describe the basics of the ECM phenomenon, and the state of the knowledge that existed on the subject prior to the current project. For the following discussions, it is assumed reader has a basic knowledge on corrosion theory; therefore focus is given to the problem of electrochemical migration. Following books will be helpful if the reader needs basics on corrosion theory: Winston and Uhlig [39] and for atmospheric corrosion Leygraf and Graedel [3]). For a description of other corrosion issues of electronics following references can be used [14,40].

An attempt is made in this thesis to explain in detail mechanisms of the ECM of tin and this given in the appended paper entitled “On the mechanism of electrochemical migration of tin”. Therefore, a discussion on this will be avoided in this part, but focus only on the basic concepts of ECM and available literature.

Before proceeding with the literature review, a short discussion on the specific terminologies are provided below for the reader to understand the difference between **electro**migration and electro**chemical** migration, as this is usually confused by many.

3.1 DEFINITIONS AND TERMS

Electrochemical migration is defined by IPC standard IPC-TR-476A [41] as follows:

> *"... as the growth of conductive metal filaments on a Printed Wiring Board (PWB) under the influence of a DC voltage bias. This may occur at an external surface, an internal interface, or through the bulk material of a composite (e.g. paper/phenolic laminate). Growth is by electro-deposition from a solution containing metal ions which are dissolved from the anode, transported by the electric field and redeposited at the cathode. We are thus excluding phenomena such as field induced metal transport in semiconductors and diffusion of the products arising from a metallic corrosion."*

The widely cited work by Krumbein [42] divides metallic electromigration into ionic and solid state, where ionic electromigration is what is here termed electrochemical migration. The terminology can be illustrated by the sketch in Figure 3.1:

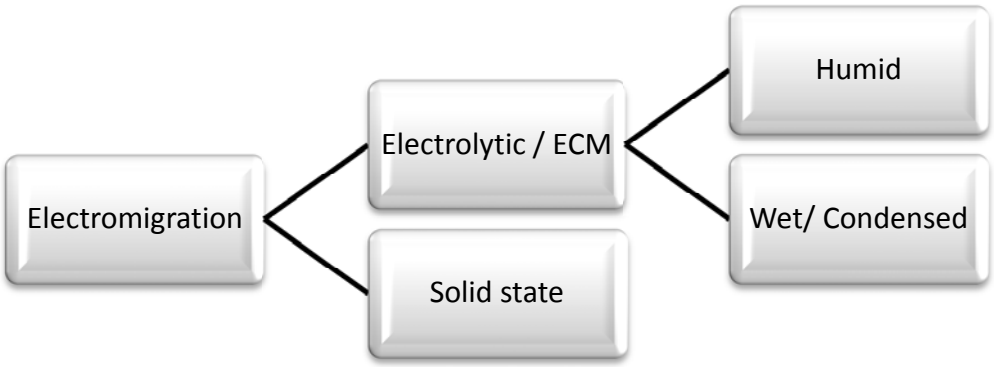

Figure 3.1: Definition of terminology by Krumbein [42].

However, as the two phenomena rely on completely different mechanisms[4] it would be natural to make a clear distinction between the two subjects. The distinction is that the solid state migration takes place by an electron momentum transfer process under a potential gradient, while the ionic migration (ECM) is due to electrochemical process and ion transport in the presence of an aqueous media. Therefore, a better classification might be as given in Figure 3.2.

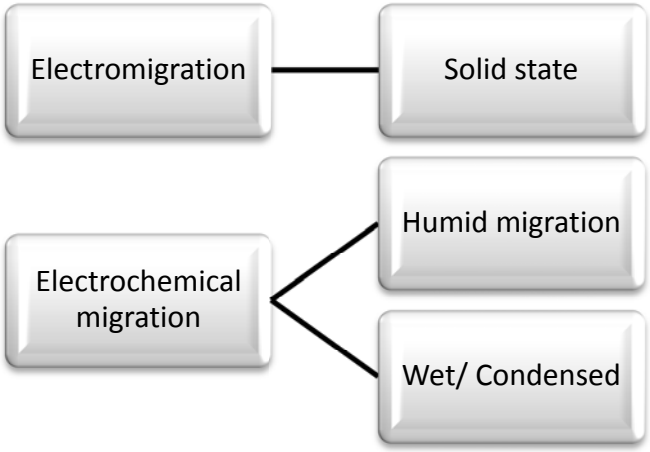

Figure 3.2: Classification separating electromigration and electrochemical migration. .

Unless otherwise stated throughout the thesis, use of word 'migration' refers to "Electrochemical migration".

[4] *Electromigration relies on solid state electron momentum transfer while ECM is an electrochemical phenomenon*

Tin whisker formation is also often incorrectly termed as electrochemical migration. However, it is stressed that tin whisker formation is not an electrochemical process, but attributed to the crystallography of the tin coatings [41,42]

Electrochemical migration can take place in two forms [43], one is when a non-condensing, humid layer of water exists on the surface which connects the two electrodes (adsorbed water molecules are believed to form a few molecular layers on the surfaces in contact with humid air [44]), while another form is when a visible, condensed water layer has nucleated on the surface and the water connects the two electrodes.

Humid ECM is when metal ions are migrating within the adsorbed water layer (few nanometre or molecular layers) on a surface that is exposed to humid environment. Krumbein [42] references work were silver and to a very limited extent copper showed humid ECM [45-54], and it is stated that tin could possibly also migrate in humid conditions [55-57], though the references given are rather attributing the migration to improper cleaning which could have formed a condensed water layer, rather than humid ECM [55,56]. Due to the unstable nature of tin ions in the presence of especially oxygen, it seems unlikely that the tin ions could be able to travel through adsorbed water of few molecular layers. As most technical surfaces will have a certain degree of roughness in the µm range (e.g. the ceramic part on the chip components), the migration of the tin ion could be regarded as moving a football across a mountain range and an inter-electrode distance in the scale of mm is a very large distance at these scales.

In IPC-TR-476A [41]**,** the laminate material is said to have an influence on the migration properties, and the moisture absorption properties of the polymer is said to be of key importance. Humid ECM could therefore be related to the metal transport through the absorbed water in the polymer or even through flux residues mixed with water, rather than as a surface transport phenomenon. Humid migration has only been little investigated in the current project. Limited number experiments on tin and silver at high humidity in non-condensing environment showed no sign of ECM even after 3 weeks of testing [58].

Therefore, special care should be taken when attributing the humid migration on a PCBA to metal ion transport through the water layer, as the surfaces on the PCBA invariably has roughness, solder flux residues, ionic residues from plating baths, and adsorption of various kinds of impurities from ambient air, which makes it reasonable to think that the layer of water formed will be much thicker to get a condensed ECM rather than humid ECM.

3.2 Electrochemical Migration in Electronic Devices

As mentioned earlier, structural dimensions of the electronic components get smaller, the risk of condensation of water and having a pathway for electrochemical reactions between the conductors is high. The conventional understanding of electrochemistry in bulk electrolytes is insufficient at such scales due to the micro-volumes of electrolyte involved, overlapping of diffusion layers between the closely spaced electrodes, and electrode potentials that are much higher than usually dealt with in conventional electrochemical experiments related to corrosion at higher scales.

Electrochemical migration is a process, which occurs when two oppositely biased electrodes are connected by an aqueous electrolyte. In electronics, electrodes could be conducting patterns on a printed circuit board, component leads or terminals such as electrodes of a chip resistor or capacitor (see example in Figure 3.3).

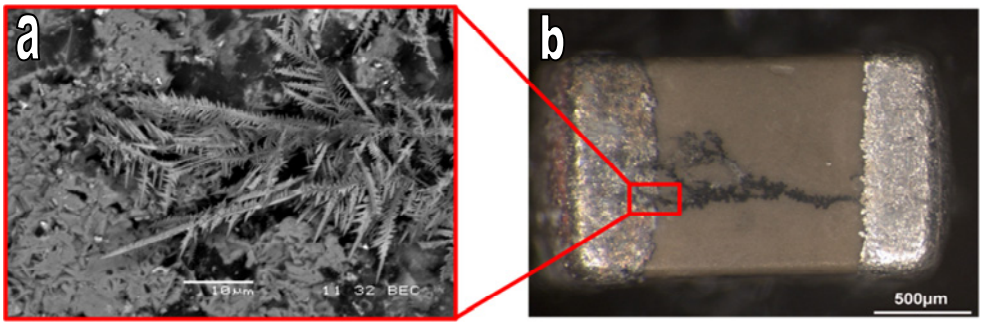

Figure 3.3: Example of electrochemical migration on a ceramic chip resistor: a) SEM image of the dendrite-anode contact point and b) optical microscopy image showing the whole dendrite. The cathode is on the right and the anode is on the left.

Electrochemical migration, as described earlier can cause a short circuit in an electronic device and even an intermittent failure in a critical electronic device. The positively charged metal ions will tend to be attracted to the negatively charged cathode at sites where the electric field is strongest, e.g. a protrusion on the cathode where they can get reduced to their metallic state if it is energetically favourable. As this happens, the inter-electrode distance at that site will become shorter, and that particular site will be more attractive for further deposition of metal ions leading to dendrite growth.

Takemoto et al. [59] have predicted that the electrochemical migration will become one of the most severe reliability issues for the electronics industries in the future, due to the miniaturization of the devices and increased sensitivity to contamination. As many of the failures are intermittent, it is extremely difficult for manufacturers to detect the root cause of a failed device, and electrochemical migration is indeed suspected to be the root cause of many field failures that have been labelled: “no failures found” [60,61]. The main factors controlling the ECM can be listed as the flow chart in Figure 3.4. Co-existence of all the factors makes the ECM possible on a PCBA.

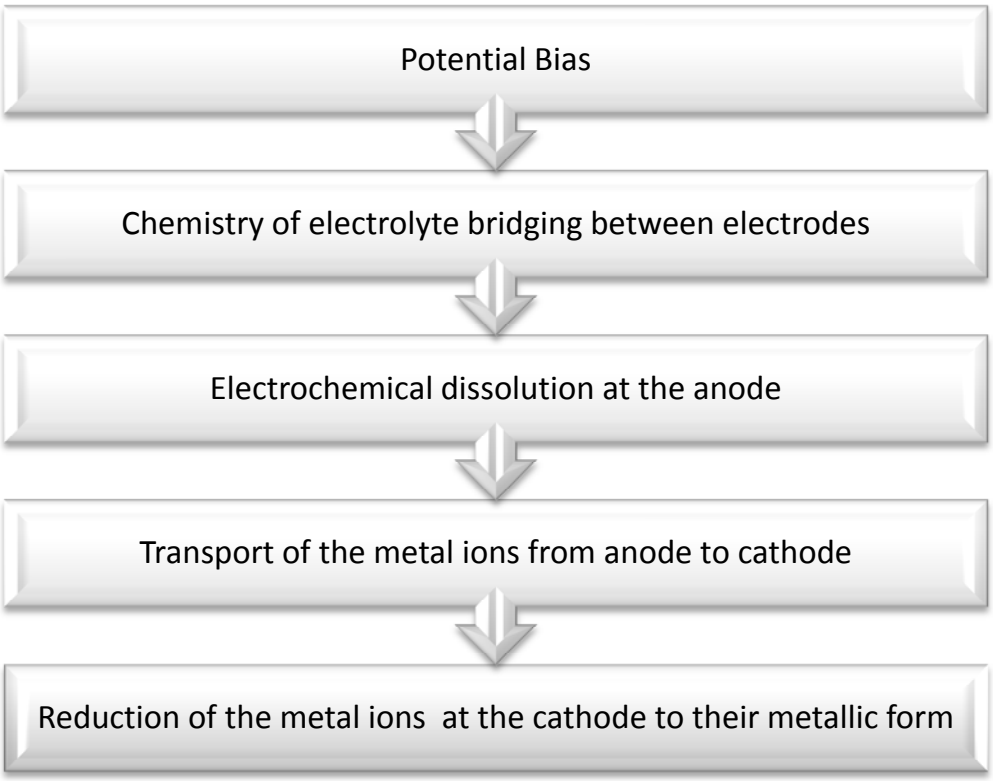

Figure 3.4: Main process steps in the ECM. If one of these steps is hindered, migration will not occur.

A comprehensive review of ECM failures of all susceptible metals on a PCBA is extensive and beyond the scope of this thesis, therefore only the ECM behaviour of tin is discussed in detail. Tin is also an important material when considering the corrosion of electronics as tin based surface finish (immersion tin or hot levelled solder alloys with tin) is the major PCB surface finish used today. Figure 3.5 shows an example of a PCBA of an industrial device. The hot air levelled surface finish on the PCB, tin based electrodes of the component, and solder alloy occupy more than 80% of the surface area indicating the importance of tin corrosion and migration in electronic corrosion failures.

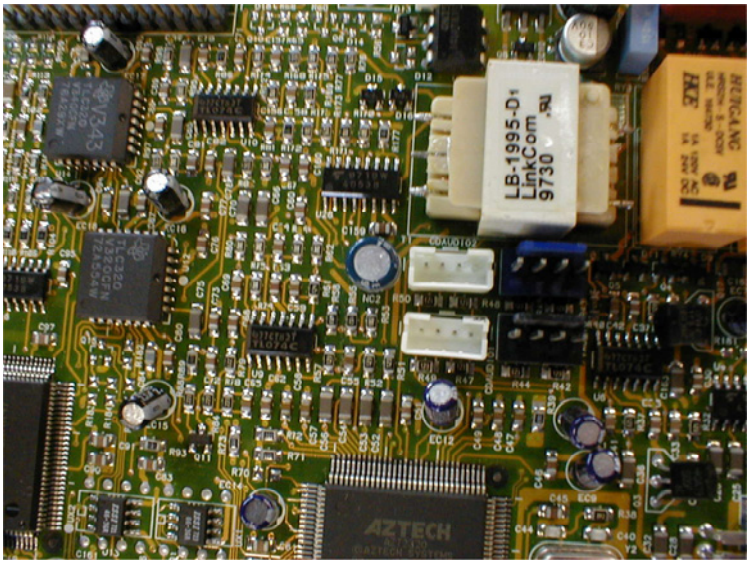

Figure 3.5: Example of components on a printed circuit board. A large fraction of the metallic surfaces that are exposed to the outside environment consists of tin and tin alloys.

3.3 ELECTROCHEMICAL BEHAVIOUR OF TIN

3.3.1 BASIC ELECTROCHEMISTRY OF TIN

Tin is having the atomic number 50 and is in the main group of metals, group 14. In normal conditions white tin is stable having a body centred tetragonal (termed β-tin) while grey tin having a diamond lattice (α-tin) forms at temperatures below 13°C [62]. Electrochemically, tin has two valence states; Sn^{2+} (stannous) and Sn^{4+} (stannic) which are almost equally stable and readily convertible.

Pourbaix [63] calculated the thermodynamic stability of the tin-H_2O system and the standard E_h-PH (Pourbaix diagram) for tin is shown in Figure 3.6.

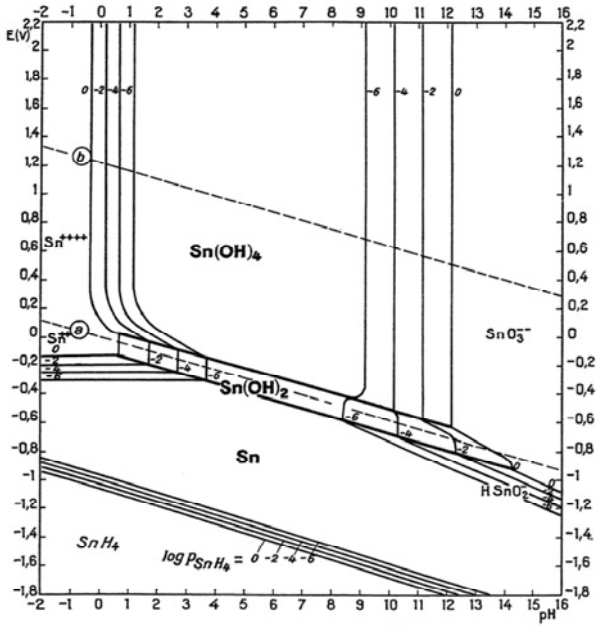

Figure 3.6: Pourbaix diagram for tin including the hydroxides $Sn(OH)_2$ and $Sn(OH)_4$ [63]. Stability lines are shown for varying tin concentrations. Dashed lines (a) and (b) indicate stability lines for water reduction and oxidation respectively. (© NACE International 1974, reprinted with permission. Markings that are irrelevant for present context have been deleted from the original figure)

The diagram shows stability domains for the dominant species and it should be noted that other species can therefore co-exist across the domains shown.

Important electrode reactions of tin in the presence of water are:

Anode:

$$Sn \rightarrow Sn^{2+} + 2e^- \quad \text{Eq. 1}$$

$$Sn^{2+} \rightarrow Sn^{4+} + 2e^- \quad \text{Eq. 2}$$

$$Sn^{4+} + 4H_2O \rightarrow Sn(OH)_4 + 4H^+ \quad \text{Eq. 3}$$

$$Sn + 4H_2O \rightarrow Sn(OH)_4 + 4H^+ + 4e^- \quad \text{Eq. 4}$$

$$2H_2O \rightarrow O_2 + 4H^+ + 4e^- \quad \text{Eq. 5}$$

Cathode:

$$O_2 + 2H_2O + 4e^- \rightarrow 4OH^- \quad \text{Eq. 6}$$

$$H_2O + 2e^- \rightarrow H_2 \uparrow + 2OH^- \quad \text{Eq. 7}$$

Tin is amphoteric meaning that it is soluble in acid and alkali. In acidic conditions tin is dissolved as stannous or stannic ions depending on the potential as described by Eq. 1 and 2. Stannous ions are reported to exist to a certain extent as

Sn^{2+} aquo ion in slightly acid solutions [62]. However, at pH values above ~1.0, stannous or stannic ions will be rapidly hydrolysed as various tin hydroxides, where $Sn(OH)_4$ is dominant. Eq. 3 and 4 represents formation of stannic hydroxide either by hydrolysis of Sn^{4+} (Eq. 3) or by direct oxidation tin to $Sn(OH)_4$ (Eq. 4). In highly alkaline conditions tin dissolves as stannate ions represented by Eq. 8.

$$Sn(OH)_4 + 2OH^- \rightarrow (Sn(OH)_6)^{2-} \qquad \text{Eq. 8}$$

More detailed discussion on the stability of tin species as a function of pH is explained while elucidating the mechanism in paper 4 in chapter 8 and is therefore not repeated here.

3.3.2 RELEVANT LITERATURE ON THE ELECTROCHEMICAL BEHAVIOUR OF TIN

Ammar et al. [64] compiled an extensive review on the electrochemistry of tin and tinplate, though much of the work is focused on tin for use for food conservation. Some important discussions in the review paper relevant to the present thesis are the following.

House and Kelsall [65] constructed several Eh-pH diagrams based on calculations for tin in the presence of mononuclear and polynuclear hydroxy species and chloride, which was not included in the original work by Pourbaix [63]. A three-dimensional E-pH diagram is created with the activity of tin on the third axis, which serves as an excellent illustration of the complexity of the thermodynamic stability of tin species.

Awad and Kassab [66] studied the anodic dissolution in 0.1-10N NaOH by polarization measurements and found that tin passivates at high current densities due to stannic oxide formation, while at low current densities a mechanism was proposed that excludes tetravalent tin. Golubev and Kadyrov [67] studied the dissolution of tin in NaOH/NaCl mixtures, and found that the anodic behaviour included dissolution of tin as Sn^{2+} and formation of SnO. The anodic dissolution was found to be affected by the OH^-/Cl^- ratio, where with increasing ratio (pH>11) a second anodic process occurred which was attributed to the oxidation of SnO to SnO_2. Brainia et al. [68] studied the electrochemical behaviour of tin in HCl

electrolytes by inverse voltammetry and found that several positive, neutral, and negative complex ions were produced while Johnson and Liu [69] found that the apparent valence of the dissolved tin ions in acidic chloride solutions was dependent on the nature and concentration of the electrolyte and on the current density. Complexing of Sn^{2+} had an important effect and the dominant product was $SnCl_3^-$. Yarunia et al. [70] found that dissolution of tin in HCl electrolyte has a first step which is electrochemical in nature, followed by a second step which is chemical in nature using polarization experiments.

Passivation of tin anodes in alkaline NaOH solutions was studied by Stirrup and Hampson [71]. Passivation was found to involve a primary and secondary mechanism, where primary passivation was found to involve dissolution-precipitation of stannous species and secondary passivation was found to be a combination of both oxidation of Sn^{2+} to Sn^{4+} species and direct oxidation of tin as stannic species. At higher potentials, passive film was found to dehydrate to make a more efficient passivation. This is supported by the X-ray Photoelectron Spectroscopy (XPS) studies of Ansell et al. [72], where anodic films of tin in NaOH solutions are found to contain stannous oxide and hydroxide in the pre-passive region, while stannic oxide and hydroxide was formed at higher potentials. Ammar et al. [73] studied the polarisation and passivation of tin in neutral solutions containing halide ions Cl^-, Br^- and I^- at potentials up to 4V, and results are explained based on formation of oxides, hydroxides, and halogen-containing compounds in the passive film.

Gobom [74] studied the hydrolysis of Sn^{2+} ions by potentiometric titrations in the pH range 2.7-3.7 as an extension of similar work by Tobias [75], and discussion on the complex ions $SnOH^+$, $Sn_3(OH)_4^{2+}$ and $Sn_2(OH)_3^+$ and their predominance is given.

Clifford [76] suggested that an approximation of solubility product constant of species having largely covalent bonds can be made on the basis of the difference in electronegativity of the species. This relation is claimed to hold as a first approximation for sulphides and hydroxides in case experimental results do not exists.

As an overall summary, tin can form a large variety of positively, negatively charged and neutral species and the stability of these species are highly dominated by pH, potential and by the presence of halides. In the case of electronic corrosion, the stability of dissolved tin ions will be greatly influenced by the impurities that exist on the PCBA surface, which will have an influence on the electrochemical migration.

3.4 Relevant Literature on ECM of tin

3.4.1 Industrial standards

The industrial standard closely related to the current subject is IPC-TR-476A [41] on electrochemical migration. However a large variety of closely related standards exist of relevance to corrosion of electronics and environmental testing. A thorough listing of relevant standards for electronic corrosion is given by Hienonen and Lahtinen [1].

During 1990, IPC did a survey on ECM with a number of electronic manufacturers. From the 27 responses they received, there were 25 separate definitions on ECM phenomenon [41]. Among the manufacturers testing for ECM, about 50 per cent were following the IPC test guidelines, along with in-house developed tests. The literature on ECM of tin is quite limited, and most of the work published is based on reliability studies on case specific material combinations where the test method predominantly is the surface insulation resistance (SIR) as described by the IPC-TR-476A [41] standard.

3.4.2 General reviews on ECM

General reviews on ECM have been published by Krumbein [42], Steppan et al. [77], and Harsányi [78]. Krumbein [42] gives an excellent review of the various types of electrochemical migrations that occur in humid and wet environment based on references from reliability studies, including the effect of some contaminants. However, little information is given on the mechanistic aspects of ECM for the various materials. Harsányi [78] divides ECM into five types which is electrochemical migration based on the “classical model” where metal ions migrate

from one electrode to the other, “contamination induced migration” where effects such as metal complex formation is included, “anodic dendritic growth” which is also termed conductive anodic filament (CAF) formations, “migration of reduced isolating constituents” explaining dendritic growth of dielectric constituents and “virtual migration” where dielectric constituents are reduced to form conductive dendrites by hydrogen ions. The classical model is described using Ag as example and is based on a three step process namely: (i) metal ions are formed by the anodic corrosion, (ii) metal ions migrate towards the cathode, and (iii) Electrochemical metal deposition of metal ions lead to the dendrite formation. The contamination induced migration is discussed for Au, Pd, and Pt in the presence of chloride ions and the process is described by the formation of negative and positive complexes, where the positive complexes can migrate to the cathode and form dendrites. ECM of tin is scarcely discussed in this review. Steppan et al. [77] reviews Ag, Au, Co, and aluminium, and divides the review into literature from reliability studies and literature from mechanistic studies. The review clearly indicates that most investigators do not discuss the pre-treatment or surface conditions of conductors prior to accelerated tests, and stresses that the clean and reproducible surfaces are necessary to obtain reproducible results. A very useful summary of acceleration tests is given in the table form. This brings up a key issue related to ECM testing and analysis, which is the lack of description of clear experimental procedures in many publications and reports, so that the repeatability and comparison between works become extremely difficult.

3.4.3 General research papers on ECM

Harsányi [79] has investigated the effect of chloride impurities on migration failures. Highly precious metals (Au, Pd, and Pt) lost their ability to resist migration when chloride is present, while migration of other metals such as Ag, Cu, Sn, and Pb can both be accelerated and hindered by the ionic contamination. Chloride contamination can originate from salt spray of the seas, dust particles, fingerprints, air contaminants, residual fluxes, and adhesives or cleaning solvents. The most important effect of chloride and ionic contaminants are summarized to:

- Increase conductivity of the electrolyte,
- Increase of anodic dissolution of metal ions due to breakdown of the surface oxide film,
- Forming precipitates or salts with the metal ions,
- High ionic conductivity of the solution makes the electric field distribution more uniform at the cathode promoting uniform plating,
- Ionic contaminants are often present in the form of inorganic salt, which can attract condensation at relative humidity levels less than 100% due to their hygroscopic nature. E.g. NaCl will attract enough humidity from water vapour in humid air to form a condensed nucleus of saturated solution at RH higher than 75% (at ambient temperatures) [1,4].

Harsányi and Inzelt [80] proposed using cyclic voltammetry (CV) as a new method for comparing migration abilities of metal conductors and found that the ability for ECM for tested metals was in the order of Ag>Pb>Cu>Sn which was confirmed both using CV and water drop testing. However, the CV technique must use a 3 electrode setup and usually done using bulk electrolyte unless the experiment is carried out at the miniaturized scales similar to electrolytic cell formation during ECM on a PCBA. Effects originating from the micro-volume of electrolyte, which is encountered in electronics, can therefore not be investigated using this technique. Investigations reported in the present thesis have clearly shown that the chemistry within the micro-volume environment is the key factor determining the ECM of tin. However, polarization and cyclic voltammetric techniques could provide general information on the electrode reaction kinetics at varying potential levels.

Meilink et al. [81] investigated Cu dendrite formation using thin solution layers and bulk pH1 H_2SO_4 electrolytes with various concentrations of Cu^{2+} ions added. It was found that the dendrite growth rate in bulk electrolytes was two orders of magnitude smaller than those predicted theoretically. For weak electrolytes, the IR drop through the solution is higher, but the dendrite growth velocities were found to be higher than those for the bulk electrolytes, which was attributed to increased Cu ion concentration in the confined space of the thin volume. Zamanzadeh et al. [82] investigated ECM of Cu at constant humidity on alumina substrates that were

contaminated by $CuCl_2$ salts. Results showed that the dendrites grew through condensed layers of water which nucleated on the $CuCl_2$ salts at RH above 70%. Devos et al. [83,84] investigated the optical appearance and current transients of Cu dendrites in oxalic acid media and found that the dendritic structures where more straight and needle like at high current densities as compared to low current densities where more branched dendrites are formed and the observations are in agreement with the findings of Wranglén [85]. The growth rate of Cu dendrites was found to increase with increasing oxalic acid concentration, potential and activation current, and it was shown that the dendrite formation could be avoided by addition of buffer or inhibitor solutions. Flow of the electrolyte was induced, and it was shown that the dendrite formation was influenced by the flow direction, where flow from anode towards the cathode increased migration and flow perpendicular to the electrodes decreased dendrite formation.

Rathinavelu et al. [86] investigated Cu migration under conformal coatings, and found that solder flux residues significantly reduced adhesion strength between the coating and the PCB as well as promoting the formation of Cu dendrites.

Ready et al. [87] proposed a novel test circuit for ECM and CAF testing using surface insulation patterns, where an operational amplifier is used in order to avoid burn outs of dendrite or filaments during measurement sequence. Noh and Jung [88] found that ECM is affected by the PCB laminate material, though experimental results are found to be inconclusive. Van Soestbergen et al. [89] made a mathematical model for metal ion migration through plastic encapsulations. The model only describes the initial ion flux from the anode to cathode, but not the dendrite formation or dendrite growth. Also, the model does not include the possibility of the metal ion to react with the chemical species inside the polymer, and therefore assumes rather stable metal ions, such as silver. However, the model could be interesting in relation to investigations on humid migration.

3.4.4 Relevant research directly related to ECM of tin

Takemoto et al. [59] notes that many inconsistencies exist in the literature ECM of tin. E.g. DerMarderosian reported that pure tin migrates in pure water while

Kawanobe and Otsuka [90] classified tin as one of the most resistant metals to ECM. Takemoto et al. [59] investigated ECM of Sn and Sn solder alloys in deionised (DI) water. Specimens were prepared by cold rolling of the solder alloy that was cut to shape and two electrodes of the same alloy were then placed between glass plates. Potential was either applied as fixed potential or it was swept at a fixed rate towards higher potential and similar results were obtained for both methods. In Sn-Pb alloy system, pure lead was found to have highest susceptibility to ECM, alloys containing up to 60% Sn showed similar behaviour, and alloys with higher tin content showed less or no migration. However, pure tin samples having a different surface roughness than those in the original test setup was found to show ECM. In this case increased surface roughness of the anode has increased dissolution rate of tin to cause ECM.

Yoo and Kim [91] compared the corrosion properties with the susceptibility for ECM for SnPb solders in dilute Cl^- and SO_4^{2-} electrolytes. Pure tin showed similar time to failure intervals in chloride and sulphate solutions, while an increase in the time to failure was found for the samples with high amount of Pb in sulphate solution. It was concluded that the anodic dissolution rate did not influence the ECM susceptibility, which is contrary to other work [59,81,92-94]

Lee et al. [93,94] compared the ECM of Pb and Sn at potentials in the range of 0.5-3V by water drop testing and potentiodynamic anodic polarization in dilute NaCl and Na_2SO_4 electrolytes, and attributed the decreased tendency of tin migration (as compared to Pb) to passivation of the tin surface. In the presence of high chloride, the passivation of tin was impaired, and higher tendency for tin to ECM was observed. Specimen preparation was done by thermal evaporation and screen printing of SIR patterns on oxidized Si wafers.

Yu et al. [95] has studied the ECM of several SnPb and lead free solders in distilled water. Solder was cold rolled and two pieces of solder were glued to a PCB laminate opposite to each other at a fixed distance and a droplet of DI water was added. For Sn-Pb systems, Pb was the migrating species, for Sn-Ag and Sn-Ag-Cu alloys Sn migrates, and for Sn-Zn-Bi systems both Sn and Zn were found to

migrate. Authors suggest that the important factors influencing ECM migration are metal dissolution at the anode and ionic transport through the solution. Metal dissolution is closely related to the electrochemical potential of the involved metals in the investigated environment and ionic transport is related to the solubility product of the metal oxides/hydroxides.

In another study, Yu et al. [96] investigated the migration of lead free solders by both water drop test (DI water) and temperature/humidity testing using SIR patterns. Reflow solder paste was applied on a base pattern (Cu with immersion tin surface coating) and solder paste was then melted either by hot air (specimens for water droplet tests, temperature of the air is not specified) or using a reflow oven (specimens for temperature/humidity testing 225°C or 250°C depending on the solder type). No-clean flux residues were washed off using acetone in ultrasonic bath for experiments where clean sample was tested, whereas similar solder pastes from different manufacturers were used in order to obtain surfaces with different flux residues. Bromide was found in the EDS results from some of the dendrites from lead free solders, though this is not discussed in the paper. However, the presence of halides such as bromide could have an impact on metal dissolution and hence migration behaviour.

Jellesen et al. [97] studied the electronic corrosion at device level by cyclic humidity testing of an electronic device or PCBA while it was powered. Electrochemical migration of tin on SM components was found to provide failures to the device, and the number of cycles required to induce a failure was greatly reduced if contaminants were deliberately added to selected sites of the device. Hansen et al. [98], studied the decomposition of no-clean solder flux and found that active components of the solder flux such as adipic acid remains on the PCB until temperatures around 250-275°C reached depending on the heating rate. Jellesen et al. [99] investigated corrosion and migration failures due to extensive use of hand soldering flux to fix tactile switches on to the PCB of an electronic add-on device and found corrosion of Sn, Ag and Ni, which was caused by the flux residues. Excessive use soldering flux was a direct result of the PCBA design in this case where a large copper area sitting directly below the tactile switch area

makes it difficult to solder due to the high heat capacity of copper. This indicate the importance of PCB design, local material mass, and their thermal properties in determining local temperature on the PCB during soldering and therefore local flux residue levels. Key findings of high relevance to the work done in the present project are summarized in Table 3.1 below:

Table 3.1: Summary of some key findings from research papers that are of high relevance to the work in this thesis.

Paper	Material	Parameter
Devos et al. [83,84]	Cu in Oxalic acid	Current density (CD): • CD↑= Needle like dendrite • CD↓=Branched dendrite
Takemoto et al. [59]	Sn in DI water	Surface roughness influence ECM
Yu et al. [95]	Sn solder alloys	Preferential dissolution of less noble metals
Yu et al. [96]	Sn solder + Flux	Flux affects migration. Br in some dendrites from lead free solders.

3.5 GASEOUS CORROSION ON PCBAS:

Many metals/alloys on a PCBA are susceptible to corrosion by corrosive gases such as sulphur dioxide, hydrogen sulphide, ozone, ammonia, chlorine etc. depending on the user environment. However, corrosion of silver due to sulphur containing gases and ozone is frequently found on electronic devices and much literature exists on failure analysis e.g. [27,100-108] and on the mechanisms of sulphidation [109-124]. Presence of ozone is easy to find in large electronic installations with high voltage switching devices due to sparking in air, which convert oxygen into ozone [125]. Interaction between sulphur containing gases such as sulphur dioxide or hydrogen sulphide with silver can result in the growth of silver sulphide crystals. The problem is well known in environments even with low concentrations of H_2S (under 50ppb) [115].

Part of the work (one paper) in this PhD thesis is related to the corrosion of silver in sulphur containing environment. Therefore more detailed discussion on this subject could be found in appended paper entitled “Morphological study of corrosion of silver in sulphur environments”.

4 METHODOLOGY FOR ECM TESTING

Some dedicated experimental setups have been developed under this PhD programme. A detailed description of these techniques is given below. However, since the work carried out in this PhD programme is presented as appended papers, some overlapping on this description is unavoidable.

4.1 DEVELOPMENT OF EXPERIMENTAL SETUPS

Most PCBAs are complex and directly investigating the ECM on the board for test purpose will not provide reliable and reproducible data as the number of parameters involved are many and therefore extremely difficult to single out the effect of various factors influencing the ECM. The investigations on ECM in our lab are conducted in three hierarchical levels for a holistic understanding namely at component level, PCB level, and finally at device level. Present PhD project focused on single component and PCB level testing, and two novel experimental set ups for this purpose have been designed and fabricated during the project. These are called Single Component Electrochemical Migration (SCECM) set up and CELCORR Test PCB set up. Figure 4.1 provide an overview of the three levels of testing with increasing levels of complexity, while the first two were employed for the present PhD project. More on device level testing can be found in Jellesen et al. [97]

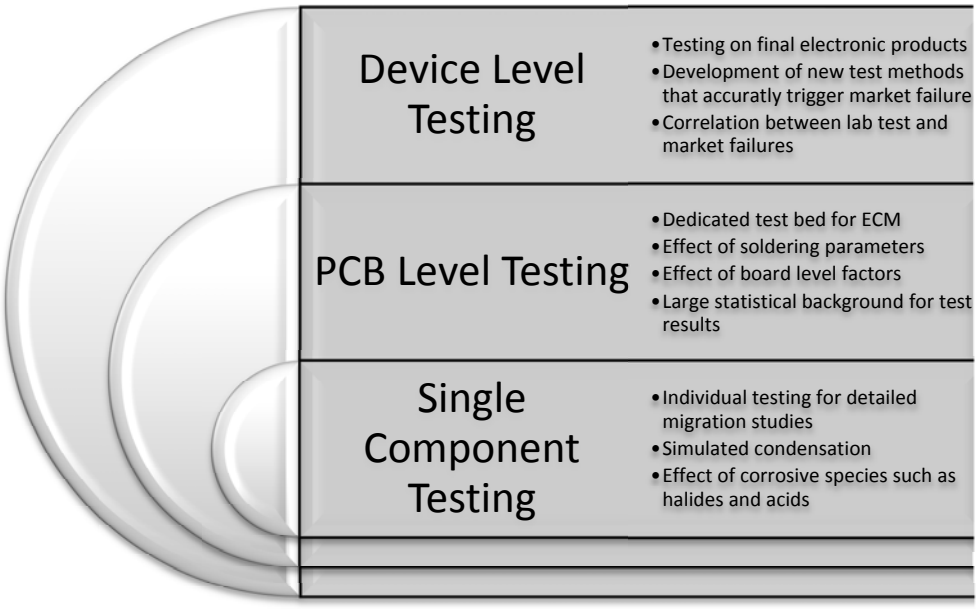

Figure 4.1: Overview of the three hierarchical level testing approach used for electronic corrosion testing. Each level is intended to add additional complexity to the testing.

The single component testing is intended for well controlled experiments directly on components varying only one parameter except for the component variability (such as surface roughness, slight variation in constituent materials, and cleanliness factors). The PCB level testing introduce much more variability due to introduction of multiple components, laminate, soldering etc. However, in this case experiments are carried out at board level on a number of components to get statistical average.

4.1.1 SINGLE COMPONENT ELECTROCHEMICAL MIGRATION (SCECM) SETUP

By doing experiments directly on individual components, all parameters associated with the soldering process are removed.

For this purpose a novel experimental set up was designed and fabricated called SCECM setup. A detailed view of the SCECM set up is shown in Figure 4.2 including experimental set ups to control humidity and video microscope for in-situ videoing. The SCECM is an electrochemical cell setup consisting of three holders for surface mount components such as chip resistors or chip capacitors, allowing three simultaneous experiments. As shown in Figure 4.2a, components are

suspended between two probes in the SCECM set up, which also acts as electrical contact. The probes were coated by electrically conductive diamond like carbon or CrN coatings (PVD process performed by The Danish Technological Institute) in order to provide the hardness and mechanical durability to the probe tip, and an additional silicone coating was finally introduced in order to avoid the possibility of galvanic contact between the terminal and the probe, in case the contact area comes in contact with the aqueous media. Attached video microscope has the capability to rotate the lens so that three dimensional scanning of the component during the experiment is possible to view the dendrite formation from all the sides.

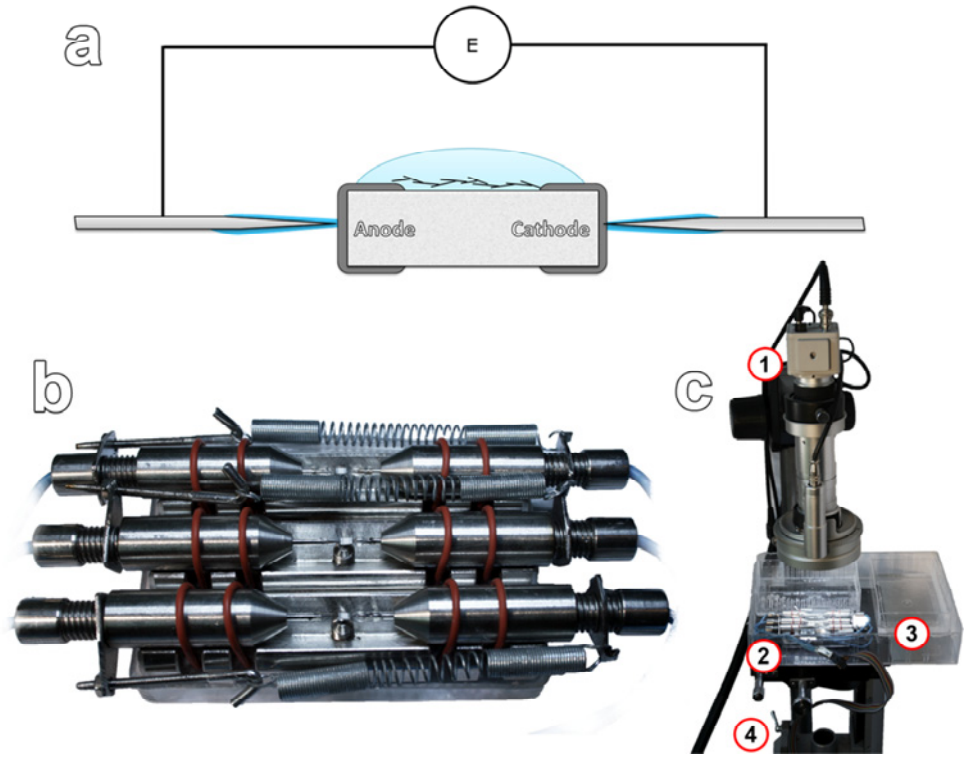

Figure 4.2: SCECM setup. a) Schematic of the principle, b) actual SCECM cell setup and c) whole arrangement including 1) Video microscope, 2) SCECM holders, 3) Closed box with container for water/ saturated salt solution to control humidity, and 4) XYZ-stage.

The SCECM holders were kept in a closed box with a transparent lid to control the humidity levels. Application of the desired electrolyte on the components in the present work is done by manually adding a droplet of water to the top of each component using a micro pipette tip. If water condenses on a PCBA, the better surface wetting properties of chip components make them favourable sites for the nucleation of water droplet. This is illustrated in Figure 4.3 where an unbiased PCBA was cooled gradually to ~6°C in open atmosphere at ambient conditions (~20°C and 45%RH) and a time lapse video was recorded. The images show how the water nucleates preferentially at the metallic and ceramic surfaces as they have better wetting properties than the solder mask. Due to the geometry of the component, a large water droplet is seen to form on top of the component, thereby bridging the two terminal electrodes.

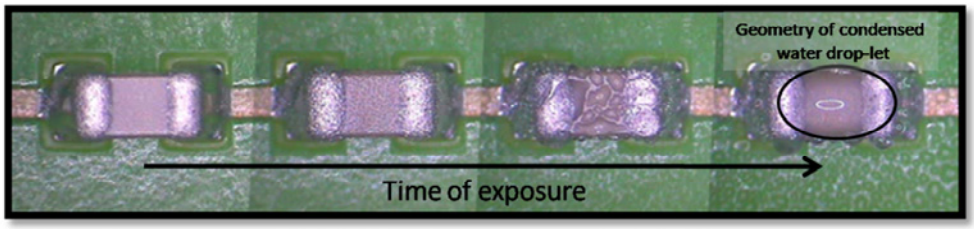

Figure 4.3: Example of the formation of condensation on an unbiased chip capacitor soldered to a PCB.

However, in the present investigation, manual application of water by a micro pipette was employed to create a water droplet similar to the one shown in Figure 4.3. The manual application of water provided two key advantages: (i) droplets of the same size can be added (to keep volume constant), and (ii) droplets can deliberately be contaminated with species that need to be investigated with known concentration e.g. chlorides.

The power source attached to the SCECM system for measurement was a multichannel potentiostat (Biologic VSP multichannel potentiostat, Bio-Logic Instruments, France, equipped with three individual potentiostat units having 0-20V compliance voltage and 1 nA resolution). The probes were connected to a potentiostat for the electrochemical experiment such as potentiostatic measurement by application of the constant potential and monitoring the current as a function of time. Cell connection is made by connecting the working electrode connection to one of the probes, while the reference electrode and counter electrode connections are shorted together to the other probe.

A typical output from the SCECM set up is shown in Figure 4.4. It provides video recording of the one channel at high magnification (which can be changed during the experiment), while the electrochemical curves, three channels are simultaneously displayed.

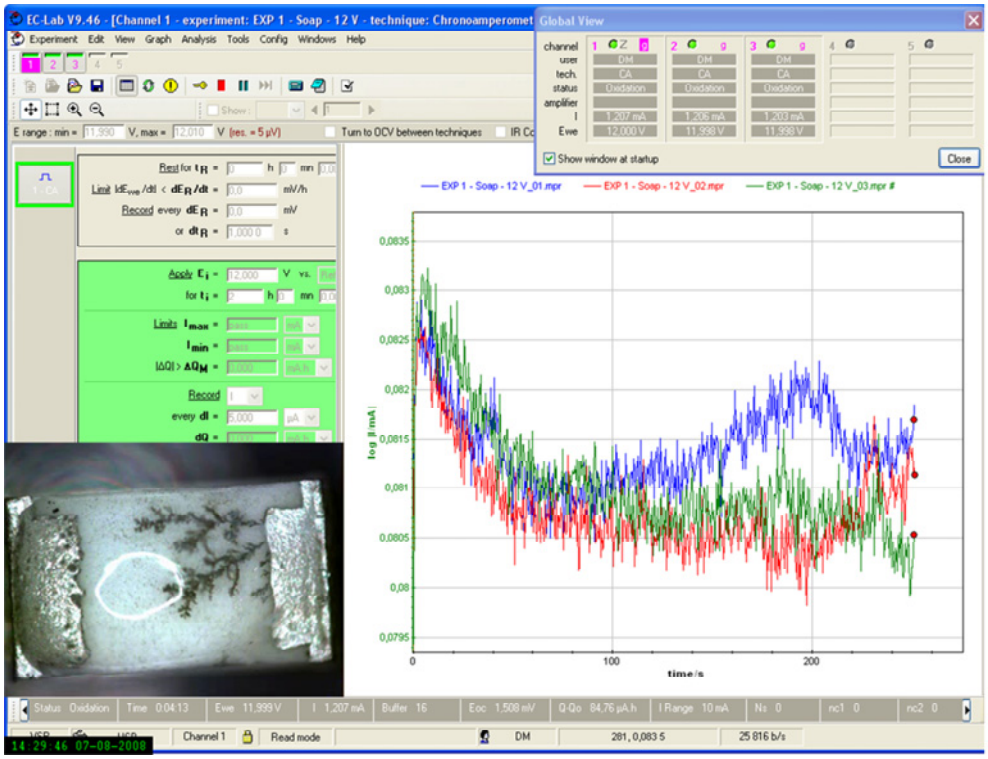

Figure 4.4: Example of typical outcome from SCECM setup. Current time curves are shown for all three potentiostat channels, while in-situ video recording is made only on one specimen due to the resolution needed for detailed observation of dendrites.

4.1.2 Design and Development of a test PCB System

For PCB level testing of electronic corrosion, especially ECM, a dedicated test rig was designed and developed under this PhD programme. The intention of the CELCORR TestPCB set up is to:

1. Provide a well-controlled test rig for PCB level testing of electrochemically induced corrosion such as ECM,
2. Testing of multiple components to provide statistical average to determine the effect of board level parameters and variations on ECM susceptibility.
3. Well defined electrical and electronic parameters due to the use of known components and circuitry.
4. Basis for PCB level testing of conformal coating with components for performance evaluation.

The developed TestPCB consists of 20 circuits: 18 containing SMD components and 2 SIR (Surface Insulation Resistance) patterns. One SIR pattern is covered by a soldermask, while the other has reflow solder surface finish. However, the surface finish and types of components can be changed depending on the requirement keeping the basic PCB design and data acquisition instrumentation. Figure 4.5 shows the CELCORR TestPCB pattern used for the investigations in the present project.

- Each of the 18 circuit channels consists of 10 identical SM components in parallel.
- Half of the (nine out of 18) circuits are resistors having resistances of from 68Ω to 1 MΩ and of sizes 0805, 0603 and 0402.
- Rest of the (nine out of 18) circuits are reserved for capacitors having capacitances in the range of 22pF to 100nF and sizes of 0805, 0603 and 0402

Application of the desired electrolyte on the components in the present work is done by manually adding a drop-let of water to the top of each component using a micro pipette tip. However, the set-up has the capability to produce a condensed water layer on the components directly by cooling down the cell set up using a Peltier stage under various levels of humidity.

Detailed description on the instrumentation for data acquisition, manufacturing of the test PCB and on the components are given in paper 5 in chapter 9 and will not be repeated here. However, further details and specifications that are not given in the paper are included in Appendix A

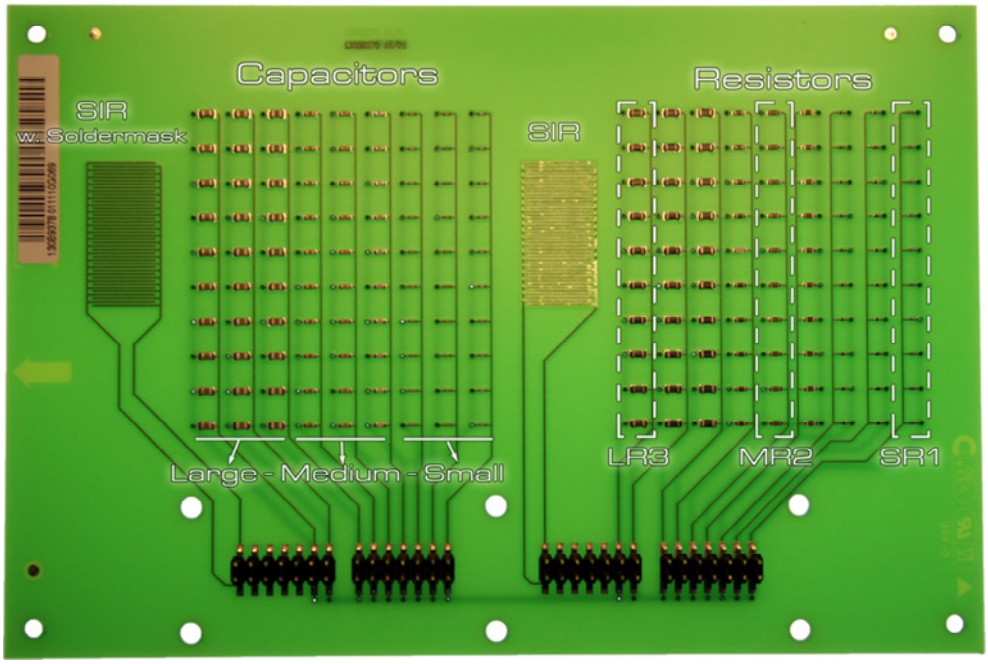

Figure 4.5: Mounted CELCORR TestPCB. The PCB has 20 circuits, 9 containing capacitors, 9 containing resistors and two SIR patterns.

REFERENCES

[1] R. Hienonen, R. Lahtinen, Corrosion and climatic effects in electronics, Vtt Publications. (2000).

[2] D. White, Influence of humidity on corrosion rate, Anti-Corrosion Methods and Materials. 39 (1992) 4–5.

[3] C. Leygraf, T.E. Graedel, Atmospheric corrosion, New York, USA, Wiley-Interscience, 2000.

[4] F.E.M. O'Brien, The control of humidity by saturated salt solutions, Journal of Scientific Instruments. 25 (1948) 73–76.

[5] E. Johansson, Korrosion på elektronik i inomhusmiljö in: "Temadag om Fuktskador och Fuktskydd", Korrosionsintitutet, Stockholm (1995).

[6] S. Brunauer, P.H. Emmett, E. Teller, Adsorption of gases in multimolecular layers, Journal of the American Chemical Society. 60 (1938) 309–19.

[7] C.F. Coombs, Printed circuits handbook, McGraw-Hill Professional, 2007.

[8] S.J. Sangwine, Electronic components and technology, 2nd ed., Florida, USA, CRC Press, 1994.

[9] R.P. Prasad, Surface mount technology, Springer, 1997.

[10] M. Pecht, Y. Deng, Electronic device encapsulation using red phosphorus flame retardants, Microelectronics and Reliability. 46 (2006) 53–62.

[11] Personal Conversation with R. Enemærke, PRI-DANA Elektronik A/S, (2010).

[12] C. Young, V. Illingworth, J. Young, The Penguin dictionary of electronics, Penguin Books, 1988.

[13] S. Gibilisco, Teach yourself electricity and electronics, McGraw-Hill, 2002.

[14] R. Ambat, P. Møller, Corrosion and environmental effects on electronics, in: Proceedings of Korrosion- Mekanismer, Havarier, Beskyttelse, 2005: pp. 161-178.

[15] T. MATSUMOTO, M. NOGUCHI, K. ASO ET AL., LEAD FRAME MATERIAL, US006117566A, 2000.

[16] M.A. Ju-sheng, F. Huang, L. Huang, G. Zhi-ting, N. Hong-long, H.A.N. Zhen-yu, Trends and development of copper alloys for lead frame [J], Journal of Functional Materials. 1 (2002).

[17] Creative Commons Licence - Attribution-Noncommercial-Share Alike 2.0 Generic, Http://Creativecommons.org/Licenses/by-Nc-Sa/2.0/Deed.en. (2010).

[18] Z.H. Levine, B. Ravel, Identification of materials in integrated circuit interconnects using x-ray absorption near-edge spectroscopy, Journal of Applied Physics. 85 (1999) 558.

[19] G.K. Rao, Multilevel interconnect technology, McGraw-Hill, 1993.

[20] M. Ohring, Reliability and failure of electronic materials and devices, Academic Press, 1998.

[21] R.D. Jones, Hybrid circuit design and manufacture, New York, USA, Marcel Dekker, 1982.

[22] J.J. Licari, L.R. Enlow, Hybrid Microcircuit Technology Handbook: Materials, Processes, Design, Testing and Production, 2nd ed., New Jersey, USA, Noyes Publications, 1998.

[23] GNU Free Documentation License, Http://Commons.wikimedia.org/Wiki/Commons:GNU_Free_Documentation_License. (2010).

[24] C.A. Harper, Passive electronic component handbook, 2nd ed., New York, USA, McGraw-Hill Professional, 1997.

[25] M. Kahn, D.P. Burks, I. Burn, W.A. Schulze, Ceramic Capacitor Technology, in: L.M. Levinson (Ed.), Electronic Ceramics, New York, USA, Marcel Dekker, 1988: pp. 191-

275.
[26] Personal conversation with K. Blohm, Danfoss Drives, (2007).
[27] C. Hillman, J. Arnold, S. Binfield, J. Seppi, Silver and Sulfur: Case Studies, Physics, and Possible Solutions, in: SMTA International, 2007.
[28] V. Solberg, Design guidelines for surface mount and fine pitch technology, New York, McGraw-Hill Professional Publishing, 1996.
[29] Personal conversation with K. Stentoft, Danfoss Drives, (2007).
[30] G.L. Ginsberg, Surface mount and related technologies, New York, Marcel Dekker, 1989.
[31] Hakko Corporation, Technical Note: Flux Residues and What to Do About Them, Technical Note Nr. TN00000030. (2002).
[32] P. Westermann, Investigation of Process related residues during PCB manufacturing, Master Thesis, Technical University of Denmark, 2008.
[33] P. Biocca, Flux Chemistries And Thermal Profiling: Avoiding Soldering Defects In SMT Assembly, in: Proceedings of SMTA International 2001, Chicago, USA, SMTA - Surface Mount Technology Association, 2001.
[34] S. ARORA, A. SCHNEIDER, K. TELLEFSEN, SOLDERING FLUX, U.S. Patent WO/2001/039922, 2001.
[35] F. Classon, Surface mount technology for concurrent engineering and manufacturing, New York, USA, McGraw-Hill, 1993.
[36] R. Strauss, Surface mount technology, Oxford, UK, Butterworth-Heinemann, 1994.
[37] C. Capillo, Surface Mount Technology Materials, Processes, and Equipment, 1st ed., New York, 1990.
[38] M.S. Jellesen, P. Westermann, D. Minzari, U. Rathinavelu, P. Møller, R. Ambat, Investigation of thermal decomposition of solder flux, residue formation, and effect on corrosion of electronics, In Manuscript. (2010).
[39] R.W. Revie, H.H. Uhlig, Corrosion and corrosion control, Wiley-Interscience, 2008.
[40] G.S. Frankel, J.W. Braithwaite, Corrosion of Microelectronic and Magnetic Storage Devices, in: P. Marcus (Ed.), Corrosion Mechanisms in Theory and Practice, New York, USA, Marcel Dekker Inc, 1995: p. 547.
[41] IPC-TR-476A, Surface Insulation Resistance Handbook, Northbrook, IL, USA, IPC, Institute for Interconnecting and Packaging Electronic Circuits, 1996.
[42] S. Krumbein, Metallic electromigration phenomena, Components, Hybrids, and Manufacturing Technology, IEEE Transactions On. 11 (1988) 5-15.
[43] S.J. Krumbein, Electrolytic models for metallic electromigration failure mechanisms, IEEE Transactions on Reliability. 44 (1995) 539–549.
[44] C. Leygraf, T.E. Graedel, Atmospheric corrosion, Wiley-Interscience, 2000.
[45] A. DerMarderosian, C. Murphy, Humidity threshold variations for dendrite growth on hybrid surfaces, in: Proc. Reliability Physics Symp., 1977: p. 92.
[46] D.E. Yost, Silver migration in printed circuits, in: Proc. Symp. on Printed Circuits, Philadelphia, PA, 1955.
[47] D.J. Lando, J.P. Mitchell, T.L. Welsher, Conductive anodic filaments in reinforced polymeric dielectrics: Formation and prevention, in: Proc. 17th Annu. Reliability Physics Symp., 1979: p. 51.
[48] G. DiGiacomo, Metal migration (Ag, Cu, Pb) in encapsulated modules and time-to-fail model as a function of the environment and package properties, in: Proc. Int. Reliability Physics Symp., 1982: p. 27.
[49] J.N. Lahti, R.H. Delaney, J.N. Hines, The characteristic wear out process in epoxy-glass printed circuits for high density electronic packaging, in: Proc. 17th Annu. Reliability Physics Symp., 1979: p. 39.
[50] G.T. Kohman, H.W. Hermance, G.H. Downes, Silver migration in electrical

insulation, Bell Syst. Tech. J. 34 (1955) 1115.

[51] R. Gjone, The migration failure mechanism on pin grid array VLSI packages, in: 1983 Int. Forum of the National Assoc. of Corrosion Eng., Anaheim, CA, USA, 1983: p. 231.

[52] S. Krumbein, A.H. Reed, New studies of silver electromigration, in: Proc. 9th Int. Conf. on Electric Contact Phenomena, 1978: p. 145.

[53] S.W. Chaikin, J. Janney, F.M. Church, C.W. McClelland, Silver migration and printed wiring, Indust. Eng. Chem. 51 (1959) 299.

[54] T.L. Welsher, J.P. Mitchell, D.J. Lando, CAF in composite printed-circuit substrates: Characteristics, modelling, and a resistant material, in: Proc. 18th Annu. Reliability Physics Symp., 1980: p. 235.

[55] P. Dumoulin, J.P. Seurin, P. Marce, Metal migrations outside the package during accelerated life tests, IEEE Transactions on Components, Hybrids, and Manufacturing Technology. 5 (1982) 479–486.

[56] R.R. Sutherland, I.D.E. Videlo, Accelerated Life Testing of Small-Geometry Printed Circuit Boards, Circuit World. 11 (1985) 35–40.

[57] P.J. Dudley, Electrical and environmental testing of UV curable and dry film solder masks, (1983).

[58] D. Minzari, M.S. Jellesen, P. Møller, R. Ambat, Unpublished Results, Technical University of Denmark. (2009).

[59] T. Takemoto, R.M. Latanision, T.W. Eagar, A. Matsunawa, Electrochemical migration tests of solder alloys in pure water, Corrosion Science. 39 (1997) 1415-1430.

[60] R. Williams, J. Banner, I. Knowles, M. Dube, M. Natishan, M. Pecht, An investigation of ‘cannot duplicate ‘failures, Quality and Reliability Engineering International. 14 (1998) 331–337.

[61] D.A. Thomas, K. Ayers, M. Pecht, The ”trouble not identified ”phenomenon in automotive electronics, Microelectronics Reliability. 42 (2002) 641–651.

[62] M. Schlesinger, M. Paunovic, Modern electroplating, Wiley New York, NY, 2000.

[63] M. Pourbaix, Atlas of electrochemical equilibria in aqueous solutions, M. Pourbaix, Published 1974 by NACE, 644. (1974).

[64] I. Ammar, S. Darwish, M. Khalil, S. El-Taher, A review on the electrochemistry of tin, Materials Chemistry and Physics. 21 (1989) 1-47.

[65] C. House, G. Kelsall, Potential--pH diagrams for the Sn/H2O---Cl system, Electrochimica Acta. 29 (1984) 1459-1464.

[66] S.A. Awad, A. Kassab, Mechanism of anodic dissolution of tin in sodium hydroxide solutions, Journal of Electroanalytical Chemistry. 26 (1970) 127–135.

[67] A. Golubev, M. Kadyrov, Study of Anodic and Cathodic Processes on Sn in Neutral Media, Zhur Priklad Khim. 44 (1971) 1297–1301.

[68] K.H.Z. Brainina, I.N. Nikulina, V.I. Kurbatova, Inversion Voltammetry of Sn in Chloride Solutions and the Analysis of Heat Resistant Alloys, Ind. Lab. 39 (1973) 1028–1033.

[69] J.W. Johnson, E.C. Liu, The anodic dissolution of tin in acidic chloride solutions, Journal of the Less Common Metals. 34 (1974) 113–120.

[70] G.V. Yarunina, I.N. Nikulina, K.H.Z. Brainina, Electrodissolution of Metals From the Surface of an Inert Electrode. Pt. 11. Processes Involving a Rapid Chemical Reaction, Elektrokhimiya. 10 (1974) 1464–1470.

[71] B. Stirrup, N. Hampson, Anodic passivation of tin in sodium hydroxide solutions, Journal of Electroanalytical Chemistry. 67 (1976) 45-56.

[72] R.O. Ansell, T. Dickinson, A.F. Povey, P.M.A. Sherwood, X-Ray Photoelectron Spectroscopic Studies of Tin Electrodes after Polarization in Sodium Hydroxide Solution, Journal of the Electrochemical Society. 124 (1977) 1360.

[73] I.A. Ammar, S. Darwish, M.W. Khalil, A. Galal, Electrochemical Polarization and Passivation of Tin in neutral solutions of chloride, bromide and iodide ions, Materialwissenschaft Und Werkstofftechnik. 13 (1982) 376-385.

[74] S. Gobom, The hydrolysis of the tin (II) ion, Acta Chem. Scand. 30 (1976) 745–750.

[75] R.S. Tobias, Studies on the Hydrolysis of Metal Ions, Acta Chem. Scand. 12 (1958).

[76] A.F. Clifford, The Prediction of Solubility Product Constants, Journal of the American Chemical Society. 79 (1957) 5404–5407.

[77] J.J. Steppan, J.A. Roth, L.C. Hall, D.A. Jeannotte, S.P. Carbone, A review of corrosion failure mechanisms during accelerated tests, Journal of the Electrochemical Society. 134 (1987) 175.

[78] G. Harsanyi, Electrochemical processes resulting in migrated short failures in microcircuits, IEEE Transactions on Components, Packaging, and Manufacturing Technology, Part A. 18 (1995) 602–610.

[79] G. Harsányi, Irregular effect of chloride impurities on migration failure reliability: contradictions or understandable?, Microelectronics Reliability. 39 (1999) 1407-1411.

[80] G. Harsanyi, G. Inzelt, A new method for comparing migration abilities of conductor systems based on conventional electroanalytical techniques, in: 2000 Proceedings. 50th Electronic Components and Technology Conference, Las Vegas, NV, USA, 2000.: pp. 1666-1673.

[81] S.L. Meilink, M. Zamanzadeh, G.W. WARREN, P. Wynblatt, Modeling the Failure of Electronic Devices by Dendrite Growth in Bulk and Thin Layer Electrolytes, Corrosion. 44 (1988) 644-651.

[82] M. Zamanzadeh, Y.S. Liu, P. Wynblatt, G.W. Warren, Electrochemical Migration of Copper in Adsorbed Moisture Layers, Corrosion. 45 (1989) 643-648.

[83] O. Devos, C. Gabrielli, L. Beitone, C. Mace, E. Ostermann, H. Perrot, Growth of electrolytic copper dendrites. I: Current transients and optical observation, Journal of Electroanalytical Chemistry. 606 (2007) 75-84.

[84] O. Devos, C. Gabrielli, L. Beitone, C. Mace, E. Ostermann, H. Perrot, Growth of electrolytic copper dendrites. II: Oxalic acid medium, Journal of Electroanalytical Chemistry. 606 (2007) 85-94.

[85] G. Wranglén, Dendrites and growth layers in the electrocrystallization of metals, Electrochimica Acta. 2 (1960) 130-143.

[86] U. Rathinavelu, M.S. Jellesen, P. Møller, R. Ambat, Performance of Conformal Coatings on Electronic Printed Circuit Boards Under Harsh Environmental Conditions, in: Proceedings of Eurocorr 2009, Nice, France, 2010.

[87] W.J. Ready, L.J. Turbini, R. Nickel, J. Fischer, A novel test circuit for automatically detecting electrochemical migration and conductive anodic filament formation, Journal of Electronic Materials. 28 (1999) 1158–1163.

[88] B.I. Noh, S.B. Jung, Characteristics of environmental factor for electrochemical migration on printed circuit board, Journal of Materials Science: Materials in Electronics. 19 (2008) 952–956.

[89] M. van Soestbergen, A. Mavinkurve, R. Rongen, L.J. Ernst, G. Zhang, Modeling electrochemical migration through plastic microelectronics encapsulations, in: 2009 International Conference on Electronic Packaging Technology & High Density Packaging, Beijing, China, 2009: pp. 1079-1082.

[90] T. Kawanobe, K. Otsuka, Metal migration in electronic components, in: Proceeding of the 32nd Electronic Component Conference, 1982: pp. 220–228.

[91] Y.R. Yoo, Y.S. Kim, Influence of corrosion properties on electrochemical migration susceptibility of SnPb solders for PCBs, Metals and Materials International. 13 (2007) 129–137.

[92] B. Noh, J. Lee, S. Jung, Effect of surface finish material on printed circuit board for

electrochemical migration, Microelectronics Reliability. 48 (2008) 652-656.

[93] S. Lee, M. Jung, H. Lee, T. Kang, Y. Joo, Effect of Bias Voltage on the Electrochemical Migration Behaviors of Sn and Pb, IEEE Trans. Device Mater. Relib. 9 (2009) 483-488.

[94] S. Lee, M. Jung, H. Lee, Y. Joo, Effect of initial anodic dissolution current on the electrochemical migration phenomenon of Sn solder, in: 2009 59th Electronic Components and Technology Conference, San Diego, CA, USA, 2009: pp. 1737-1740.

[95] D.Q. Yu, W. Jillek, E. Schmitt, Electrochemical migration of Sn-Pb and lead free solder alloys under distilled water, Journal of Materials Science: Materials in Electronics. 17 (2006) 219–227.

[96] D.Q. Yu, W. Jillek, E. Schmitt, Electrochemical migration of lead free solder joints, Journal of Materials Science: Materials in Electronics. 17 (2006) 229–241.

[97] M.S. Jellesen, D. Minzari, U. Rathinavelu, P. Møller, R. Ambat, Corrosion in Electronics at Device Level, in: ECS Transactions, Vienna, Austria, 2009: pp. 1-14.

[98] K.S. Hansen, M. Jellesen, P. Møller, P.J. Westermann, R. Ambat, Effect of Solder Flux Residues on Corrosion of Electronics, in: Proc. of RAMS Conference, Texas, USA, (2009),: p. 502.

[99] M.S. Jellesen, D. Minzari, U. Rathinavelu, P. Møller, R. Ambat, Corrosion failure due to flux residues in an electronic add-on device, Engineering Failure Analysis. (2010).

[100] R. Bauer, Sulfide corrosion of silver contacts during satellite storage, Journal of Spacecraft and Rockets. 25 (1988) 439.

[101] B.H. Chudnovsky, S.D. Co, O.H. West Chester, Degradation of power contacts in industrial atmosphere: silver corrosion and whiskers, in: Electrical Contacts, 2002. Proceedings of the Forty-Eighth IEEE Holm Conference On, 2002: pp. 140-150.

[102] Y. Fukuda, T. Fukushima, A. Sulaiman, I. Musalam, L.C. Yap, L. Chotimongkol, et al., Indoor Corrosion of Copper and Silver Exposed in Japan and ASEAN Countries, Journal of The Electrochemical Society. 138 (1991) 1238.

[103] Y. Ishikawa, T. Ozaki, L. Hitachi, H.C. Ltd, Corrosion Failure Characteristics of Electronic Components and Perspectives For Prevention and Control, in: Corrosion and Reliability of Electronic Materials and Devices: Proceedings of the Fourth International Symposium, 1999: p. 59.

[104] D.W. Rice, R.J. Cappell, P.B.P. Phipps, P. Peterson, Indoor Atmospheric Corrosion of Copper, Silver, Nickel, Cobalt and Iron, Atmospheric Corrosion. (1980) 651-666.

[105] K. Rogers, C. Hillman, M. Pecht, S. Nachbor, Conductive filament formation failure in a printed circuit board, Circuit World. 25 (1999) 6–8.

[106] R. Schueller, D. Inc, T. Austin, Creep Corrosion on Lead-free Printed Circuit Boards in High Sulfur Environments, Smta News and Journal of Surface Mount Technology. 21 (2008) 21.

[107] P. Zhao, M. Pecht, S. Kang, S. Park, Assessment of Ni/Pd/Au-Pd and Ni/Pd/Au-Ag Pre-Plated Leadframe Packages Subject to Electrochemical Migration and Mixed Flowing Gas Tests, IEEE Transactions on Components and Packaging Technologies. 29 (2006) 818.

[108] Y. Zhou, M. Pecht, Investigation on Mechanism of Creep Corrosion of Immersion Silver Finished Printed Circuit Board by Clay Tests, (n.d.).

[109] K. Aoki, K. Shimizu, R.A. Osteryoung, Electrochemical behavior of sulfide at the silver rotating disc electrode: Part II. Mechanism of silver sulfide film formation, Journal of Electroanalytical Chemistry. 129 (1981) 171-180.

[110] M.D. Benari, G.T. Hefter, The corrosion of silver and silver sulphide in halide solutions in water and dimethylsulphoxide, Hydrometallurgy. 28 (1992) 191-203.

[111] V.I. Birss, G.A. Wright, The kinetics of the anodic formation and reduction of phase silver sulfide films on silver in aqueous sulfide solutions, Electrochimica Acta. 26

(1981) 1809-1817.
[112] R.B. Comizzoli, R. Frankenthal, P.C. Milner, J.D. Sinclair, Corrosion of Electronic Materials and Devices, Science. 234 (1986) 340-345.
[113] J. Drott, Growth of silver sulphide whiskers, Acta Metallurgica. 8 (1960) 19-22.
[114] J.P. Franey, G.W. Kammlott, T.E. Graedel, Corrosion of silver by atmospheric sulfurous gases., Corrosion Science. 25 (1985) 133-143.
[115] T.E. Graedel, Corrosion Mechanisms for Silver Exposed to the Atmosphere, Journal of The Electrochemical Society. 139 (1992) 1963.
[116] T. Graedel, J. Franey, G. Gualtieri, G. Kammlott, D. Malm, On the mechanism of silver and copper sulfidation by atmospheric H2S and OCS, Corrosion Science. 25 (1985) 1163-1180.
[117] M. Hepel, S. Bruckenstein, G.C. Tang, The formation and electroreduction of silver sulfide films at a silver metal electrode, Journal of Electroanalytical Chemistry. 261 (1989) 389-400.
[118] S. Jaya, T.P. Rao, G.P. Rao, Nucleation and Growth of Anodic Films. IV. Anodic Deposition of Silver Sulphide, Key Eng. Mater. Vol. 20-28. 20-28 (1988) 627-632.
[119] S. Juanto, R.O. Lezna, A.J. Arvia, Optical and electrochemical study of the sulphide/silver system, Electrochimica Acta. 39 (1994) 81-85.
[120] A. Stefánsson, T.M. Seward, Experimental determination of the stability and stoichiometry of sulphide complexes of silver(I) in hydrothermal solutions to 400°C, Geochimica Et Cosmochimica Acta. 67 (2003) 1395-1413.
[121] L. Volpe, P. Peterson, The atmospheric sulfidation of silver in a tubular corrosion reactor, Corrosion Science. 29 (1989) 1179-1187, 1189-1196.
[122] C. Wagner, Investigations on silver sulfide, The Journal of Chemical Physics. 21 (1953) 1819.
[123] S. ZAKIPOUR, C. LEYGRAF, Quartz crystal microbalance applied to studies of atmospheric corrosion of metals, British Corrosion Journal. 27 (1992) 295-298.
[124] P. Zhao, M. Pecht, Mixed flowing gas studies of creep corrosion on plastic encapsulated microcircuit packages with noble metal pre-plated leadframes, IEEE Transactions on Device and Materials Reliability. 5 (2005) 268–276.
[125] J.S. Chang, P.A. Lawless, T. Yamamoto, Corona discharge processes, IEEE Transactions on Plasma Science. 19 (1991) 1152–1166.

APPENDED PAPERS

5 PAPER1: ELECTROCHEMICAL MIGRATION ON ELECTRONIC CHIP RESISTORS IN CHLORIDE ENVIRONMENTS

Daniel Minzari, Morten S. Jellesen, Per Møller, Pia Wahlberg, Rajan Ambat

Abstract—Electrochemical migration behaviour of end terminals on ceramic chip resistors was studied using a novel experimental setup in varying sodium chloride concentrations from 0 – 1000 ppm. The chip resistor used for the investigation was 10kΩ ceramic chip resistor size 0805 with end terminals made of 97Sn3Pb alloy. Anodic polarization behaviour of the electrode materials was investigated using a micro-electrochemical set up. Material makeup of the chip resistor was investigated using SEM/EDS and FIB-SEM. Results showed that the dissolution rate of the Sn and stability of Sn ions in the solution layer plays a significant role in the formation of dendrites, which is controlled by chloride concentration and potential bias. Morphology, composition, and resistance of the dendrites were dependant on chloride concentration and potential.

Index Terms— Failure, Corrosion Testing, Electrochemical analysis, Environmental testing, Tin.

NOMENCLATURE

CCR	*Ceramic Chip Resistor*
ECM	*Electrochemical Migration*
EDS	*Energy Dispersive Spectroscopy*
FIB	*Focused Ion Beam*
OCP	*Open Circuit Potential*
PCB	*Printed Circuit Board*
SCECM	*Single Component Electrochemical Migration*
SEM	*Scanning Electron Microscopy*
SHE	*Standard Hydrogen Electrode*

Manuscript received December 23, 2008.
Current research has been conducted as part of the CELCORR consortium. Authors would like to acknowledge the Danish Ministry of Science, Technology and Innovation for the funding of the CELCORR project.
Daniel Minzari, Morten S. Jellesen, Per Møller, Rajan Ambat are with the Department of Mechanical Engineering, Technical University of Denmark, DK 2800 Kgs. Lyngby, Denmark (Corresponding Author: Daniel Minzari, phone: +45 4525 2118, Fax: +45 4593 6213, email: dm@mek.dtu.dk)
Pia Wahlberg is with the Department for Micro technology and Surface Analysis, Technological Institute of Denmark, DK 2630 Tåstrup, Denmark.

5.1 INTRODUCTION

Corrosion of electronic devices in humid environment is of serious concern today due to the combination of multimaterial use, potential bias and miniaturization on Printed Circuit Boards (PCB). Process and service related contaminations accelerate corrosion by making the environment more aggressive [[1],[2]]. Due to corrosion problems, life span of the product is reduced [[3]], and failure or loss of functionality of the device leads to severe economic loss, plant down time and customer dissatisfaction.

Miniaturization at all levels is one of the key factors reducing corrosion reliability. Over the last 10 years, size of the electronics has been reduced by over 70%. For flip chip ICs, miniaturization amounts to ~ 90%. The closer spacing increases the electric field (E = V/d where E is the electric field, V is the applied potential and d is the distance between the terminals), which makes corrosion cell formation easy during local condensation under humid environments. At constant voltage, the electric field between the conductors rises inversely with the conductor spacing, and corrosion phenomena such as electrochemical migration are known to be enhanced under high electric fields [[6]-[7]].

Under humid conditions a nano scale water layer is formed locally on the PCB components giving rise to a conducting path for current flow and thereby establishment of electrochemical cell between two points on PCBs. The potential bias on the PCB at adjacent points or dissimilar material combinations serves as thermodynamic driving force for the corrosion cell. Fig. 5.1 shows two possibilities for the corrosion cell formation on the surface of the PCBs due to material combinations and potential bias. Process and service related contamination makes it easy to form the water layer as they are good water absorbers, while they also serve as a source of ions for solution conductivity.

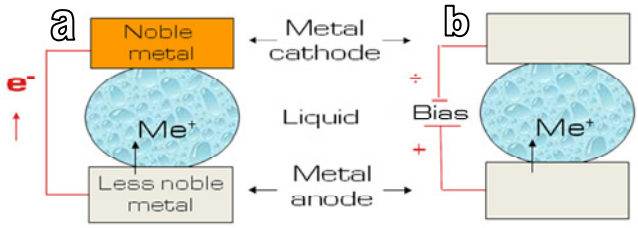

Fig. 5.1: Two possibilities for corrosion cell formation on a PCB with condensed electrolyte: (a) Galvanic coupling due to different materials on PCB and (b) Formation of electrochemical cell between similar electrodes due to applied bias.

ElectroChemical Migration (ECM) is a typical form of corrosion found on electronic systems [[3]-[4]] due to the presence of susceptible metals such as Cu, Ag, Sn, Pb etc. ECM occurs due to the presence of a potential gradient between two susceptible conductors (Cu, Ag, Sn, Pb etc. on PCB) connected by a thin layer of solution. For example two terminals of a chip capacitor or resistor on a PCB could act as anode and cathode if they are connected by a water layer. In this case, dissolved metal ions from the positive electrode (anode) migrate towards oppositely charged negative electrode (cathode) to deposit there. The process is similar to metal plating except for the dendritic morphology of the deposit formation extending from cathode to anode. Growth of dendrites finally leads to electric short between two points on the PCB, which cause component failure or malfunction.

However, not all metals on the PCB can cause electrolytic migration. Whether a specific metal is susceptible to electrolytic migration or not depends on the stability of the dissolved metal ion in aqueous solution and of the overvoltage required for deposition compared to hydrogen overvoltage. Metal compounds with low solubility product give fewer ions for migration, while those with high hydrogen overvoltage will not deposit. Therefore, on a PCB surface, only metals like Cu, Ag, Sn and Pb are susceptible to electrochemical migration at least over a range of potentials and pH predicted by the Pourbaix diagram [[5]]. Tin and lead exists in the form of solder alloy on the PCB surface and also as outer layer of electrodes of components for example chip resistors and capacitors. Migration of these metals on a PCB surface leads to malfunction or failure of devices during service.

ECM has traditionally been roughly divided into two sub-categories: *humid* ECM where a thin invisible moisture film is adsorbed to the surface and *condensed* ECM

where a visible layer of condensed water is present [[8]]. Though Brunnauer et al. [[9]] found an exponential increase in surface conductivity, not all metals that are susceptible to ECM have been found to migrate under *humid* conditions. Silver and to some extent copper has been reported to migrate under humid conditions [[10]-[15]], while other susceptible metals usually require a visible water layer (*condensed* conditions) [[8],[16]-[26]]. However, as distances on the PCBs are getting smaller due to miniaturization, the risk of having a condensation nucleus expanding over two conductors increase, and the relevance for ECM under wet (*condensed*) conditions is therefore increasing.

The exact mechanism of electrolytic migration and influencing factors on a PCB surface vary from one application to another, and many factors are still unknown. Contaminations such as chloride ions have significant effect on corrosion, while pH of the solution layer determines the stability of the dissolved metal ions in the water layer for migration to occur [[5]]. Localized pH changes are also likely to occur during migration due to water dissociation and hydrolysis at the electrodes.

A problem encountered when investigating ECM phenomenon directly on the PCB is the number of parameters influencing the system such as solder process, solder flux and heating profile to name a few. B. Noh and S Jung [[1]] found, that ECM migration is more likely to occur on a glass-epoxy FR-4 (flame resistant-4) PCB than on a polyimide PCB. Yoo and Kim [[28]] investigated the influence of the corrosion properties on ECM in varying Pb concentrations. Sample preparation was done by applying solder paste of varying Pb content on to a silicon wafer and passing it through a reflow oven. However, solder paste contain flux and for varying Pb content, the flux chemistries could be different and remnants of the solder flux could greatly affect the migration process. Also, the surface roughness of the solder on a silicon wafer could be different than on a PCB thereby influencing the ECM behaviour [[4]]. Such factors make reliable reproduction of experiments extremely difficult, thereby complicating interpretation and comparison of experimental results.

In this paper, ECM on ceramic chip resistors in condensing environment has been investigated in detail using a Single Component ElectroChemical Migration

(SCECM) setup in which a single electronic component can be directly loaded and electrochemical migration process can be investigated. The setup is attached with a video microscope for *in-situ* observation. In this work the effect of chloride ion concentration and potential bias was investigated. Basic electrochemical behaviour of the chip resistor electrode materials was investigated using a microelectrochemical setup with a tip diameter of 350µm. The material make up, microstructure, and corrosion morphology was investigated using Scanning Electron Microscope (SEM), Energy Dispersive Spectroscopy (EDS), Focused Ion Beam Scanning Electron Microscope (FIB-SEM), and optical microscopy.

In the SCECM setup, a single chip component can be loaded with applied potential on both sides to be exposed to micro-volumes environment, thus simulating the condensed corrosion environment encountered on a PCB. The resulting migration current can be monitored together with time lapse videoing of the migration phenomena. A great advantage of this experimental setup is that the components can be investigated in the as received condition, without any soldering process. Chloride is known to be an aggressive corrosion promoter. As chloride impurities are commonly found on electronic circuits through dust, handling or external exposure it is relevant to investigate the effect it has on ECM. Increased chloride content on a PCB is expected to result in increased kinetics of metal dissolution in a condensed humidity environment. However, the effect of chloride concentration on ECM is not yet understood, nor is the synergistic effects of chloride with other impurities on a PCB (e.g. solder flux or dust). Work in this paper focus on the effect of chloride concentration on electrolytic migration behavior. Most electronic components will be exposed to field environments that are mainly humid, and condensed environments are believed to be limited to fewer cases, though the relevance of condensed environments has increased dramatically in the past decade due to the increased mobility of electronic devices. Work is currently underway using the SCECM setup in a humid environment, with and without corrosive gasses, such as H_2S, SO_2 and NH_3. Results from these investigations will be published separately.

5.2 MATERIALS AND METHODS:

5.2.1 ELECTRONIC COMPONENTS

The electronic component used for investigation in this work is a commercially available 10kΩ Ceramic Chip Resistor (CCR) size 0805 (Fig. 5.5). The dimension of the chip resistor is: 2.0x1.2x0.45 mm. The component chosen for this investigation represent a large number of chip resistors used for the electronic PCB production.

5.2.2 SCECM SYSTEM:

The SCECM set up consists of a glass chamber where opposite sides are fitted with two tiny adjustable probes, which act as connections to each end of the components, in this case chip resistor (Fig. 5.2). One of the probes is fixed, while the other can be controlled in the transverse direction with micrometer precision. The probes are covered with silicone rubber, which is penetrated by the probe when a load is applied, thereby allowing electrical contact while at the same time providing corrosion protection to the probes.

The potentiostat used for the SCECM experiments was a Gill AC potentiostat from ACM instruments. For 12V experiments, a current divider was used for increasing the potential output of the potentiostat.

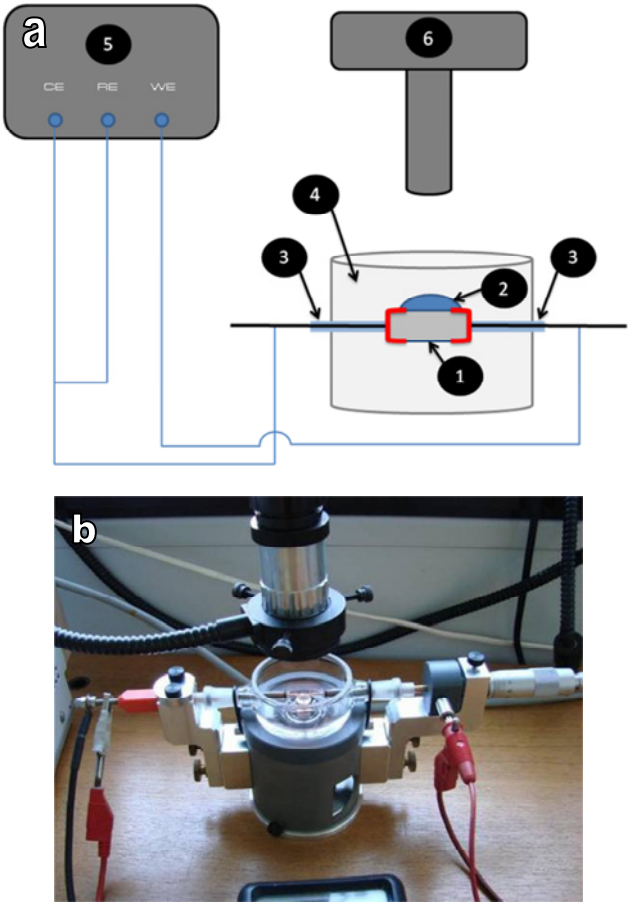

Fig. 5.2: (a) Schematic of the SCECM setup: 1. Specimen for investigation, 2. Droplet of solution, 3. Needles covered by silicone for electrical contact, 4. Experiment chamber, 5. Potentiostat and 6. Video microscope. (b) Image of actual setup.

A droplet of solution is then added on to the surface of the resistor (as shown in Fig. 5.3) and required DC bias is applied between the two electrodes of the component. Simultaneously the time lapse video recording is started (Fig. 5.2) for in-situ videoing of the migration sequence.

Experiments are conducted on the bottom side of the resistor, due to the better color contrast between the dendrite and Al_2O_3 substrate, which facilitates in-situ visual documentation of dendrite formation.

Leakage current flowing through the water layer is measured as a function of time until a permanent short is observed. During the experiment, the chamber was covered with a glass lid to minimize evaporation of the liquid.

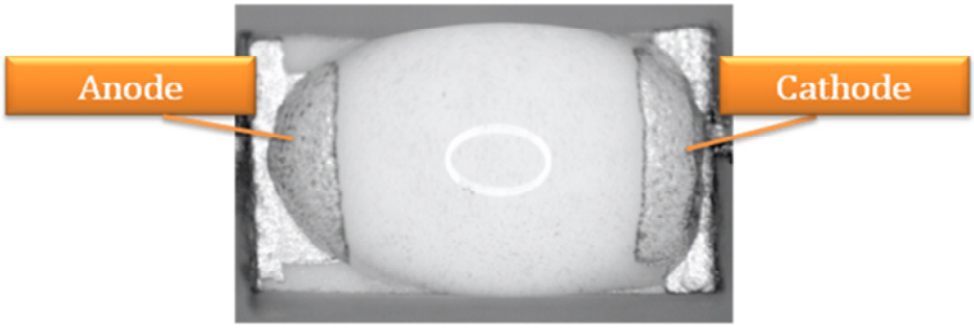

Fig. 5.3: CCR with water droplet added for simulating local condensation.

5.2.3 MICRO-ELECTROCHEMICAL SETUP:

A micro-electrochemical setup was used for potentiodynamic anodic polarization measurements on the resistor terminal in 10, 100 and 1000 ppm NaCl. The set up consists of an electrochemical head containing the solution, counter and reference electrodes, which is attached to the carousel of an optical microscope. The cell is connected to a pipette, which makes contact with a local region of the working electrode (for e.g. electrodes of the CCR). The lateral resolution of the technique is determined by the dimensions of the pipette tip, in this case ~350 µm in diameter. As the electrode area on CCR is small, part of the surface covered by the electrolyte is the Al_2O_3 substrate, which is inactive in the electrochemical measurements. By image analysis of corroded specimens, an electrode area of 0.003 cm^2 was found.

All Micro-electrochemical experiments were conducted using a CH Instruments 600 B electrochemical analyzer and an Ag/AgCl reference electrode (3M NaCl giving a potential of 215 mV vs. SHE). Open Circuit Potential (OCP) was held for 300 s after which anodic polarization was conducted from OCP -20mV to 2000mV with a scan rate of 2 mV/s. Electrolyte in the micro-electrochemical tip was purged between each experiment.

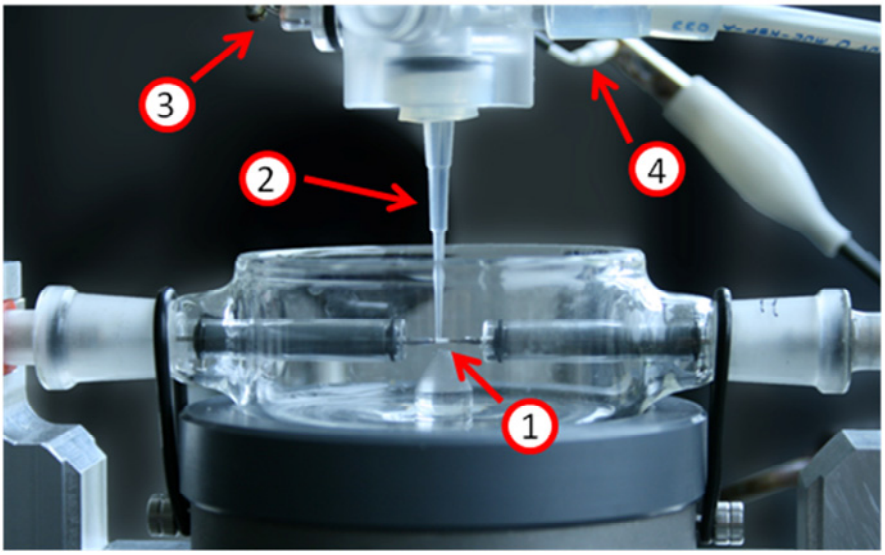

Fig. 5.4: Micro-electrochemical setup used in combination with the SCECM holder: 1. Specimen to be investigated, 2. Tip containing electrolyte, 3. Connection for counter electrode, and 4. Connection for reference electrode.

5.2.4 SPECIMENS AND SOLUTIONS

For SCECM measurements, chip resistors were handled by polymer tweezers to avoid any mechanical damage during handling. Sodium chloride solutions of concentrations 0, 10, 100, and 1000 ppm in de-ionized water were used for the experiments. All the solutions were prepared using A.R grade NaCl. All the experiments were carried out in the aerated conditions. Experiments using each set of parameters were repeated for 6 times to get a statistical average of the behaviour.

5.2.5 SEM/EDS AND FIB-SEM ANALYSIS

Microstructural characterization of the components before and after SCECM experiments were done using SEM (JEOL 5900 instrument) and chemical analysis was carried out using EDS (Oxford Link ISIS) analyzer attached to the SEM. FIB-SEM was performed using a Zeiss 1540EsB cross beam for the cross sectioning of dendrites for detailed investigation of microstructure.

5.3 RESULTS

5.3.1 MATERIAL MAKE UP AND MICROSTRUCTURE OF CHIP RESISTOR

The ceramic chip resistor (Fig. 5.5) is a surface mount component that consists of a sintered ceramic body, on top of which a resistive layer is placed.

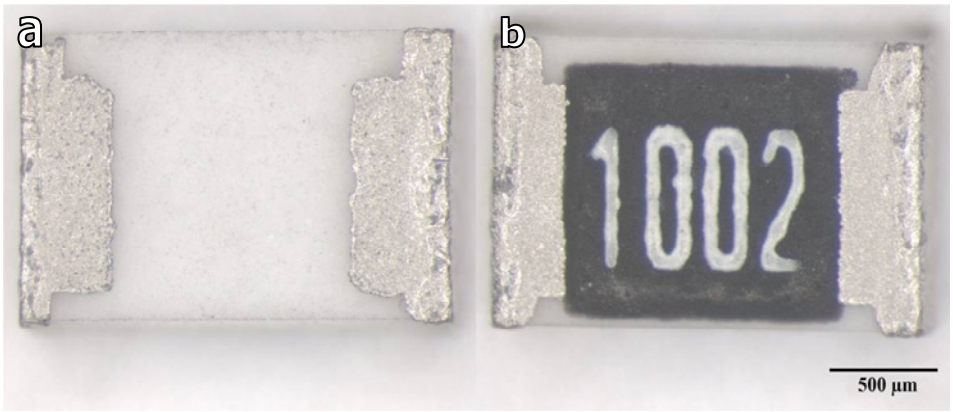

Fig. 5.5: Ceramic chip resistor with size 0805 used in this work: (a) bottom side and (b) top side. Resistance of the component is 10 kΩ.

An inert glass coating is applied in order to protect the resistive layer and connections to the resistive layer are made by adding metal terminals at the ends of the component. A schematic of the material makeup is presented in Fig. 5.6.

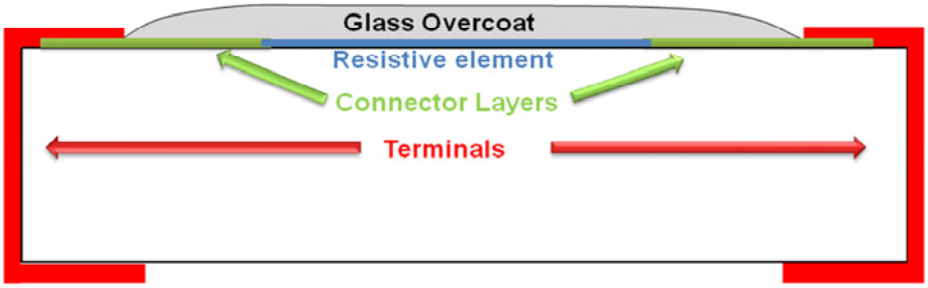

Fig. 5.6: Schematic of Surface mount chip resistor material make-up.

Fig. 5.7 shows SEM picture of the surface of the electrodes. EDS analysis showed that the top surface of the electrodes are made of tin containing 3 wt. % lead (Sn3Pb). Surface morphology of the electrode shows that the surface is non-uniform with rough areas indicative of a barrel plating technique used for manufacturing of the outer layer of these resistors.

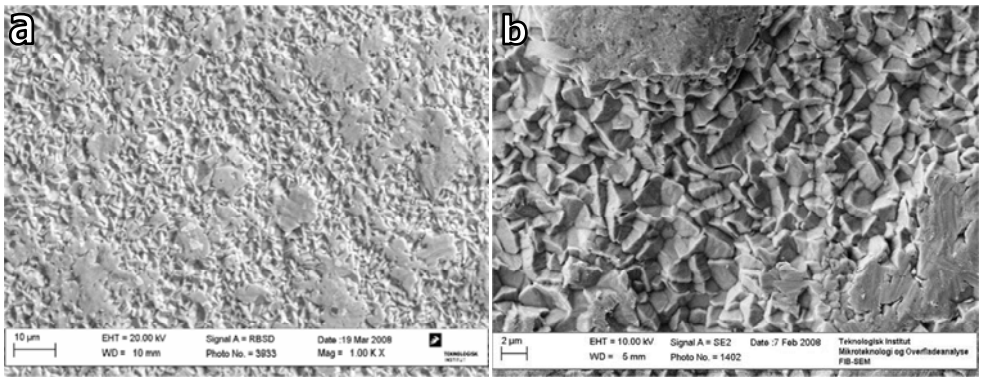

Fig. 5.7: SEM images of terminal electrode surface layer: (a) Low magnification view, and (b) High magnification picture of rough areas.

Fig. 5.8 shows the cross section of the resistor and different layers of electrode materials and resistive element. Table 5.1 shows a summary of the EDS analysis of various components with major and minor elements. The resistive layer was analysed using EDS and was found to contain oxides of Pb and Si with smaller amounts of Ca, Ti, Cr, Zn and Ag. This layer is covered by a silicon oxide glass layer. The Ag layers are used to connect the resistive layer to the terminals that consist of a Sn3Pb outer layer on top of Ni layer, which is placed on top of Ag layer. The ceramic body is made of aluminum oxide, with small amount of silicon oxide. Particles containing Cu, Ag and Bi where found at the outer 20 µm of the ceramic body, probably impurities from the sintering process.

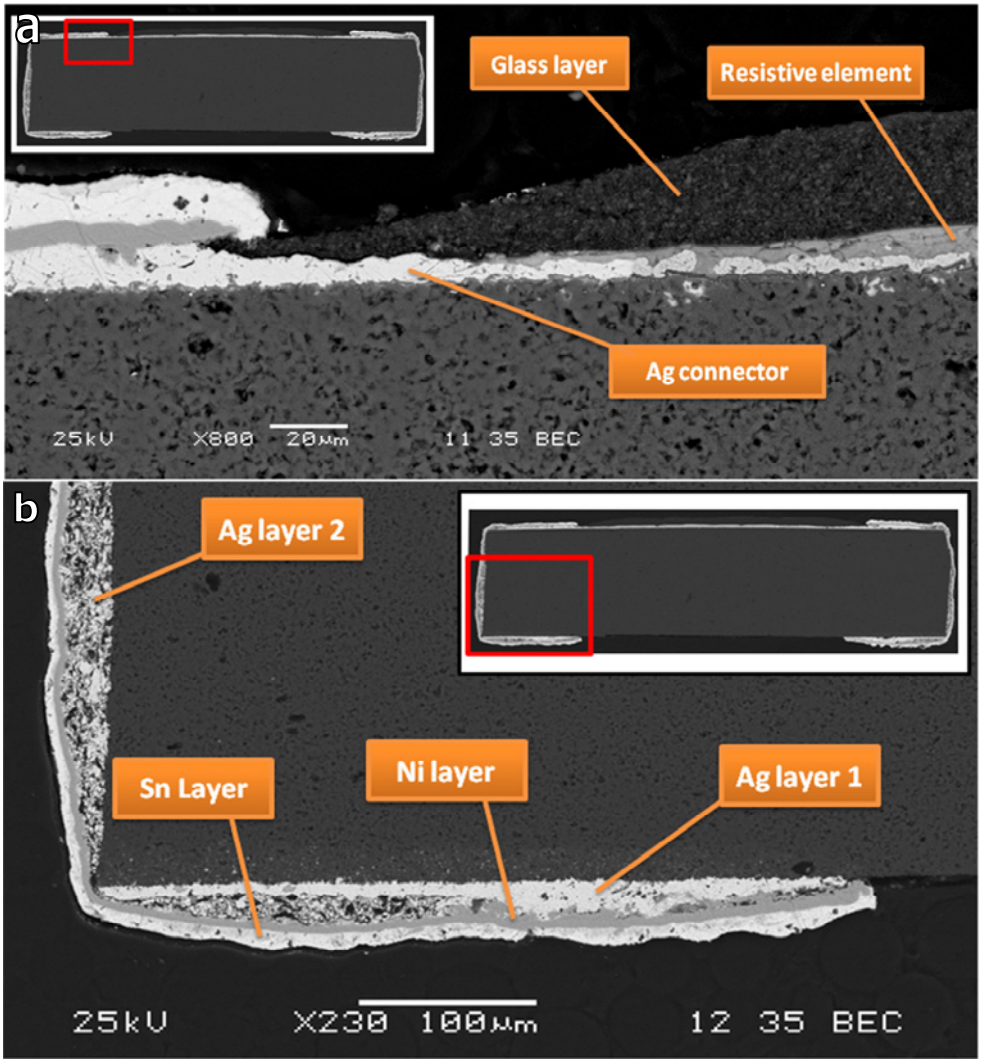

Fig. 5.8: SEM cross sections of chip resistor: ***(a)*** *terminal-resistive element connection and* ***(b)*** *Bottom side of terminal. An overview of the whole cross section is shown on each image. The position of the image acquisition is marked by a square.*

In order to understand how Ni and Ag layers are distributed inside the resistor electrode, a FIB cross sectional analysis was made as shown in Fig. 5.9 on part of the electrode termination area.

Table 5.1: Elemental composition of component parts (all results in wt. %)

Comp. part	O	Al	Si	Ca	Ti	Cr	Sn	Ni	Ag	Pb
Terminals:										
***Sn layer**							97			3
***Ni layer**								100		
***Ag layer**									100	
Glass layer	30		70							
Resistive element	9	3	18	1	2	2			7	58
Ceramic Body	29	69	2							

The multiple metallic layers can be seen in the FIB cut area with Ni and Sn layers as described before. It is also clear that the Ag and Ni layer is hidden beneath the Sn layer, and therefore not exposed to the surface.

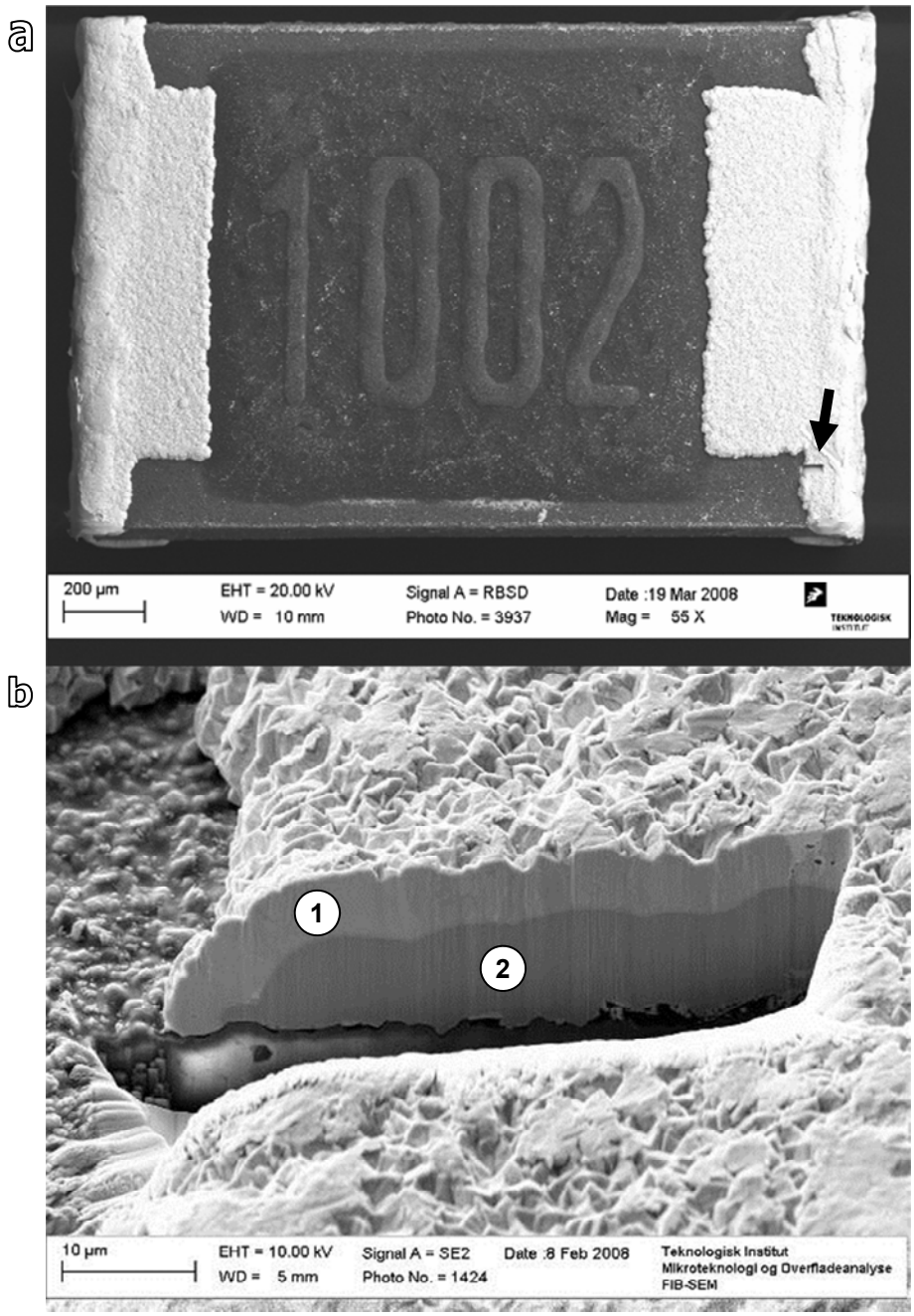

Fig. 5.9: SEM micrographs of chip resistor: (a) Top side of resistor with FIB cross section (marked by arrow) and (b) High magnification of FIB cross section revealing Sn layer (1) with Ni under layer (2).

5.3.2 ANODIC POLARIZATION OF COMPONENT TERMINALS

The Tafel plots overlay of the anodic polarization curves for the solder terminal in increasing chloride concentrations is shown in Fig. 5.10. The current density axis is in logarithmic scale, and therefore currents are positive irrespective of whether it is cathodic or anodic. The potential value (intersection of both curves) where the current changes from negative to positive (or the potential value at which the cathodic current is equal to the anodic current), is called the steady state corrosion potential, $E_{corr.}$ This can be seen on the curves as a "notch" at potentials between -200 mV and -400 mV. At potential less than these values, the current is negative, and the surface is in the cathodic domain. At potentials larger than the E_{corr}, the current is positive, and anodic dissolution of tin is observed. Active dissolution of tin is observed up to a potential of approx. E_{corr}+ 100 mV. Above this value current flattens as the ohmic limit of the solution is reached. The dissolution rate of the tin is seen to increase with the chloride concentration. Almost a decade increase in current was observed with 10 times increase in chloride concentration. At high potentials, polarization curves flatten as the ohmic limit of the solution is reached and little increase in current density is seen with increase in potential.

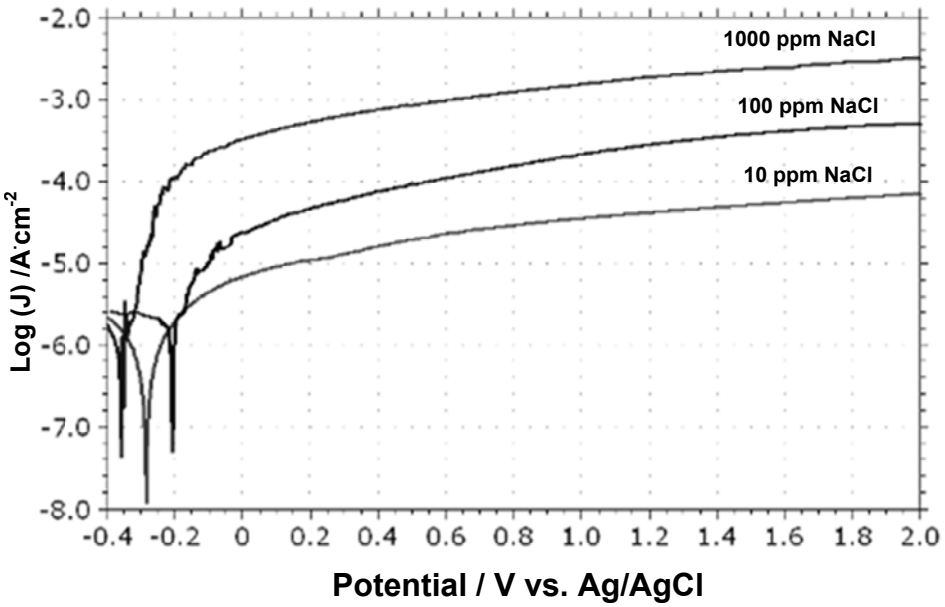

Fig. 5.10: Anodic polarization curves for solder terminals on ceramic chip resistor. The Y-axis is showing the logarithm to the current density (J) and the X-axis has the potential vs. Ag/AgCl reference electrode (215 mV vs. SHE).

Corroded area after 1000 ppm NaCl anodic polarization experiment was investigated using SEM and X-ray mapping as shown in Fig. 5.11. The X-ray mapping clearly shows selective dissolution of tin exposing nickel layer beneath. Islands containing higher amount of tin and oxygen are seen, probably corrosion products.

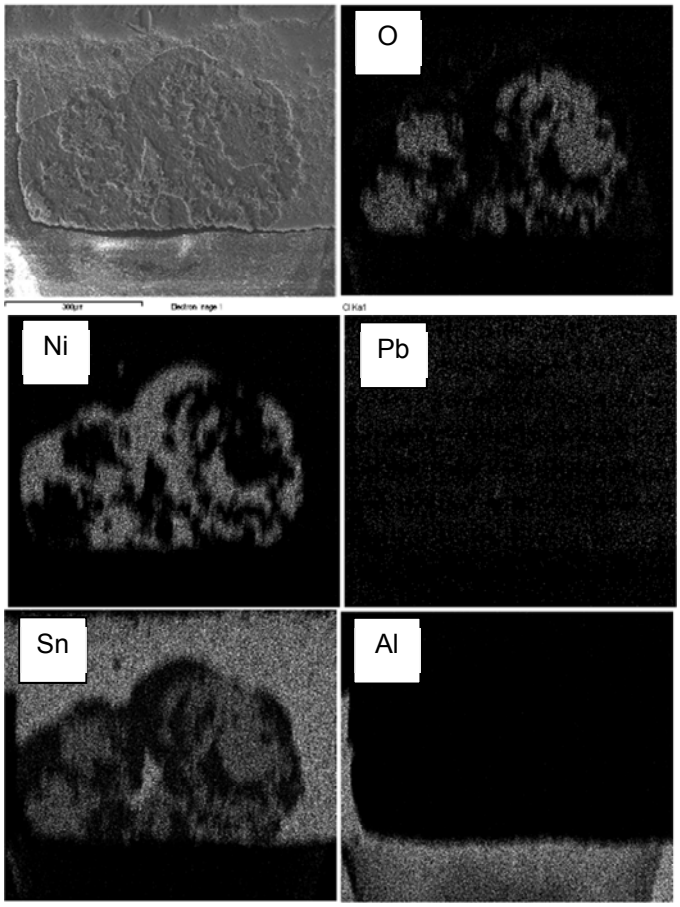

Fig. 5.11: Top left: SEM image of corroded area after anodic polarisation in 1000 ppm NaCl to 2000mV vs. Ag/AgCl electrode. Rest: EDS mappings showing O, Ni, Pb, Sn and Al signals respectively.

5.4 ELECTROLYTIC MIGRATION EXPERIMENTS IN CHLORIDE SOLUTIONS

5.4.1 MIGRATION AS A FUNCTION OF TIME IN 10 PPM NACL UNDER A 3V BIAS

Fig. 5.12 shows the current-time curve along with images of the dendrite formation as a function of time in 10 ppm NaCl in DI water under 3V bias. Before application of the solution, the base current level was measured to 300µA, as expected for a 10kΩ resistor at 3V bias.

Image 1 on Fig. 5.12 shows the initial condition, just as the potential bias was applied, as illustrated by the dotted line added to the current-time curve. First

visible dendrite nucleation was observed after approx. 7 min 30 sec (image 2). At this stage a little corrosion is observed at the anode and some corrosion products are seen in the solution, most likely tin hydroxides. After first visible nucleation of a dendrite was observed, a period of approximately 2 min dendrite growth was observed (image 3) until the dendrite finally reached the anode short circuiting the system (image 4).

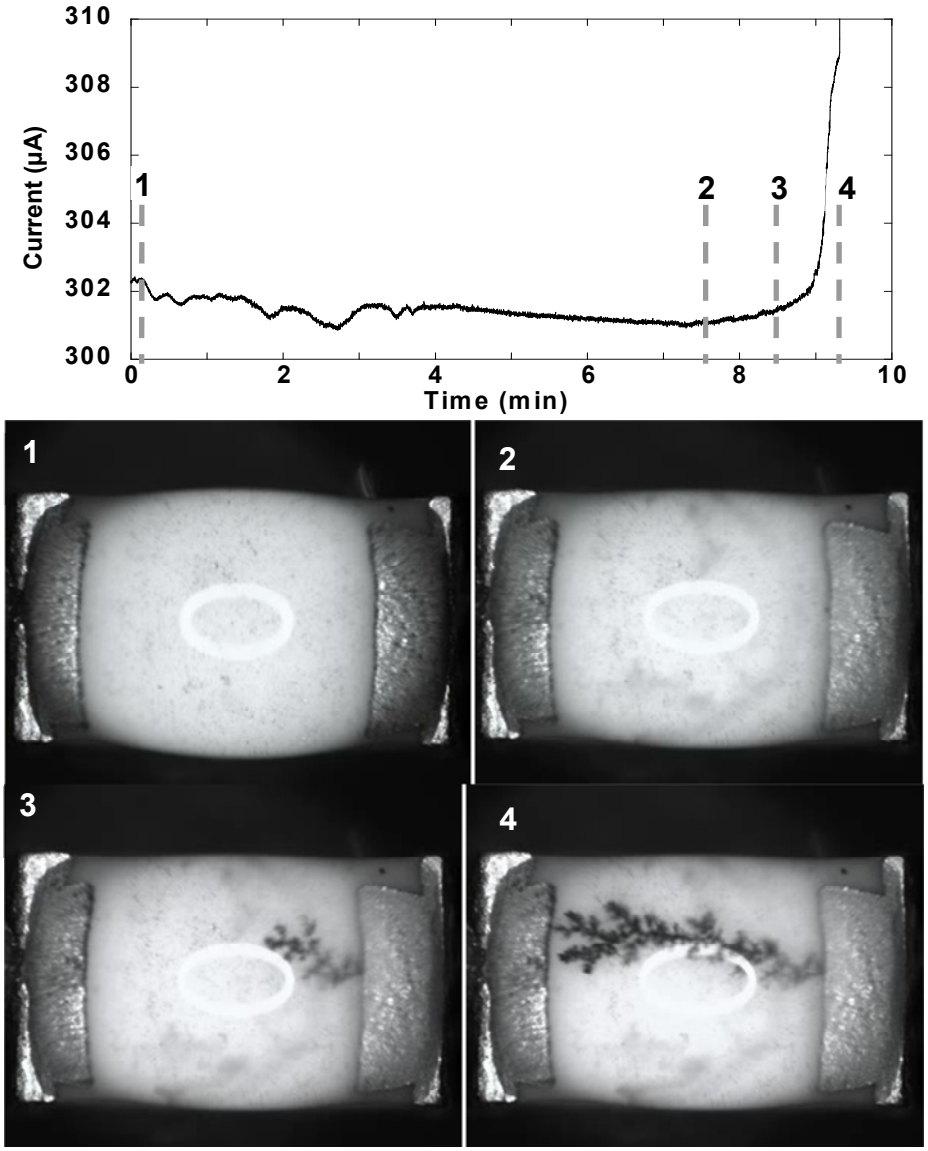

Fig. 5.12: Current-time curve for dendrite formation during SCECM experiment in 10 ppm NaCl solution at 3V bias along with images of the various stages of dendrite formation. For all images, cathode is on the right and anode is on the left. The times of image acquisition are marked by dotted lines on the current-time curve.

The current-time curve for the whole experiment is shown in Fig. 5.13 along with images of dendrite at the time of first short (image 1), condensation (images 2+3) and at the end of the experiment where the solution has dried out (image 4).

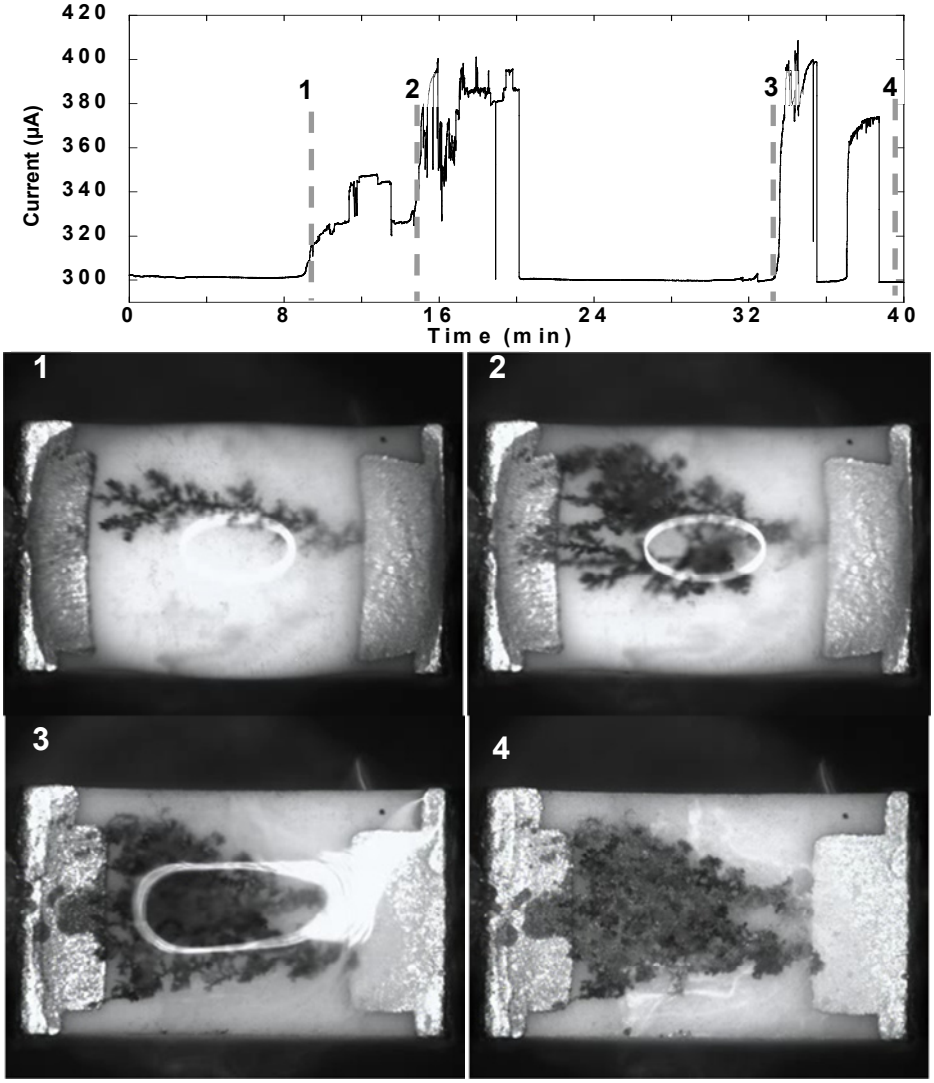

Fig. 5.13: Current-time curve for dendrite formation until electrolyte has evaporated for 10 ppm NaCl at 3V bias experiment, along with images at selected stages. For all images, cathode is on the right and anode is on the left. The times of image acquisition are marked by dotted lines on the current-time curve.

The dendrite is seen to increase the current to the level of 400 μA, until the dendrite bridge degrades (burns off) at approx. time = 20 min. At this stage current drops back to the base level of 300 μA. After 33 min a new dendrite bridge is formed which is again degraded, and this behavior continues until the solution is completely evaporated from the component.

5.4.2 EFFECT OF CHLORIDE CONCENTRATION AND POTENTIAL BIAS

Fig. 5.14 and Fig. 5.15 show specimens after SCECM experiments at 3V and 12V respectively and in varying chloride concentrations. Images are acquired at the time where the dendrite first reaches the anode. For experiments with no migration, the image presented is taken after the experiment has finished and the solution has dried out.

At 3V, dendrite formation was observed even at 0ppm sodium chloride, while at 12V no migration was observed. Also at 1000ppm sodium chloride, experiments at 3V did not show dendrite formation, while formation of dendrite was observed at 12V. Dendrites formed at 12V in general were thinner and less branched than those observed at 3V.

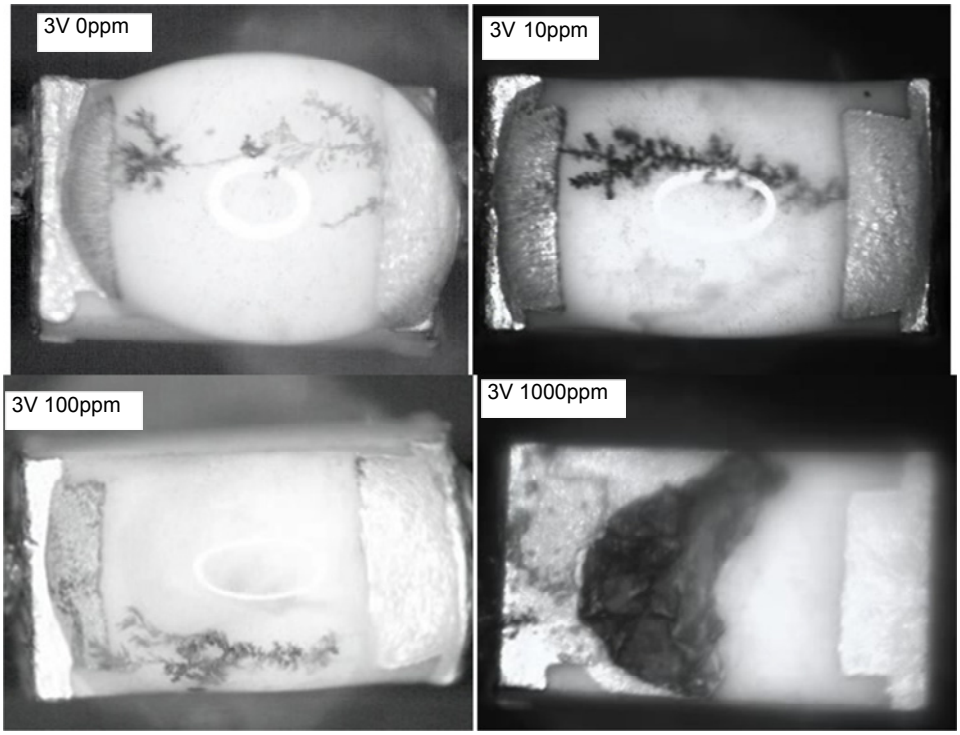

Fig. 5.14: Dendrite and corrosion morphology for 3 V experiments in varying sodium chloride concentrations. For all images, cathode is on right and anode is on left. For experiments with no migration, the image presented is taken after the experiment has finished and the solution has dried out.

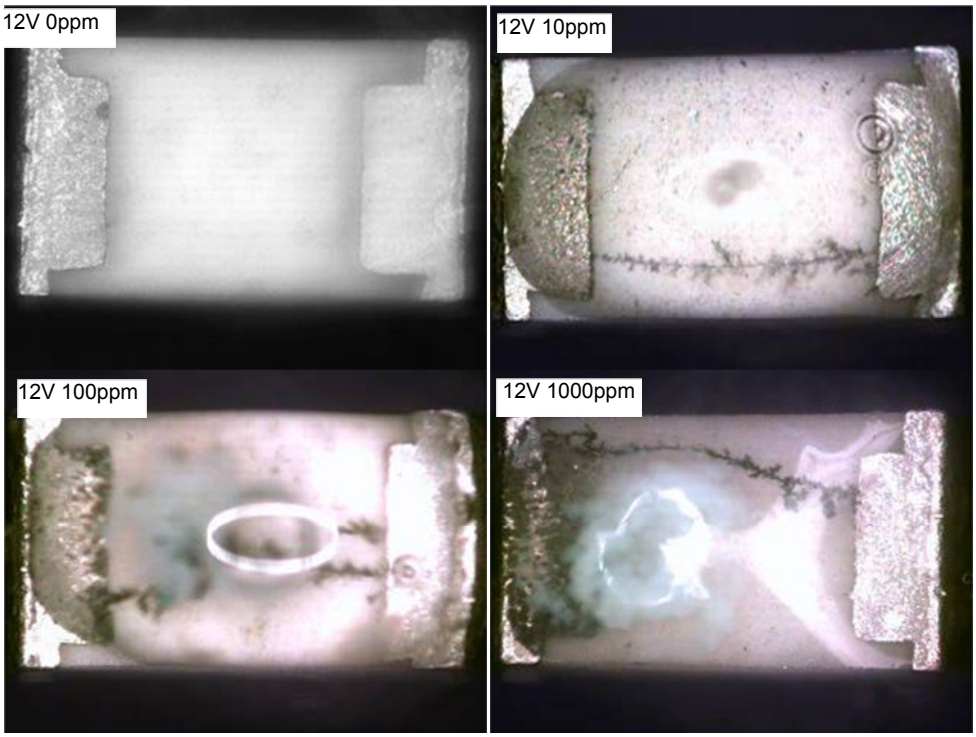

Fig. 5.15: Dendrite and corrosion morphology for 12 V experiments in varying sodium chloride concentrations. For all images, cathode is on right and anode is on left.

For 12V experiments using 100 and 1000 ppm NaCl, a grey/turquoise corrosion product can be seen (Fig. 5.15). The EDS analysis showed presence of Ni, Sn and O, indicating that the corrosion product is a mixture of hydroxides of these. However, Ni was not detected in the dendrites.

The probability of experiencing a short due to dendrite formation during the experiment time is given in Fig. *5.16* and the time for first short circuit is plotted in Fig. *5.17*. These data are deduced from the current-time curves obtained during the migration experiments and represents the average of 6 experiments carried out in each case (similar to the current-time curve in Fig. 5.13).

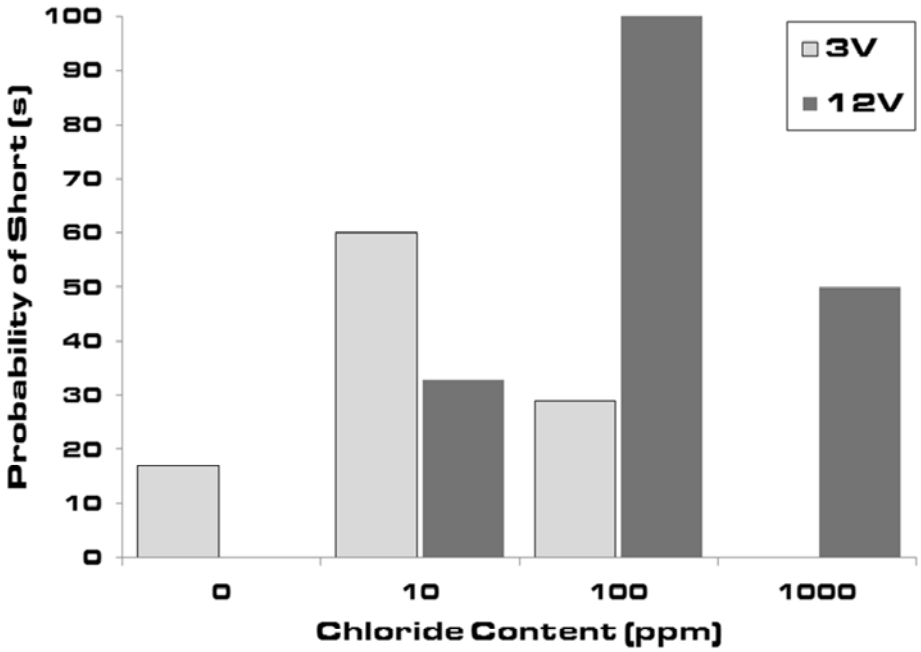

Fig. 5.16: Probability of electrochemical migration for 3V and 12V at varying sodium chloride concentrations.

It can be observed that the electrochemical migration is most likely to occur at sodium chloride concentrations in the range of 10-100 ppm (Fig. 5.16), while higher values of sodium chloride concentrations result in heavy corrosion of the anode with less tendency of dendrite formation (see images in Fig. 5.14 and Fig. 5.15). Repeated experiments with 0 ppm NaCl (DI water) on various components have shown that migration is rare, but could happen (at both 3 and 12V). It could be argued that the one experiment in 0 ppm NaCl which showed migration should be excluded as a statistical abnormality. However, we have chosen to include this experiment to show that even at very small contaminations could lead to migration. The origin to these contaminations could be impurities from the manufacturing process, although further investigation is needed to prove this fact.

Fig. 5.17 shows the time for first short deduced from the current-time curves. Time required for short circuiting in general is longer for the 3V compared to 12V bias (Fig. 5.17). No values are shown for 0 ppm 12V and 1000 ppm 3V experiments since no migration was observed for these experiments.

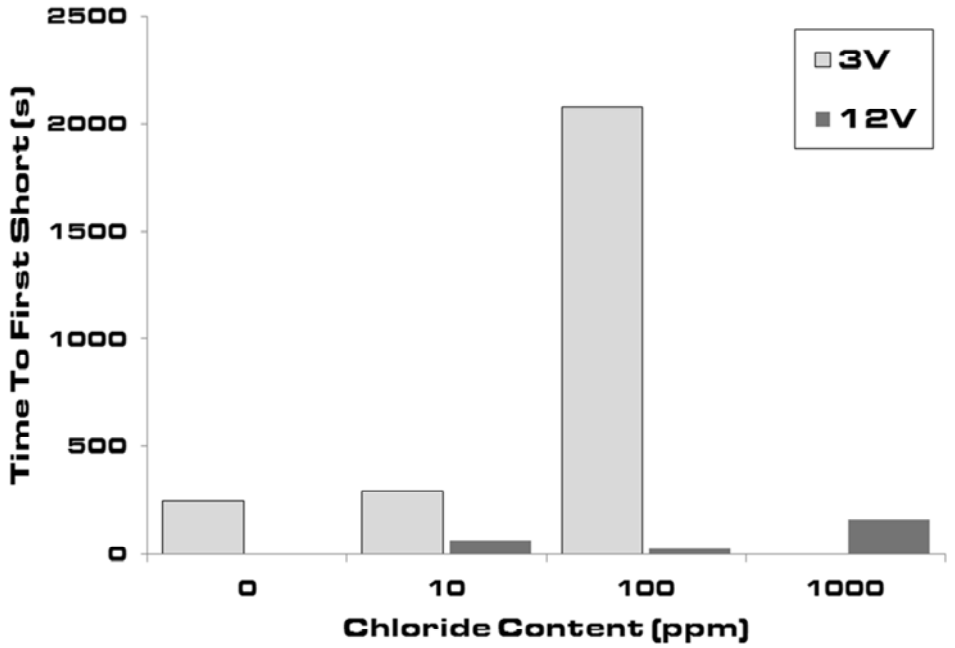

Fig. 5.17: Time for first short circuit due to electrochemical migration for 3V and 12V at varying sodium chloride concentrations.

5.4.3 ELECTRICAL PROPERTIES OF DENDRITES AS FUNCTION OF POTENTIAL BIAS AND CHLORIDE CONCENTRATION:

Current – time curves for various experiments at 3V and 12V bias are presented in Fig. 5.18. Current passed through the electrolyte is very small compared to that passing through the dendrite bridge and dendrite formed at 3 and 12V showed large differences in the capacity for current flow.

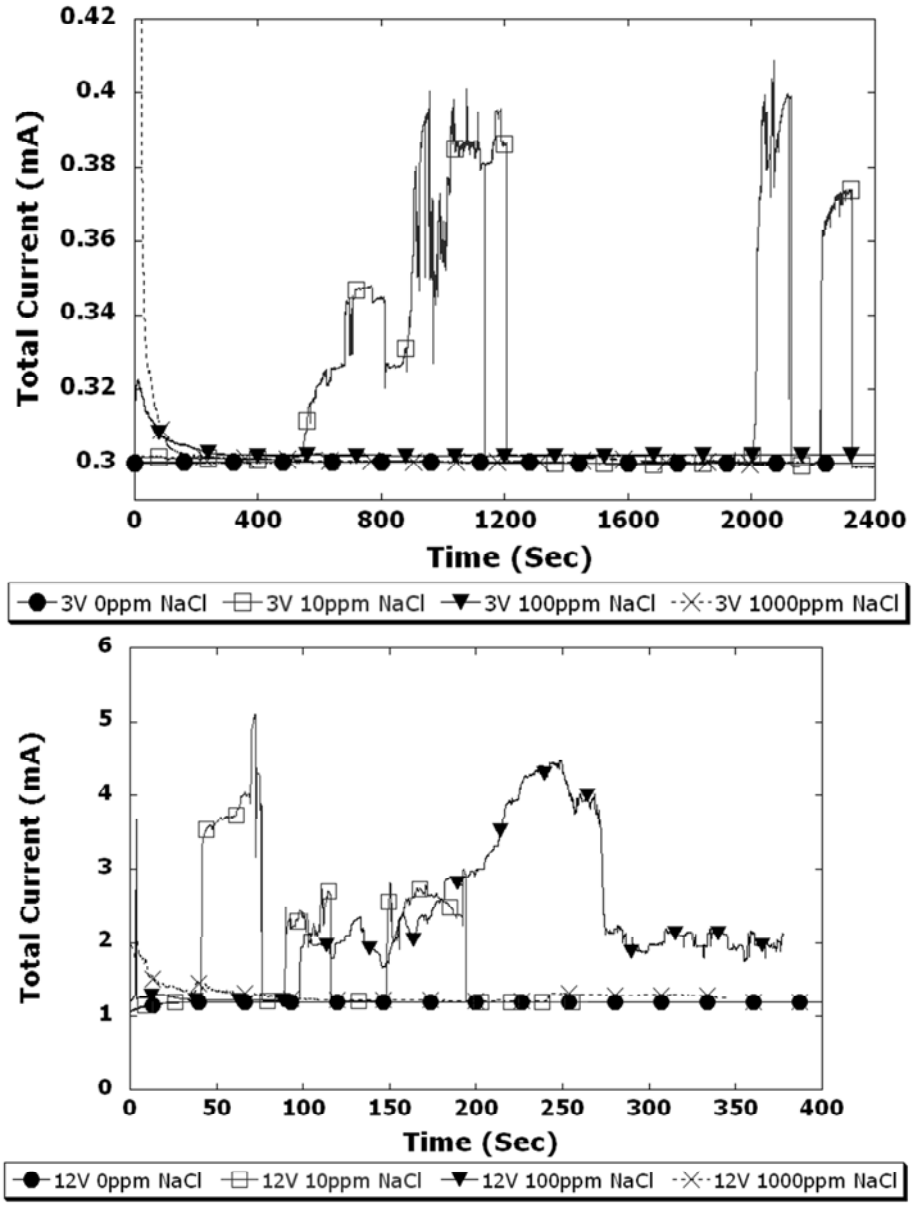

Fig. 5.18: Current time curves for 3V and 12V at varying sodium chloride concentrations.

As the dendrite is formed on the surface of the component, the system can be simplified into an equivalent circuit consisting of parallel resistances as shown in Fig. 5.20.

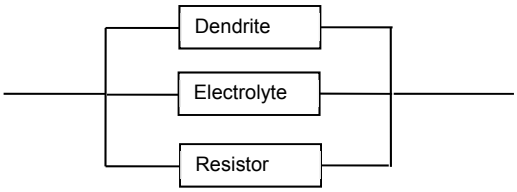

Fig. 5.19: Simple equivalent circuit for the resistor-electrolyte-dendrite system

As the resistance of the electrolyte is very high compared to the resistance of resistor and dendrite, this can be neglected. The resistance of the dendrite can then be roughly estimated using simple Ohms law to provide quantitative estimates.

In order to estimate the resistance or conductivity of the dendrite, the maximum current measured during the experiments were used. Fig. 5.20 shows the dendrite resistance as a function of the chloride concentration. Values shown are average values only taken from experiments where dendrite formation was observed.

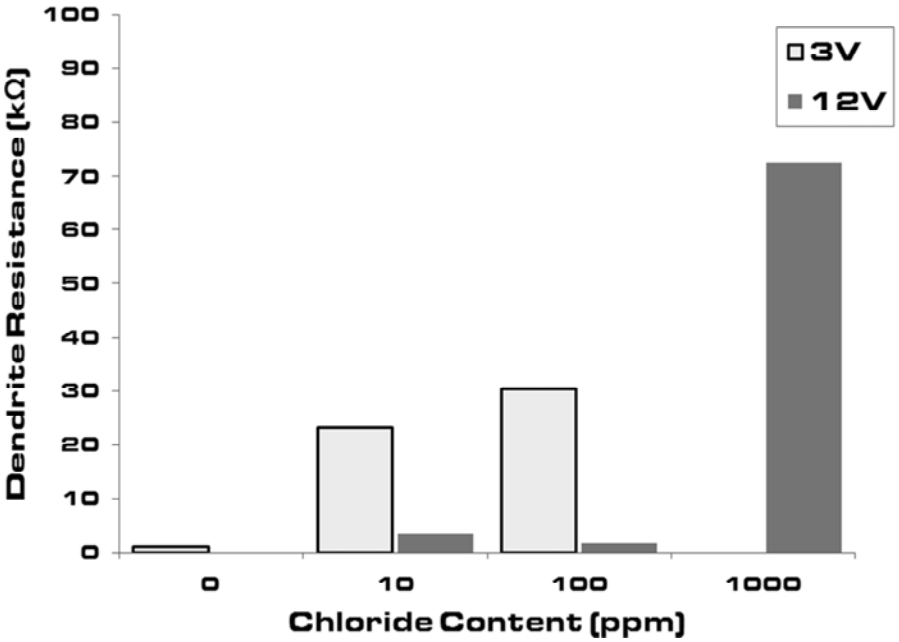

Fig. 5.20: Dendrite resistance at varying sodium chloride concentrations for 3V and 12V experiments.

The backbone of a typical dendrite has been observed to be in the magnitude of ~200nm (see Fig. 5.21).

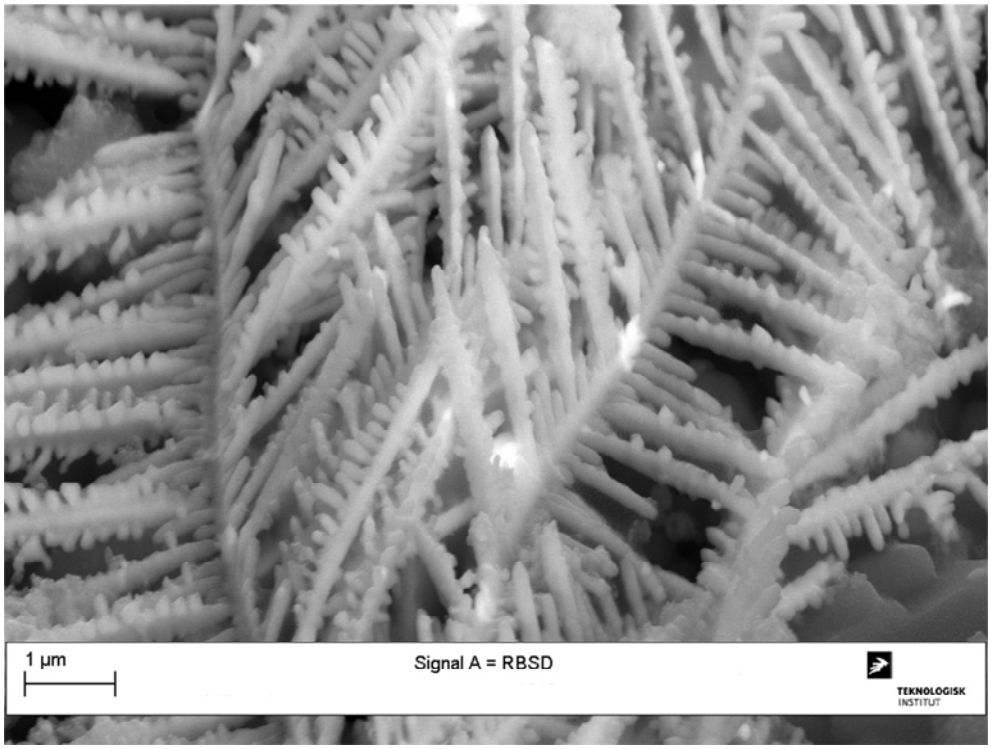

Fig. 5.21: Example of SEM image of dendrite at high magnification.

This backbone is the continuous line carrying the current from one terminal to the other. Approximating the dendrite to a wire with a diameter of 200nm having a length of approximately 1 mm (distance between the two terminals on the resistor), a dendrite made of metallic tin should have a resistance of about 3.5kΩ (resistivity of tin used is ~ $1.09 \cdot 10^{-7}$ Ωm). This value fit quite well with the lowest resistances observed in the magnitude of 1kΩ, when it is considered that the dendrite does not consist of one backbone but several branches, thereby lowering the resistance. However, many dendrites were observed to have resistances in the scale of 20-75 kΩ, and here it is especially noted, that the dendrites having high resistances at 3V, 10-100 ppm NaCl where the ones that appeared thicker as compared to those at 12V (see Fig. 5.14 and Fig. 5.15).

In order to get an idea of dendrite life and cumulative damage to the component, the total charge passed during the experiments was calculated by integrating the current-time curves. Fig. 5.22 shows the results obtained at 3 and 12 V. The values

where obtained by assuming the baseline to that of the current level for a dry resistor, and then integrating the current exceeding that level. As the current contribution from the faraday current through the electrolyte is very small compared to that when a dendrite makes a short (Fig. 5.18), this calculation can practically be regarded as the charge passed through the dendrite. An interesting observation is that at higher chloride concentrations total charge passed is less due to intermittent burning of the dendrite once it is formed.

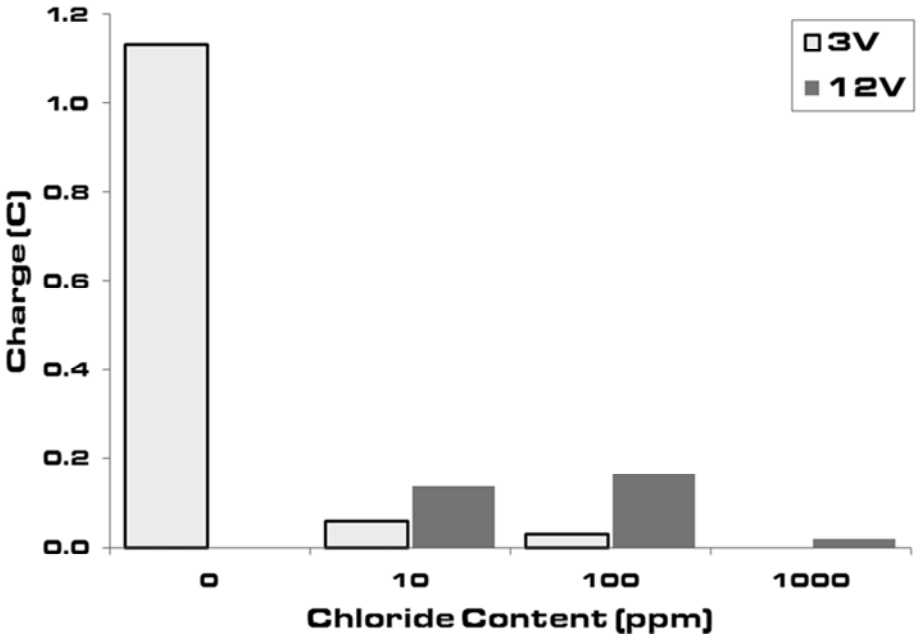

Fig. 5.22: Charge passing through the dendrites during experiment at varying sodium chloride - concentrations for 3V and 12V experiments.

5.5 DISCUSSION

Chip resistors tested in this investigation was found to be susceptible to electrolytic migration in chloride environments due to the presence of susceptible electrode materials. Susceptibility to migration, dendrite morphology, and dendrite resistance were a function of the chloride content and potential bias. Results showed some scatter in migration behavior for similar components with some of them showing dendrite formation while others not, although test parameters were kept similar. This clearly indicates the variability that could be observed on a PCB if many

components are present. Therefore, experiments in each case were repeated several times and the results reported in this paper represent typical behaviors observed.

Migration was observed in one out of six experiments at 0 ppm NaCl (pure DI water) using 3V potential bias, while no migration was observed at 0ppm NaCl at 12V bias. However, it is likely that the migration is due to an uncontrolled parameter, such as impurities from manufacturer of the components.

Overall, the probability of experiencing a short was found to increase initially with change in sodium chloride concentration from 0 to 10 ppm at 3V, but further increase in concentration reduced the probability for short. Similar behavior was observed at 12V except for the shift in the sodium chloride concentration to 100 ppm. It is clear from the polarization curves that increased sodium chloride ion concentration increases the dissolution of the anode on the chip resistor. However, it is assumed that the increased metal ion concentration in the solution layer will result in precipitation of hydroxides as the product of concentration of metal ions and hydroxyl ions reach above the solubility limit. Local changes in pH (alkalization at the cathode) can assist this process by increasing the hydroxyl ion concentration. Formation of hydroxides impedes migration as hydroxides are neutral compounds and therefore they will not migrate under the electric field. Further investigation is needed to elucidate the exact reason for this behavior, but it appears to be due to change in local pH change resulting from increased faradaic reactions with bias voltage and corresponding change in the stability of the metal ions. At 12V 1000 ppm NaCl, migration still occurred in 50% of the experiments, whereas at 3V 1000 ppm NaCl no migration was observed, but heavy corrosion of the anode was observed (see Fig. 5.14-5.16). As seen in the anodic polarization curves, presented in Fig. 5.10, the anodic dissolution of tin is at the diffusion limited region at both 3 and 12V. The migration observed at 12V could therefore be explained by difference in the local pH distribution inside the droplet, or due to the co-dissolution of nickel from the terminal underlayer, which could possibly have an effect on the stability of the tin ions in solution, though no evidence is readily given for this at present. However, this might suggest that the migration behavior is

influenced by the tin-layer thickness and of the morphology of the metal underlayers.

Noh et al [[27]] found, that the tendency for ECM followed the same trend as the rate of corrosion on materials such as electroless Ag, electroplated Sn, and ENIG (electroless nickel on immersion gold) surfaces when comparing ECM experiments using DI water to corrosion experiments in 1.0 wt. % NaCl solutions, and that the tendency for ECM for various metals were in the order Ag>Sn>ENIG. In this work however, it is found that the dissolution rate at the anode under ECM conditions play a significant role on whether ECM is possible or not. Also, an Ag underlayer is present on the electrode terminal of the ceramic chip resistor used in the present work, but no silver migration or silver corrosion products where observed. This shows that even though silver has a higher trend for ECM, when combined with Sn and Ni, the galvanic coupling between Sn, Ni and Ag layer might not allow dissolution of silver ions.

Yoo and Kim [[28]] have investigated the influence of varying Pb content on ECM using NaCl and Na_2SO_4 solutions (all neutral pH conditions). In Na_2SO_4 the tendency for ECM is seen to decrease due to passivation of Pb, while in NaCl solution no significant change in the tendency for ECM is observed when the Pb content is increased. The NaCl solution used by Yoo and Kim was 0.001 wt. % equivalent to the 100 ppm solution used in the present work. The time to failure of pure tin in 100 ppm NaCl at 3V potential bias found by Yoo and Kim was approximately 60 s, differing significantly from the values found in present work (Fig. 5.17). However, the distance between the electrodes used by Yoo and Kim was 350 µm, whereas the distance between the electrodes in the present work is 1100 µm. This strongly illustrates the importance of conductor spacing when investigating ECM. Further work is presently carried out investigating ECM on a large number of components having varying sizes with varying potential bias and environments.

Another important aspect is the morphology and resistance of the dendrite that determines the stability and current leakage through the dendrites. Fig. 5.20 clearly shows the variations in the resistance values of the dendrites, indicating the

possibility of variation in composition of the dendrites formed at different parameters. Increased dissolution kinetics at higher chloride concentrations results in more dissolution of tin ions as explained before. Higher concentration of tin ions in the solutions results in precipitation of tin hydroxide, which could be incorporated into the dendrite to increase its resistance. Incorporation of the hydroxide particles changes morphology and resistance of the dendrites. Attempts have been made to analyze the dendrite composition after migration experiments in various NaCl concentrations using EDS, but due to the large sampling volume of the X-Rays produced (approx. 1 μm^3) no conclusive results can be presented. The problem is more complicated due to the large variations in the dendrites formed, since dendrite growth conditions could change due to electric field and pH changes within the droplet. It is believed that the dendrite consist of an inner metallic conductor, embedded by hydroxides or hydrochlorides. Further analysis is underway on investigating dendrite morphology using FIB-SEM and EDS.

Electrolytic migration and dendrite formation observed with no chloride is assumed to be due to low levels of residues from the component, which dissolves into the water layer. It clearly indicates risk of electrolytic migration in actual practice where only very low amounts of residues are sufficient to cause ECM if there is suitable potential bias. Increased amounts of chlorides or other ions will further accelerate the migration process, while the contamination on the components itself can produce migration if water layer is present.

At higher potentials it seems that the dendrites are thinner and less branched compared to that at lower potentials. This behavior is believed to be due to the higher electric field acting between terminals, which results in subsequent deposition of the metal ions at the tip of the dendrite rather than branching.

As expected, the time to first short was found to be longer at lower potentials (3V) compared to that at 12 V bias due to slow dissolution and deposition kinetics. Also, the droplet used for 3V experiments had less tendency to evaporate, indicating less generation of heat in the component (resistor heating) during the experiment.

Both aspects correlate with the use of higher voltage that results in higher current through the resistor to heat up and higher voltage also increases the migration kinetics.

In general electrolytic migration of the chip resistor was found to be a function of the amounts of chloride ions in solutions and potential bias between electrodes. Presence of chloride ions also increases the dissolution of the anode to provide the metal ions necessary for migration. This is important as the analysis of many field failures shows signs of chloride contamination on the components. Such contamination on a PCB can arise from the use of halide containing flux, human handling or from service environments. Material make up, surface morphology of electrode layer, and solution chemistry all play a big role in controlling migration due to combined effects. Humidity absorption is easy on a rough surface, while dissolution of the top layer of a component electrode can expose the metal underneath causing galvanic corrosion, especially if the potential bias is switched off. Similarly the continuous changes in solution chemistry during the experiments determine the stability of dissolved ions in solution. As shown before, stability of the metal ions in the solution layer can alter migration and dendrite formation behaviour as well as the resistance of the dendrites.

5.6 CONCLUSIONS

1. Chip resistor electrode terminals are found to be susceptible to electrolytic migration in sodium chloride solutions under a potential bias of 3 and 12V.
2. Sodium chloride concentrations around 10-100 ppm was found to significantly increase the probability of electrochemical migration depending on the potential bias. Chloride concentration also increased the anodic reactivity of the electrode material.
3. Lower migration kinetics at 3V experiments resulted in higher time-to-short values. The dendrites formed at 3V in general had higher resistance than those formed at 12V.

4. SCECM setup was found to be a good tool for corrosion studies of single electronic components in *condensing* environments.

ACKNOWLEDGMENTS

Authors would like to acknowledge project partners Danfoss A/S, Grundfos A/S, Vestas A/S and GPV Chemitallic A/S, Danish Technological Institute and IPU for their commitment to this project.

REFERENCES:

[1] B. Noh, S. Jung, "Characteristics of environmental factor for electrochemical migration on printed circuit board", J MATER SCI-MATER EL, Vol. 19, No. 10, **2008**

[2] B. A. Smith, L. J. Turbini, "Characterizing the weak organic acids used in low solids fluxes", J ELECTRON MATER, Vol. 28, No. 11, **1999.**

[3] R. Ambat and P. Møller, Proceedings of "Korrosion- mekanismer, havarier, beskyttelse", DMS Vintermødebog, pp.161-178, **2005**.

[4] T. Takemoto R. M. Latanision, T. W. Eagar and A. Matsunawa, "Electrochemical migration tests of solder alloys in pure water", CORROS SCI, Vol. 39, No. 8, pp. 1715-1430, **1997.**

[5] M. Pourbaix, "Atlas of electrochemical equilibria in aqueous solutions", NACE, Cebelcor, **1974.**

[6] T. Kawanobe, K. Otsuka, "Metal Migration in Electronic Components", Proc. Electronic Components Conf., p. 220, **1982.**

[7] S. Nishigaki, J. Fukuta, S. Yano, H. Kawabe, K. Noda, M. Fukaya, "New low temperature fireable Ag multilayer ceramic substrate having post-fired Cu conductor (LFC-2)", Proc. Int. Society of Hybrid Microelectronics, p. 429, **1986**.

[8] S. J. Krumbein, "Tutorial: Electrolytic Models for Metallic Electromigration Failure Mechanisms", IEEE T RELIAB, Vol. 44, No. 4, **1995.**

[9] S. Brunauer, P.H. Emmett, and E. Teller, "Adsorption of Gases in Multimolecular Layers," Journal of the American Chemical Society, vol. 60, p. 309, **1938.**

[10] D. E. Yost, "Siver migration in printed circuits", Proc. Symp. Printed Circuits, Philadelphia, **1955.**

[11] G.T. Kohman, H.W. Hermance, G.H. Downes, "Silver migration in electrical insulation", Bell System Tech. J, vol 34, pp. 1115, **1955.**

[12] S.W. Chaikin, J. Janney, F.M. Church, C.W. McClelland, "Silver migration and printed wiring", Indust. Eng'g Chemistry, vol51, pp. 199, **1959.**

[13] S. J. Krumbein, A. H. Reed, "New studies of silver electromigration", Proc. 9th Int'l Conf. Electric Contact Phenomena, pp. 145, **1978.**

[14] A. Der Marderosian, C. Murphy, "Humidity threshold variations for dendrite growth on hybrid surfaces", Proc. Int'l Reliability Physics Symp, pp. 92, **1977.**

[15] G. DiGiacomo, "Metal migration (Ag, Cu, Pb) in encapsulated modules and time-to-fail model as a function of the environment and package properties", Proc. Int'l Reliability Physics Symp, pp. 27, **1982.**

[16] L.J. Turbini, J.A. Jachim, G.B. Freeman, J.F. Lane, "Characterizing water soluble fluxes: Surface insulation resistance vs Electrochemical migration", Proc. CHMT Int '1 Electronics Mfr'g Technology Symp, pp. 80, **1972.**

[17] D. Shangguan, A. Achari, W. Green, "Application of lead-free eutectic Sn-Ag solder in no-clean thick film electronic modules", IEEE Trans. Components Packaging Mfr'g Technology part B, Vol.17, pp. 603, **1994.**

[18] M. Zamonzadeh, S.L. Moilink, G.W. Warren, et al, "Electrochemical examination of dendritic growth on electronic devices in HC1 electrolytes'', Corrosion, Vol. 46, pp. 665, **1990.**

[19] C. W. Jennings, "Filament formation on printed wiring boards", IPC Tech. Rev, pp. 9-16, **1976.**

[20] A. Shumka, R. R. Piety, "Migrated gold resistive shorts in microcircuits", Proc. Reliability Physics Symp, pp. 93, **1975.**

[21] F.G. Grunthaner, T.W. Griswold, P.J. Clendening, "Migratory gold resistive shorts: chemical aspects of a failure mechanism", Proc. Reliability Physics Symp, pp. 99, **1975.**

[22] A. Shumka, "Analysis of migrated-gold resistive short failures in integrated circuits", Proc. Tech. Program Int'l Microelectronic Conf, pp. 156, **1976.**

[23] P. E. Rogren, "Electro migration in thick film conductor materials", Proc. Tech. Program Int '1 Microelectronic Conf, pp. 267, **1976.**

[24] A. Der Marderosian, "Humidity threshold variations for dendrite growth on hybrid substrates", Proc. 20th Ann. Mtg. IPC, (IPC-TP-156), Tech Paper 13, **1977.**

[25] N. L. Sbar, "Bias humidity performance of encapsulated and unencapsulated Ti-Pd-Au thin-film conductors in an environment contaminated with Cl", BEE Trans. Parts, Hybrids, Packaging, Vol. PHP-12, pp. 176, **1976.**

[26] R. P. Frankenthal, "Corrosion failure mechanisms for gold metallizations in electronic circuits", J. Electrochemical Soc, Vol. 126, pp. 1718, **1979.**

[27] B. Noh, J. Lee, S. Jung, "Effect of surface finish material on printed circuit board for electrochemical migration", MICROELECTRON RELIAB, 48, pp. 652-656, **2008**

[28] Y. R. Yoo and Y. S. Kim, "Influence of corrosion properties on electrochemical migration susceptibility of SnPb solders for PCBs", MET MATER INT, 13, 3, pp. 129-137, **2007**

6 PAPER 2: ELECTROCHEMICAL MIGRATION OF TIN IN ELECTRONICS AND MICROSTRUCTURE OF THE DENDRITES

Daniel Minzari[6], Flemming Bjerg Grumsen, Morten S. Jellesen, Per Møller, Rajan Ambat

Section for Materials and Surface Technology, Department for Mechanical Engineering, Technical University of Denmark

ABSTRACT

The morphology and structure of tin dendrites, formed by electrochemical migration on a surface mount chip resistor having Sn 2wt. % Pb electrodes was investigated by SEM, TEM/EDS and electron diffraction. The tin dendrites were formed under 5 or 12V potentials in dilute NaCl electrolyte. Electron diffraction showed that the dendrites consist of metallic tin having sections of single crystal orientation and lead containing intermetallic particles embedded. At certain areas, the dendrites were found to be surrounded by a tin oxide due to unstable growth conditions.

Keywords: A. Tin, B. Potentiostatic B, SEM, B. TEM, C. Electrochemical Migration, C. Dendrite

6.1 INTRODUCTION

Electrochemical migration (ECM) is a phenomenon of outmost importance in relation to corrosion of electronic devices. If condensation occurs locally on an electronic device where two closely located biased points get connected to form a corrosion cell, ECM results in the formation of a metallic dendrite that can bridge two conductors and form a short circuit within a short interval of time if the right conditions are present. If two metallic conductors are connected by a water layer, the water will act as an electrolyte and metal ions will be dissolved at the anode. Depending on the thermodynamic nature and stability of these metal ions they will migrate though the electrolyte to the cathode where they can be deposited to their metallic state in a manner similar to electroplating. However, due to the high electric fields, low conductivity, and other uncontrolled conditions in the electrolyte,

[6] *Corresponding Author: Daniel Minzari, Department of Mechanical Engineering, Technical University of Denmark, Kgs Lyngby DK-2800, Denmark, Tel : +45 4525 2118, Fax : +45 4593 6213, Email: dmin@mek.dtu.dk*

the electrodeposit will rarely form smooth plating at the cathode, but rather grow preferentially at high energy sites producing a dendritic growth starting at the cathode and growing towards the anode. Such failures are often intermittent, as the contact though the dendrite bridge is lost due to dendrite burn off during the surge in current or when the condensed water layer has evaporated due to the heat generated as high currents are transported through the fragile dendrite structure. Due to the small distances in electronic circuits and high packing density of the components, failures due to electrochemical migration are often overseen as the dendrites can be difficult to observe, even in an electron microscope.

Electrochemical migration of tin and tin alloys is of high interest, as they make up a significant part of the metallic materials that are directly exposed on the surface of an electronic printed circuit board assembly (PCBA) where tin solder finish (hot levelled) surface is used and in most cases the component electrodes are made of pure tin or tin based alloys.

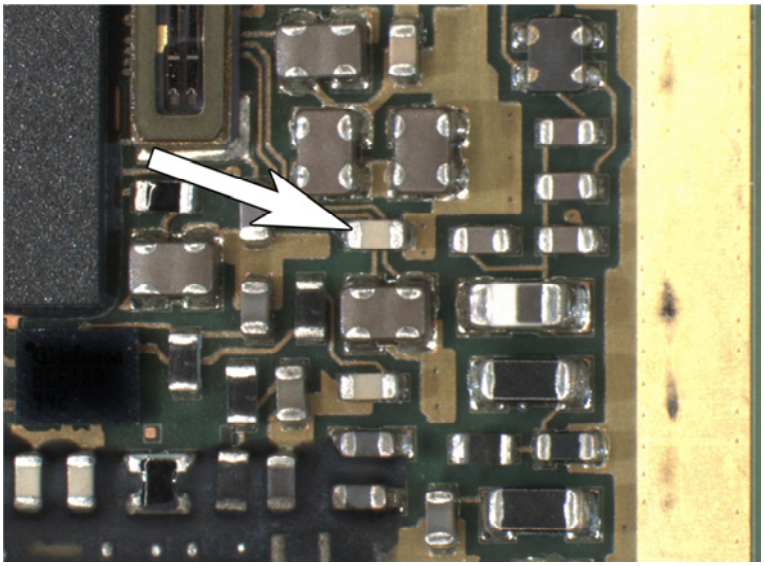

Figure 6.1: Example of a PCBA with various components mounted. Arrow shows the electrode terminals of a chip component which is found in large numbers on a PCBA. Most of these components has terminals made from tin or tin alloys.

There have been many inconsistencies in the literature regarding electrochemical migration of tin. Takemoto et al [1] references examples of DerMarderosian [2] who reported that pure tin migrates in pure water while Kawanobe and Otsuka [3]

classified tin as one of the most resistant metals to ECM. Takemoto et al [1] investigated ECM of Sn and Sn solder alloys in deionised (DI) water. In Sn-Pb alloy system, pure lead was found to have highest susceptibility to ECM, alloys containing up to 60%Sn showed similar behaviour and alloys with higher tin content showed less or no migration. However, pure tin samples having a different surface roughness than those in the original test setup was found to migrate and it was found that migration occurred when surface of the anode was rough which was attributed to the dissolution rate of tin. Yoo and Kim [4] compared the corrosion properties with the susceptibility for ECM for SnPb solders in dilute Cl^- and SO_4^{2-} electrolytes. Pure tin showed similar time to failure intervals on both chloride and sulphate solutions, while increases in the time to failure was found on samples with high amount of Pb in sulphate solution. It was concluded that anodic dissolution rate did not influence ECM susceptibility, which is contrary to other reported work [1,5-8]. Lee et al [7,8] compared ECM of Pb and Sn at potentials in the range of 0.5-3V by water drop testing and potentiodynamic anodic polarization in dilute NaCl and Na_2SO_4 electrolytes, and attributed the decreased tendency of tin migration to passivation of the tin surface. Yu et al [9] has studied the ECM of several SnPb and lead free solders in distilled water. For Sn-Pb systems Pb was the migrating species, for Sn-Ag and Sn-Ag-Cu alloys Sn migrates and for Sn-Zn-Bi systems both Sn and Zn was found to migrate. Authors suggest that the important factors influencing ECM migration are metal dissolution at the anode and ionic transport through the solution. Metal dissolution is closely related to the standard potential of the involved metals and ionic transport is related to the solubility product of metal oxides/hydroxides.

Previous works by the present authors [10-12] showed that during ECM of tin, appearance, resistance, and structure of dendrite was a function of the chemistry of the electrolyte and potential bias. It has been reported that the morphology of the dendrite changes with current density [13,14] and metal ion concentration [5]. Increased tin dissolution due to increased potential bias or aggressiveness of the solution has more chance to produce a dendrite mixed with oxides of the migration species. Resistance of the dendrite also change as the morphology and

composition varies [10]. However, until now no attempt has been made in the literature on looking into the detailed morphology and microstructure of tin dendrites formed during ECM.

In this paper the macro, micro, and nano-scale morphology and microstructure of tin dendrites formed during ECM was investigated using various levels of microscopic technique namely Optical microscopy, Scanning Electron Microscopy (SEM), and Transmission Electron Microscopy (TEM). Two samples with dendrites grown in 10 ppm NaCl electrolyte at two different potential biases, namely 5 and 12V DC where used as the dendrites for detailed investigation.

6.2 MATERIALS AND METHODS

6.2.1 ELECTRONIC COMPONENT USED FOR INVESTIGATION:

The electronic component used for investigation in this work is a commercially available 10kΩ Ceramic Chip Resistor (CCR) size 0805. The dimension of the chip resistor is: 2.0x1.2x0.45 mm and end terminals consist of Sn 2 wt. % Pb. Detailed analysis of the materials make-up of the chip resistor is found in Minzari et al [10].

6.2.2 ECM TESTING USING SINGLE COMPONENT ELECTROCHEMICAL MIGRATION (SCECM) SET UP:

The SCECM set up [10] consists of a sample holder having two tiny adjustable probes, which acts as connections to each end of the components, in this case a ceramic chip resistor. The probes are covered with silicone rubber, which is penetrated by the probe when a load is applied, thereby allowing electrical contact while at the same time providing corrosion protection to the probes. The SCECM holders are shown in Figure 6.2, where three holders are used in order for simultaneous experiments using a multichannel potentiostat.

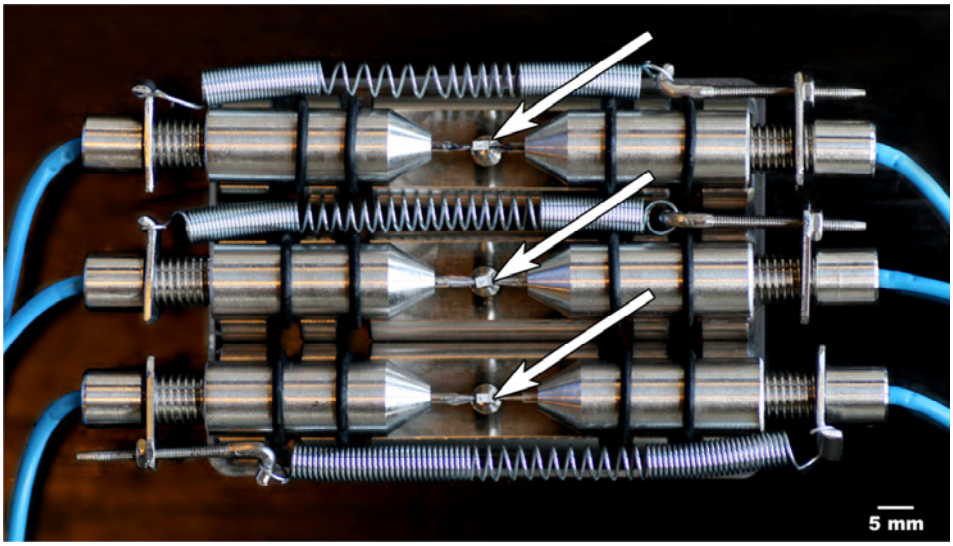

Figure 6.2: Three SCECM holders allowing simultaneous experiments on three components using a multichannel potentiostat. White arrows show the CCR components.

A droplet of approx. 2µL of 10 ppm NaCl (prepared using analytical grade chemical and de-ionized water) electrolyte was added on to the surface of the resistor and required DC bias was applied between the two electrodes of the component. Simultaneously, a time lapse video recording is started for in-situ videoing of the migration sequence.

Experiments were conducted on the bottom side of the CCR, due to the better colour contrast between the dendrite and the white Al_2O_3 substrate of the chip resistor, which facilitates in-situ visual documentation of dendrite formation.

Current flowing through the CCR and electrolyte layer was measured as a function of time using a potentiostat (Biologic VSP multichannel potentiostat, Bio-Logic Instruments, France, having 0-20V compliance voltage) until a dendrite was observed to bridge the cathode and anode, and a short circuit (large increase) in the current was observed. At this stage, the potential bias was manually switched off and the specimen was taken for subsequent SEM or TEM analysis as described below. TEM grids used were 300 mesh Cu grids with Lacey carbon film (Agar Scientific, Essex, UK).

6.2.3 *PREPARATION OF SAMPLES FOR TRANSMISSION AND SCANNING ELECTRON MICROSCOPY:*

Usual methods used for TEM sample preparation such as Focussed Ion Beam (FIB) and ultramicrotomy of dendrites cast in epoxy was attempted, however, it was not useful due to the very fragile nature of the dendritic structure and poor adhesion between dendrite and epoxy matrix. However, in this investigation a simple method was adopted in which the dendrite was carefully transferred on to the copper grid directly after the ECM experiments. Since the dendrite thickness was at nano-meter scale, it was found that it could be directly used for the TEM analysis without any post sample preparation procedure. In order to do this, the potential bias was switched off and the dendrite was then transferred on to the TEM grid by placing it over a piece of filter paper, and the resistor was then placed on the grid with the dendrite facing the grid surface (see Figure 6.3). Fragmentation of the dendrite could not be avoided during this process; however, this method provides parts of dendrites which can be directly observable with the TEM. The TEM microstructures results presented in this paper are therefore from areas that were found to be representative from the fragments observed, but its exact position on the overall dendrite could not be established.

In order to get better overview of the change in microstructure at the various parts of the dendrite, conventional SEM on similarly exposed samples with dendrites was performed. The SEM samples were prepared similarly to the TEM samples, where the potential bias was switched off immediately after the dendrite was seen to form a short circuit of the electrodes. After this, the electrolyte was left to evaporate from the component surface by exposure to ambient conditions and the sample was then mounted to the SEM sample holder.

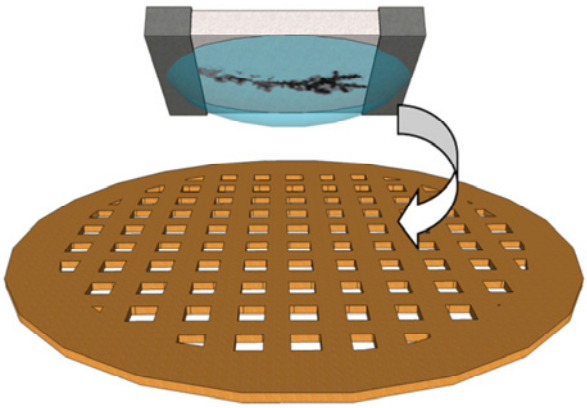

Figure 6.3: Sketch illustrating the transfer of dendrite fragments to the TEM grid.

6.2.4 INSTRUMENTS:

SEM analysis was performed using a Zeiss Ultra55 Scanning Electron Microscope. TEM analysis was performed using a Jeol JEM-3000F Field Emission Electron Microscope operated at 300kV with equipped with Oxford instruments EDS analysis.

6.2.5 ELECTRON DIFFRACTION IN TEM:

All CBED convergent beam electron diffractions were obtained using 80 cm camera length. Calculations of indices were done using “EMS on line” software, Centre Interdépartemental de Microscopie Electronique, EPFL, Lausanne.

6.3 RESULTS

Figure 6.4 shows the overall the morphology of the dendrite formed during the ECM experiments in 10ppm NaCl solutions at 5V and 12V bias for SEM and TEM observations. These pictures were extracted from the in-situ video of the ECM experiment corresponding to the time at which the experiment was stopped. For all the images shown throughout this paper, except for the TEM images, the cathode is on the right and the anode is on the left. The dendrites grown at 5V appear to be more branched than those grown at 12V. The 5V TEM sample is seen to have two contact points for the dendrites to the anode, whereas the rest of the samples only have one point of contact. The two branches of the 5V TEM sample grew

simultaneously and reached the anode at the same time. The 12V TEM sample is seen to be slightly covered by a blurry light grey precipitate while no precipitates can be observed on the 12V SEM sample. The 12V TEM sample was seen to encounter a period where the dendrite growth was unstable and stopped at periods, and the bulky dendrite area on the component at a distance of about 2/3 from the cathode corresponds to this, where the dendrite partly collapsed.

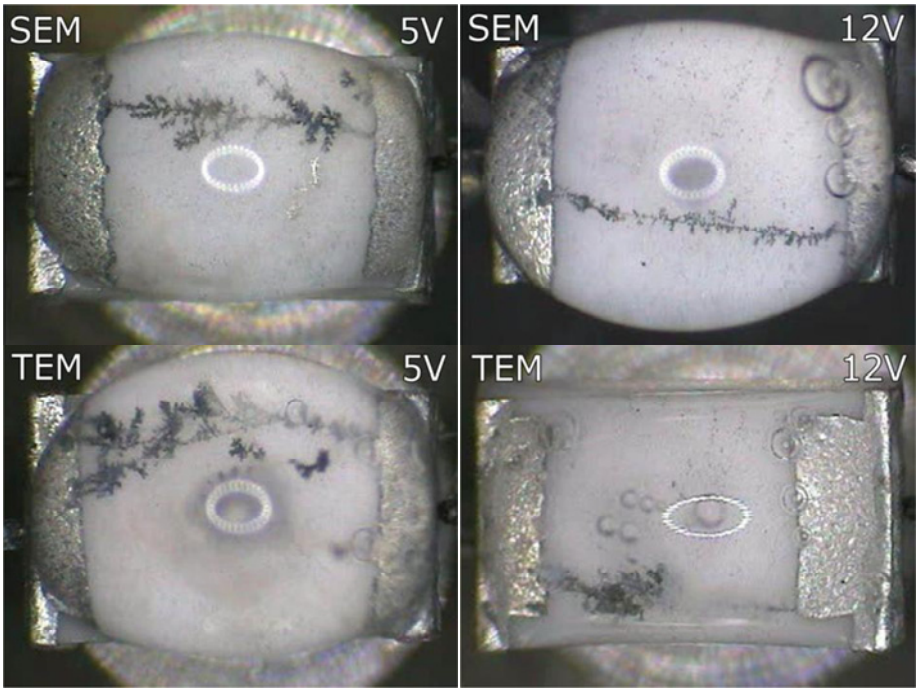

Figure 6.4: Images extracted from in-situ video recording at a time corresponding to the potential bias was switched off at 5 and 12V (Legends SEM and TEM means that the respective samples subsequently use for SEM/TEM analysis). In all images, anode is at the left and cathode at the right.

The current-time curves resulting from the above experiments are shown in Figure 6.5.

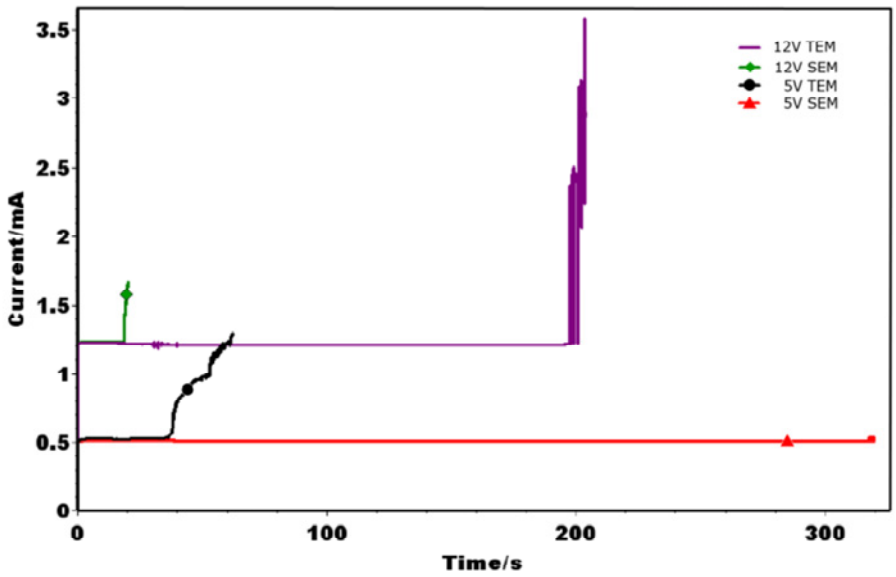

Figure 6.5: Current-Time curves from the ECM experiments 5 and 12V corresponding to components shown in Figure 6.4.

The curves in Figure 6.5 shows the sudden spikes in the current as the dendrite bridge forms between anode and cathode resulting in short circuit of the resistor. The time required for dendrite bridging was not same for similar sets of experiments for e.g. at 5V or 12V. However, not all experimental results are directly accessible from the current-time curve alone, but needs to be compared with the in-situ video for e.g. the dendrite growth time (the time interval required for the dendrite to bridge the gap starting from a visible nucleation of the dendrite was observed at the cathode and until it reaches the anode) cannot be seen on the curves. Figure 6.6 shows the important parameters that could be deduced from the current-time curve in combination with time lapse video for better understanding of the dendrite formation. As an example, $t_{nucleus}$ is the time where the dendrite is first visually observed as a nucleus at the cathode (see arrow and circle in Figure 6.6). The notation t_{short} is the time at which the dendrite has short circuited the two electrodes. Rest of the time interval in the curve is named as $\Delta t_{growth,}$ which indicate the time interval the dendrite was allowed to grow after shorting. Similarly I_{MAX} is the maximum current observed in the experiment, but as this value is influenced by how long the manual process of stopping the potential bias takes,

the current after 2 seconds of the short circuit, I_2, is used for comparison. The base current running through the resistive element in Figure 6.6 is 0.500 mA. A current level above this value corresponds to the current from the electrochemical reactions and, after shorting, the current through the dendrite which can be regarded as a resistance in parallel coupling to the resistive element.

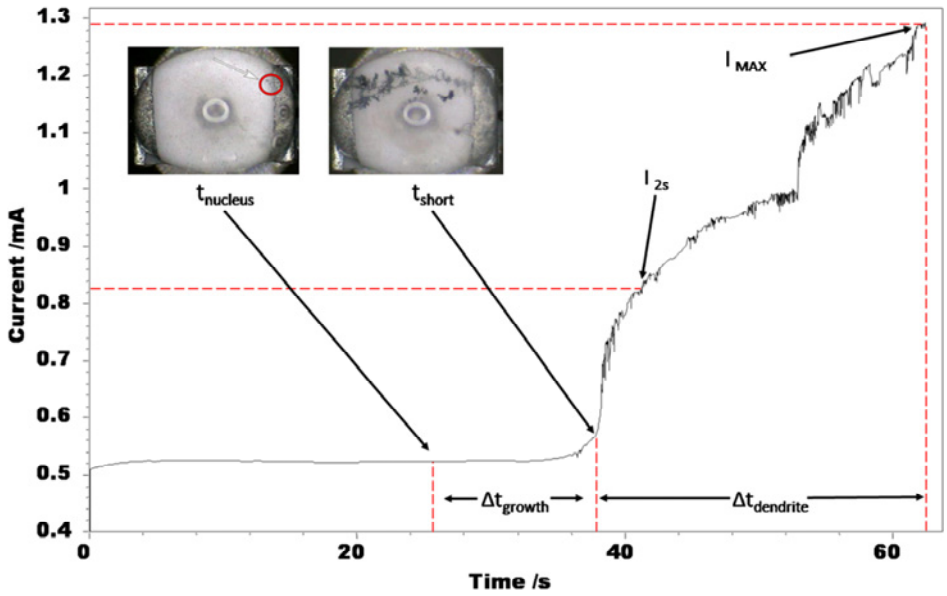

Figure 6.6: Current-time curve from the 5V TEM experiment showing important parameters that could be extracted together with in-situ video.

Table 1 shows the values of the mentioned parameters for various experiments for comparison. The value $R_{dendrite}$ is the minimum resistance measured through the dendrite and is calculated using the maximum current measured, I_{MAX} using simple Ohms law relation where the current passes though the dendrite in parallel with the resistive element which has a known resistance, in this case 10kΩ. The difference in the dendrite resistance is related to the varying time taken for the manual removal of the potential bias. The values should therefore not be compared from a quantitative point of view, but it provides a way to differentiate between dendrites used for microstructural investigation. For better comparison of the dendrite

resistance, the dendrite resistance corresponding to 2 seconds after short circuit, R_{2s} was calculated.

Table 6.1: Various experimental data related to dendrites extracted using current-time curves and in-situ video recording.

Sample:	$t_{nucleus}$ (s)	t_{short} (s)	Δt_{growth} (s)	R_{2s} (kΩ)	$R_{dendrite}$ (kΩ)
5V SEM	18	317	299	13.2	13.2
5V TEM	27	36	9	17.4	6.33
12V SEM	14	18	4	25.5	25.5
12V TEM	8	197	189	9.54	5.04

The t_{short} values showed a large scatter compared to the time for nucleation, showing that the dendrite growth is very much influenced by the chemistry and physical disturbances in the solution. Despite the large fluctuations in the growth intervals, the overall current through the dendrite immediately after the shorting (2 seconds after) was almost uniform and correspondingly the dendrite resistance at this point is almost in a similar range. The final resistance, $R_{dendrite}$, depends on further growth which is difficult to predict, though the resistances were still in the kilo Ohm range. The 5V SEM and 12V TEM samples had a rather long growth interval, which in the time-lapse video was observed as periods where the growth seemed unstable, leading to collapsing of the dendrite front or temporary halts in the growth. However, there does not seem to be a correlation between the growth interval and the resistance of the dendrite.

6.3.1 SEM ANALYSIS:

Figure 6.7 and 8 show the SEM images from various areas of the dendrite for 5 and 12V samples respectively. Images have been acquired at various sites along the dendrite growth direction, labelled A1-A4 where A1 is near the cathode and A4 is near the anode.

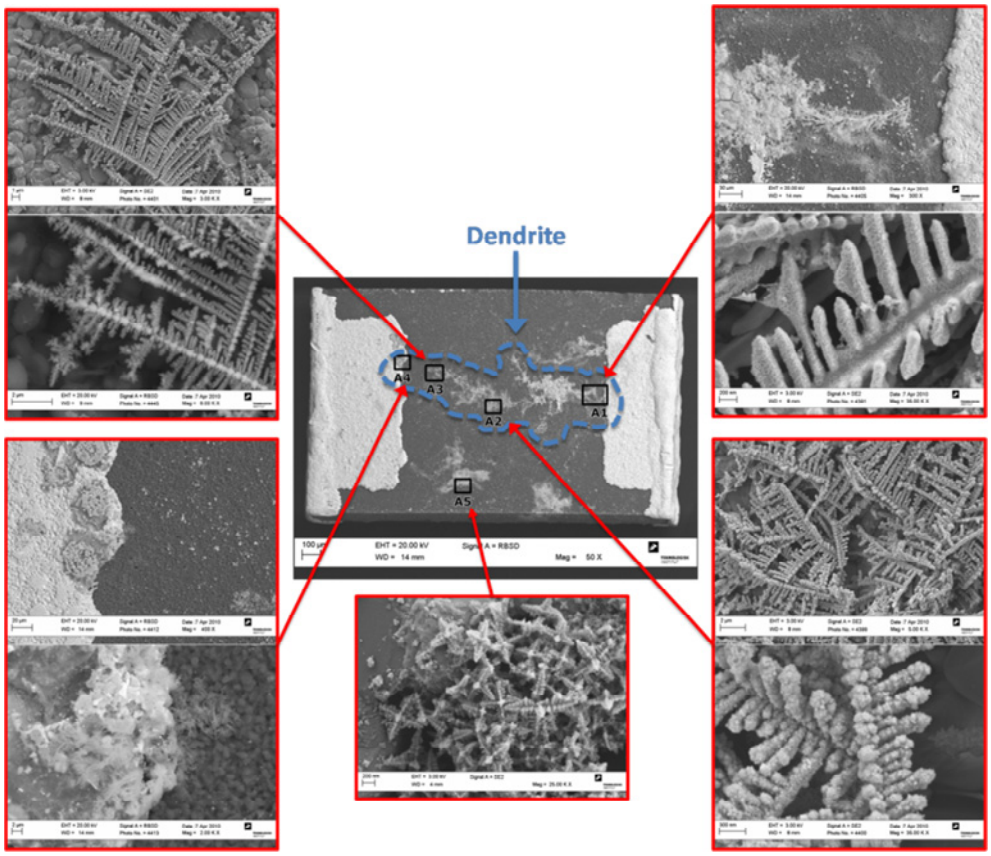

Figure 6.7: SEM images 5V sample at various sites of the dendrite. (Anode is on the left and cathode is on the right side). Image from the site labelled A5 is from an agglomeration of oxides, and has no dendrite.

Picture in Figure 6.7 for the 5V sample reveals that the dendrite has contracted during the evaporation of the electrolyte, so that the dendrite has no contact at the cathode and anode interfaces in the ex-situ observations. The dendrite near the cathode (A1) is seen to grow within a bulky agglomeration of oxides, and the dendrite appears have a smooth surface texture. Correspondingly, at the A2 and A3 areas of the dendrite is more bulky and has a rougher surface. The contrast difference observed on the high magnification image on A3 suggests that the dendrites at these areas are having a more heterogeneous material distribution. At A2, the dendrite structure appears dense but rather irregular, while at the A3 site the growth is clearly directed towards the anode, and secondary, tertiary, or more branches grow from the main branch. At the anode interface (A4), corroded areas

of the anode is seen as the dark areas on the overview image, and a few dendrite fragments were found towards the corroded areas, though the main dendrite has retracted during the evaporation of the electrolyte.

At the A5 site, an agglomeration of small particles are seen which appear to be crystalline due to their symmetric geometry. Such particles were found to consist of tin oxides, most likely in a hydrated form (see analysis in the TEM section). Same type of particles was found at several places on the specimen surface, both around the dendrite, as agglomerations across the specimen surface and on the TEM samples.

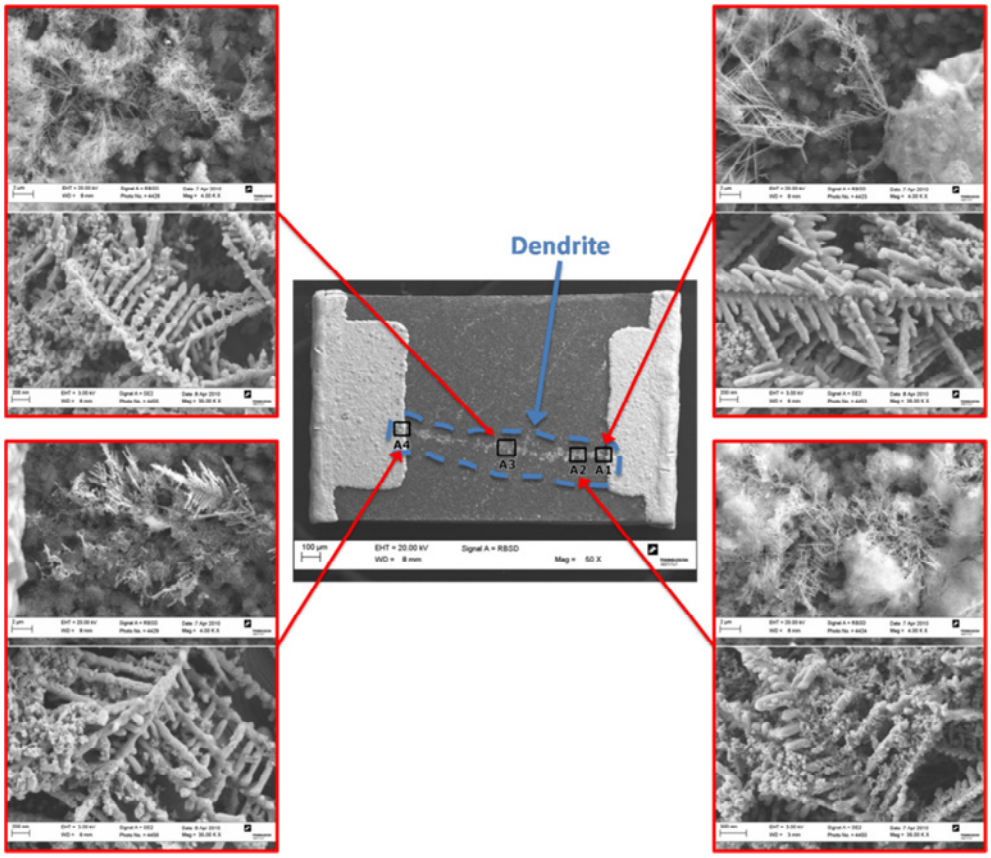

Figure 6.8: SEM images from 12V sample at various sites of the dendrite. (Anode is on the left and cathode is on the right side).

Though the dendrite of the 12V SEM sample appeared rather straight and with less braches in the optical image on Figure 6.4, the SEM images presented in Figure

6.8 shows that it consist of a web of many branches that grow within a cloudy layers of the hydroxide. At the dendrite initiation/nucleation site, A1, it is seen that few dendrite branches makes the actual contact from the cathode, and these branches rapidly spreads into a network of dendritic branches. The dendrite branch near the cathode appears dense with small closely spaced side branches. Area A2 is not far from the cathode while A3 is approximately at the middle of the dendrite along the length direction. At both sites, the dendrite network is seen to grow within the bulky hydroxide layers. The dendrites are dense and are partly covered with the precipitates of hydroxide. At areas A1 and A2, the dendrites were in general observed to consist of mainly long primary branches with relatively short secondary branches and few ternary branches growing out. Dendrites around A3 seemed more unordered and very dense while near the anode at A4, more directionality towards the anode was seen. All along the length of the dendrite, oxides was seen to closely embed the dendritic structure unlike in the case of 5V potential bias.

6.3.2 TEM ANALYSIS:

The TEM micrographs of dendrites from the 5V and 12V samples are presented in Figure 6.9. Images A and B are from the 5V sample and images C and D are from the 12V sample. Image A shows an overview of a 5V dendrite fragment. A number of dendrite branches are seen with side branches that grow with varying angles to the main branch. On the side-branches, some growth is seen parallel to the main branch, indicating that the growth of the dendrite was towards the bottom right of the image. The square on image A shows the area where the magnified view of the dendrite was acquired, which is presented in image B. Image B shows that the dendrite appears to have a rather homogenous overall material distribution with small particles of darker contrast incorporated. Thickness fringes are seen at several places, and side-branches protruding out from the main dendrite branch are having a different contrast due to the 3 dimensional structure. Image C shows an overview of a dendrite fragment on the 12V sample, and image D is the magnified view of the area marked by a square on image C. This dendrite is seen to have a rougher surface structure than the one seen on the 5V sample in Figure

6.9B. The numbers on images B and D show the location of EDS measurements which are presented in Table 6.2.

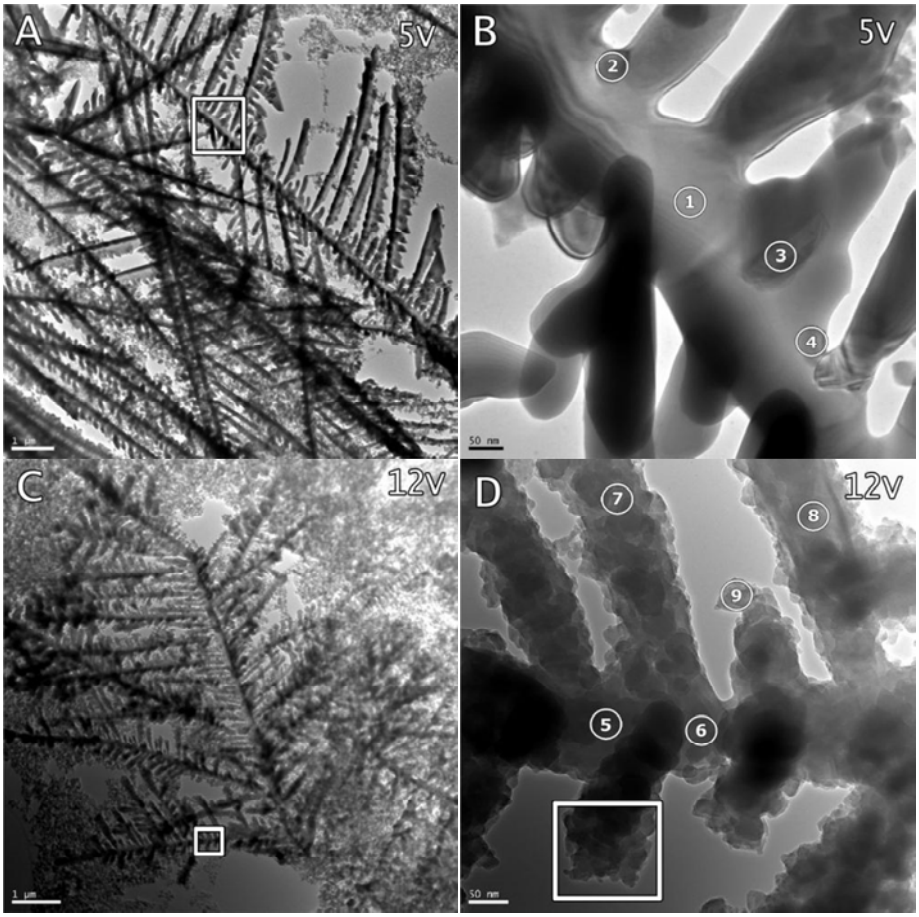

Figure 6.9: TEM micrographs showing A) an overview image of the dendrite fragment from the 5V sample, B) Magnified view of the square area on image A, C) Overview image of 12V sample, and D) Magnified view of the square area on image C. The square on image D shows the origin of the image in Figure 6.13. Numbered labels on image B and D show the location of EDS measurements, presented in Table 6.2.

The EDS spectra for the 5 and 12V samples are presented in Table 6.2. The spectra 1-4 are from the 5V sample (see labels on Figure 6.9B) and shows that the dendrite consists mainly of tin and various amounts of lead, possibly with small amounts of oxygen. Spectrum 1 is seen to consist almost entirely of tin while spectra 2-4 are on the dark coloured particles which are seen to have high amounts of lead. Analysis at several places on the main body of the dendritic

structure shows a composition similar to the spectrum 1. On the 12V sample, the dark coloured particles could not be observed, probably due to the rough surface structure. The EDS spectra (spectra 5-9) are seen to have rather low contents of lead. The oxygen content is generally higher on the 12V sample than on the 5V sample, and especially spectrum 9 which was obtained on the edge of the dendrite contain high levels of oxygen.

Table 6.2: Elemental composition of the dendrites from EDS analysis at places marked in Figure 6.9B and D. All results are in At.%

Sample	Spectrum	O	Sn	Pb
5V	Spectrum 1	4	95	1
	Spectrum 2	2	79	19
	Spectrum 3	3	15	82
	Spectrum 4	3	58	39
12V	Spectrum 5	3	97	0
	Spectrum 6	7	92	1
	Spectrum 7	15	84	1
	Spectrum 8	2	97	1
	Spectrum 9	46	54	0

Electron diffraction patterns at three different zone axes were acquired on each of the 5 and 12V samples and are presented in Figure 6.10. The point of analysis was at the center of the main dendrite branch which was at spots 1 and 5 in Figure 6.9 for the 5 and 12V samples respectively. The diffraction patterns clearly show crystalline nature of the dendrite at these sites, and diffraction patterns A-C have been indexed to the [5,3,3], [1,1,1] and [3,5,1] zone axes while D-F have been indexed to the [3,1,7], [2,1,5] and [1,1,3] zone axes respectively, using the tetragonal structure of metallic tin with the lattice parameters a= 0.5820nm and c= 0.3175nm. The high magnification image presented in Figure 6.11 shows the highly ordered crystalline structure of the tin dendrite for the 5V sample. The image was acquired at the spot labelled 1 in Figure 6.9B and oriented along the [5,3,3] zone axis. The $(0\bar{1}0)$ planes of metallic tin are clearly seen on the image revealing a highly ordered microstructure. In order to assess whether the dendrite structure is single- or polycrystalline, dark- and bright field images were obtained on the 12V

sample (Figure 6.12), using an aperture that only allowed electrons scattered along the [1,1,3] zone axis (see Figure 6.10F) to pass to the detector.

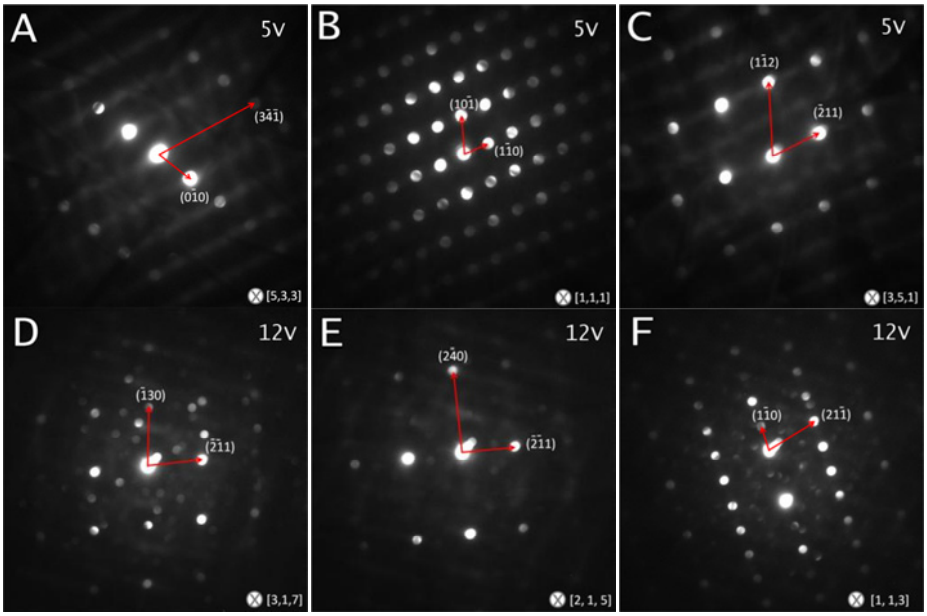

Figure 6.10: Electron diffraction patterns from dendrites: A-C: 5V sample and D-F: 12V sample. A-C was obtained at spot 1 on Figure 6.9B and D-F was acquired at spot 5 on Figure 6.9D. Patterns were obtained by tilting the specimens at three different angles.

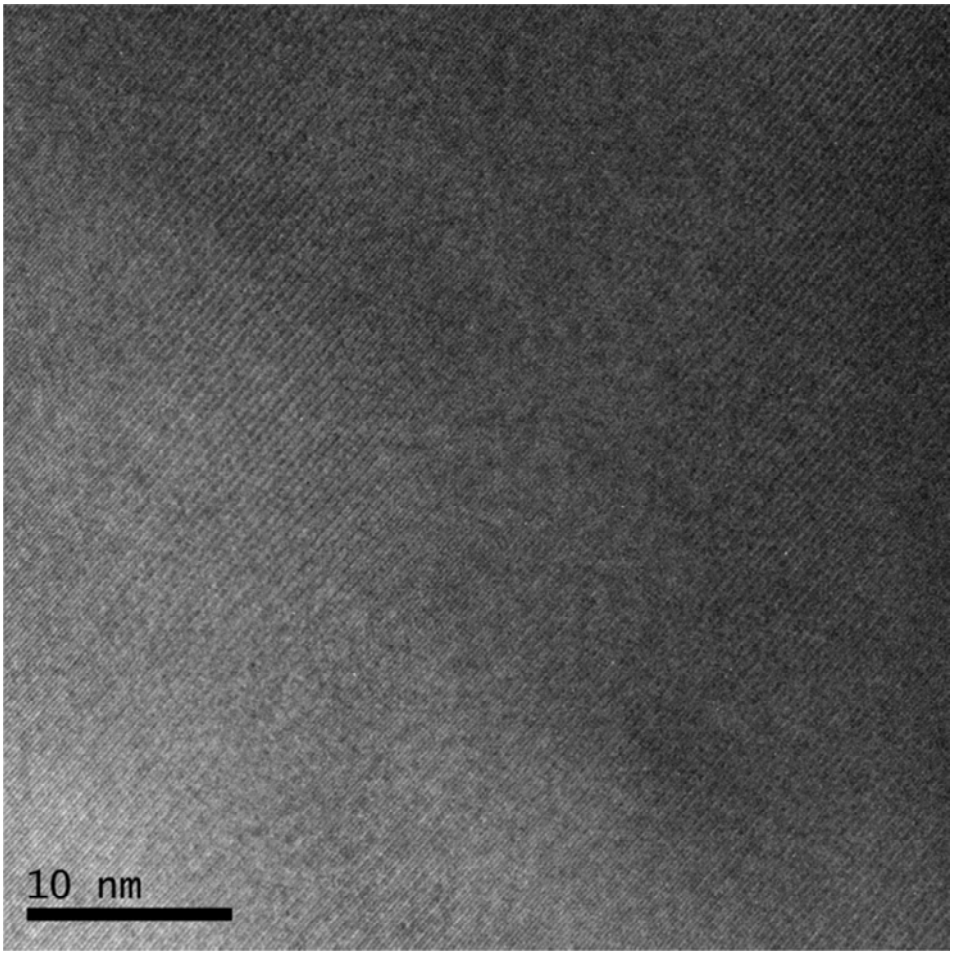

Figure 6.11: High magnification image showing highly ordered crystal planes of tin on the dendrite along the [5,3,3] zone axis (see diffraction pattern in Figure 6.10A. Image was acquired at the spot labelled 1 on Figure 6.9B (5V sample)).

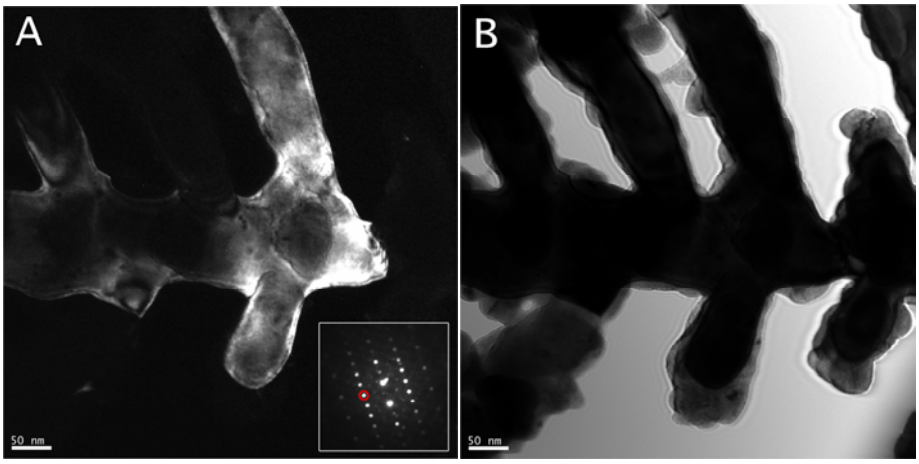

Figure 6.12: A) Dark field and B) bright field images, obtained from the $(\bar{2}1\bar{1})$ direction as indicated by the red circle on the diffraction pattern (insert in image A. Orientation is along the [1,1,3] zone axis (see Figure 6.10F)). Dendrite branch is from the location shown in Figure 6.9D (12V sample).

Magnification of the end of a dendrite side branch (area marked by a square on Figure 6.9D) is presented in Figure 6.13. The origin of the site is marked by the square in Figure 6.9D. The side branch is seen to consist of a core of dark contrast and an outer layer of bright contrast. Two EDS spot measurements were performed at the core and outer layer (see Table 6.3), which shows that the outer layer has higher oxygen content. Image B is a cut-out of image A showing nanocrystalline nature of the outer layer. The electron diffraction pattern on image B (insert) was acquired on the oxide layer and shows a mixture of crystalline pattern and ring-like nanocrystalline pattern.

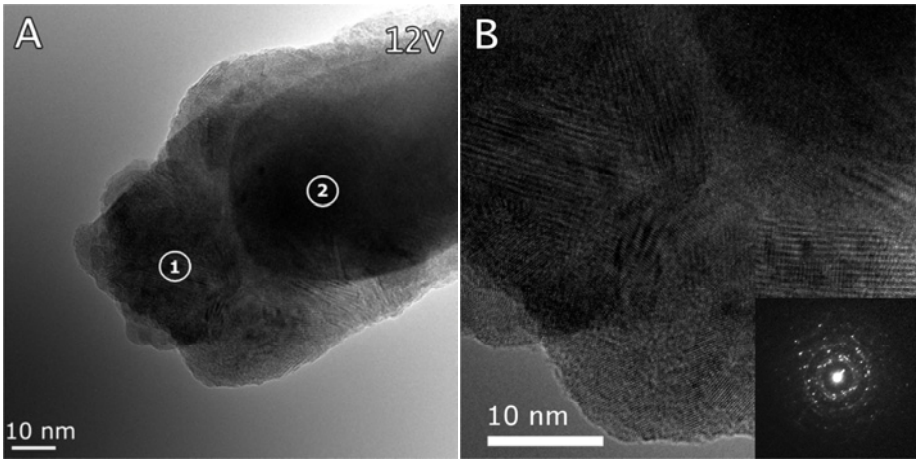

Figure 6.13: A) TEM micrograph of the end of a dendrite side branch on 12V sample, showing an inner core and an outer layer which is more electron transparent and B) Cut-out of image A showing the nanocrystalline structure of the outer layer with electron diffraction pattern (insert).

Table 6.3: Elemental composition at the spots marked in Figure 6.13A. All results are in At.%

Spectrum	O	Sn	Pb
Spectrum 1	25	74	1
Spectrum 2	14	85	1

Agglomerations of small particles were found dispersed around the TEM grid on both 5 and 12V samples. Particles having symmetrical shape (Figure 6.14A insert) as well as more irregular bulky particles (Figure 6.14B insert) were observed on both samples. EDS analysis at several places on many particles showed similar results, with oxygen contents ranging from 40-50 at.%, tin 50-60 at.% and lead 0-2 at.%. Both types of particles also showed similar nanocrystalline structure with ring-like electron diffraction patterns as shown in Figure 6.14A and B.

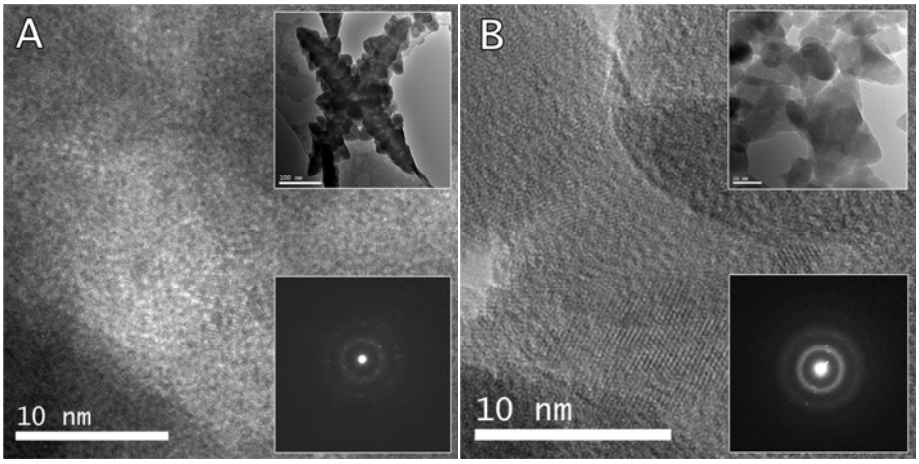

Figure 6.14: TEM images two types of particles seen together with dendrites on 12V sample A) Symmetrically shaped particle and B) irregular bulky particles.

6.3.3 DISCUSSION

The microstructural analysis of the dendrites formed during ECM presented in this paper clearly shows that the main structure of the dendrite corresponds to that of metallic tin irrespective of the voltage used, however with significant difference in surface morphology and composition due to the incorporation of the oxide. It is clear that the chemistry of the solution and stability of tin ions determines the formation of tin hydroxide species in the micro-volumes of environment and incorporation into the dendrite structure. The electrochemical migration mechanism of tin is complex as strong pH gradients will form within the micro-volume electrolyte due to the electrode reactions involving dissociation of water and hydrolysis of the tin ions. Hydrolysis of tin ions and anodic dissociation of water will produce hydrogen ions creating an acidic pH at the anode extending towards the cathode, while the opposite happens at the cathode (alkaline pH) due to cathodic dissociation of water producing hydroxyl ions. A detailed discussion on the electrochemical aspects is beyond the scope this paper and could be found elsewhere [15]. To illustrate this pH change, two micrographs are presented in Figure 6.15 showing the evolution of localized pH changes during application of potential bias in chloride solution containing universal pH indicator. At the anode, pH is shifted towards acidic values, while at the cathode pH shift to alkaline values.

The local pH conditions are also seen to rapidly change within the droplet and pH gradients are affected by convection from gas evolution and changes in the kinetics of the electrochemical reactions with time.

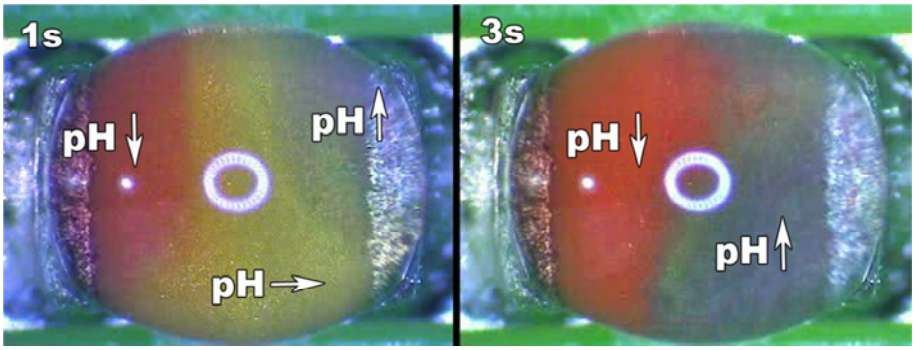

Figure 6.15: Example of pH gradient formation on a chip component under 12V at 1 and 3 seconds after potential was applied (solution consist of approx. 30 ppm NaCl and 30 vol.% pH indicator). Indication for low, neutral and high pH is illustrated by the arrows..

Tin ions are soluble at acidic pH conditions as Sn^{2+}/Sn^{4+} ions and in highly alkaline conditions as stannate ions [16]. However, in the neutral region Sn ions will be precipitated as $Sn(OH)_4$ [16]. Applying thermodynamic stability pattern [16] to the observation in Figure 6.15 shows that the tin ions could exists in all the three forms in the solution depending on the pH and tin ion concentration on the component surface, and this determines the composition of the dendrite. Resistance of the dendrite and therefore the shorting current varies with (i) the chemistry of the solution that determines the stability of tin ions and (ii) bias voltage which determines the amount of tin dissolution into the micro-volumes of environment. In our earlier investigation, based on averages from several experiments, it was found that the dendrites grown at higher potentials (12V) generally had lower resistance than those at lower potential (3V), despite that the dendrites at high potentials generally appeared less branched [10]. This was surprising because the structure having more branches should intuitively conduct more current if each branch is regarded as a very small wire of tin. If one assumes that the dendrite is composed of a tin wire of a diameter similar to that observed on a dendrite branch (magnitude of 100 nm), resistance should be much less than the resistance measured for dendrite at all conditions investigated [10]. This lead to the hypothesis, that the dendrite structure could be a mixture of metallic tin and tin hydroxides though no

clear conclusions could be drawn from the SEM work that was done, and no literature on the detailed microstructure of tin dendrites are available. The diffraction patterns in Figure 6.10 shows that the main body of the dendritic structure consists of metallic tin for both the 5 and 12V samples. The EDS measurements (spectra 1-8 in Table 6.2) show low oxygen content which support this, while the crust-like layer surrounding the metallic core on the 12V sample is most likely the hydrated oxides of tin with small amounts of lead (spectrum 9 in Table 6.2 and spectrum 1 in Table 6.3). It should be noticed that the quantification of oxygen by TEM at 300kV acceleration voltage is unreliable, and the oxygen contents should therefore not be considered exact. Therefore, the tin to oxygen ratio from these analyses is not to be used to establish the nature of the tin hydroxides observed. Both the tin oxide particles and tin oxide layers on the dendrites which were observed in the TEM showed a nanocrystalline crystal structure. This could be from recrystallization due to dehydration of tin hydroxide ex-situ. The electron diffraction patterns shown as inserts in Figure 6.13 and 14 could not be indexed to neither metallic tin nor any of the tin oxides/hydroxides that was available to the authors from diffraction databases. The dehydration processes of tin oxides are complicated [17,18], and detailed analysis of the tin oxides will not be attempted here. The diffraction pattern of the oxide crust surrounding the metallic core in Figure 6.13B (insert) showed partly nano crystalline pattern as well as indication of some singe crystalline orientation. This could be due to a large crystal grain dominating at the spot of acquisition. By overlay of the diffraction patterns obtained from both the oxide particles and the oxide surrounding the metallic core (see Figure 6.16) it is seen that the ring patterns are of similar size, and therefore it seems that one type of oxide is dominant on the surface.

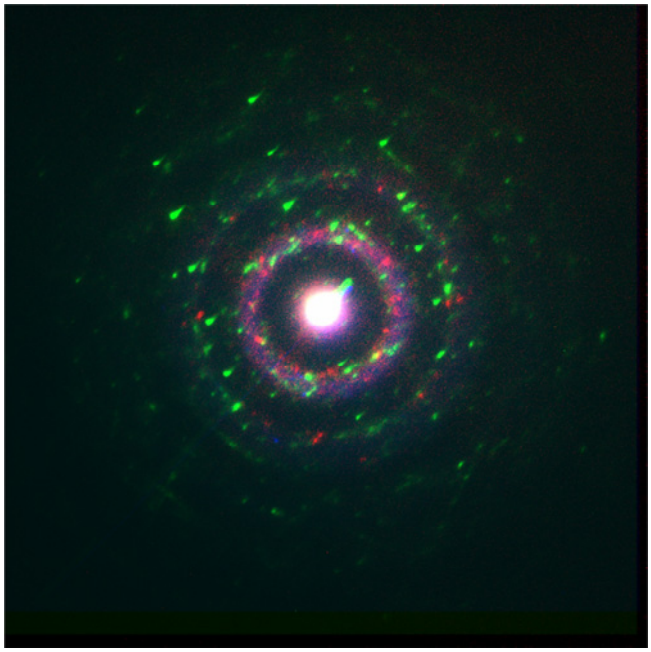

Figure 6.16: Overlay of diffraction patterns from tin oxide analysis. Green is Figure 6.13B, Red is Figure 6.14A and Blue is Figure 6.14B

The dark field image (Figure 6.12A) shows that the crystal orientation extends to a large part of the dendrite, including some but not all of the side branches, while the bright field image (Figure 6.12B) shows that the outer oxide layer with the metallic core inside. There is an abrupt ending of the crystal orientation at the right side of the bright field image, even though the main branch of the dendrite is seen to continue on the dark field image and on Figure 6.9D. This suggests that the defects exist along the dendrite growth direction, and the dendrite structure is not single crystalline along its entire length. During the growth of the dendrite, rearrangements of the structure are often seen from the time-lapse video, which could probably be due to the local changes in the concentration of chemical species or of the electric field. Such changes could provide stresses within the dendritic structure, thereby causing deformations in the crystal structure. The areas investigated on the 5V sample appear metallic with clearly visible lead containing inter-metallic particles embedded, while the 12V sample was found to consist of a metallic core having a structure similar to the 5V sample, but surrounded by an oxide layer.

The SEM images of the 5 and 12V samples show that the dendrite structure is heterogeneous along the growth direction. On the 5V SEM sample, areas are found having a rough and heterogeneous surface structure, which could be similar to the features that were observed on the 12V TEM sample. As these features are localized, it is likely that the rough/oxidized surface is due to the unstable growth conditions. Both the 5V SEM and the 12V TEM samples indeed had long growth times, as seen in Table 6.1. The difference in the structural features observed in the TEM for the 5 and 12V samples are therefore more likely to be related to the chemical/electrochemical conditions in the micro-volume of electrolyte during the growth rather than differences related to the applied potential bias.

The resistances of the dendrites from all experiments (Table 6.1) are higher than the resistance that could be expected from a metallic tin wire which connects the two electrodes (a purely metallic tin wire of 200 nm diameter and a length of 1mm should have a resistance in the magnitude of 3.5kΩ). As the dendrites have several branches for conducting the current, the resistance should be expected to be less than that of the actual tin wire. Although, in the TEM analysis no areas where found that did not show a metallic core (though the fraction of sample that is analyzed in the TEM is small), the higher resistance of the dendrite could still be due to the low levels of composition changes of the dendrites and possibly resistance offered by the contact point between the dendrite and the anode. As the dendrite reaches the anode surface, strong electrostatic forces will act on the dendrite which could give the attraction for the contact to occur, while the nature of contact could vary in each case.

6.4 CONCLUSIONS

1. The dendrites grown by the electrochemical migration in this study were found to consist of metallic tin having sections of single crystalline orientation. Electron diffraction patterns at several directions and at several sites was indexed to metallic tin and high magnification images of the main branch of the dendrite showed highly ordered crystalline lattice. Defects in the crystalline structure were found along the main dendritic branch, probably due to rearrangement of the dendritic structure during the growth stage. The dendrites grown at 5V had longer side branches than the dendrites grown at 12V, but no unambiguous differences in the structure could be found from the TEM analysis that could be related to the potential bias.

2. An oxide layer was found to surround the metallic tin core at local areas along the growth direction, which attributed to unstable growth during the electrochemical migration stage. Such oxide containing areas were found on both 5 and 12V specimens and no direct evidence was found that this oxide is affecting the conductivity of the dendrite as metallic core was still observed in the oxidized dendrite.

3. Both symmetrically shaped and bulky tin oxide particles were found dispersed on sample surfaces. The nature of the tin oxide could not be established from the analysis made in the current study, but the electron diffraction patterns showed similar nanocrystalline structure for both types of particles.

ACKNOWLEDGEMENTS

Current research has been conducted as part of the CELCORR consortium. Authors would like to acknowledge the Danish Ministry of Science, Technology and Innovation for the funding, project partners Danfoss A/S, Grundfos A/S, Vestas A/S and PRI-DANA Elektronik A/S, Danish Technological Institute and IPU for their commitment and help. Kathrine Bjørneboe from the Danish Technological Institute, Tåstrup, Denmark is greatly acknowledged for SEM work.

REFERENCES

[1] T. Takemoto, R.M. Latanision, T.W. Eagar, A. Matsunawa, Electrochemical migration tests of solder alloys in pure water, Corrosion Science. 39 (1997) 1415-1430.

[2] A. DerMarderosian, The Electrochemical Migration of Metals, Proc. Int. Society of Hybrid Microelectronics. (1978) 134.

[3] T. Kawanobe, K. Otsuka, Metal migration in electronic components, in: Proceeding of the 32nd Electronic Component Conference, 1982: pp. 220–228.

[4] Y.R. Yoo, Y.S. Kim, Influence of corrosion properties on electrochemical migration susceptibility of SnPb solders for PCBs, Metals and Materials International. 13 (2007) 129–137.

[5] S.L. Meilink, M. Zamanzadeh, G.W. Warren, P. Wynblatt, Modeling the Failure of Electronic Devices by Dendrite Growth in Bulk and Thin Layer Electrolytes, Corrosion. 44 (1988) 644-651.

[6] B. Noh, J. Lee, S. Jung, Effect of surface finish material on printed circuit board for electrochemical migration, Microelectronics Reliability. 48 (2008) 652-656.

[7] S. Lee, M. Jung, H. Lee, T. Kang, Y. Joo, Effect of Bias Voltage on the Electrochemical Migration Behaviors of Sn and Pb, IEEE Trans. Device Mater. Relib. 9 (2009) 483-488.

[8] S. Lee, M. Jung, H. Lee, Y. Joo, Effect of initial anodic dissolution current on the electrochemical migration phenomenon of Sn solder, in: 2009 59th Electronic Components and Technology Conference, San Diego, CA, USA, 2009: pp. 1737-1740.

[9] D.Q. Yu, W. Jillek, E. Schmitt, Electrochemical migration of Sn-Pb and lead free solder alloys under distilled water, Journal of Materials Science: Materials in Electronics. 17 (2006) 219–227.

[10] D. Minzari, M.S. Jellesen, P. Møller, P. Wahlberg, and R. Ambat, "Electrochemical migration on electronic chip resistors in chloride environments," *IEEE Transactions on Device and Materials Reliability*, vol. 9, 2009, pp. 392–402.

[11] M.A. Johnsen, Effect of contamination on electrochemical migration, M. Sc. thesis, Technical University of Denmark, 2009.

[12] R. Ambat, M.S. Jellesen, D. Minzari, U. Rathinavelu, M.A. Johnsen, P. Westermann, Solder flux residues and electrochemical migration failures of electronic devices, in: Proceedings of Eurocorr 2009, Nice, 2009.

[13] M. Zamanzadeh, Y.S. Liu, P. Wynblatt, G.W. Warren, Electrochemical Migration of Copper in Adsorbed Moisture Layers, Corrosion. 45 (1989) 643-648.

[14] G. Wranglén, Dendrites and growth layers in the electrocrystallization of metals, Electrochimica Acta. 2 (1960) 130-143.

[15] D. Minzari, M.S. Jellesen, P. Møller, R. Ambat, On the Electrochemical Migration Mechanism of Tin in Electronics, To Be Submitted to Journal of the Electrochemical Society. (2010).

[16] M. Pourbaix, Atlas of electrochemical equilibria in aqueous solutions, M. Pourbaix, Published 1974 by NACE, 644. (1974).

[17] S. Cho, J. Yu, S. Kang, D. Shih, Oxidation study of pure tin and its alloys via electrochemical reduction analysis, Journal of Electronic Materials. 34 (2005) 635-642.

[18] E.W. Giesekke, H.S. Gutowsky, P. Kirkov, H.A. Laitinen, A proton magnetic resonance and electron diffraction study of the thermal decomposition of tin(IV) hydroxides, Inorganic Chemistry. 6 (1967) 1294-1297.

7 PAPER 3: SOLDER FLUX RESIDUES AND ELECTROCHEMICAL MIGRATION FAILURES OF ELECTRONIC DEVICES

Rajan Ambat, Morten S. Jellesen, Daniel Minzari, Umadevi Rathinavelu, Marianna A. K. Johnsen, Peter Westermann, and Per Møller

Department of Mechanical Engineering, Technical University of Denmark, Denmark, Email: ram@mek.dtu.dk

ABSTRACT

Corrosion reliability is a serious issue today for electronic devices, components, and bare printed circuit boards (PCBs) due to factors such as miniaturization, globalized manufacturing practices, and global usage. The result is reduced life span for electronic products and heavy economic loss due to failures. Miniaturization at all levels is one of the key factors reducing corrosion reliability. Over the last 10 years, size of the electronics has been reduced by over 70%. For flip chip ICs, miniaturization amounts to ~ 90%. The closer spacing increases the electric field (E = V/d), which makes corrosion cell formation easier during local condensation under humid environments. Process related residues (contamination) on PCB surfaces results from all stages of manufacturing process starting from base PCB production to components mounting, soldering, inspection and testing, device assembly, and packing are all process that will have great influence on corrosion. A particularly important factor is the residue resulting from no clean flux especially from the wave soldering process as this is one of the step in the PCB manufacturing processes. Such residues can easily absorb water under humid conditions, and can accelerate the corrosion problems by providing conducting ions, participating in corrosion reaction, or as a site for entrapment of dust.

This paper focuses on mechanistic investigation of the role of no-clean flux residues on electrochemical migration failures, which is a dominant corrosion failure mode in electronic devices. During electrochemical migration, a suitable metal ion such as Sn, Pb, Cu etc. dissolves in to the condensed water layer from a positively biased point on a PCB and migrates through the water layer to a nearby negatively charged part to deposit there in the form of dendrites. As it progress, dendrites will bridge the gap between two points, which will lead to an electric short. This paper investigate in detail how no-clean flux residues are present on the PCBs, their composition, morphology, interaction with humid environments, and their electrochemical behaviour in aqueous environments. A novel Single Component Electrochemical Migration set up (SCECM) was used for investigating electrochemical migration under various flux residue conditions on tiny electronic components, while spectroscopic studies and SEM/EDX were used for understanding the residue composition and morphology. Detailed analysis of the dendrite morphology and composition was carried out using FEG-SEM. Results shows that the organic acids in the flux residue can some time act as corrosion inhibitors to reduce migration problem, however the exact effect depends

on combination of factors such as amount, morphology, and presence of other ions such as chlorides. Composition of the dendrite, and therefore its conductivity was a function of stability of the corresponding metal ions in the respective environments.

Key words: Electronic corrosion, solder flux, electrochemical migration, capacitor

7.1 INTRODUCTION

The miniaturization of electronic systems and the explosive increase in their usage has augmented the risk of corrosion in electronics devices. Problems are compounded by the fact that these systems are built by multi-material combinations and reasons such as process related residues, bias voltage, and unpredictable user environment. Demand for miniaturized device has resulted in higher density packing with reduction in the component size, closer spacing, and thinner metallic parts. Material loss of the order of nano-grams can cause reliability problems [1] in such cases especially with the present day use of the electronics in all walks of life.

Over the last 10 years, the pattern of electronics usage has been considerably changed due to the increased use of electronically controlled machines, use of more electronics in the transportation sector, and rapid growth in the consumer electronics. The consumer electronics sector is one area where the user environment is highly unpredictable. One such example is the wide-spread use of cell phones [2]. Global manufacturing net-works with unpredictable component supply chain and unclean components are another factor contributing to the corrosion reliability.

Miniaturization at all levels is one of the key factors reducing environmental reliability. Over the last 10 years, size of the electronics has been reduced by over 70%. For the flip chip ICs, miniaturization amounts to ~ 90%. The closer spacing increases the electric field (E = V/d), which makes the corrosion cell formation easy during local condensation under humid environments.

The average size of dew droplet formation on surfaces at different temperatures varies from 20 – 50 μm at about 50% RH [3]. Hence smaller distance on the PCBs makes it easy for the local electrochemical cell to form. Figure 7.1 shows a

schematic of how a tiny water droplet, electric field and miniaturization can create a local corrosion cell on a PCB. Condensing may result in functional failures caused by corrosion, flash over or leakage currents. Some of the failures will be permanent and other may disappear when the condensed water has evaporated.

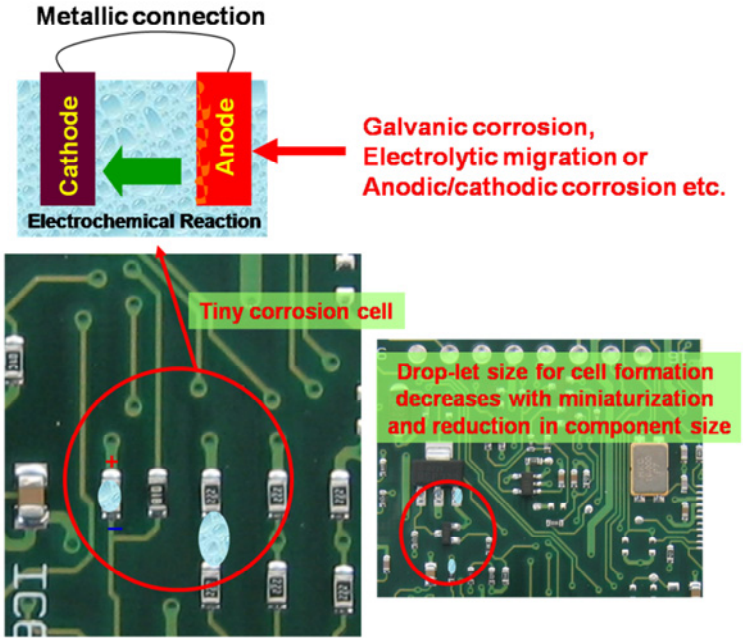

Figure 7.1: Schematic showing relation between miniaturization, local condensation and electrochemical cell formation on PCBA

The term local condensing is used where a small part of the product is still cold enough to form condensation. Thermal heavy components and air flow are important factors in formation of local condensation. Also the ability to evaporate condensed water is important for a product to be able to survive local condensing. Therefore, high levels of design factors are involved in products response to humidity and condensation.

In general, the corrosion problems experienced by the electronic systems can be generalized as due to the following key factors. These are the miniaturization together with: (i) unfavorable material combinations, (ii) DC or AC electric field applied to the system in use, (iii) process related ionic residues on the PCB surface

[1,4-6], and (iv) application related factors such as high humidity, gases, aggressive ions, dust, etc. [1,4-6].

Presently the mechanistic knowledge on electronic corrosion is limited especially related to the synergistic effects of process related residues and contamination coming from service conditions. This paper focuses on the effect of no-clean wave solder flux residue together with the effect of natural dust collection on components during service on the Electrochemical Migration (ECM) on single chip capacitors. ECM is a dominant electronic corrosion failure mechanism. During electrochemical migration, a suitable metal ion such as Sn, Pb, Cu etc. dissolves in to the condensed water layer from a positively biased point on a PCB and migrates through the water layer to a nearby negatively charged part to deposit there in the form of dendrites. As it progress, dendrites will bridge the gap between two points, which will lead to an electric short. In this paper ECM was investigated on single chip components using a novel Single Component Electrochemical Migration (SCECM) set up. Morphology of the flux residues and the capacitors after ECM experiment was analyzed using optical microscopy, FEG-SEM and EDS.

7.2 MATERIALS AND EXPERIMENTAL METHODS

7.2.1 ELECTRONIC COMPONENTS

A multilayer ceramic chip capacitor, C33 (Figure 7.2) was used as the test component for all the investigations. The capacitance of the component is 100 nF and dimensions of the component is 2.0x1.2x0.45 mm with end terminals consisting of 100 % Sn. Components used for the experiments are representative of a large number of chip capacitors used for the electronic PCB production.

7.2.2 SCECM SYSTEM:

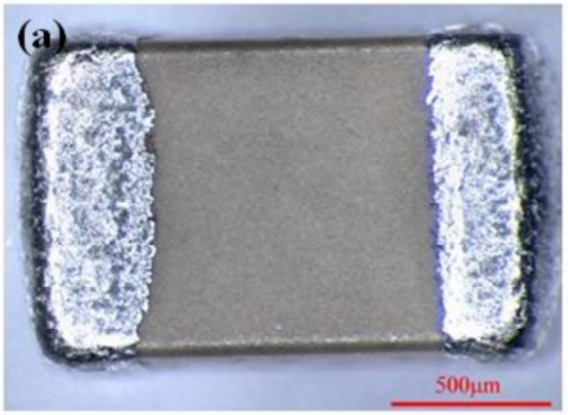

Figure 7.2: Ceramic capacitor (C33) used in this work.

A novel Single Component Electrochemical Migration Setup (SCECM) was used for ECM investigations. Set up consists of three electrode pairs with a provision to load tiny bi-polar components like the chip resistors and capacitors as shown in Figure 7.3. Using the two adjustable electrodes, components can be held for the corrosion experiments in contact with a drop-let of solution in order to simulate the condensing humidity. The pair of electrodes also provides electrical contact to the electrodes on both sides of the capacitor (Figure 7.2). The probes are covered with silicone rubber, which is penetrated by the probe when a load is applied, thereby allowing the electrical contact while at the same time providing corrosion protection to the probes.

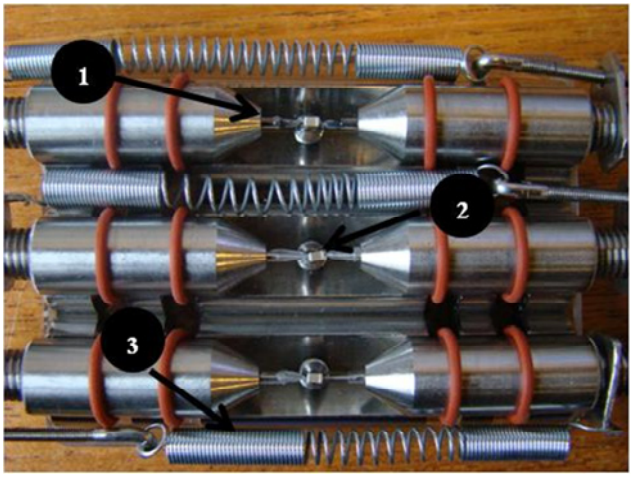

Figure 7.3: The SCECM set up with three electrode holders for the components. Components are fixed between the probes: (1) Probe covered with silicone rubber for corrosion protection, (2) Chip capacitor fixed between the electrodes, and (3) attached spring for keeping the holders tight.

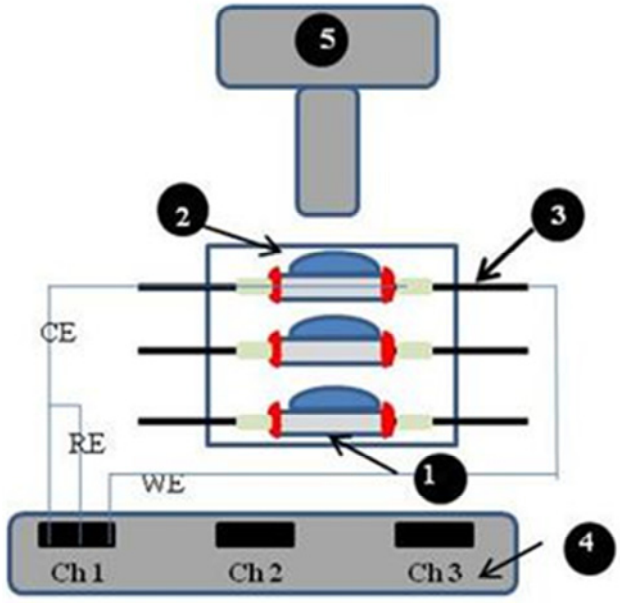

Figure 7.4: Schematic view of the overall SCECM set-up: (1) Chip capacitor, (2) Drop-let of required solution on top of the component, (3) Needle covered with silicone rubber, (4) Multi-channel potentiostat, (5) Video microscope.

Figure 7.4 shows an overall schematic of the SCECM set up consisting of various parts. Required environment (in this study, DI water) is placed on each component as a drop-let. Required DC bias is applied between the two electrodes separately for each component using a multi-channel potentiostat. Simultaneously the time lapse video recording is started for in-situ videoing of the migration sequence. The leakage current flowing through the water layer is measured as a function of time until a permanent short is observed due to ECM.

For the SCECM experiments, chip capacitors were handled by polymer tweezers and gloves to avoid any mechanical damage and human related contamination during handling. The potentiostat used for the SCECM experiments was a multi-channel Bio Logic VSP potentiostat.

7.2.3 INTRODUCING THE FLUX RESIDUE ON CHIP CAPACITORS

For studying the effect of flux residue on ECM, C33 capacitors were dosed with no-clean flux by dipping in the flux solution. The components were dried in air and subsequently heated to high temperature (in this study 235°C) for 45 seconds to simulate the heating condition during the wave soldering process. Maximum temperature attained during the wave soldering profile for Sn-Pb solders is ~235°C and overall time interval of the profile is ~45 seconds. However in this study, components are heated at constant temperature for 45 seconds.

7.2.4 MICROSCOPIC ANALYSIS

Surface morphology of the components, flux residues, and the electrochemically migrated components were analyzed using optical microscopy, Scanning Electron Microscopy (SEM - JEOL 5900) and chemical analysis using the attached EDS system (Oxford Link ISIS). Field Emission Gun Scanning Electron Microscopy (FEG-SEM) was performed using a Zeiss 1540EsB cross beam for the high resolution images of surface topography of the solder terminals.

7.3 RESULTS AND DISCUSSION

7.3.1 MORPHOLOGY AND MATERIAL MAKE UP OF CHIP CAPACITOR

The capacitor (Figure 7.5a) is a surface mount component that consists of a sintered ceramic body with two electrodes on both sides for mounting it on to the Printed Circuit Board (PCB). As shown in Figure 7.5b, the electrodes consist of three metal layers with copper at the bottom followed by a thin layer of nickel, and a top layer made of Sn (Table shown in Figure 7.5). Stacked layers of capacitor lines made of nickel can be seen inside of the capacitor (Figure 7.5b). Usually the inner electrodes layers are made by thick film technique and the outer Sn layer is barrel plated.

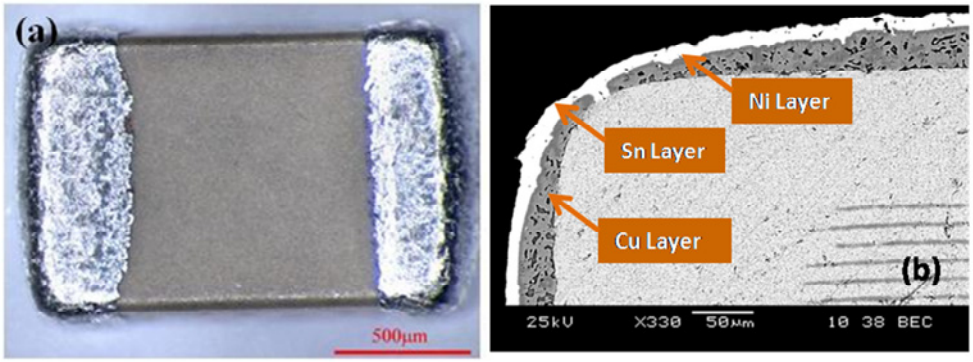

Spectrum	Al	Ni	Cu	Sn	Total
Spot 1				100.00	100.00
Spot 2		99.17		0.83	100.00
Spot 3	0.57	0.78	98.65		100.00

Figure 7.5: (a) Magnified view of a chip capacitor (C33), (b) SEM picture of the cross section of the capacitor close to one of the electrode together with results of chemical analysis (in wt.%).

Surface morphology of the electrode shows that the outer surface is non-uniform and the rough areas indicative of a barrel plating technique. Roughness and uniformity of the surface layer is important from the corrosion point of view as it increases the surface area for corrosion, and assists trapping and the condensation of water during service. Non-uniform surface layer with pores and cracks also expose inner layers to the service environment causing galvanic corrosion. Copper migration is often found simultaneously with Sn migration on these components due to the exposure of copper at various locations on the electrode surface [7].

7.3.2 FLUX RESIDUES AND THEIR COMPOSITION ON PCBS

Wave soldering process is widely used for PCB assembly process to mount through-hole components. In order to activate the metallic parts prior to soldering process, fluxes are applied on to the bottom of the PCB which is transported inside the wave soldering oven through a conveyor belt. During the flux spraying process, drop-lets of flux solution can also fall onto the top part of the PCB or rise onto the top surface through the via holes. After the spraying process, PCBs will be passed

through several stages of heating from the ambient to the soldering stage at ~235^{o}C for the lead containing solder. Depending on the temperature attained at various parts of the PCB, varying levels of flux residues will be left behind. Most commonly used solder flux for the wave soldering presently is named as 'No-clean' fluxes (NCF) meaning that it is not necessary to clean the PCBs after the soldering process. The NCFs are mainly made of three major components: (i) Solvent – a medium for mixing all the components of the flux, (ii) Activators – mainly weak organic acids, and (iii) Vehicle – a non-volatile compound such as a resin or ester stable through all temperature of the soldering profile. The assumption behind this process is that the aggressive chemicals used in the flux solution will burn off during the soldering process so that it leaves minimum residue of aggressive nature. However, in practice this seldom happens, but mostly substantial amounts of flux residue including the activator components could be seen on the PCBA. Presently, the use of NCF has become prevalent in the electronic industry and is estimated that about 70% of the assemblies produced in North America are not cleaned after the soldering process [8,9,10].

The activating species in the NCF often consists of one or more of the weak organic acids (WOA), especially the short-chain carboxylic or dicarboxylic acids such as adipic acid, glutaric acid, succinic acid, malic acid or formic acid. These acids are capable of reacting with the oxide layers on the metallic parts of the PCB and should vaporize as a result of the thermal exposure during the soldering leaving only minimal benign residue. Resin component in the NCF will usually consists of small amounts of non-volatile organic compounds like the rosin or synthetic resins made from polyhydric alcohols or fatty acid esters, and the solvents are often a mix of organic alcohols with different boiling points like isopropyl alcohol or ethanol [10,11,12].

The main organic acid in the NCF used for the present work is adipic acid (~ 1- 2 %) and a resin component (~1 – 2 %), water (~1 %), and rest the solvent isopropyl alcohol. If the flux is sprayed onto a substrate similar to the wave soldering process, which upon drying results in residues of the resin and acid components. Morphology of such residues formed at room temperature has the appearance as

shown in Figure 7.6. The acid crystals (mainly the adipic acid) are embedded inside the resin component. This type of morphology is significant for corrosion as resin part can act as a good trapping agent for the dust and other solid particles from the environment, while the acid component can also be water absorbing.

Figure 7.6: Morphology of the flux residue formed at ambient temperature by drying of the flux solution.

Figure 7.7 shows the optical pictures of the remaining flux residues on a glass plate formed after heating to various temperatures for 45 seconds. It can be seen that the amount of flux residue decreases with increase in temperature, however, even at 170^{o}C (temperature corresponds to the top side of the PCB during wave soldering) and 250^{o}C (above wave soldering peak temperature) considerable amount of residue still remain on the surface. Ion chromatographic analysis showed substantial amounts of acid component in the residue formed at 170^{o}C and 250^{o}C.

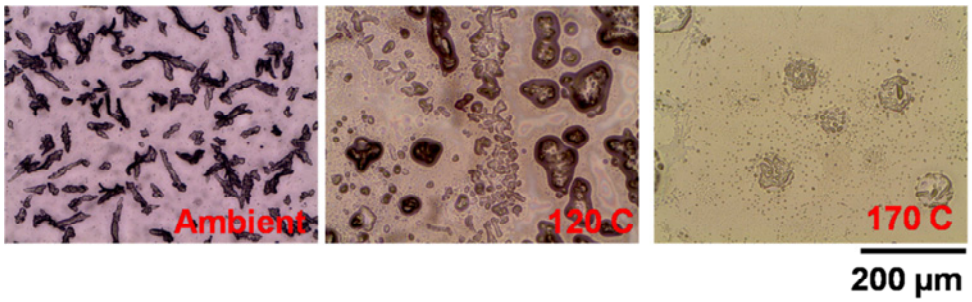

Figure 7.7: Morphology of flux residue formed at various temperatures.

Presence of the acid components in the residue in principle can influence the corrosion of electronic components in many ways. These are: (i) by changing the pH of condensed water layer which will modify the stability of the dissolved metal ions, (ii) increasing conductivity of the water layer so that higher leakage current between the electrodes for migration, and (iii) depending on the nature of acid, it can either act as an activator for corrosion or inhibitor.

The resin component may not directly influence the corrosion because of its non-ionic nature, but it can act as a good trapping agent for the solid particles such as dust in the service environment. This means that although the resin component initially appears to be benign for corrosion and non-wetting, with time it can become a good site for water absorption and source of ions due to the collection of dust particles and embedded acid components as shown in Figure 7.6.

7.3.3 SINGLE COMPONENT ECM INVESTIGATIONS USING SCECM

Effect of flux residue on ECM

Effect of flux residue formed at room temperature and at 235^{o}C on ECM was investigated on chip capacitors using the SCECM set up. As described earlier, the flux residue on capacitor was introduced by dosing the capacitor with the flux solution followed by heating at required temperature. The flux residue at room temperature means that the drying is carried out at ambient temperature, while 235^{o}C means that the component is heated to 235^{o}C after dosing with the flux solution. Six capacitors were tested in each case to provide a good statistics. A set of as-received (without any flux residue) components was also tested for comparison. Drop-let of the solution placed on the top of each capacitor for migration testing was DI water.

Table 7.1 shows the summary of test results. As-received capacitor did not show any migration at 5V and 10V showing that the set of components chosen were clean without significant levels of impurities to increase the conductivity or migration. However, it is interesting to observe that among the samples with the flux residue formed at room temperature and at 235^{o}C, only one of them showed

the migration, while others did not although strong electrochemical activity and gas evolution was evident at the electrodes at least initially. Soon after applying the potential bias, the anode showed a passivation effect although gas evolution was continued to some extent. As the potential on electrodes is of the order of ± 5V and ± 10V, bias is sufficient for oxygen evolution reaction at the anode and hydrogen evolution reaction by water dissociation at the cathode. Potentiodynamic polarization experiments using pure Sn in solution containing varying amounts of the adipic acid also showed similar passivation behavior with increase in the acid concentration [7]. This shows that the acid component might be acting as an anodic inhibitor reducing the metal dissolution. It is well known that a number of organic acids could act as corrosion inhibitors.

Table 7.1 Summary of the effect of flux residue on ECM on capacitor, C33

Sample	Voltage	Migration	Total migration
As-received	5V	0 out of 6	0 out of 12
	10V	0 out of 6	
RT	5V	0 out of 6	0 out of 12
	10V	0 out of 6	
235 °C	5V	0 out of 6	1 out of 12
	10V	**1 out of 6**	

Figure 7.8 shows the results from the in-situ video of dendrite formation observed on one of the capacitors tested with flux residues at 235^{o}C. Sequence of pictures shown in Figure 7.8 corresponds to the times indicated in the current vs. time curve. Immediately after the application potential bias, within an interval of 200 seconds the dendrite formation was started at the cathode. Rate of growth of dendrite was very fast so that within 10 seconds the entire gap was filled with dendrite to introduce an electrical short. This indicates that if the available metal ions in the solution and other parameters are conducive enough nucleation,

growth, and electrical shorting occurs very fast. Peaked current was immediately dropped due to burning of the dendrite as a result of the current surge. In this particular experiment only one event of dendrite formation was observed, but in many other cases the dendrites forms again after the burning to give many intermittent shorting events.

Figure 7.9 shows the current vs. time curve measured during the SCECM experiments for one set of the samples biased to 10V (As-received, RT, and at 235^{o}C). Effect of the acid component in the flux residue is clearly evident as the RT samples with higher flux residue shows higher current levels. This is assumed to be due to the increased conductivity of the solution together with oxygen evolution rather than due to increased metal dissolution. At high temperature, the residue is partially burned off. The decreased amount of the acid correspondingly reduces the current due to the lower conductivity. For both cases, the current is significantly higher than that for the as-received component exposed to the DI water.

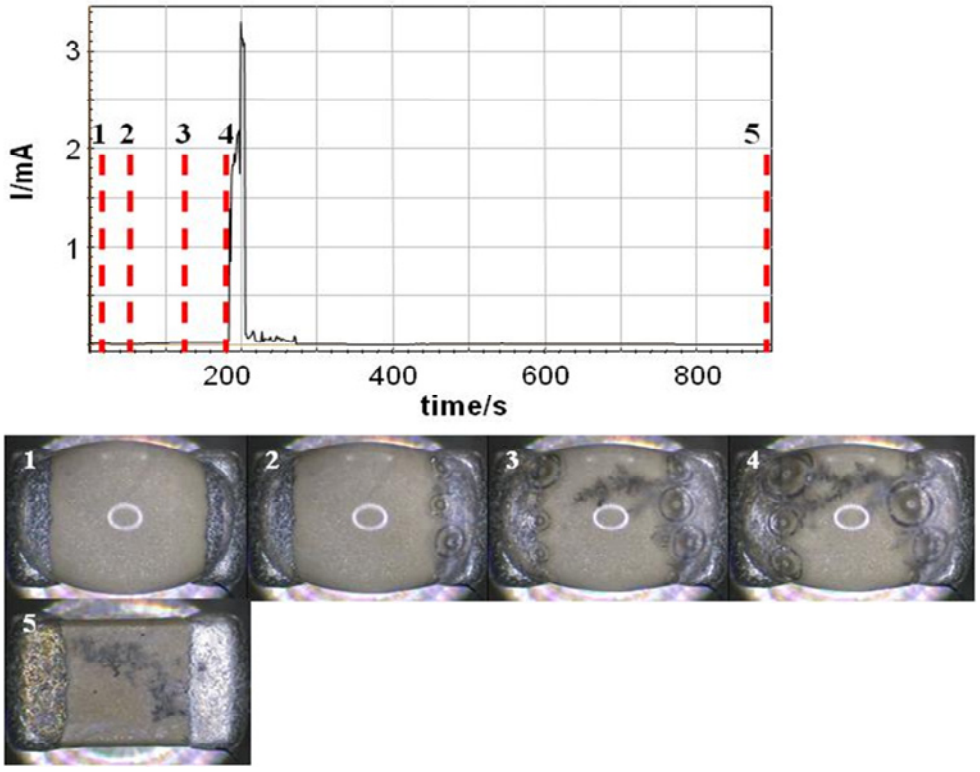

Figure 7.8: Current vs. time curve from the migration experiment with flux residue (potential bias 10V) and sequence of pictures corresponding to various points shown in the curve.

Effect of natural dust on ECM

Effect of natural dust collection on components on the ECM was investigated by exposing the capacitors for 2 months in a kitchen followed by the SCECM testing. Activity in the kitchen was mainly related to the use of food items, but no active cooking. Therefore, the source of dust can be from the particles from food items used in the kitchen (such as bread etc.), human related contamination, and the dust coming through the openings and windows. Analysis of such dust showed clear signs of active ions such as chloride, although a detailed chemical analysis is presently being carried out. However, the effect of this type of dust settling on components on ECM was very clear from the SCECM experiments as all the six components tested in this case with a potential bias of 10V showed migration and electrical short within a short period of time. Comparing with the results presented in Table 7.1 showing no migration for as-received capacitors, the results obtained after exposing to the dust clearly shows the aggressiveness and danger of such dust on electrochemical migration. This is due to the fact that the dust must contain both organic and inorganic compounds, and ions that could accelerate corrosion as well as increase conductivity of the solution layer. For example it was found that human contamination such as finger print can cause almost 100 times increase in the leakage current through a condensed water drop-let compared to pure water due to the dissolution active components from the finger prints [13].

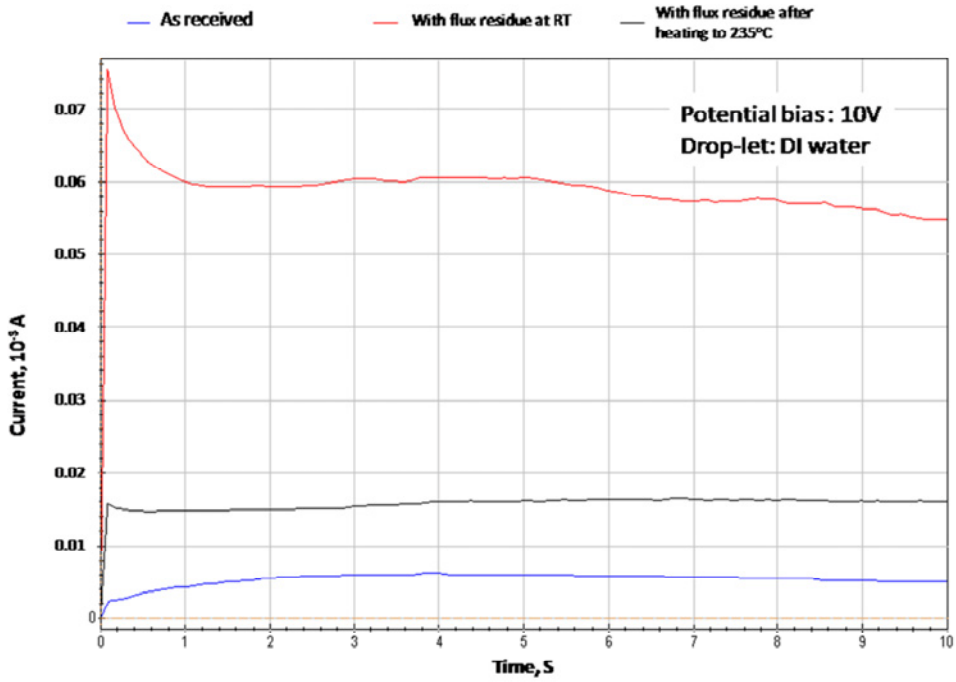

Figure 7.9: Current vs. time curve corresponds to one of the ECM experiments with flux residue for the first 10 seconds.

Figure 7.10 shows the current vs. time curve and the sequence of pictures from the in-situ video for one of the migrated component after exposing to the dust. Initially the current was low, but after an interval ~450 seconds, dendrites started nucleating at the cathode. The dendrites grow with time towards the anode until it electrically short (maximum current). The short remain in place for about 300 seconds and then it breaks off more due to the evaporation of the solution. In this case, therefore a permanent short was observed once the dendrite filled the gap between electrodes indicating that the dendrites was stable to carry required current without burning and the environment on the component is aggressive enough to support continued growth of the dendrites.

Effect of flux residue and natural dust on ECM

Synergistic effect of flux residue and natural dust on ECM was investigated for the capacitor using components initially dosed with the flux and heated to 235^{o}C followed by exposure to the dust in a kitchen similar to earlier set of experiments.

The idea of the experiment is to understand how the dust collection could alter the inhibiting effect if flux residue alone is present. It is important from the point of view of field applications as the flux residue can clearly attract the dust, but at the same time act as a decelerator for migration. The question then is that the aggressiveness of the dust could overcome the inhibitive effect of flux residue so that with time it can introduce failures.

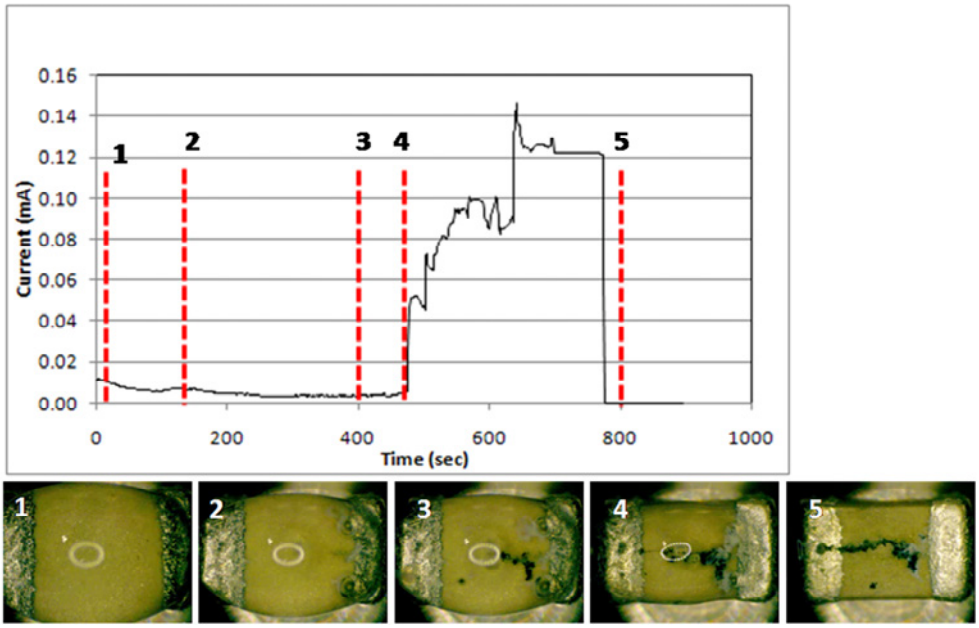

Figure 7.10: Current vs. time curve from the migration experiment on components with collected natural dust (potential bias 10V) and sequence of pictures corresponding to various points shown in the curve.

Similar to the results found for samples with dust, all the six samples tested at 10V showed migration. This shows that the environment created by the dust with DI water was aggressive enough in this case to overcome the effect of flux residue. Flux residue alone is supposed to inhibit the migration as described earlier (Table 7.1).

Figure 7.11 shows the current vs. time curve and sequence of pictures from in-situ video for one of the component tested for the migration with flux residue and dust. Initially the current was low, but in this case after an interval of ~250 seconds, dendrites started nucleating at the cathode. With time dendrites grow towards the

anode making an electrical short, which remains in place for about 200 seconds and then burns off. Compared to the experiments only with dust, although the dendrites formation started earlier, the stability of the dendrite is shorter. However, the current levels under dendrite short was much higher than that observed in Figure 7.8 and Figure 7.10 indicating that the dendrite formed in this case was either thick or more conducting (means more metallic in nature without much intermixed oxides [14]). In agreement with this higher degree of electrochemical activity was observed on the sequence of pictures compared to one without flux residue. In summary, the result obtained with the flux residue and dust shows that the presence of flux residue must have increased the conductivity, however presence of dust could have further increased the conductivity and acted as a source of ions for corrosion to occur.

7.3.4 SEM ANALYSIS OF DENDRITES:

Figure 7.12 shows the FEG-SEM images of one of the migrated capacitor with dust alone. Figure 7.12a shows overall view of the migrated capacitor. Dust collection on the surface can be clearly seen (see arrows). Figure 7.12a and b shows that the dendrites are very much branched and connected to the anode at many points. Figure 7.12c provides a magnified view of the dendrites showing that the branches are not adhered to the surface of the component.

The SEM pictures of one of the migrated capacitors with the flux residue and dust is shown in Figure 7.13. Figure 7.13a shows that the amount of dust collected in this case is more than without flux (See arrows). Similar to that observed for one with dust, dendrites are branched (Figure 7.13a and b), but the concentration of dendrites on the surface is much larger in this case. This is also evident in Figure 7.13c where a large number the dendrite branches are seen. Higher density of dust on the surface in this case might be the reason for higher reactivity compared with the one only with dust.

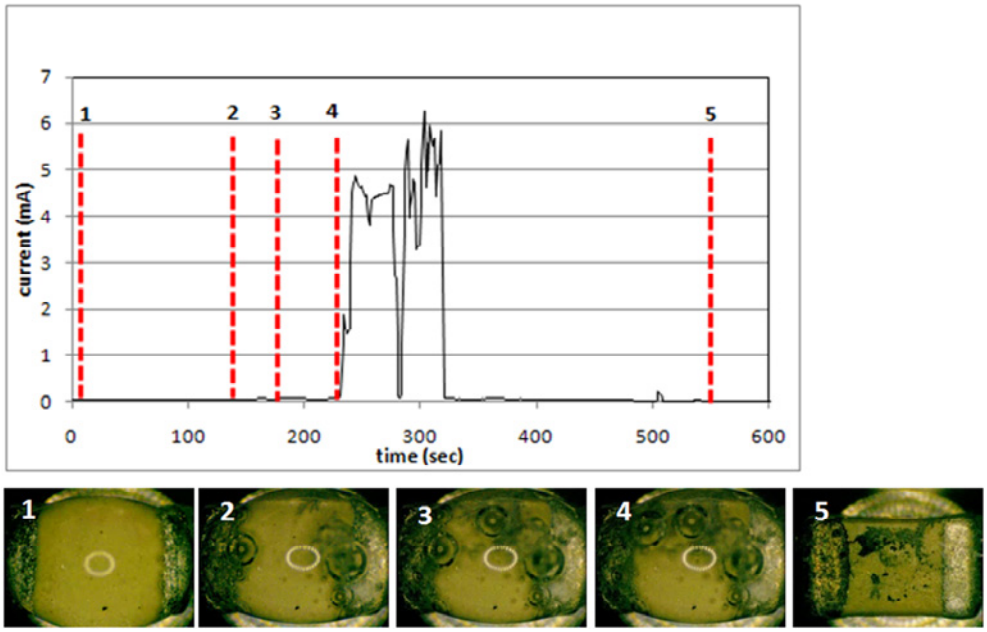

Figure 7.11: Current vs. time curve from the migration experiment on capacitor with the flux residue and collected dust (potential bias 10V) and sequence of pictures corresponding to the various points shown in the curve.

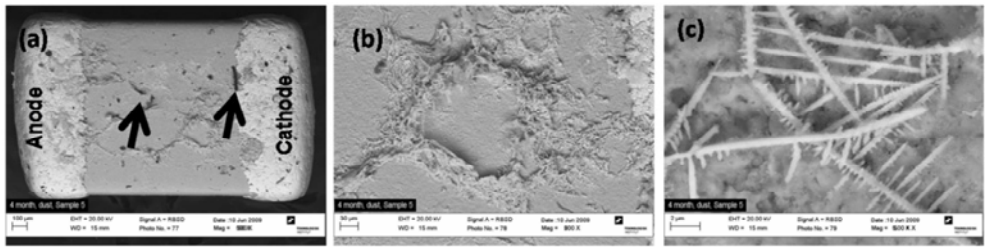

Figure 7.12: SEM pictures of migrated capacitor after exposing to dust.

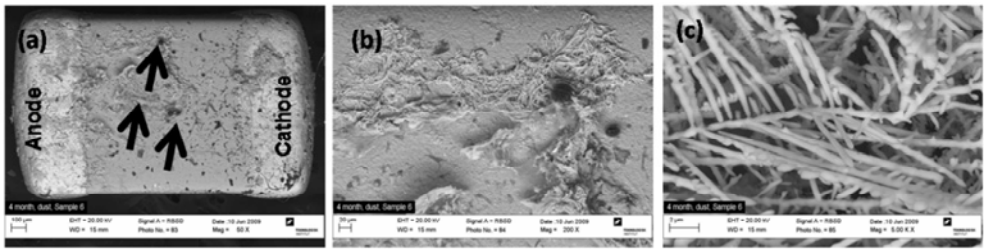

Figure 7.13: SEM pictures of migrated capacitor after exposing to flux residue and dust.

In summary, the results from the experiment with dust and flux residue + dust suggest that although the flux residue alone is not dangerous for ECM, but with time collection of dust can alter the behavior to give severe ECM. In this respect, flux residue can act as a most probable site for dust collection.

7.4 CONCLUSIONS

Considerable amounts of flux residue with both the activator and resign component was found even after heating the flux to 170^{o}C and 250^{o}C. Flux residue showed morphology with acid crystals embedded in the resin component.

Presence of flux residue alone did not create any ECM on the capacitors although the conductivity of the solution layer was increased due to the presence of acid component.

Collection of natural dust on the surface has increased the reactivity giving ECM for all the samples tested. The dendrites were highly branched and crisscrossed without adhering to the surface.

Presence of the dust together with the flux residue has diminished the inhibiting effect of the flux residue on migration to severe ECM on all the samples tested. More dust collection was found on the components with flux, and thick dendrites with crisscrossed pattern.

ACKNOWLEDGEMENTS

Current research has been conducted as part of the CELCORR consortium. Authors would like to acknowledge the Danish Ministry of Science, Technology and Innovation for the funding for the CELCORR project and project partners Danfoss A/S, Grundfos A/S, Vestas A/S and PRI-DANA Elektronik A/S, Danish

Technological Institute and IPU. Pia Wahlberg from the Danish Technological Institute is acknowledged for the FEG-SEM work.

REFERENCES

[1] M. Yunovich, Appendix Z – Electronics, pp. Z1-Z7, www.corrosioncost.com/pdf/electronics.pdf

[2] R. Ambat and P. Møller, Corrosion Science 49 (2007) 2866–2879

[3] S. Matsumoto, "The measurement of tiny dew droplets at the initial deposition stage and dew point using a phase-shift interference microscope", Meas. Sci. Technol. 14 (2003) 2075-2080.

[4] H. Risto, R. Lahtinen, Reima, Corrosion and climatic effects in electronics, Published by VTT Automation, Finland, 2000.

[5] R. Lahtinen, R. Heinonen, Corrosion and reliability of electronic materials and devices, Electrochemical Society Proceedings 99-29(1999)155-163.

[6] G. Di Giacomo, Reliability of electronic packages and semiconductor devices, McGarw-Hill, USA, 1996.

[7] D. Minzari and R. Ambat, Unpublished results, Technical University of Denmark, 2009.

[8] 'Solder Joint Reliability', John H. Lau Van Nostrand Reinhold, 1991, ISBN: 0-442-00260-2

[9] Flux Chemistries And Thermal Profiling Avoiding Soldering Defects In SMT Assembly, Peter Biocca, Loctite / Multicore Solders Inc., Richardson, Texas

[10] Residue Effects of Weak Organic Acid (WOA) Flux Activators, Terry Munson, President of Foresite Inc., PDF-file at www.residues.com, June 2009.

[11] Electronic Materials Handbook - Volume 1, Packaging, Merrill L. Minges, Technical Chairman, ASM International, 1st Edition, 1989, ISBN: 0-87170-285-1 (v.1)

[12] B.A. Smith and L. Turbini, Journal of Electronic Materials, 28(1999)11.

[13] P. Westermann, Investigation of process related residues during PCB manufacturing, Master thesis, Technical University of Denmark, 2008.

[14] D. Minzari, M.S. Jellesen, P.Møller, P.Wahlberg, R.Ambat, Electrochemical migration on electronic chip resistors in chloride environments, Accepted for publication in IEEE Transactions on Reliability (2009)

8 PAPER 4: ON THE ELECTROCHEMICAL MIGRATION MECHANISM OF TIN IN ELECTRONICS

Daniel Minzari[7], Morten S. Jellesen, Per Møller, Rajan Ambat

Department of Mechanical Engineering, Technical University of Denmark, DK 2800 Kgs. Lyngby, Denmark

ABBREVIATION

ECM Electrochemical Migration
PCB Printed Circuit Board
PCBA Printed Circuit Board Assembly
SMD Surface Mounted Device
DI De-Ionized
SIR Surface Insulation Resistance

ABSTRACT

ElectroChemical Migration (ECM) of tin and tin alloys on an electronic Printed Circuit Board Assembly (PCBA) can result in the growth of a metal deposit with a dendritic structure from cathode to anode. Necessary conditions for ECM of tin in electronics are two closely spaced conductors on the PCBA made of tin or tin alloys with sufficient potential difference, a layer of water formed due to humidity, and sufficient conductivity in the water layer. Dendrite formation can short circuit the system, potentially leading to intermittent or complete failure of the device. The electrochemical migration mechanism of tin is extremely sensitive to any ionic species and to the local pH changes that develop within the micro-volumes of environment, which determines the thermodynamic stability of dissolved tin ions in solution. The ECM experiments carried out in various environments such as chlorides, bromides, solder flux residues, and various pH conditions showed that the stability of tin ions and various other species, controlled by the chemistry of the solution, play a major role in the dendrite nucleation and growth, and therefore ECM susceptibility of tin. In this paper, mechanistic aspects of ECM of tin are discussed in detail using the experimental results on the susceptibility in various environments, potential bias, and results on local pH changes combining with thermodynamic stability of tin species as depicted in the Pourbaix diagram.

8.1 INTRODUCTION

Electronic circuits are becoming a growing part of our everyday life, and during the past two decades a significant change has occurred where electronic devices have become consumable items rather than luxury goods. Since 1996, the electronics

[7] Corresponding Author: Daniel Minzari, phone: +45 4525 2118, Fax: +45 4593 6213, email: dm@mek.dtu.dk

industry has been the largest industry in the world, having a turnover of more than US$1 trillion a year [1]. Integrated Circuits (IC's) are becoming faster, smarter, and cheaper, while increased battery efficiency allows complex devices to become portable. However, the number of components required on a device is increasing, as certain components such as capacitors cannot be implemented into the IC's. As the trend is to make electronic devices smaller and lighter, a significant decrease in component sizes has allowed closer packing on the PCBA. The trade-off for these technological changes is that the electronic devices become increasingly prone to failures due to corrosion in the harsh environments that can be encountered when they are brought out from the protected shelves of our living rooms, into our daily life. The scenario is not different for industrial electronics where wide spread applications of electronics as control systems experience mild to harsh environmental conditions.

Electrochemical migration (sometime referred to as electrolytic migration) is a form of corrosion, which significantly compromise the corrosion reliability of electronic devices. This process occurs when two oppositely biased and closely spaced electrodes are connected by an aqueous electrolyte. The two biased points could be a pair of exposed conduction lines, legs of components or two electrodes on a bipolar component (resistors or capacitors as shown in Figure 8.1b) on a PCBA on which a layer of water has developed in contact with atmospheric humidity. During electrochemical migration, metal ions are dissolved at the anode and migrate towards the negatively charged cathode, where they can be deposited to their metallic state [2]. Electrochemical migration should therefore not be mistaken for electromigration, which is an electron momentum transfer phenomenon resulting from the movement of ions in solid state [3]. During electrochemical migration, if the conditions are conducive, the deposit grows in a dendritic structure outward from the cathode extending towards the anode within tenths to hundreds of seconds, which eventually results in a short circuit between the two electrodes. An example of electrochemical migration on a ceramic chip resistor is shown in Figure 8.1, which can result in an intermittent fault or permanent failure of an electronic device. As the electric field between conductors is inversely proportional to the

distance, the driving force for electrochemical migration is highly influenced by the inter-electrode distance, and therefore the miniaturization of electronics.

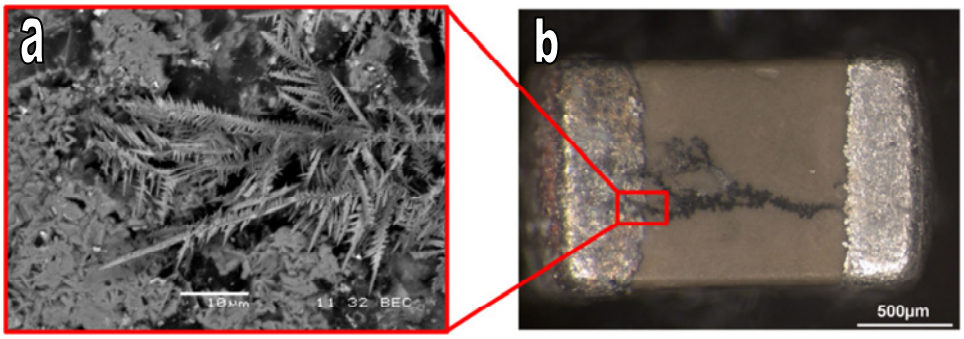

Figure 8.1: Electrochemical migration and dendrite formation on a chip capacitor: (a) SEM picture showing magnified view of the dendrite and (b) optical migration showing overall view of the dendrite. Dendrite has grown from right (cathode) to left (anode).

Only few metals on a PCBA such as Sn, Pb, Cu, Ag, and Au are susceptible to electrochemical migration [3]. In general, metals that cannot be electroplated (such as aluminium) from aqueous solutions can be regarded as safe from ECM. In order for anodic dissolution of metal ions to occur and dissolved metal ions to migrate, some conductivity for the condensed layer of water is needed. This is provided by the tiny levels of ionic contamination on the PCBA or on component. Low conductivity of the solution will in general cause uneven electric field distribution on the surface of the cathode under potential bias helping preferential nucleation of dendrites at some locations (Figure 8.1b). Once the dendrite formation initiate, the reduced distance between the tip of the dendrite and anode will cause a strong gradient of electric field to the dendrite tip, thereby making subsequent metal ion deposition to continue at this point. If the growth is allowed to continue until the dendrite reaches the anode, the two electrodes will be short circuited, and a sudden increase in the current flow between the two electrodes will be observed. The dendritic branch, which shorts the two electrodes, commonly has a backbone structure with a diameter in the magnitude of ~100nm, and the lifetime of the conductive dendritic bridge can be few seconds, minutes or it can be permanent.

Electrochemical migration is commonly divided into humid and wet/condensed migration [3], where humid conditions are defined as having a thin invisible moisture film adsorbed to the surface, while in condensed conditions a nucleated

visible layer of water is present. Though Brunnauer et al. [4] found an exponential increase in surface conductivity with increasing humidity, not all metals that are susceptible to ECM have been found to migrate under humid conditions. Silver and to some extent copper has been reported to migrate under humid conditions [3,5-10], while other susceptible metals such as Au, Sn, Ni, Pb, Pd, etc. usually require a visible water layer (condensed conditions) [3,9,11-20]. As more and more electronic applications are being used in severe environments with thermal cycling, migration in condensing conditions is of high relevance.

Takemoto et al. [21] have predicted that electrochemical migration will become one of the most severe reliability issues for the electronic industries in the future due to the miniaturization of the devices and increased sensitivity to contamination. As many of the failures are intermittent, it is extremely difficult for manufacturers to detect the root cause of a failed device, and electrochemical migration is indeed the reason for failures that have been labelled: “no failures found” [22,23]. It is hard to establish the exact cost of electronic devices failures due to ECM, but the importance is due to the fact that it can cause a whole device to malfunction or fail, unlike conventional corrosion where slow damage to the device is expected over a longer time-scale.

On a PCBA (e.g. the PCBA with condensed water shown in Figure 8.2), majority of the exposed area is covered by the solder mask or by a component housing/encapsulation. The metallic surfaces that are directly exposed to the environment are mainly the component electrodes, solder joints, and contact/connector areas. A hot air levelled solder finish (usually a surface with lead free tin based solder alloy is used today) PCBA is widely used for industrial applications [24]. Therefore, large part of the exposed metallic areas is made of tin or tin solders. The new lead free solder alloys commonly used for soldering in the electronic industries consists of almost 95% tin, while the rest is copper, silver, and/or tiny levels of other metals. Due to this reason electrochemical migration of tin is extremely important in connection with corrosion reliability of electronic devices.

For electrochemical migration of tin to occur, one needs a condensed layer of water. The properties of the condensed layer will depend on the wettability of the surface, and therefore droplets of water will have a higher tendency to form at sites such as the electrode surface and ceramic bodies of Surface Mount (SM) components where the good wetting properties of metals and ceramics are combined with a rough surface morphology. In this regard, two material combinations are relevant; pure tin which is commonly used as the electrode material for the SM components, and tin solder material that is used to fix the SM components to the PCBA. A schematic presenting an example of condensation on a PCBA and material makeup is presented in Figure 8.2.

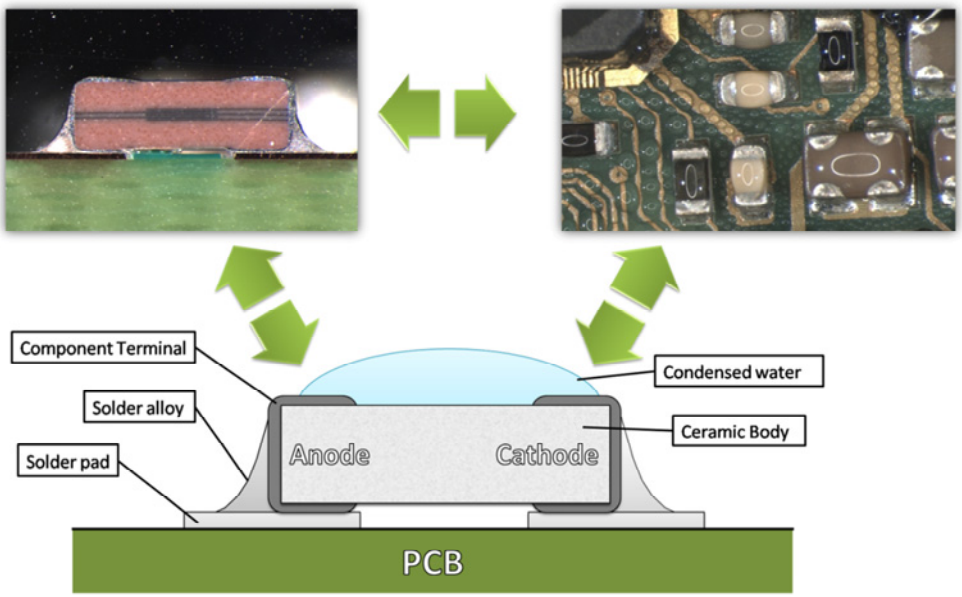

Figure 8.2: Sketch presenting an example of condensation on a PCBA, a cross section of an SMD chip capacitor on a PCBA, and a simplified sketch showing the material makeup.

A number of investigations in our laboratory on ECM susceptibility of tin using chip components have shown that the condition for dendrite formation in general depends on various parameters such as chemistry of the solution, distance between the electrodes, pH of the solution, potential bias etc. A general trend was observed on the probability of dendrite formation by ECM of tin linking to the stability of tin ion in solution, which is to a large extend determined by the local pH

changes during electrochemical reactions. This paper attempts to bring together these experimental observations and to elucidate a general mechanism for tin migration based on thermodynamic stability factors, supported by various ECM experimental results. All the experimental work reported are carried out on single chip components such as SM chip resistors and capacitors with electrodes made of tin.

8.2 MATERIALS AND EXPERIMENTAL METHODS:

8.2.1 COMPONENTS USED FOR THE EXPERIMENTS:

All the experimental work reported in this paper was carried out using Surface Mount (SM) chip components. These are: (i) 10kΩ Ceramic Chip Resistor (CCR) housing size 0805 (New Sincere Electronics Company Ltd., Taiwan type CR05T10NF10K), and (ii) Ceramic Chip Capacitor (CCC) housing size 0805 (Yageo Phycomp, Taiwan Type 2238 580 15649). The electrodes of (i) are made of Sn 2 wt. % Pb and (ii) are made of pure tin.

8.2.2 SINGLE COMPONENT ELECTROCHEMICAL MIGRATION SET UP (SCECM) AND TESTING:

Electrochemical migration experiments reported in this paper were carried out using an in-house developed Single Component Electrochemical Migration (SCECM) setup shown in Figure 8.3. In the SCECM set up, SM chip components can be suspended between two needles that are covered by silicone, so that the electrical contact can be established without experiencing galvanic corrosion between the needle and component electrode. More information on the SCECM setup can be found elsewhere [25].

For ECM experiments, a droplet of approx. 2μL of electrolyte was added on the surface of the components mounted on the SECEM and DC bias was applied between the two electrodes. Simultaneously, a time lapse video recording was started for in-situ recording of the migration sequence.

Current flowing through the component and electrolyte layer was measured as a function of time at constant applied potential using a potentiostat and the

experiment was continued until the electrolyte droplet had evaporated from the component surface.

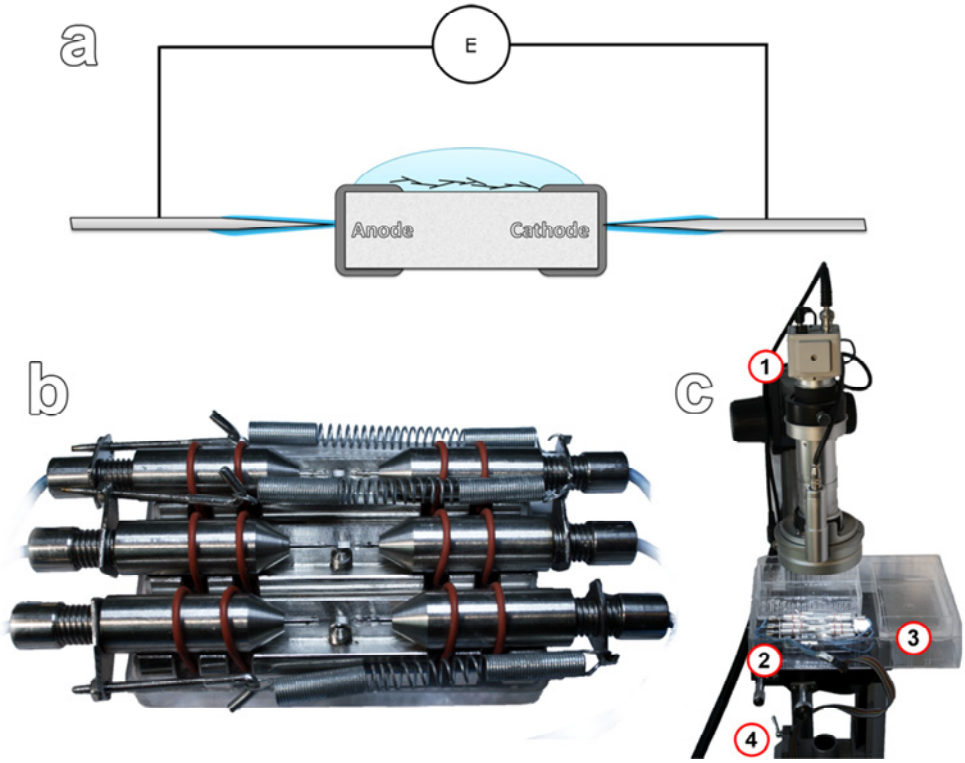

Figure 8.3 a) Schematic of the cell holder principle of SCECM set up, b) SCECM multiple cell holders, and c) the whole SCECM setup including: 1) Video microscope, 2) SCECM cell setup, 3) Closed box with container for water/ saturated salt solution to control humidity, and 4) XYZ-stage.

8.2.3 INVESTIGATED ENVIRONMENTS:

The ECM experiments reported in this paper have been conducted in the following environments and the idea of conducting experiments in each environment is briefly explained:

Chloride ions: Many electronic device failures due to ECM can be directly correlated to the presence of low levels of chloride ions. Sources of chloride contamination on the PCBA can be from the manufacturing process as a contamination (PCB manufacturing process, halogen containing flux, or human handling etc. as source) or from the service environments. Solutions with chloride

concentrations ranging from 10 – 1000 ppm were used for the present investigations.

Bromide ions: The ECM experiments in bromide solution is conducted due to the possibility of finding brominated species on a PCBA resulting from the use of Tetrabromobisphenol A (TBBA) as fire retardant in the PCB laminate. Heating during soldering can result in degassing of a number of brominated species from TBBA [26] especially enhanced by the use of higher temperature for lead free soldering (approx. 250°C, but locally, the temperature can be 270°C).

Adipic acid: Effect of adipic acid on the ECM was investigated because the no-clean solder flux residue usually found on a PCBA from the manufacturing process consists of di-carboxylic acids. One of the most commonly found di-carboxylic acid in no-clean flux residue is adipic acid [27,28].

Effect of pH: Solutions with pH values ranging from 0 – 11 on ECM of tin were investigated using de-ionized water with pH adjusted using HNO_3 or NaOH.

Effect of dust: Dust from various sources can enter the electronic device, which is very detrimental for corrosion. One reason for the increased corrosion in the presence of dust is due to the ability of dusts to provide ions that contribute to the conductivity of the solution and corrosion. Results on the influence of two types of dusts on ECM are presented in this paper namely a mild dust (collected indoor in household) and an aggressive dust (collected in a pig farm). The exact chemical composition of these dusts is very complex, however, for indexing of the aggressivity of each categories, ion chromatographic analysis shows that the aggressive dust provides higher ionic equivalent to the solution (e.g. ~6-10 ppm chlorides, ~3-5 ppm sulphate, ~3-4 ppm ammonium ions) than mild dust (e.g. ~2-3 ppm chlorides, ~1 ppm sulphate, ~0.5–2.5 ppm ammonium ions) [29]. For the ECM experiments on the effect of dust, components were exposed at respective places for 2-4 months. Electrochemical migration experiments were later carried out by placing a drop-let of clean deionised water on the component. Soluble ionic species from the dust are hereby dissolved into the solution.

8.2.4 VISUALIZATION OF LOCALIZED pH CHANGES DURING MIGRATION:

Experiments using Gel:

A gel made using a mixture of agar gel (Agar type A7002, Sigma-Aldrich Chemie GmbH, Germany) and universal indicator (Universal pH indicator range pH 3-10, Sigma-Aldrich Chemie GmbH, Germany) was used for visualizing pH gradients. Concentration of agar gel was 3g/100 ml of solution and pH indicator was 15 ml/100ml. The indicator gel was prepared at a temperature of 80°C in the liquid form and was casted on the components to be tested on the PCBA. The thickness of the cast gel layer on the component was approximately 1 mm and the gel acts as the electrolyte during the electrochemical experiments. Required potential bias was applied between the electrodes of the component (anode and cathode) by connecting the PCBA to the potentiostat, and the localized pH changes resulting from the electrochemical reactions and the colour change was recorded in-situ using a video microscope.

Experiments using pH indicator in solution:

A tiny drop-let (2 µl) of de-ionized water mixed with universal pH indicator (50 ml/50 ml of water) was applied to the components mounted on to the SCECM set up. Required potential was applied between the electrodes using a potentiostat and the localized pH changes resulting from the electrochemical reactions and the colour change was recorded in-situ using a video microscope.

8.2.5 EQUIPMENTS USED:

All electrochemical experiments were carried out using Biologic VSP multichannel potentiostat, Bio-Logic Instruments, France, having 0-20V compliance voltage. SEM analysis was performed using a Zeiss Ultra55 Scanning Electron Microscope. TEM analysis was performed using a Jeol JEM-3000F Field Emission Electron Microscope operated at 300kV equipped with Oxford instruments EDS analysis.

8.3 RESULTS AND DISCUSSION:

8.3.1 EFFECT OF SOLUTION CHEMISTRY ON ECM OF TIN:

Typical results that are representative of the ECM behaviour of tin electrodes on chip components in various environmental conditions are presented below. These include the effect of chloride, bromide, adipic acid, dust particles, pH of the solution, and potential bias. The aim of presenting this summary of results from various sets of investigations is to show the general trend on tin migration with respect to the aggressiveness of the environment, pH, and potential bias.

Figure 8.4 shows the summary of a series of ECM experiments carried out in chloride solutions under different potential bias [25]. Typical optical micrographs shown in Figure 8.4 shows that at low concentrations of chloride (10 ppm), a clear dendrite formation was observed, while at 1000 ppm chloride (Figure 8.4b) there was no dendrite formation although heavy corrosion was observed at the anode. In-situ video for 1000 ppm experiment also showed vigorous gas evolution in the solution and heavy precipitation was observed instead of dendrite formation as shown in the picture in Figure 8.4b, which is extracted frame from the video. Increase in potential bias from 3 to 12V also had a somewhat similar effect on the dendrite formation where less migration by heavy corrosion was observed at high chloride concentration. At 12V, the dendrites formed were generally thinner as illustrated in Figure 8.4c, although heavy electrochemical activity was observed in the solution in the in-situ video. Similar behaviour was observed for chip capacitors with different chloride concentrations and potential values.

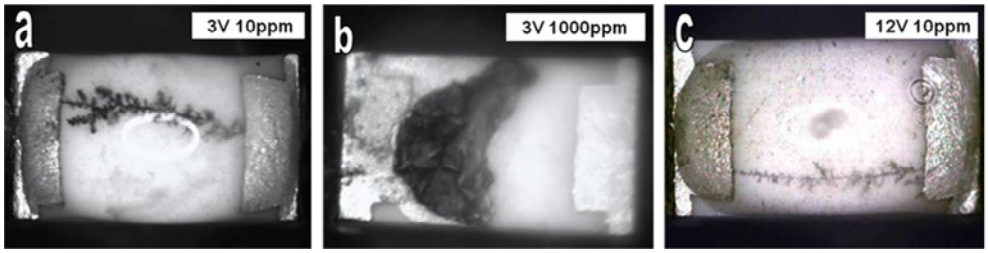

Figure 8.4: Effect of chloride and potential on the ECM of tin during experiments using chip resistor: (a) 3V, 10 ppm, (b) 3V, 1000 ppm, and (c) 12V, 10 ppm. (Anode is on the left and cathode is on the right). Dimensions of the components are 1.5x0.8mm (0605 housing).

Figure 8.5 shows the effect of various concentrations of bromide on ECM using chip capacitor [29]. Typical pictures extracted from the respective in-situ videos in Figure 8.5 illustrates a tendency similar to the chloride, where higher concentrations of bromide reduces the dendrite formation probability, although severe electrochemical activity was found in the in-situ video and formation of a white blurry layer on the surface for 250ppm bromide concentration.

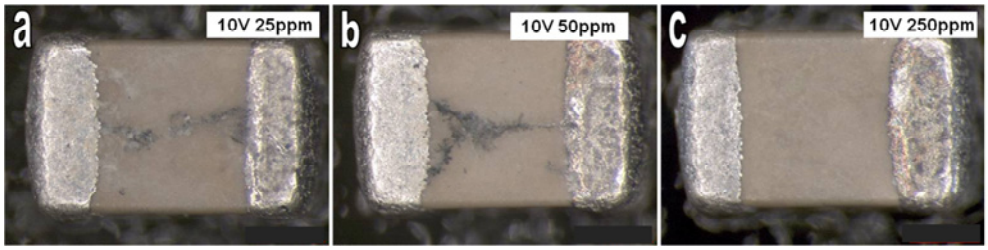

Figure 8.5: Effect of bromide on the ECM of chip capacitor at 10V in: (a) 25 ppm, (b) 50 ppm, and (c) 250 ppm. (Anode is on the left and cathode is on the right). Dimensions of the components are 1.5x0.8mm (0605 housing).

The role of adipic acid on ECM was investigated at various concentrations for isolating the effect of one of the widely used activator components in the commonly used no-clean flux systems. Generally a no-clean flux typically consists of three major components: (i) Solvent – a medium for mixing all the components of the flux, (ii) Activators – mainly weak organic acids, and (iii) Vehicle – a non-volatile compound such as a resin or ester stable through all temperature of the soldering profile. Assumption behind the no-clean flux based soldering process is that the aggressive chemicals used in the flux solution will react or burn off during the soldering process so that it leaves minimum residue of aggressive nature. However, in practice this seldom happens, but mostly substantial quantity of flux residue including the activator components could be found on the PCBA [27]. The activator components in the no-clean flux often consists of one or more of the weak organic acids (WOA), especially the short-chain carboxylic or dicarboxylic acids such as adipic acid, glutaric acid, succinic acid, malic acid or formic acid, but major part in most flux systems is adipic acid.

Figure 8.6 shows the effect of adipic acid concentration on the susceptibility of ECM. The effect of no-clean flux residue on chip component was also investigated by adding a known quantity of flux on to the component and heating to the desired

temperatures prior to the ECM testing [30]. A common observation on the effect of flux residue and adipic acid was that the increasing amount of unreacted flux residue or adipic acid has decreased the probability of tin migration. The micrographs in Figure 8.6 reveals this observation, where at low concentrations of adipic acid dendrite formation occurred, although the lifetime of the dendrite was very short and it rapidly collapsed, while at higher concentration there was no dendrite formation. Behaviour similar to 1000 ppm was shown by saturated solution of adipic acid (pH 2.6).

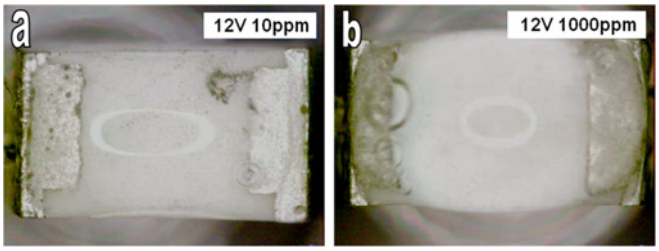

Figure 8.6: Effect of adipic acid on the ECM of chip resistor at 12 V: (a) 10 ppm (pH 4.4), and (b) 1000 ppm pH (3.2). Dimensions of the components are 1.5x0.8mm (0605 housing).

Presence of adipic acid in solution can shift the bulk pH of the micro-droplet towards acidic pH. In order to understand the effect of bulk pH on ECM, experiments were conducted in acidic (adjusted by HNO_3) and alkaline (adjusted by NaOH) environments. As shown in Figure 8.7, very low pH levels did not favour dendrite formation (Figure 8.7a), however increasing the pH value to 4.0 seems to produce a little dendrite formation (Figure 8.7b) at high voltages. It is clear from the pictures in Figure 8.7a that at 0 pH severe corrosion occurred on the anode, however only a white blurry layer of precipitate forms instead of dendrite growth. However, the current density for 0 pH experiment was very high, therefore it was difficult to differentiate the presence of tiny dendritic structure from the white blurry layer. Shift towards alkaline pH values (Figure 8.7c and d) showed dendrite formation at pH 9 and 11, while the dendrites rapidly collapsed in the case of pH 9. Overall the effect of pH suggests that the ECM of tin is pH dependant, and highly acidic or alkaline pH seems to be most favourable for dendrite formation. Presence of adipic acid to a significant amount can also act as acidic buffer, however the

presence of adipic acid in solution was also found to promote the passivation of the tin surface (see section 8.3.6).

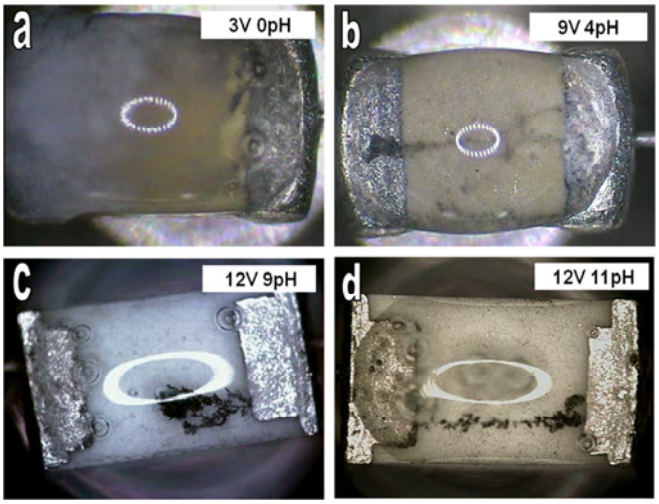

Figure 8.7: Effect of pH on the ECM on Tin using chip resistor: (a) 0 pH (3V), (b) 4 pH (9V), (c) 9 pH (12V), and (d) 11 pH (12V). Acidic pH was obtained by addition HNO_3 and alkaline pH was obtained by addition of NaOH. Dimensions of the components are 1.5x0.8mm (0605 housing).

Figure 8.8 shows the effect of a mild (indoor dust) and aggressive dust (typically found inside the electronics used in pig farms) on the electrochemical migration possibility on a chip capacitor [29,31] . Only the presence of mild dust at lower levels resulted in ECM (Figure 8.8a), while the increased amount of mild dust or aggressive dust has reduced the migration susceptibility (Figure 8.8b,c,d), instead, white precipitates were formed on the component surfaces similar to that observed in the earlier cases.

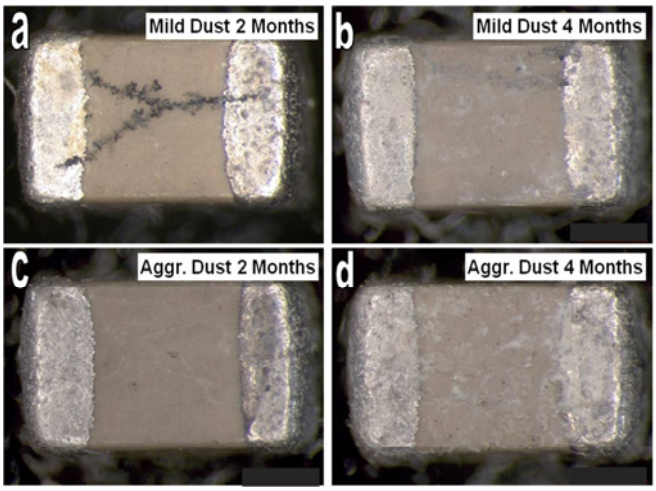

Figure 8.8: Effect of dust on ECM of chip capacitor at 10 V potential bias: (a) mild dust, collection period 2 months, (b) mild dust, collection period 4 months, (c) aggressive dust, collection period 2 months, and (d) aggressive dust, collection period 4 months. Dimensions of the components are 1.5x0.8mm (0605 housing).

Table 8.1 provides the summary of the data from a number of repeated experiments using the above environmental conditions (some of them are not shown in the above figures). Probability values in the table represent the number of repeated experiments showed stable dendrite growth against a total number of experiments conducted. Dendrites formed that do not short circuit (unstable growth) are therefore not included. The data clearly shows a general trend in ECM probability, irrespective of the environment. Probability of dendrite formation in general increases initially with increase in aggressiveness of the solution (more concentration of aggressive ions or other contaminations) and then decreases as the aggressiveness of the solution gets above a certain value.

Table 8.1: Summary of probability of migration data from ECM experiments described above.

Solution	Potential bias	Probability of ECM
10 ppm chloride	3V	3/5
100 ppm chloride	3V	2/6
1000 ppm chloride	3V	0/6
10 ppm chloride	12V	2/6
100 ppm chloride	12V	6/6
1000 ppm chloride	12V	3/6
10 ppm bromide	10V	0/6
25 ppm bromide	10V	1/6
50 ppm bromide	10V	4/6
250 ppm bromide	10V	1/6
Mild dust	10V	5/6
Aggressive dust	10V	2/6
1 ppm adipic acid	12V	2/6
10 ppm adipic acid	12V	0/6
1000 ppm adipic acid	12V	0/6
Saturated adipic acid	1, 2, 3, and 12V	0/6
0 pH	1V	0/3
0 pH	3V	0/3
4 pH	3V	0/3
4 pH	9V	1/3
9 pH	12V	1/6
11 pH	12V	2/6

Dendrites formed at high voltages was generally observed to be less branched than those formed at lower voltages [25,29,32], which corresponds well with the findings of Devos et al. [33,34] and Wranglén [35]. However, a common feature observed with increase in aggressiveness of the environment, and therefore the increased corrosion at the anode is that the dendrites formed under more aggressive conditions are more covered with or embedded in oxides/hydroxides

compared to the one formed at less aggressive conditions. All the dendrites showed some oxides, however the one formed in higher concentrations of contaminants showed more oxides/hydroxides in their structure.

A common denominator in all the observations described above is that the very aggressive environment instead of increasing the probability of dendrite formation (more tin dissolution and therefore more ions for dendrite formation) rather decreases the probability. Even in cases where the dendrites have formed, increase in aggressiveness of the environment cause more inclusion of precipitates of oxides/hydroxides to the dendrites [29,32]. Dendrite formation is possibly also a function of the pH of the solution as shown in Figure 8.7 where a high and slightly lowered pH conditions favours the migration, but no migration at very low starting pH levels. This is in good agreement with tin plating technology where both acidic and alkaline plating baths exist [36] for tin. In summary, the results reveals that the increased dissolution of tin does not necessarily result in increased migration even if conducting ions are present in the solution to transport substantial current through the solution. Further, increased tin dissolution also correlates with the formation of white blurry layer without dendrites. This shows that the migration of tin is a delicate process where the formation of dendrites requires a balance of various factors in the micro-volume of environment inside the droplet.

8.3.2 POSSIBLE ELECTRODE REACTIONS AT THE ANODE AND CATHODE, AND PH CHANGE

The anode and cathode reactions expected for tin electrodes in aqueous based electrolytes having a starting pH close to neutral and applied potential between 3V-12V are:

Anode:

$$Sn \rightarrow Sn^{2+} + 2e^{-} \quad \textit{Eq. 1}$$

$$Sn^{2+} \rightarrow Sn^{4+} + 2e^{-} \quad \textit{Eq. 2}$$

$$Sn^{4+} + 4H_2O \rightarrow Sn(OH)_4 + 4H^{+} \quad \textit{Eq. 3}$$

$$Sn + 4H_2O \rightarrow Sn(OH)_4 + 4H^{+} + 4e^{-} \quad \textit{Eq. 4}$$

$$2H_2O \rightarrow O_2 + 4H^{+} + 4e^{-} \quad \textit{Eq. 5}$$

Cathode:

$$O_2 + 2H_2O + 4e^{-} \rightarrow 4OH^{-} \quad \textit{Eq. 6}$$

$$2H_2O + 2e^{-} \rightarrow H_2 \uparrow + 2OH^{-} \quad \textit{Eq. 7}$$

Electrode potentials of tin in acidic media are presented below in Figure 8.9.

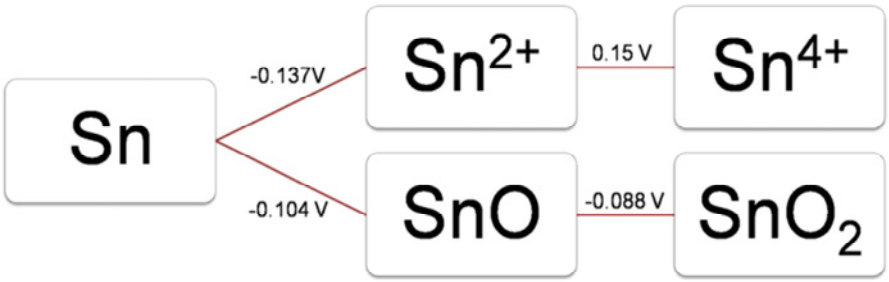

Figure 8.9: Tin electrode potentials vs. SHE in acidic media.

Eq. 1 represents the anodic dissolution of tin as stannous, which exist to a certain extent as Sn^{2+} aqueous ion in slightly acid solutions [36]. Stannic ions formed by Eq. 2 co-exist with the stannous ions, but unless very low pH is present, it will rapidly hydrolyze as various tin hydroxides through intermediate species, where $Sn(OH)_4$ is dominant. Eq. 3 and Eq. 4 represents the formation of stannic hydroxide either by hydrolysis of Sn^{4+} (Eq. 3) or by direct oxidation of tin to $Sn(OH)_4$ (Eq. 4). Eq. 3 and 4 are preferred as the pH increases towards the neutral side. Oxygen evolution by water dissociation is also possible at the anode (potentials values above 1.2 V vs SHE), as described by Eq. 5 although the over potential required on tin might be higher. However, under the potential bias conditions used in the present investigations this reaction seems to be possible, as the potentials values are between 3 – 12 V. Eq. 3-5 at the anode also generates H^{+} ions making the local environment more acidic. At the cathode, oxygen

reduction (Eq. 6) and hydrogen evolution from water dissociation (Eq. 7) will create a local alkaline environment, although the dominant cathodic reactions within the potential regime used (3 – 12 V) might be water dissociation.

In order to understand the local pH shift in the micro-volume of environment during ECM testing, and possible effects on the electrochemical migration, two types of experiments were carried out to visualize the local pH development with time. For the first set of experiments, an agar gel media with pH indicator was used so that the relatively immobile gel media gives a clear visualization of the pH change. Figure 8.10a shows the result of this experiment on many of the two chip components on a test PCBA. Figure 8.10b shows the standard Pourbaix diagram for tin indicating the regions of tin stability to which the local pH change observed during the experiment belongs.

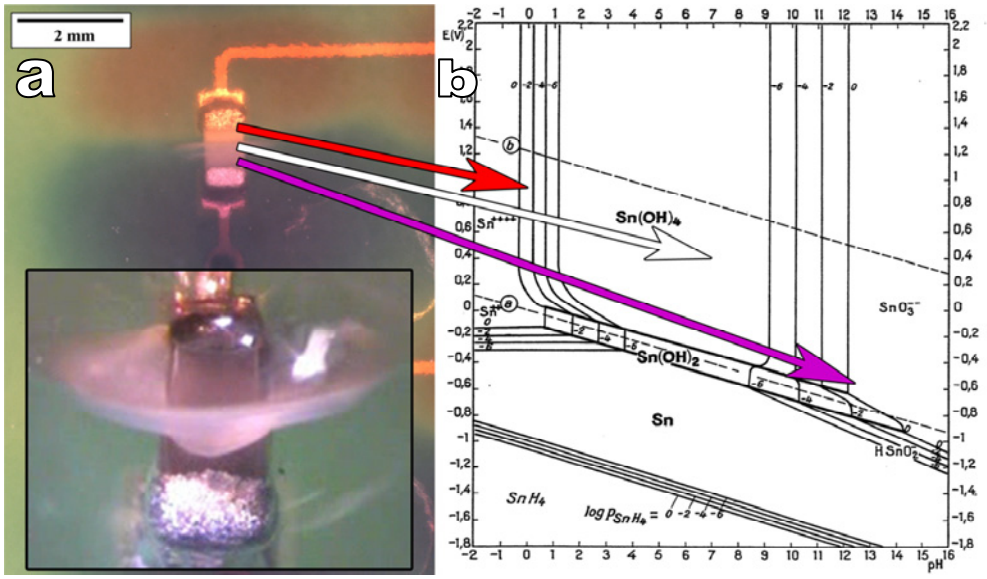

Figure 8.10: (a) Visualization of localized pH change using agar gel containing pH indicator under 3V potential bias on two SMD ceramic chip capacitors on a PCBA, inset shows hydroxide formation in the middle after extended duration of the experiment. (b) Standard Pourbaix diagram for tin. (Image b is © NACE International 1974 [37]. Markings that are irrelevant for present context have been deleted from the original figure)

Figure 8.10 clearly shows the visual evidence for the pH change where top parts of the components (anode, red in colour) with time develops an acidic pH, while the bottom part (cathode, green in colour) turns to alkaline. This happens within a time

interval of 5-10 seconds and the colours from the pH indicator are at the minimum or maximum values of the indicator for acidic and alkaline regions respectively, corresponding to pH values of pH 4 or below for acidic region and pH 10 or above for alkaline. Since the rate of development of the localized pH is fast, there is also a sharp boundary separating the two layers where a white layer is observed (see white arrow) similar to precipitation of hydroxides. A magnified view of the white blurry layer at the interface of two pH regions (shown as inset in Figure 8.10a) shows a conical shape pattern extending in the middle towards the cathode. Overall, the alkaline area is larger than the acidic area. This might be attributed to the distribution of current at the anode for various other reactions not involving hydrogen ion production, while at the cathode all the current is consumed by the dominating reaction of water dissociation.

To elucidate the pH change in the micro-volume of environment on the component during ECM experiments in actual practise (where no gel is present), another set of experiment was conducted by adding the pH indicator directly into the solution without using agar gel. The local changes in pH and associated colour change was recorded in-situ using a video microscope. In this case, the dynamic movements of the pH regions when the bias was applied could be visualized in the in-situ video. Figure 8.11 shows few typical pictures extracted from the in-situ video at various time intervals to provide an overview of local pH development. The dynamics of the pH changes were extremely fast and significant pH changes were observed to occur within seconds. However, electrochemical migration could not be observed in this case. After approx. 20s formation of brown coloured precipitations were observed near the anode which was attributed to agglomeration of the pH indicator and hydroxide species.

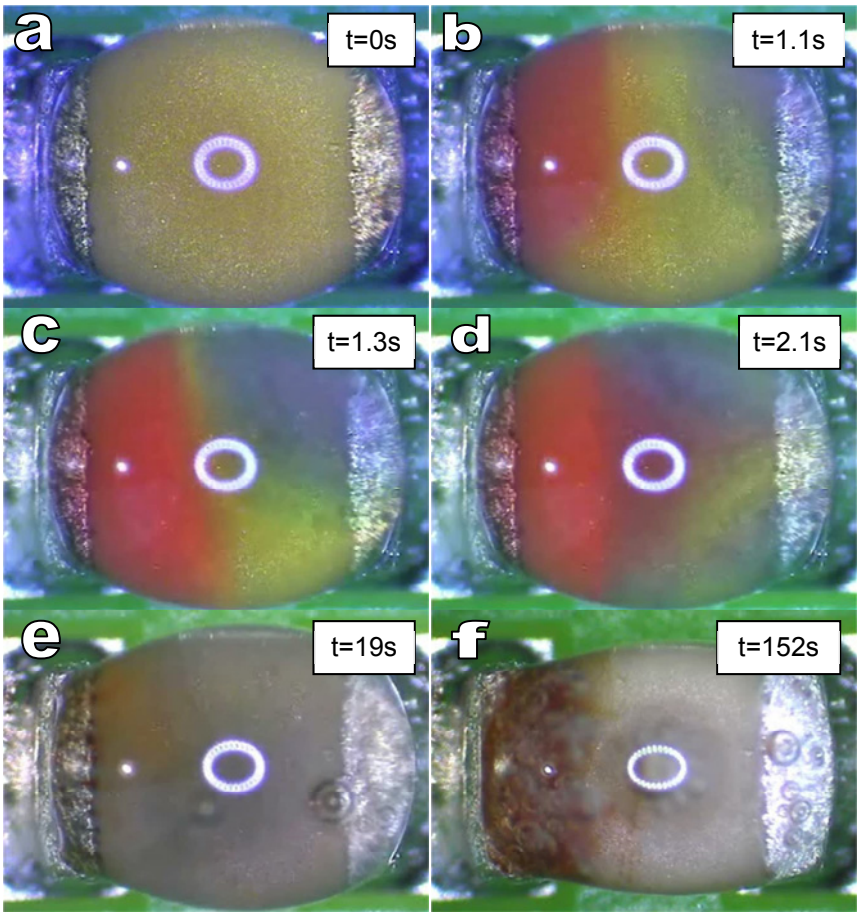

Figure 8.11: Visualization of localized pH change using pH indicator in solution under 3V potential bias on a single chip component. Time of image acquisition after application of potential bias is marked on each image. Dimensions of the components are 1.5x0.8mm (0605 housing).

Similar to that observed in agar gel, local pH regions were developed within ~1 second after the application of potential bias indicated by the red, yellow, and purple colour respectively for acidic, neutral, and alkaline conditions in Figure 8.11b. The acidic and alkaline areas spread out with time (Figure 8.11c and Figure 8.11d), while rapid disturbances in the solution due to convection was found. This movement cause uneven distribution of pH regions, in this case in the middle of the component, though the behaviour seemed close to random when comparing several experiments. Overall the regions close to anode remains acidic (colour code of indicator shows a pH of 4 or below) and cathode remains alkaline (colour

code shows a pH of 10 or above), while smaller regions of neutral pH (yellow colour) appears in the middle.

The pH gradient is largely influenced by the inter-electrode distance. In bulk electrolytes, the diffusion layers by the electrodes gradually decrease with distance from the electrode surface and after a certain distance, natural convection will make it reasonable to assume that the pH is the same as the bulk solution. The magnitude of such diffusion layers depend on temperature, diffusion constants and electric field, but are typically in magnitudes of μm-mm. At short distances, however, where electrodes are closely spaced as on small electronic components, there could be an overlap between the pH regions originating from the electrodes, so that a very strong pH gradient will form at the boundary where the pH regions from the anode and cathode meet. In the case of large distance between the electrodes (distance much larger than the scale of the pH influenced regions), a comparatively large area of bulk pH will be present. This will have an important influence on the stability of the tin ions in solution and migration through the solution, and therefore on the electrochemical migration properties. However, the disturbances and convection within the solution due to gas evolution and other ionic movements can to some extent even out the pH gradients and create fluctuations across the specimen surface. For these reasons, the experimental procedures and test parameters used for ECM testing are very important and needs to be reported clearly as the results from two different distance of separation between the electrodes should be compared with caution.

8.3.3 STABILITY OF TIN SPECIES IN SOLUTION AND CONNECTION TO ECM

Once the pH gradient develops within the micro-droplet, tin dissolution at the anode will produce stannous and stannic ions in the local acidic environment. As the positively charged ions are attracted to the negatively charged cathode, it will move through the solution into a region with higher pH within the micro-droplet. The local chemistry experienced by the tin ions during the movement from anode to cathode has serious implication on the formation of the dendrite and ECM behaviour as it determines the transformation of tin ions into various other stable species as a function of pH. Considering the variations in pH due to the electrochemical

reactions at the electrodes and corresponding stability of tin species, Pourbaix diagrams [37] can be used for the analysis. The Pourbaix diagram for the Sn-H_2O system at 25°C showing the stability of various tin species is shown in Figure 8.10b.

A Pourbaix diagram provides an overview of the thermodynamic stability of the dominant species, but other species can also co-exist in respective areas to a lesser extent. The diagram is also limited by the thermodynamic data that is available for relevant tin species, and therefore some tin hydroxyl ions are excluded [37]. Relatively low levels of other Sn(IV) species such as $Sn(OH)^{3+}$, $Sn(OH)_2^{2+}$ and $Sn(OH)_3^{+}$ which are the precursor for $Sn(OH)_4$ will also be observed in solution at concentrations rapidly decreasing with increasing pH from the anode.

Following the stability of various tin species (Figure 8.10b), when the tin ions move away from anode it experiences various pH levels so that it is possible that it will tend to precipitate as $Sn(OH)_4$ (and possibly some $Sn(OH)_2$). As these species are neutral, they will not be further attracted towards the cathode, and migration will be initially stopped, unless it can be converted to ionic species that could migrate and get reduced at the cathode. In general, this is expected to be the basis for electrochemical migration of tin where pH condition acquired through the local chemistry changes determine the stability of tin species including the amount of $Sn(OH)_4$.

However, if the alkaline environment created by the cathode reactions (Eq. 6 and Eq. 7) extends to a region where the stannate species are present, $Sn(OH)_4$ precipitates will disproportionate into ($Sn(OH)_6^{2-}$) complex as described by Eq. 8. Formation of the stannate species ($Sn(OH)_6^{2-}$) is very important for the dendrite formation as now there is an ionic species at the cathode, which can reduce to form metallic tin similar to the process in the alkaline plating of tin. This shows that the stability of stannate region in the Pourbaix diagram is very important for the dendrite formation and growth.

$$Sn(OH)_4 + 2OH^- \rightarrow (Sn(OH)_6)^{2-} \quad \text{Eq. 8}$$

$$(Sn(OH)_6)^{2-} + 4e^- \rightarrow Sn + 6OH^- \quad \text{Eq. 9}$$

$$(Sn(OH)_6)^{2-} \leftrightarrow Sn^{4+} + 6OH^- \quad \text{Eq. 10}$$

$$Sn^{4+} + 4e^- \rightarrow Sn \quad \text{Eq. 11}$$

In a relatively static micro-droplet on the component, the development of these stability regions could be schematically expressed as shown in Figure 8.12. As the dissolved stannous and stannic ions from the anode migrate towards the cathode, these ions get hydrolysed into many intermediate species, but mainly stannic hydroxide, which will eventually converted to stannate as it encounter the high alkaline conditions at the cathode similar to a travel through the pH regions in the Pourbaix diagram from lower pH levels to higher pH conditions.

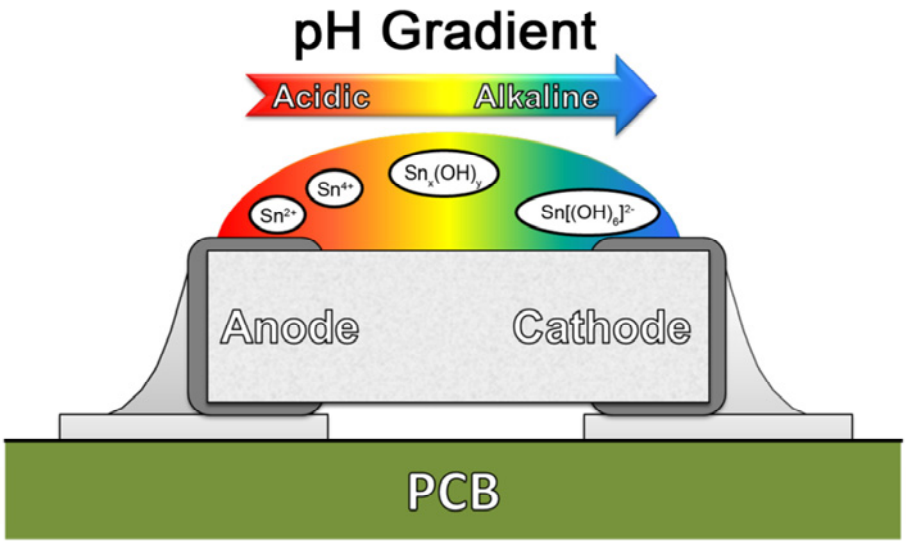

Figure 8.12: A schematic of the pH gradient formation inside the droplet over a SM chip component with tin electrode illustrating the areas of stability for various species with local chemistry changes.

Formation of dendrite during the migration process is therefore most likely to have a mechanism similar to the alkaline plating of tin. Alkaline plating of tin was described by Schlesinger and Paunovic [36] as a reduction of $Sn(OH)_6^{2-}$ to metallic tin (Eq. 9), but as $(Sn(OH)_6)^{2-}$ is inherently negatively charged it will be repelled by

the cathode. However, this mechanism is widely accepted for tin reduction, and the migration mechanism for the tin ion to reach the cathode could be diffusion due to a concentration gradient or, more likely, it could be due to an equilibrium between $(Sn(OH)_6)^{2-}$ and stannic ions (Eq. 10) which was proposed by Cuthbertson [38]. Stannic ions would then be reduced at the cathode according to Eq. 11, and Eq. 9 is obviously just a combination of Eq. 10 and Eq. 11.

Figure 8.13 shows the concentration of many tin(II) species as a function of pH, calculated using Medusa software [39]. Due to limitations in the thermodynamic data for Sn(IV) species, only Sn(II) is included in the graph. The graph should therefore only be regarded representative figure to show the relative stability of various tin species with the hydroxyl group.

The presence of $SnOH^+$ and $Sn_3(OH)_4^{2+}$ ions are very interesting, as they are seen to be stable in a broader pH range of approximately 2-5, whereas the stability of Sn^{2+} is seen to rapidly drop above pH 2. Similar species for tin(IV) ions in acidic media could be $Sn(OH)^{3+}$, $Sn(OH)_2^{2+}$ and $Sn(OH)_3^+$, though no thermodynamic data exist for these species to make a calculation as in Figure 8.13.

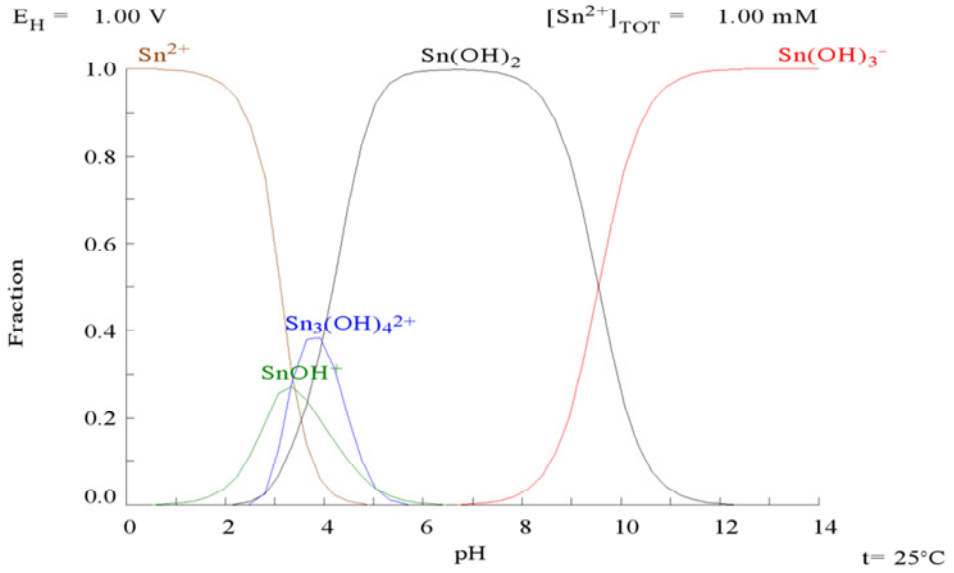

Figure 8.13: Graph showing the fraction of various tin(II) species as a function of pH, calculated by Medusa software for $[Sn^{2+}]=10^{-3}$.

8.3.4 ELECTRODE REACTION KINETICS AND SHIFT IN STABILITY LINES

As the Pourbaix diagram shows (Figure 8.10b), the exact pH at which the stannous and stannate species are stable depends on the amount of tin dissolved and therefore shift to higher pH values with increased dissolution of tin at the anode. A change in stannic ion concentration from 10^{-6} M to 1 M results in broadening of $Sn(OH)_4$ region from 9 to 12 pH. Corrosion promoting species such as chloride, bromide, flux residue etc. can increase the dissolution rate of tin. Increased anodic dissolution rate at the anode expands the stability area for $Sn(OH)_4$, which acts against the dendrite formation, as higher alkaline pH is required now in order for the Eq. 8 to run. If the anodic reaction rate is too slow, on the other hand, migration kinetics will also be slow.

Assuming an experiment where a fixed potential bias is applied, which is sufficient for tin oxidation/reduction to occur, and all parameters are held constant except the concentration of the aggressive ionic species in solution (e.g. chloride), the probability of observing dendrite formation, $P_{(migration)}$, can then be regarded as:

$$\text{Anodic rate} \uparrow \Rightarrow [Sn] \uparrow \Rightarrow \text{Stability of } Sn_xOH_y \uparrow \Rightarrow \text{P}(Migration) \downarrow$$

$$\text{Anodic rate} \downarrow \Rightarrow [Sn] \rightarrow Low \Rightarrow \text{P}(Migration) \downarrow$$

If $P_{(migration)}$ is plotted versus the anodic reaction rate, a point of optimum migration kinetics would then be found, where the highest probability for dendrite formation occurs, as shown schematically in Figure 8.14a. The experimental results on the probability of migration plotted as a function of concentration of the aggressive species in solution is shown in Figure 8.14b, which clearly show the concentration dependency where intermediate levels result in high probability, while very low or high concentration reduces the ECM. The concentration for maximum probability for migration is a function of anodic dissolution rate, applied potential, and distance between the electrodes. In Figure 8.14, the rate of dissolution of tin has increased with increasing concentration of chloride/bromide or potential bias.

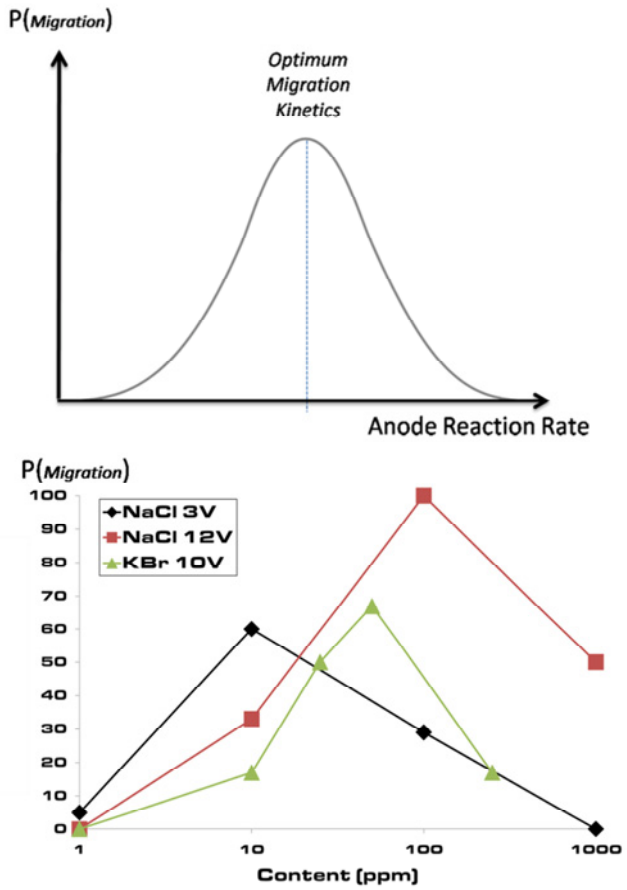

Figure 8.14: (a) Schematic plot showing the probability of migration, P(migration) as a function of anodic dissolution rate for tin where all parameters are held constant except the amount of aggressive species in solution and (b) Probability plot from experimental data for electrolytes containing NaCl and KBr.

The cathode reaction kinetics will influence the formation of local alkaline environment near the cathode, and species that influence the hydrogen overvoltage could therefore influence migration dynamics. However, the tin reduction step (Eq. 9) has generally not been observed to be the rate determining step, as dendrites have been observed to grow to form a short circuit within few seconds given the right conditions [25]. The anodic reaction rate of tin dissolution will therefore in general play a significantly larger role on migration kinetics than the cathodic rate, which corresponds well with the findings of Takemoto et al. [21] where the surface roughness and anodic dissolution was found to influence migration behaviour and with the findings of Lee et al. [40] who found a correlation

between ECM behaviour and the initial anodic dissolution rate, measured by potentiodynamic polarization in sodium chloride and sodium sulphate electrolytes.

Based on the ECM mechanisms explained above, in general the following sequence for ECM may be proposed with increasing dissolution of tin: (i) comparatively low dissolution of tin provides a more metallic dendrites due to the low levels of precipitated hydroxides, (ii) medium levels of tin ions provides dendrites with incorporated hydroxides due to its increased quantity in solution, and (iii) high levels of tin dissolution leading to just precipitation, but no dendrites as the local alkaline conditions are not enough to produce stannate ions. This is in clear agreement with the results presented on ECM susceptibility in various environments and localized pH shifts. However, the above mentioned mechanism is highly influenced by the presence of species which can form soluble tin complexes that are stable in a broad pH range and thereby aiding the migration kinetics.

8.3.5 REDUCTION OF TIN AND DEVELOPMENT OF DENDRITE STRUCTURE

Unlike in the electroplating process, lack of additives in the micro-volume of environment during migration, rough surface morphology of the electrodes, and relatively low conductivity of the electrolyte causing non-uniform current distribution on the cathode surface, and strong electric field due to the relatively short distance between the anode and cathode will often result in a deposition in the form of a dendrite. The electrodeposition mechanism is not trivial, and is highly influenced by the dissolved species in the electrolyte. Fischer [41] proposed five main growth types of polycrystalline electrodeposits:

- Field-oriented isolated crystals type (FI)
- Basis-oriented reproduction type (BR)
- Twinning intermediate type (Z)
- Field-oriented texture type (FT)
- Un-oriented dispersion type (UD)

Dendritic growth is a FI type electrodeposit. A detailed explanation of the deposit types is outside the scope of this paper, but could be found elsewhere [42]. Focus will therefore be given to the factors leading to the FI type of growth. Winand [42]

proposed that the structure of the electrodeposits is mainly influenced by the ratio of the current density, J, to the diffusion-limiting current density, J_d, (mass transfer) at the cathode and on the inhibition intensity, as illustrated by the Winand's diagram in Figure 8.15. Other factors influencing the structural growth of the electrodeposit are concentration the ions containing the metal (C_{meZ+}), agitation, temperature, pH, other cations and anions, complex formation, inhibitors, and substrate [42].

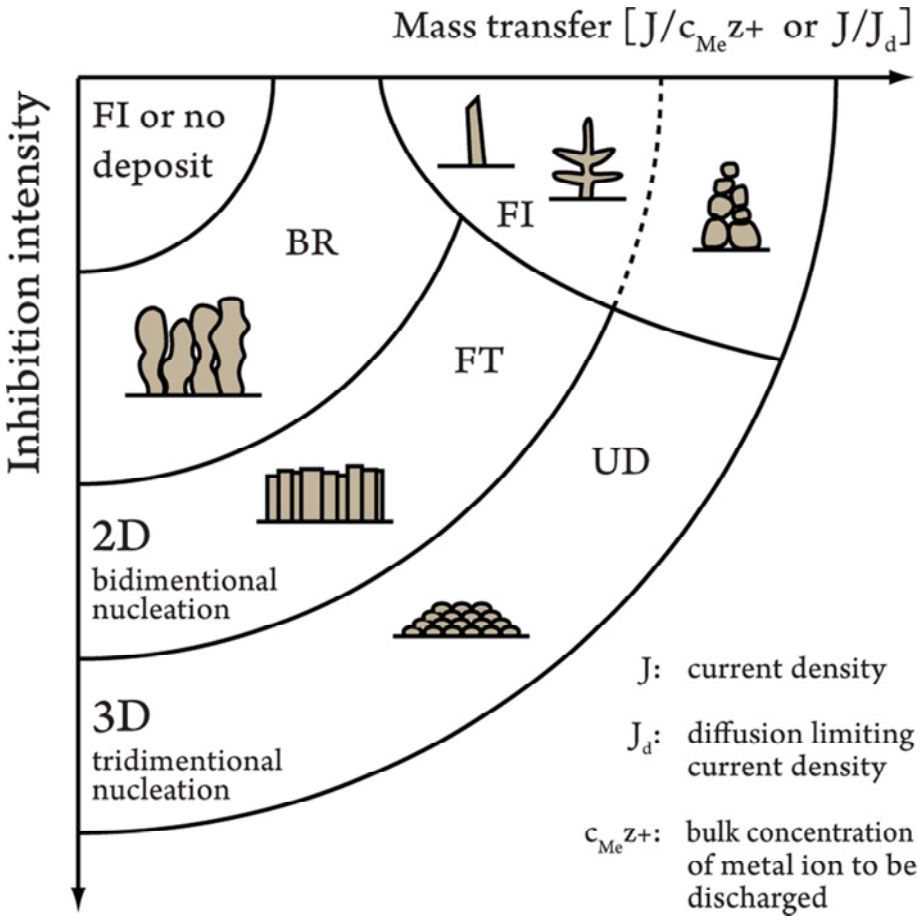

Figure 8.15: Winand's diagram relating the structure of electrodeposits to mass transfer and inhibition. Inspired by diagram proposed by Winand [42].

Inhibition intensity can be influenced by organic compounds that are adsorbed to the cathode surface, thereby reducing the efficiency of the reduction of tin ions to metallic tin (e.g. Eq. 9) at the cathode. Contaminations on the PCBA that could be

dissolved into the condensed layer of water will therefore not only contribute to a change in the conductivity of the electrolyte, but they can also dramatically change the type of electrodeposit formation at the cathode. This is particularly important for ECM in the presence of flux residues, which consists of di-carboxylic acids (see section 8.3.6).

The electrodeposit growth mechanism will not only influence the shape and rate of the dendritic growth, but also the conductivity of the dendrite shorting the two electrodes due to the variation in chemical composition. By calculating the current going through the dendrites grown in electrolytes containing various NaCl concentrations (10 – 1000 ppm range), the resistivity of the short circuited dendrites was estimated by Minzari et al [25,32] on ceramic chip resistors. Results showed that the dendrite resistivity varied with potential and NaCl concentration, and on the average, the resistance value was much higher than the resistance of pure tin with similar dimensions. Further, ex-situ electron microscopy has also shown that the dendrites are most likely to consist of a mixture of tin and tin hydroxides [29,32] especially in more aggressive conditions in which the dissolution of tin is high. Tin hydroxide particles are often found dispersed over the specimen surfaces under such circumstances as shown in Figure 8.16a where a high magnification picture of a dendrite branch on the electrode surface shows precipitate particles of approximately 1μm diameter. In-situ video of this experiment reveals incorporation of the particles to the dendrite structure (Figure 8.16a). This is in agreement with the electroplating theory by Schlesinger and Paunovic [36], where oxidized Sn(IV) colloids are reported to give coarsening and decreased solderability of an electrodeposit. In the present case, it is possible that the outer surface of the precipitated particles comes in contact with a dendrite branch due to convection, which will convert outer surface of the particles to stannate due to the local alkaline pH, and subsequent partial reduction will incorporate them to the dendrite branch. However, a thin layer of oxide crust was found on all dendrites formed irrespective of the parameters as shown in the TEM image (Figure 8.16b) of a dendrite fragment formed in 10 ppm NaCl solution under 3V potential bias as described in [32].

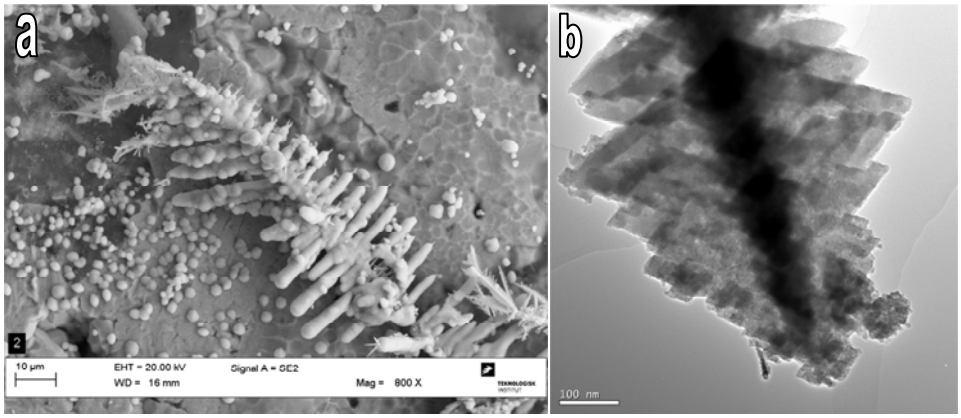

Figure 8.16: a) Example of dendrite growth in the presence of tin hydroxide particles [29], b) TEM image of dendrite grown in 10 ppm NaCl electrolyte under 3V potential bias showing oxide crust.

EDS analysis and electron diffraction in the TEM has showed that the dendrite structure has areas that are purely metallic, while the high oxygen content regions are attributed to hydroxides [32]. A schematic of the model for the incorporation of hydroxide particles to the dendrite is shown in Figure 8.17.

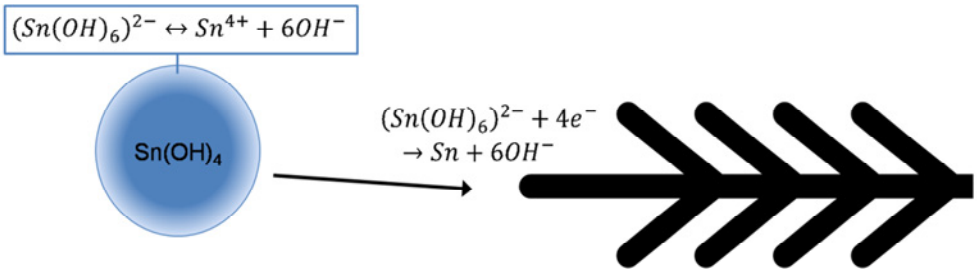

Figure 8.17: A schematic of the model proposed for the incorporation of tin hydroxide particles to the dendrite structure during it growth through the micro-droplet of solution with varying local pH values.

8.3.6 OTHER EFFECTS OF IONIC CONTAMINANTS IN MICRO-VOLUME OF ENVIRONMENT

Contamination on an electronic device or PCBA can originate from the manufacturing process or during service. Solder flux is one main source for contamination from the manufacturing process. In addition, contamination can also result from degassing of chemicals incorporated in the PCB laminate and human handling of PCBA etc. [29] During service, several other types of contaminants

can enter the PCBA surface such as chloride, dust particles (also provide conducting ions) and many other aggressive ions and gaseous species, depending on the place of application.

The activators in the no-clean flux systems [27,28] presently used for the electronic manufacturing are weak organic dicarboxylic acids as described before. There have been many investigations in the literature on the effect of flux residue on corrosion of electronic devices [11,43-53]. In general, the understanding is that the presence of flux residue (therefore carboxylic acids) increases the corrosion problems of electronics and especially the ECM. However, the exact influence of the flux residue amounts or components are not investigated or discussed. Our investigations on the contrary show that significant levels of no-clean flux residue or adipic acid stops migration of tin. Table 8.2 gives the probability of ECM as a function of flux residue formed at various temperatures on a chip capacitor followed by ECM testing using SCECM in a micro-droplet of de-ionised water. Probability of migration is higher when the quantity of flux residue is lower (The amount of flux residue is reduced with exposure to increasing temperature), while no migration was observed in the flux residue at room temperature. The effect is expected to be due to two factors, one related to the buffering effect of acid as explained before so that the pH is more conducive for precipitation rather than migration, while the other effect is related to the passivation effect of the organic compound.

Table 8.2: Probability (out of total 6 experiments) of dendrite formation with amount of flux residue.

Flux + heat treatment	RT	170°C	235°C
Probability for dendrite formation	0%	0%	33%

Electrochemical evaluation using potentiodynamic polarization experiments on tin in various concentrations of adipic acid showed passivation in the form of a thick visually observable corrosion product on the surface at higher concentrations of adipic acid. Passivation was found at adipic acid concentration of 1000 ppm or higher (pH 3.2 or less), and gas evolution was observed on the anode at potentials above ~1.9V vs standard hydrogen electrode. Passive layer was visible in the form

of a dark layer (similar to the dark appearance on the anode in Figure 8.6b). Analysis of the passive layer formed in saturated solution of adipic acid by was investigated by FIB-SEM, showing a thickness of ~2µm. At 100 ppm or less (pH 3.8 or above), corrosion was observed as large pits evenly distributed along the surface, though no visible passive layer was found. Further work is presently being carried out on this subject, and will be the subject for future publication.

Presence of ionic species in the solution such as chloride, bromide etc. will also influence the migration, however, the effects these depends on the influence on tin dissolution and on the ability of these ions to form complex with dissolved tin species. Those with strong complexing ability might stabilize more tin ions in solution similar to a plating bath, and are therefore expected to increase the probability of migration. Higher stability of such complexes avoids precipitation of tin species so that the migration possibility is increased.

8.3.7 EFFECT OF POTENTIAL BIAS AND ELECTRIC FIELD

The potential bias that is applied to a given component on a PCBA will influence both the electrochemical potentials of the electrodes, as well as the electric field within the condensed droplet. The electrochemical potential is the driving force for the reactions given in Eq. 1-2,4-6,8, and changing the electrochemical potentials of the electrodes will influence the pH gradient formation and distribution as well as the reaction kinetics (see section 3.2). The electrochemical potential is in principle independent of the inter-electrode distance, but is highly dependent of the resistance of the electrolyte. For this reason, practically no corrosion is observed for metals in very pure water (resistivity in the magnitude of 18MΩ/cm), and is the main reason for why cleanliness of electronic circuits should always have a high priority.

An increase in the electrochemical potential (controlled by the limiting current) will enlarge diffusion layers from the electrodes, thereby causing an abrupt shift in pH within the solution for closely spaced conductors. Providing that the corrosion promoting contaminants are in solution, an increase in the electrochemical

potential will increase the electrode reaction rates, thereby causing a shift in the optimum migration kinetics.

The electric field is inversely proportional to the distance between the electrodes, and will therefore be much higher for small components than for large ones. In practice, the electrode potentials are affected by the potential bias, as a short distance through the electrolyte will result in less ohmic resistance, and less conductive electrolyte could therefore lead to ECM. Surface roughness, electrolyte conductivity, and the presence of surfactant contaminations will influence the electric field distribution, and thereby whether even plating of tin or dendritic growth occurs at the cathode.

8.3.8 EFFECT OF CONVECTION IN THE SOLUTION ON DENDRITIC GROWTH

In some of the experiments reported in this paper, where a rather conductive electrolyte has been used, in-situ video showed convection in the solution which is clockwise or anti-clockwise. Such convection could be attributed to uneven distribution of the electrochemical reactions across the electrodes, thereby facilitating the migration of charged species from anode to cathode at one part of the droplet and from cathode to anode at another (see illustration in Figure 8.18). If ionic flux through the solution is high, such flux could induce convection to the solution in a manner similar to that observed by Tang and Davenport [54] for ferromagnetic species. Another possibility for the convection could indeed be due to the presence of ferromagnetic species from the metal under layers of the component in experiments with severe corrosion which would be subjected to Lorenzian forces in the electric field [54]. However, this should cause the convection to rotate in the same direction every time and therefore this explanation seems less likely, which was also supported by ex-situ EDS analysis of the corrosion products where tin is seen to corrode preferentially, and corrosion of nickel underlayer was only found in few experiments where corrosion was so severe, that almost all of the tin surface had corroded. If convection was observed in the droplet, migration would indeed often occur where the flow is from anode to cathode, which corresponds well with the findings of Devos et al [34], where current flow from anode towards the cathode was found to promote formation of Cu

dendrites. Repetition of experiments showed that the convection occurred in some experiments while in other similar experiments no convection was observed, or rotation was different, supporting that uneven distribution of the electrode reactions is causing the convection.

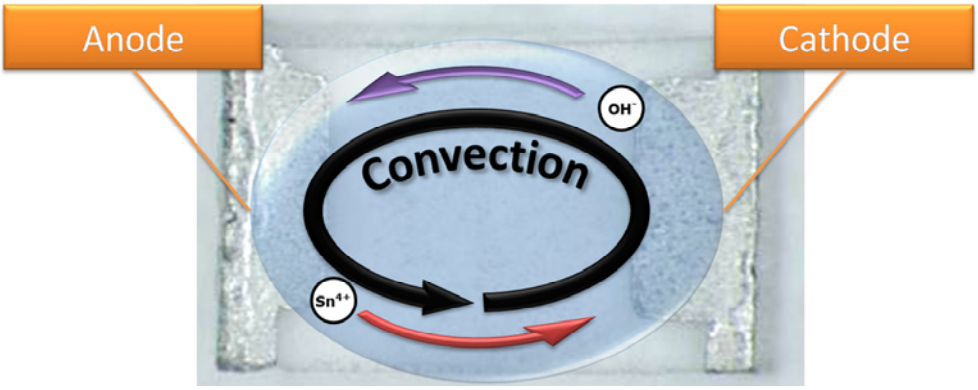

Figure 8.18: Illustration of convection in a condensed droplet on a SMD component. Species drawn in the figure are examples from many other possible ionic species.

Stirring in the solution will smoothen out the pH gradient inside the droplet and could aid transport of ions between the electrodes.

8.4 CONCLUSIONS:

1. Based on the experimental results on ECM of tin under various parameters (environment, potential, and pH), possible general mechanisms is proposed based on the local pH development during electrochemical reactions and stability of tin species in solution.

2. The proposed mechanism shows the importance of the thermodynamic stability domains of tin species, as predicted by the Pourbaix diagram in relation with ECM. Due to the formation of strong local alkaline environment at the cathode, the dendrite formation during ECM of tin is most likely to be correlated with alkaline plating of tin using stannate ions ($Sn(OH)_6^{2-}$) in the alkaline medium, though the amphoteric nature of tin also leaves the possibility of metal reduction similar to acidic plating in cases where the solution is strongly acidic, which is unlikely to exists in normal conditions on a PCBA.

3. Determined by the stability of tin species in the micro-volume of environment in which the migration is taking place, three different types of behaviour could be expected with increased dissolution of tin: (i) formation of a metallic

dendrite, (ii) metallic dendrite mixed with hydroxides, and (iii) only hydroxide precipitate, but no dendrites.

4. Potential, inter-electrode distance, complexing ability of the ionic species in solution, convection etc. alter the ECM behaviour by altering the electric field, kinetics of electrochemical reactions, stability of tin ions in solution, and ionic migration.

REFERENCES

[1] J.H. Lau, C.P. Wong, N.C. Lee, S.W. Lee, Electronics manufacturing: with lead-free, halogen-free, and conductive-adhesive materials, McGraw-Hill Professional, 2002.
[2] IPC-TR-476A, Electrochemical Migration: Electrically Induced Failures in Printed Wiring Assemblies, Northbrook, IL, USA, IPC, Institute for Interconnecting and Packaging Electronic Circuits, 1997.
[3] S. Krumbein, Metallic electromigration phenomena, Components, Hybrids, and Manufacturing Technology, IEEE Transactions On. 11 (1988) 5-15.
[4] S. Brunauer, P.H. Emmett, E. Teller, Adsorption of Gases in Multimolecular Layers, Journal of the American Chemical Society. 60 (1938) 309-319.
[5] D.E. Yost, Silver migration in printed circuits, in: Proc. Symp. on Printed Circuits, Philadelphia, PA, 1955.
[6] G.T. Kohman, H.W. Hermance, G.H. Downes, Silver migration in electrical insulation, Bell Syst. Tech. J. 34 (1955) 1115.
[7] S.W. Chaikin, J. Janney, F.M. Church, C.W. McClelland, Silver migration and printed wiring, Indust. Eng. Chem. 51 (1959) 299.
[8] S. Krumbein, A.H. Reed, New studies of silver electromigration, in: Proc. 9th Int. Conf. on Electric Contact Phenomena, 1978: p. 145.
[9] A. DerMarderosian, C. Murphy, Humidity threshold variations for dendrite growth on hybrid surfaces, in: Proc. Reliability Physics Symp., 1977: p. 92.
[10] G. DiGiacomo, Metal migration (Ag, Cu, Pb) in encapsulated modules and time-to-fail model as a function of the environment and package properties, in: Proc. Int. Reliability Physics Symp., 1982: p. 27.
[11] L.J. Turbini, J.A. Jachim, G.B. Freeman, J.F. Lane, Characterizing Water Soluble Fluxes: Surface Insulation Resistance VS Electrochemical Migration, in: Thirteenth IEEE/CHMT International Electronics Manufacturing Technology Symposium, 1992., 1992: pp. 80–84.
[12] D. Shangguan, A. Achari, W. Green, Application of lead-free eutectic Sn-Ag solder in no-clean thick film electronic modules, IEEE Trans. Comp., Packag., Manufact. Technol. B. 17 (1994) 603-611.
[13] M. Zamanzadeh, S.L. Meilink, G.W. Warren, B. Yan, Electrochemical Examination of Dendritic Growth on Electronic Devices in HCl Electrolytes, Corrosion. 46 (1990) 665-671.
[14] C.W. Jennings, Filament formation on printed wiring boards, SAND-75-0616, Sandia Labs., Albuquerque, N. Mex.(USA), 1975.
[15] A. Shumka, R.R. Piety, Migrated-Gold Resistive Shorts in Microcircuits, in: 13th International Reliability Physics Symposium, Las Vegas, NV, USA, 1975: pp. 93-98.
[16] F.J. Grunthaner, T.W. Griswold, P.J. Clendening, Migratory gold resistive shorts: chemical aspects of a failure mechanism, in: Reliability Physics Symposium, 1975. 13th Annual, 1975: pp. 99–106.
[17] A. Shumka, Analysis of Migrated-Gold Resistive Short Failures in Integrated Circuits,

in: Proc. Tech. Program of the Int. Microelectronic Conf, 1976: p. 156.
[18] P. Rogren, C. Santa Clara, Electro migration in thick film conductor materials, in: Proceedings of the International Microelectronics Symposium, 1976: p. 267.
[19] N. Sbar, Bias-Humidity Performance of Encapsulated and Unencapsulated Ti-Pd-Au Thin-Film Conductors in an Environment Contaminated with Cl2, Parts, Hybrids, and Packaging, IEEE Transactions on DOI -. 12 (1976) 176-181.
[20] R.P. Frankenthal, W.H. Becker, Corrosion Failure Mechanisms for Gold Metallizations in Electronic Circuits, J. Electrochem. Soc. 126 (1979) 1718-1719.
[21] T. Takemoto, R.M. Latanision, T.W. Eagar, A. Matsunawa, Electrochemical migration tests of solder alloys in pure water, Corrosion Science. 39 (1997) 1415-1430.
[22] R. Williams, J. Banner, I. Knowles, M. Dube, M. Natishan, M. Pecht, An investigation of 'cannot duplicate'failures, Quality and Reliability Engineering International. 14 (1998) 331–337.
[23] D.A. Thomas, K. Ayers, M. Pecht, The"trouble not identified"phenomenon in automotive electronics, Microelectronics Reliability. 42 (2002) 641–651.
[24] C.F. Coombs, Printed circuits handbook, McGraw-Hill Professional, 2007.
[25] D. Minzari, M.S. Jellesen, P. Møller, P. Wahlberg, R. Ambat, Electrochemical migration on electronic chip resistors in chloride environments, IEEE Transactions on Device and Materials Reliability. 9 (2009) 392–402.
[26] F. Barontini, V. Cozzani, K. Marsanich, V. Raffa, L. Petarca, An experimental investigation of tetrabromobisphenol A decomposition pathways, Journal of Analytical and Applied Pyrolysis. 72 (2004) 41–53.
[27] P. Westermann, Investigation of Process related residues during PCB manufacturing, Master Thesis, Technical University of Denmark, 2008.
[28] S. ARORA, A. SCHNEIDER, K. TELLEFSEN, SOLDERING FLUX, U.S. Patent WO/2001/039922, 2001.
[29] M.A. Johnsen, Effect of contamination on electrochemical migration, M. Sc. thesis, Technical University of Denmark, 2009.
[30] M.S. Jellesen, P. Westermann, D. Minzari, U. Rathinavelu, P. Møller, R. Ambat, The effect of adipic acid residue on corrosion of electronics, In Manuscript. 2010).
[31] R. Ambat, M.S. Jellesen, D. Minzari, U. Rathinavelu, M.A. Johnsen, P. Westermann, Solder flux residues and electrochemical migration failures of electronic devices, in: Proceedings of Eurocorr 2009, Nice, 2009.
[32] D. Minzari, F.G. Grumsen, M.S. Jellesen, P. Møller, R. Ambat, Electrochemical Migration of Tin in Electronics and Microstructure of the Dendrites, Submitted to Corrosion Science. (2010).
[33] O. Devos, C. Gabrielli, L. Beitone, C. Mace, E. Ostermann, H. Perrot, Growth of electrolytic copper dendrites. I: Current transients and optical observation, Journal of Electroanalytical Chemistry. 606 (2007) 75-84.
[34] O. Devos, C. Gabrielli, L. Beitone, C. Mace, E. Ostermann, H. Perrot, Growth of electrolytic copper dendrites. II: Oxalic acid medium, Journal of Electroanalytical Chemistry. 606 (2007) 85-94.
[35] G. Wranglén, Dendrites and growth layers in the electrocrystallization of metals, Electrochimica Acta. 2 (1960) 130-143.
[36] M. Schlesinger, M. Paunovic, Modern electroplating, Wiley New York, NY, 2000.
[37] M. Pourbaix, Atlas of electrochemical equilibria in aqueous solutions, M. Pourbaix, Published 1974 by NACE, 644. (1974).
[38] H.W. Dettner, J. Elze, E. Raub, Handbuch der Galvanotechnik, 2nd ed., München, Germany, C. Hanser, 1966.
[39] I. Puigdomenech, Medusa Software, ver. 17/2- 2009, Stockholm, Sweden, Division of Inorganic Chemistry, KTH- Royal Institute of Technology, 2009.
[40] S. Lee, M. Jung, H. Lee, Y. Joo, Effect of initial anodic dissolution current on the electrochemical migration phenomenon of Sn solder, in: 2009 59th Electronic

Components and Technology Conference, San Diego, CA, USA, 2009: pp. 1737-1740.

[41] H. Fischer, Elektrolytische Abscheidung und Elektrokristallisation von Metallen, Berlin, Germany, Springer, 1954.

[42] R. Winand, Electrocrystallization-theory and applications, Hydrometallurgy. 29 (1992) 567–598.

[43] C. Hunt, L. Zou, The impact of temperature and humidity conditions on surface insulation resistance values for various fluxes, Technology. 36 (1999) 43.

[44] D.Q. Yu, W. Jillek, E. Schmitt, Electrochemical migration of lead free solder joints, Journal of Materials Science: Materials in Electronics. 17 (2006) 229–241.

[45] K.S. Hansen, M. Jellesen, P. Møller, P.J. Westermann, R. Ambat, Effect of Solder Flux Residues on Corrosion of Electronics, in: Proc. of RAMS Conference, Texas, USA, 2009.: p. 502.

[46] M.S. Jellesen, D. Minzari, U. Rathinavelu, P. Møller, R. Ambat, Corrosion failure due to flux residues in an electronic add-on device, Engineering Failure Analysis. (2010).

[47] W.J. Ready, L.J. Turbini, The effect of flux chemistry, applied voltage, conductor spacing, and temperature on conductive anodic filament formation, Journal of Electronic Materials. 31 (2002) 1208–1224.

[48] W.J. Ready IV, Reliability investigation of printed wiring boards processed with water soluble flux constituents, (2000).

[49] Sheng Zhan, M. Azarian, M. Pecht, Reliability of Printed Circuit Boards Processed Using No-Clean Flux Technology in Temperature–Humidity–Bias Conditions, Device and Materials Reliability, IEEE Transactions On. 8 (2008) 426-434.

[50] D. Rocak, K. Bukat, M. Zupan, J. Fajfar-Plut, V. Tadic, Comparison of new no-clean fluxes on PCBs and thick film hybrid circuits, Microelectronics Journal. 30 (1999) 887-893.

[51] B. Smith, L. Turbini, Characterizing the weak organic acids used in low solids fluxes, Journal of Electronic Materials. 28 (1999) 1299-1306.

[52] J.E. Sohn, U. Ray, V.H. Heideman, B. Schubert, J.E. Anderson, K.M. Adams, et al., How clean is clean: effect of no-clean flux residues and environmental testing conditions on surface insulation resistance, in: Proceedings of the Technical Program, Surface Mount International, 1994: pp. 391–402.

[53] Y. Tsai, C. Hu, C. Lin, Electrodeposition of Sn-Bi lead-free solders: Effects of complex agents on the composition, adhesion, and dendrite formation, Electrochimica Acta. 53 (2007) 2040-2047.

[54] Y.C. Tang, A.J. Davenport, Magnetic Field Effects on the Corrosion of Artificial Pit Electrodes and Pits in Thin Films, J. Electrochem. Soc. 154 (2007) C362-C370.

9 PAPER 5: PCB LEVEL TESTING OF ELECTROCHEMICAL MIGRATION ON SURFACE MOUNT COMPONENTS

Daniel Minzari[8], Christian Ravn[*], Kirsten Stentoft[+], Morten S. Jellesen, Per Møller, Rajan Ambat

Section for Materials and Surface Technology, Department for Mechanical Engineering, Technical University of Denmark, DK-2800 Kgs. Lyngby, Denmark

** IPU Technology Development, DK-2800 Kgs. Lyngby, Denmark*

+ Danfoss Power Electronics A/S, DK-6300 Gråsten, Denmark

ABSTRACT

In this paper, the development of a test setup for PCB level testing of Electrochemical Migration (ECM) on surface mounted components is described. Test set up include a specially designed Printed Circuit Assembly (PCBA), and necessary electrochemical and data acquisition systems. The test PCBA used for this investigation consists of parallel rows of surface mounted chip capacitors and resistors having three different housing sizes, and for each housing size, three rows are made having components from different manufacturers. Tests are performed in simulated condensed humidity, investigating how parameters from cleaning, component housing size, bias voltage, solder joint geometry, and handling (fingerprint contamination) is affecting the tendency for ECM. Results show that small components are more prone to migration on a PCBA compared to the large ones. Additionally, it is found that the components of similar housing size, but different height have different tendency for migration due to the interference from solder geometry. Lead free (SAC) solder is found to migrate slightly less than lead containing solder, and fingerprints from human handling of the PCB are found to be very aggressive to promote migration.

NOMENCLATURE

DI	De-Ionized (water)	SEM	Scanning Electron Microscopy
ECM	Electrochemical Migration	SIR	Surface Insulation Resistance
EDS	Energy Dispersive Spectroscopy	SM	Surface Mount
IPA	Isopropyl Alcohol	SSFL	Skin Surface Film Liquids
PCB	Printed Circuit Board	TFF	Time to First Failure
PCBA	Printed Circuit Board Assembly	TP	Test Person
SAC	Sn-Ag-Cu based solder alloy	WD	Water Droplet

[8] *Corresponding Author: Daniel Minzari, Department of Mechanical Engineering, Technical University of Denmark, Kgs Lyngby DK-2800, Denmark, Tel : +45 4525 2118, Fax : +45 4593 6213, Email: dmin@mek.dtu.dk*

9.1 INTRODUCTION

Electrochemical migration (ECM) is defined by the IPC standard TR-476A as the growth of conductive metal filaments under a DC potential bias [1]. Metal ions dissolve at the anode and are transported by various mechanisms to the cathode where they are reduced into their metallic form. The growth will often be in the form of conductive dendrites, which can eventually short circuit the cathode to the anode if the dendritic growth forms a conductive bridge.

Since 1996, the electronics industry has been the largest industry in the world, having a turnover of more than US$1 trillion a year [2]. It is hard to establish the exact cost of ECM failures, but as the failures can cause an entire device to fail, it is obvious that every measure should be taken into account in order to avoid such failures, as even an intermittent failure can in a worst case scenario cause a plane to crash or a medical instrument to stop at a hospital.

Takemoto et al. [3] have predicted that ECM will become one of the most severe reliability issues for the electronics industries in the future, due to the miniaturization of the devices and increased sensitivity to contamination. As many of the failures are intermittent, it is extremely difficult for manufacturers to detect the root cause of a failed device, and electrochemical migration is indeed suspected to be the root cause of many field failures that have been labelled: “no failures found” [4,5].

Previous works from our research group showed how isolated parameters such as chloride [6], bromide [7], solder flux, dust and synergetic effects of these [8] influence the ECM of tin. The experiments in the earlier work, relied on a method where ECM testing was done on individual components, thereby eliminating any board level parameters that could influence ECM, e.g. PCB laminate, soldering process (solder alloy, solder flux, heating profile etc.), human handling etc. ECM of tin was found to be very sensitive to the local pH changes within the water layer formed by the condensed humidity [9] and the ability of tin to form a large variety of complex ions [9-11], of which the stability and solubility are highly affected by the pH.

In this work, we have developed a novel test bed for dedicated ECM studies on PCBA level. Various issues related to the development of the test PCBA and the related instrumentation are described, and experimental results related to the effect of various parameters are presented. The results have been divided into the following categories: (i) Effect of cleaning, (ii) Effect of bias voltage and size, (iii) Comparison between lead containing and lead free solder, and (iv) Effect of human handling (fingerprints).

For all the experiments reported in the present paper, the micro-volume of environment over the components was created for ECM testing by water drop (WD) method by adding de-ionized (DI) water using a micro-pipette tip. This ensures a reproducible volume of environment in each experiment to get a high level of reproducibility. However, prior to the experiments using WD, a condensation test on the test PCBA cooled gradually to ~6°C in open atmosphere at ambient conditions (~20°C and 45%RH) showed that the condensed water droplet preferably form on the component surface due to the preferential wetting (Figure 4.3) similar to the one attained by WD method.

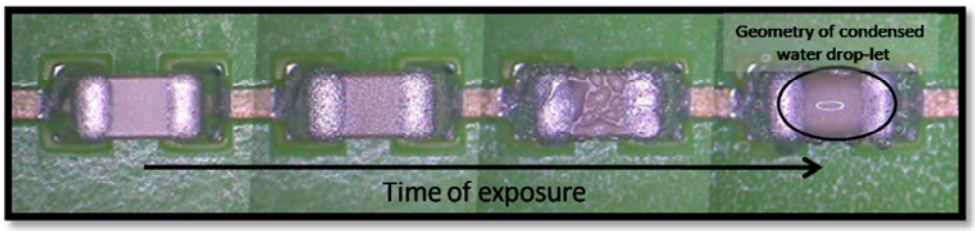

Figure 9.1: Typical geometry of condensed water layer on chip components on test PCB cooled to ~6°C at ambient conditions.

9.2 Development of Test PCB Set up

9.2.1 The CELCORR Test PCB

Actual PCBAs used in the electronic devices are too complex for basic investigations of the effect PCB level parameters on corrosion behaviour. Surface Insulation Resistance (SIR) patterns are usually tested using the industrial standards such as IPC-9201 [12] without components, and will therefore not provide information on the corrosion issues of PCBA with components and

associated process parameters for these. For a standardized PCB level corrosion testing, a PCBA was designed with a series of standard components and other parameters, named the CELCORR Test PCB set up. The test PCB consists of 20 circuits: 18 containing Surface Mount (SM) components and 2 SIR patterns. One SIR pattern is covered by a soldermask, while the other has reflowed solder surface finish.

- Each of the 18 circuits contains 10 identical SM components in parallel.
- 9 of the 18 circuits are reserved for resistors having resistances of from 68Ω to 1 MΩ and of sizes 0805, 0603 and 0402.
- 9 of the 18 circuits are reserved for capacitors having capacitances in the range of 22pF to 100nF and sizes of 0805, 0603 and 0402.

Dimensions of the 0805, 0603 and 0402 housings are presented in Table 9.1 below.

Table 9.1: Housing size dimensions in metric and imperial units

Housing	**Dimensions** *mm*	**Dimensions** *Inches*
0805	2.0 x 1.3	0.08 x 0.05
0603	1.5 x 0.8	0.06 x 0.03
0402	1.0 x 0.5	0.04 x 0.02

A series of lead containing and lead free test PCBs were manufactured, and all components, solders, materials, and processes were kept similar for the manufacturing of various set of PCBAs, except solder temperature profile, which is inherently different for lead containing and lead free solders.

Notation used for components on the test PCB

A mounted test PCB is shown in Figure 4.5. For simplicity, components with size 0805 housing are called as “Large (L)”, 0603 “Medium (M)” and 0402 “Small (S)”. Notation C represents **c**apacitors and R for **r**esistors. As there are three rows of components of same housing size (Figure 4.5), these will be denoted with numbers 1, 2 and 3 (numbered from right to left on Figure 4.5). This is summarized in Table 9.2. For e.g. LC1 means “Large capacitors in row 1”.

SIR pattern size is 13x25mm; conductor width 0.3mm and conductor distance 0.3mm.

Table 9.2: Summary of notations used for various components on the test PCB.

Notation		House	CH	Resistance / Capacitance	Power Rating (W)
SR1	Small resistors in Row 1		1	1000 Ω	0.063
SR2	Small resistors in Row 2	**0402**	2	10000 Ω	0.063
SR3	Small resistors in Row 3		3	100000 Ω	0.0625
MR1	Medium resistors in Row 1		4	100 Ω	0.10
MR2	Medium resistors in Row 2	**0603**	5	100000 Ω	0.063
MR3	Medium resistors in Row 3		6	1000000 Ω	0.063
LR1	Large resistors in Row 1		7	68 Ω	0.1
LR2	Large resistors in Row 2	**0805**	8	330000 Ω	0.125
LR3	Large resistors in Row 3		9	1000000 Ω	0.125
	Reflow surface finish		10	SIR	
SC1	Large capacitors in Row 1		11	1000 pico F	
SC2	Large capacitors in Row 2	**0402**	12	1000 pico F	
SC3	Large capacitors in Row 3		13	1000 pico F	
MC1	Medium capacitors in Row 1		14	47 pico F	
MC2	Medium capacitors in Row 2	**0603**	15	1 nano F	
MC3	Medium capacitors in Row 3		16	100 nano F	
LC1	Small capacitors in Row 1		17	22 pico F	
LC2	Small capacitors in Row 2	**0805**	18	1 nano F	
LC3	Small capacitors in Row 3		19	100 nano F	
	Coated by solder mask		20	SIR	-

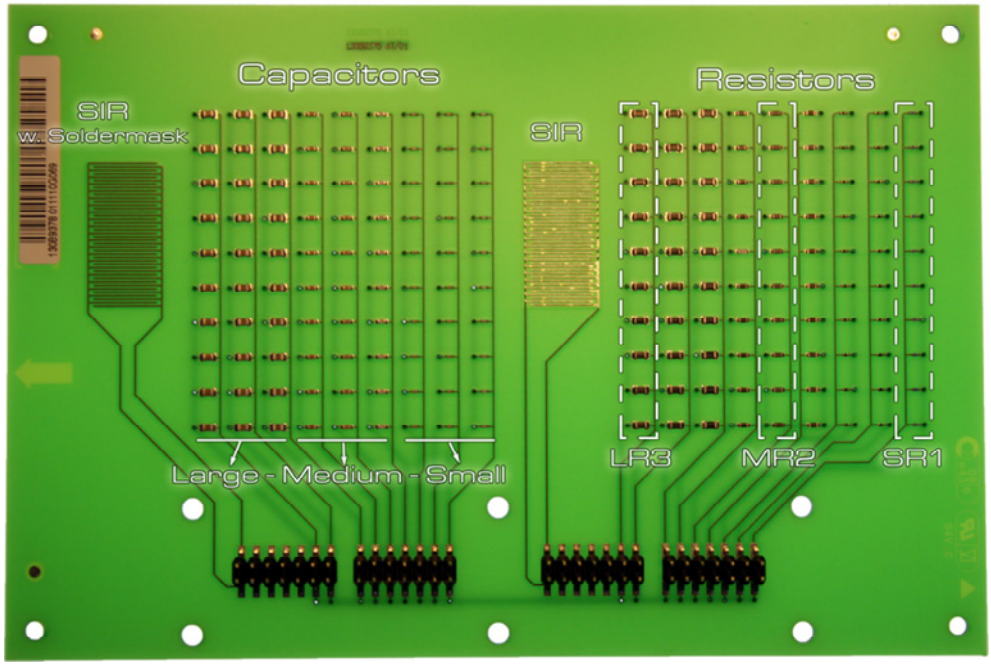

Figure 9.2: An example of Mounted CELCORR test PCB. All the component circuits are connected to pin connector for electrical contact to the PCBA.

9.2.2 INSTRUMENTATION

When performing experiments on multiple circuits, instrumentation is challenging if no interference to the electrochemical conditions shall be introduced during the measurement. First of all, the parameter to be measured is important. Surface insulation resistance has traditionally been the parameter that has been used in electronic reliability, as described by the IPC-9201 standard [12]. However, when investigating electrochemical phenomena such as ECM, there can be a complication if resistance is chosen as the instrumental parameter. Resistance is normally not measured directly, but relies on a current generator and a voltage measurement (or vice versa) that is converted to a resistance. Many instruments will apply a set current in order to measure the resulting voltage, which is then transformed into a resistance reading. This will induce an unknown voltage pulse to the system differing from the potential bias by several tens of volts [12,13], which alters the electrochemical conditions of the system being investigated. Therefore, experiments where a constant potential (voltage) is applied to a system (AC or DC)

one should preferably use current measurements if electrochemical factors are involved in the investigated process.

The ideal instrumentation would be to have one ammeter to measure the current for each circuit. However, this option is not realistic when many circuits are used. Therefore a switch relay is commonly used for such measurements, where one instrument is shared for measuring the current in various circuits, while a switching device will allow making the measurements on each circuit in a given sequence [12,13]. The implication when using this method is that as the relay contact the switches, an interruption of the voltage occurs for fraction of a second. Such interruption can alter the electrochemical behaviour of the system if corrosion is studied, as diffusion layers and movement of charged species within the electrolyte will be affected by the voltage interruption.

Therefore, the instrumentation for CELCORR test PCB employs a double switch solution, where two switches are assigned for each circuit. In this way, the ammeter is switched in first, so that it is shortly in parallel with the switch, insuring that the potential bias to the circuit is never interrupted. A very small change in the bias will occur due to the internal resistance of the ammeter, but it is in the range of few mV, which is insignificant compared to the high applied potential to the test PCB. A block diagram is presented below in Figure 9.3 illustrating the setup.

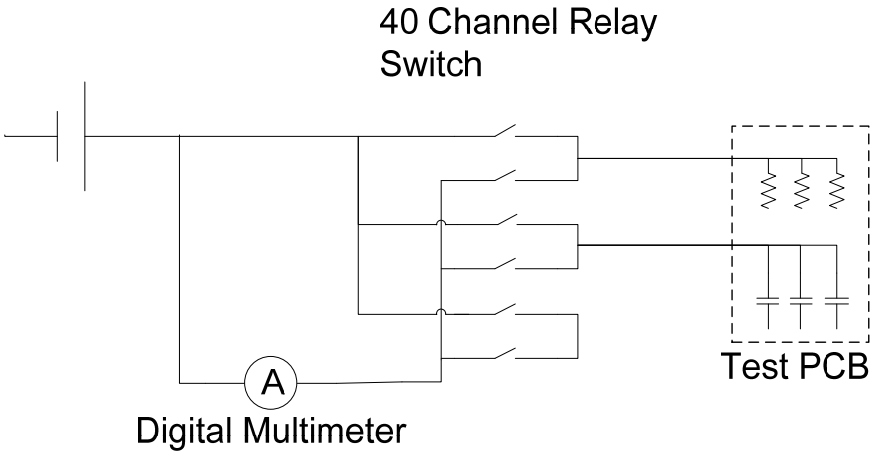

Figure 9.3: Block diagram for the CELCORR test PCB setup.

Another issue is the sensitivity of the current measuring instrument to measure low and high current levels. This is due to the fact that when the dendrite forms current jumps up by many decades (micro-amps to several milli-amps)[6,14]. If the ammeter is set to auto range measurement, the instrument need to set the required current range before each measurement, therefore the speed of the measurements per time will be impaired. In order to counter this problem, a fixed measurement range from 1µA to 100mA is used and 5 measurements on each circuit per second (total of 100 measurements per second on the entire test PCB) are possible.

9.2.3 MEASUREMENT SOFTWARE

The measurement software was programmed using Labview software (example of the display interface is given in Figure 9.4). The software allows choosing the sampling rate on each circuit and manual enabling/disabling of a given channel. The software was programmed plotting the current time curves for each circuit in real-time with the possibility to manually show/hide individual graphs. A safety upper limit value for current can be entered at which the software will interrupt the voltage from a circuit so that out of range measurements and destruction of the switch relay is avoided. If safety value is triggered on any of the channels, the program will indicate this. For each channel, the real time current value and max current attained over the period of the experiment are displayed. In this way,

dendrite formation can easily be monitored during the long term testing experiments. Figure 9.5 shows the whole set up.

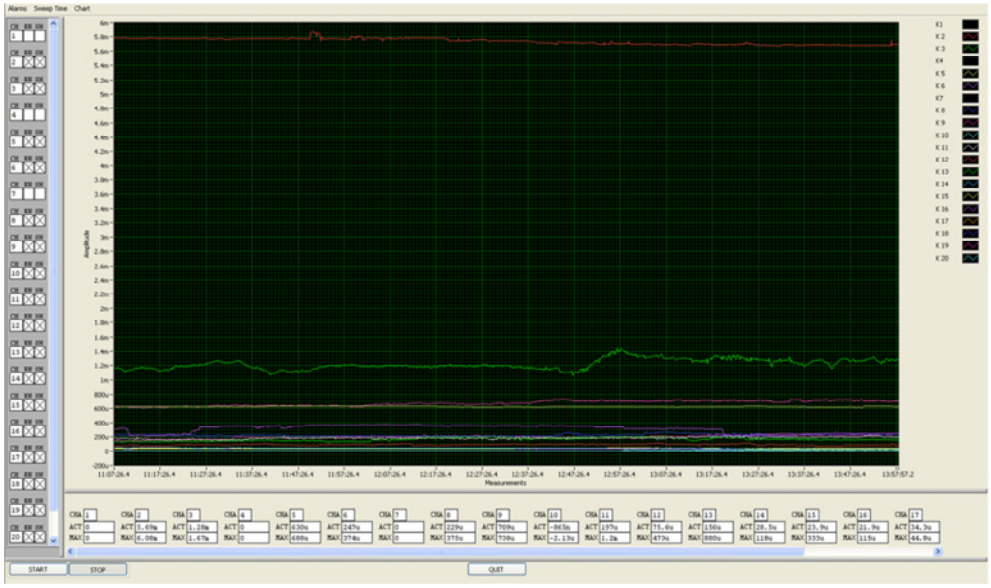

Figure 9.4: Display interface for the CELCORR test PCB software.

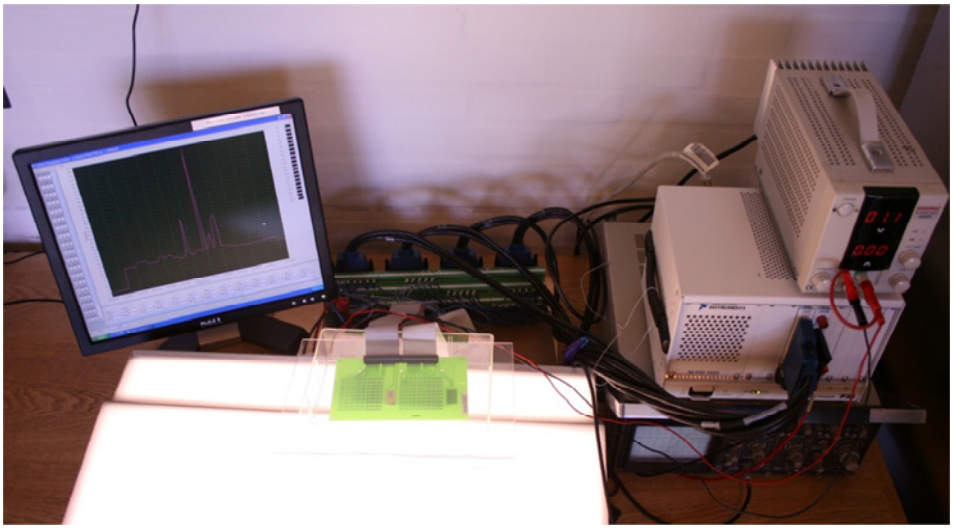

Figure 9.5: CELCORR test PCB setup for PCB level corrosion testing.

9.2.4 DATA OUTPUT FROM TEST PCB EXPERIMENTS

The data output from the test PCB experiments is the current-time curves for each channel, as illustrated by the example in Figure 9.6a. If a dendrite shorts two

electrodes on a component (at least on one component in a row) a current spike is observed in the current-time signal. Resistors have a base current running through the resistive layer, so the current measured in this case is the sum of the current through the resistor and the current through the solution layer (connected in parallel), while for the capacitors, current measured is constituted only by the current through the solution layer.

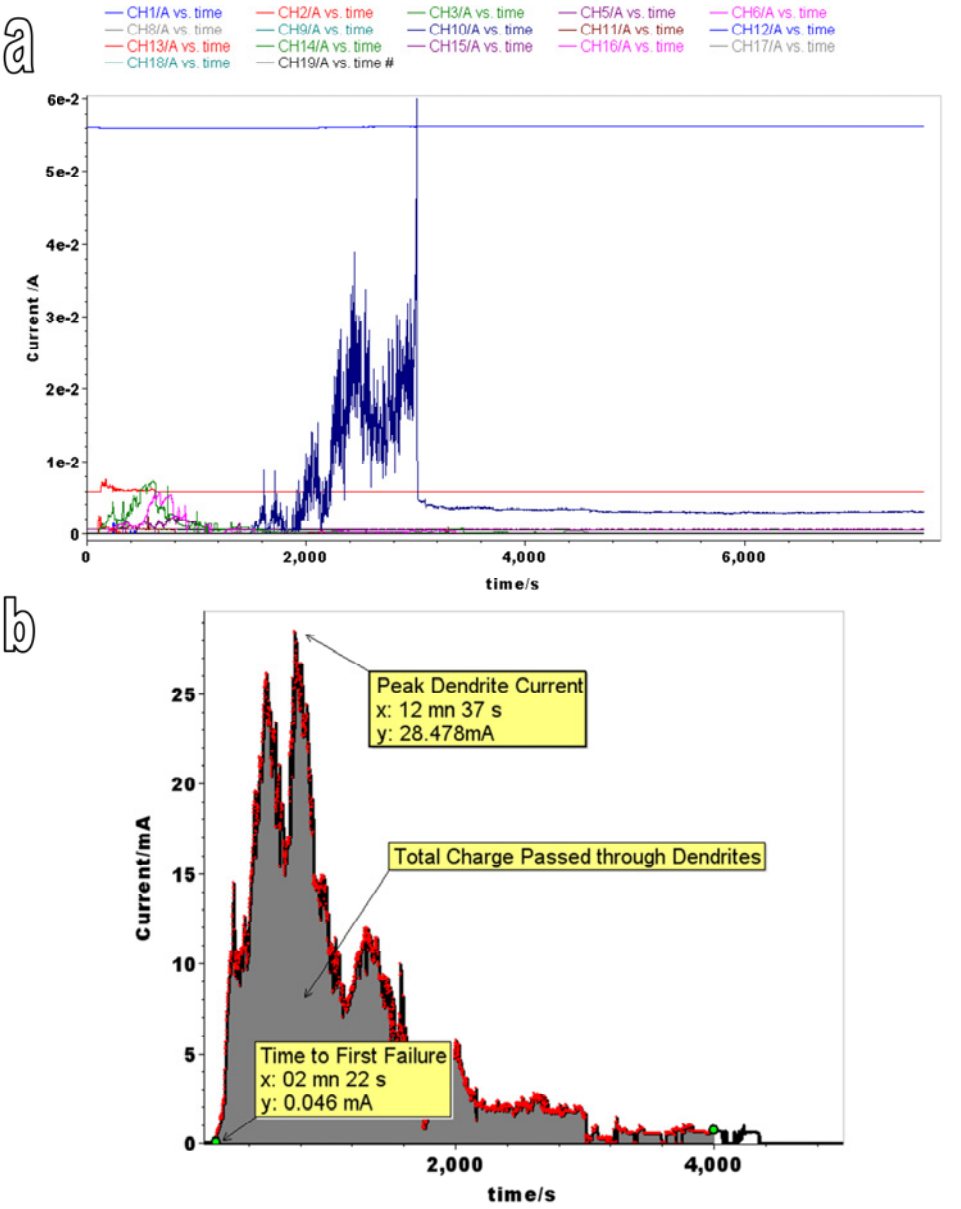

Figure 9.6: a) Example of current-time output from the test PCB during WD testing, and b) Illustration of parameters that are deduced from the curve for analysis for ECM susceptibility. .

As the measurements on each channel are done on 10 components in parallel, it is not possible to know whether the increase in current is due to migration on one component or more. However, a large number of components on the test PCB that

are investigated for each experiment provide a good statistical analysis on the overall ECM behaviour.

Figure 9.6b shows the parameters from the current-time curves that are used for analysis. The Time to First Failure (TFF) is the time where the first dendrite has bridged two conductors on a circuit, and can be read from the curve as the point where the first spike in the current occurs. The peak dendrite current can be regarded as the maximum conductivity of the dendrite/dendrites that have grown while the total charge passed is relating to the frequency of shorting, stability, and lifetime of the dendrites. Most failures from dendrite bridging of the electrodes are intermittent, as the dendrite burns off during the surge in current. However, some failures can be permanent, and for such failures the value of the total charge would depend on how long the experiment is allowed to run. In order to have charge values that can be compared, a cut-off value of 4000 s has been chosen in the present work. This cut off value is based on the evaluation of the current-time curves from several experiments showing failure due to ECM, and most failures will have burned out within this time.

9.3 MATERIALS AND METHODS

An overview of the experiments reported in this paper is given in Table 9.3, along with a short description of the purpose of the experiment.

Table 9.3: Experimental overview for PCB level ECM testing

Experiment	Solder Alloy	Environment / Test PCB / Bias	Purpose
Effect of Cleaning	Sn/Pb	DI Water As received and cleaned test PCB Bias voltage 6V	Comparison between as received and cleaned PCBs to see the effect of cleaning in isopropyl alcohol
Effect of bias voltage and size	Sn/Pb	DI Water Bias voltages: 1, 3, 6,18V	Benchmarking of components – sizes and potentials
Comparison: Sn/Pb vs. Pb-free solder	Sn/Pb + SAC	DI Water Bias 6V	Compare susceptibility for ECM of components soldered with lead and lead free solders
Effect of human handling (finger prints)	SAC	DI Water+ Fingerprint on PCBA Bias 3V	Effect of fingerprints from 5 different test persons.

9.3.1 TEST PCB MATERIALS AND PROCESS PARAMETERS

The test PCB used in the present investigation was made from a FR4 epoxy laminate in accordance to IPC-4101/21 and having a Tg (glass temperature) of min. 135° C, and produced according to PERFAG 2E specifications for production of rigid PC-boards [15]. The PCBs were delivered with a hot air levelled surface finish with either eutectic Sn/Pb solder or SAC (Sn/Ag/Cu based) solder. The boards where mounted and reflow soldered in an automated pick and place system, and soldered using the solder profiles presented in Figure 9.7. Lead containing solder was a Senju OZ2062-221C5M-40-10 (Senju Manufacturing Ltd. Bucks, UK) no-clean reflow solder having an alloy composition of Sn62, Pb36, Ag2 (melting point of 178-192°C) containing non-halide rosin based flux. Lead free solder was a Senju M705-GRN360-K-V (Senju Manufacturing Ltd. Bucks, UK) no-clean reflow solder having an alloy composition of Sn96.5, Ag3.0, Cu0.5 (melting point of 217-220°C) containing non-halide rosin based flux.

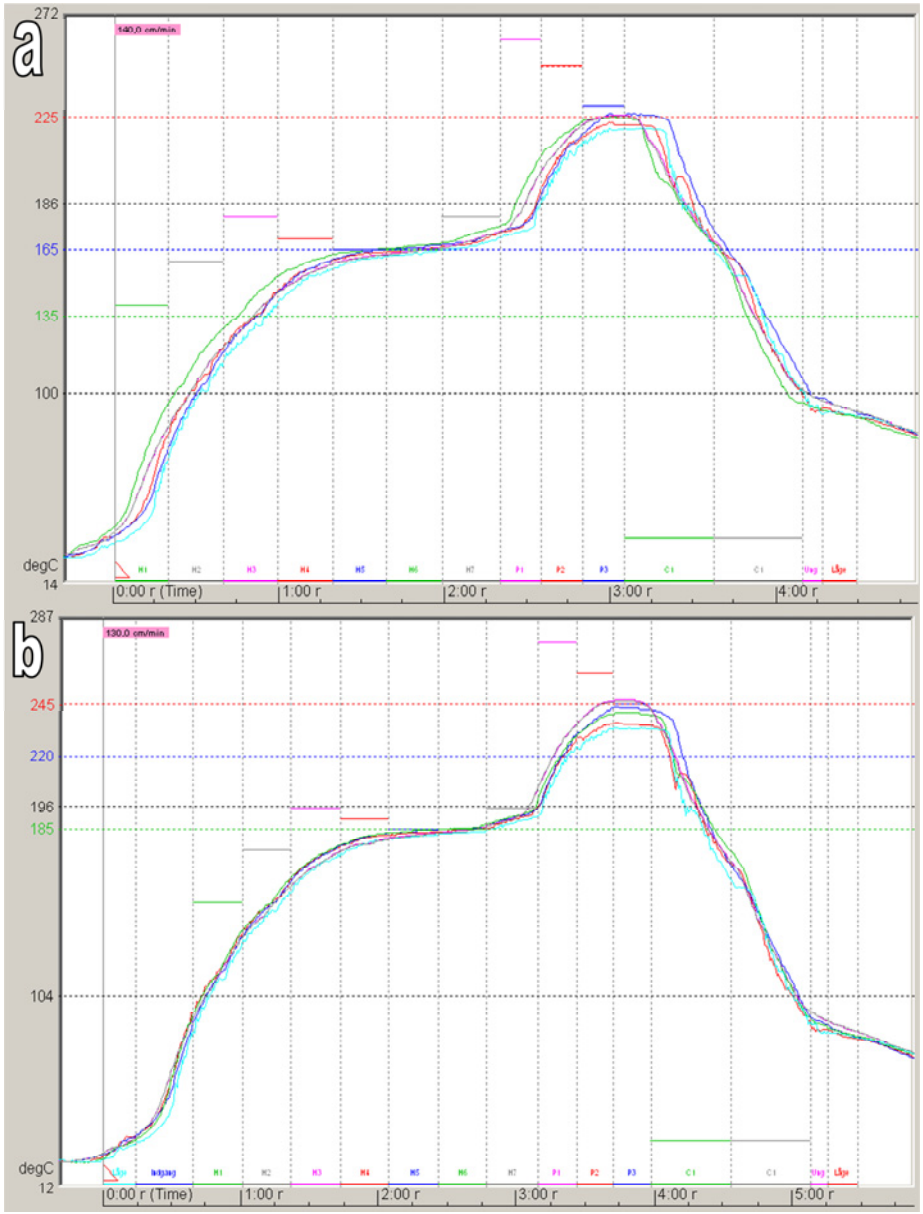

Figure 9.7: Soldering heating profiles for a) Sn-Pb and b) lead free reflow soldered test PCBs.

9.3.2 ECM TESTING USING TEST PCB

Unless otherwise stated the test PCBs were cleaned immediately prior to experiments. The cleaning procedure included ultrasonic immersion in 50/50% isopropyl alcohol (IPA) in DI water for 30 min, followed by a DI water rinse and drying at ambient temperatures.

For testing the effect of cleaning, following cleaning treatments were carried out: (i) As received boards, (ii) Boards that were cleaned by water rinse, (iii) Ultrasonic soak for 30 min in 50/50% isopropyl alcohol (IPA) in DI water, and (iv) Ultrasonic soak 2 hrs. in 50/50% IPA in DI water.

A droplet of de-ionized water was added for WD testing using a micro-pipette in order to simulate condensation. Droplet volumes were 2μL for 0805 housing, 1.3μL for 0603 housing, and 0.3μL for 0402 housing. The test PCB was placed in a transparent box where water compartments provided an environment of approx. 90-95%RH at ambient temperatures. Potential bias was applied to all circuits simultaneously and current was measured with one second intervals on each circuit. Current was measured using a digital multimeter (NI-PXI 4065, National Instruments, Denmark).

For investigating the effect of human handing, finger prints from 5 male test persons were used (persons from Korea, Iceland, Uganda, Denmark and India, and their age spanned from 31 to 50 years. Test persons were asked to wash hands 1 hour prior to the experiment and only allowed to do the ordinary office work during this one hour. A cleaned Test PCB was given to the test person, who was asked to touch the PCB regularly during one hour. Conductivity of the each person's fingerprint was measured by placing their thumb onto the SIR pattern on the test PCB under 6V, and a current curve similar to that presented in Figure 9.8 was obtained. The maximum current measured during the 30s interval was taken as the measure of the fingerprint conductivity.

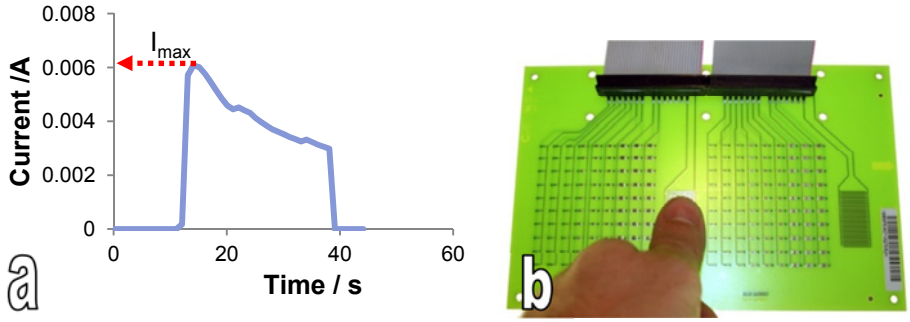

Figure 9.8: a) Example of current-time curve obtained from placing a finger over the open SIR pattern. Value used for comparison of fingerprint conductivity was the maximum current measured as indicated by the arrow. b) Image showing thumb over SIR pattern.

9.3.3 ELECTRON MICROSCOPY

Scanning Electron Microscopy (SEM) was performed using a Zeiss Ultra55 and JEOL 5900 instruments both having Energy Dispersive X-ray Spectroscopy (EDS) analysis capability (Oxford instruments).

9.4 RESULTS AND DISCUSSION

9.4.1 EFFECT OF CLEANING

Figure 9.9 shows the results from as received test PCB (soldered using lead containing solder) and cleaned by the methods described above. Plot shows the total charge passed through the dendrites for the three rows of large capacitors (0805 housing) which are representative of the overall behaviour.

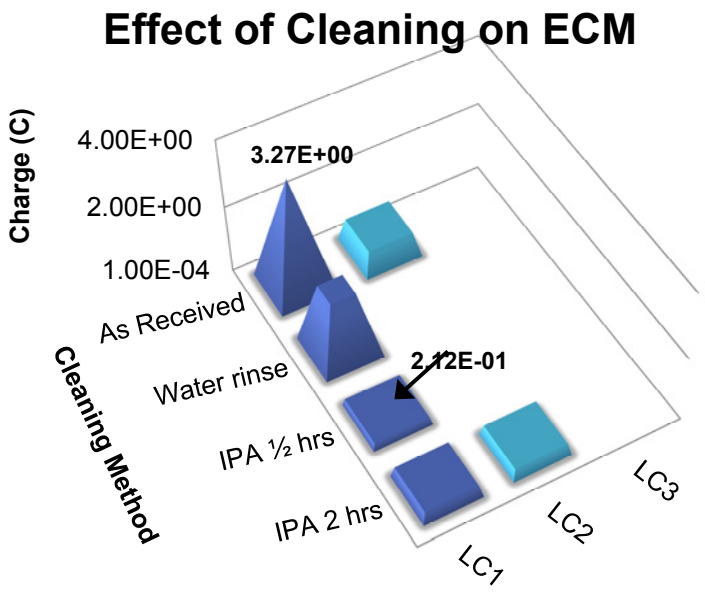

Figure 9.9: Effect of various types of cleaning on the ECM susceptibility of the PCB (total charge passed indicate accumulated damage due to ECM). Test PCBs are soldered using lead containing solder. Experiments were done under 6V potential bias. Minimum and maximum values are shown on the plot in Coulombs.

Both the water rinse and IPA cleaning reduces the susceptibility to migration shown by the reduction in charge. Tendency for ECM is in the order of as received>water rinse>IPA 2hrs>IPA ½hrs. The IPA soak is seen to have a positive effect by reducing the migration, probably by dissolving solder flux residues from the no clean flux, though extended soak is not seen to reduce the migration further, on the opposite the 2 hrs. IPA soak is seen to have a slightly increased tendency to migrate.

What is striking when regarding the test result is that for the LC3 row, no components ever migrate in DI water, while for the LC1 row migration is observed for all experiments. When carrying out migration experiments on single components similar to LC1 without the soldering process, migration has been found to be very rare in pure DI water [6]. Therefore, it seems strange that the capacitors of similar housing sizes have very much different migration behaviour when it is on the PCBA.

SEM and EDS analysis of the new LC1 and LC3 capacitors showed that there is no significant difference in the electrode surface morphology and chemical composition. In both cases terminals are found to be made of tin.

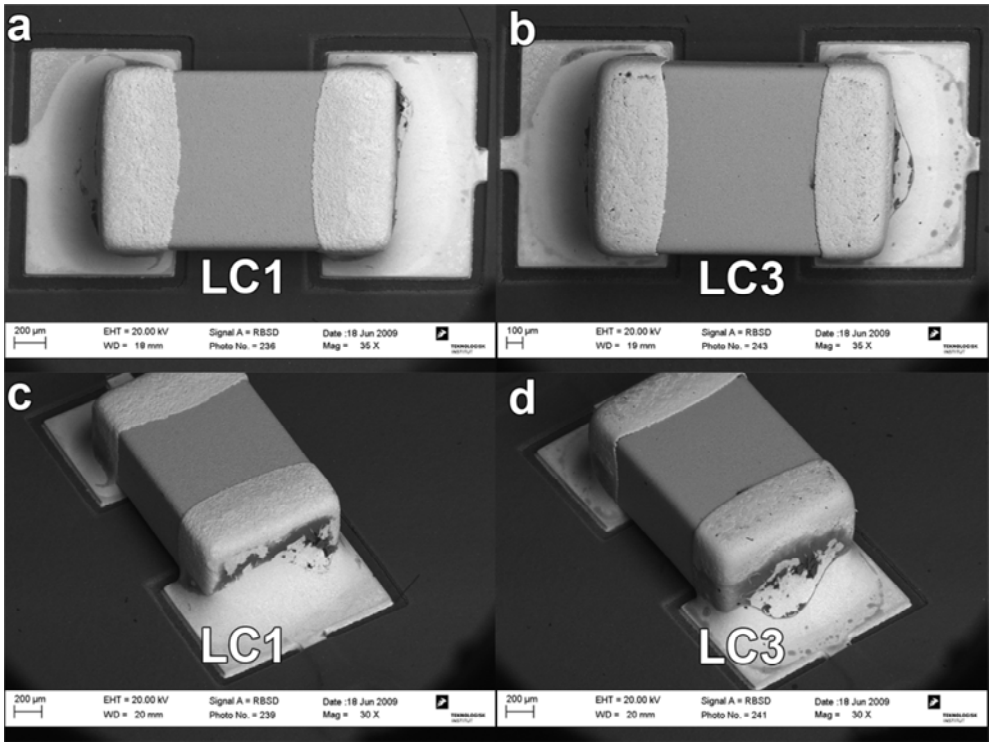

Figure 9.10: SEM images of LC1 and LC3 components on the test PCB. Images a and b are top view, and images c and d are tilted views revealing the solder joint.

SEM images from mounted LC1 and LC3 components are shown in Figure 9.10. Solder flux residues are seen as black flaky substances on both components at the interface between the solder and the component electrode. Component LC1 has little less height (0.7 mm) than LC3 (1 mm), which means that the solder alloys flow over the LC1 component during soldering process could be different from that over the LC3 component. Magnified view of the electrode surfaces of LC1 and LC3 in the backscattered mode are given in Figure 9.11. The surface of LC1 shows a second phase in bright contrast, which is absent on LC3. EDS analysis showed that the bright phase is rich in lead.

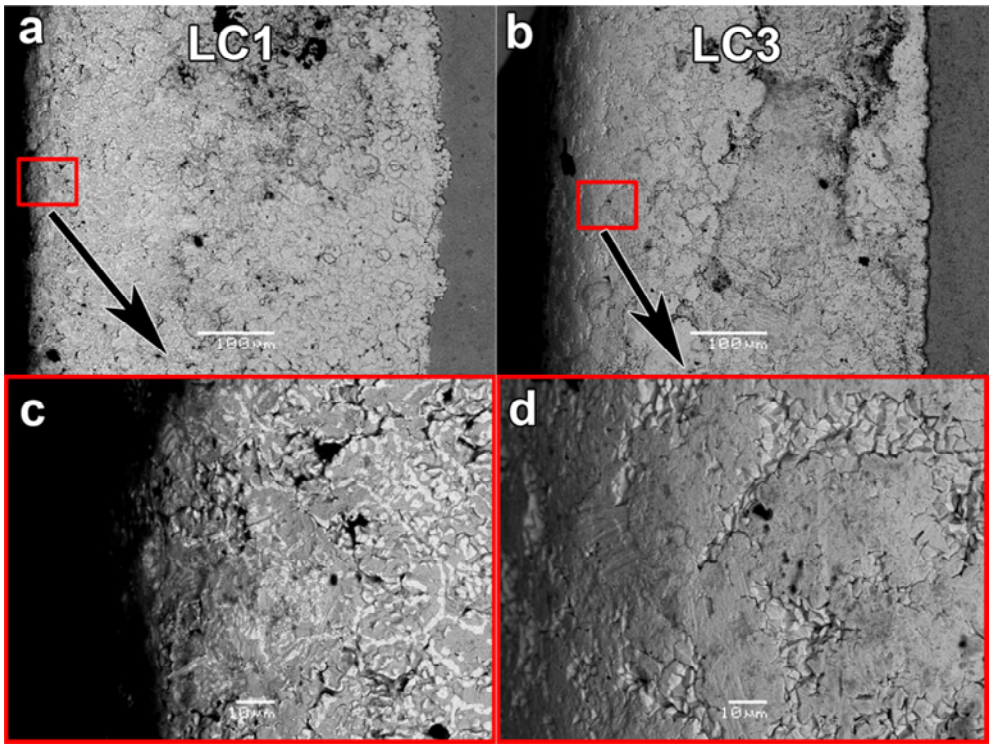

Figure 9.11: Magnified view of the electrode surfaces: (a) LC1, and (b) LC3. Image c and d are magnifications of image a and b respectively

The height of the component in relation to the amount of solder paste and size of the solder pad seems to be the determining factor on whether the solder will reach the surface of the component. Takemoto et al. [3] investigated the electrochemical migration of pure tin, pure lead, and tin-lead solder alloys in pure water, and found that for pure lead and tin-lead solders with high amount of lead, migration occurs in pure water, while pure tin did not migrate. The presence of solder alloy at the surface of the component is therefore a very likely explanation for the increased migration on the LC1 components as compared to LC3.

9.4.2 Effect of Size and Potential

The effect of component housing size and potential was investigated on the test PCBs soldered with lead containing solder. The results are presented as total charge passed (Figure 9.12) and TFF plots (Figure 9.13) for 1, 3, 6, and 18 volts

potential bias. For the charge plot, all components on the test PCB are included, while for the TFF plot, only capacitors are included. Due to current limitations, some resistor circuits with low resistance value had to be disabled at high voltages. For this reason, MR1 and LR1 were disabled for all experiments and SR1 was disabled in the 18V experiment. Experiments where a row has been disabled are marked by an "x".

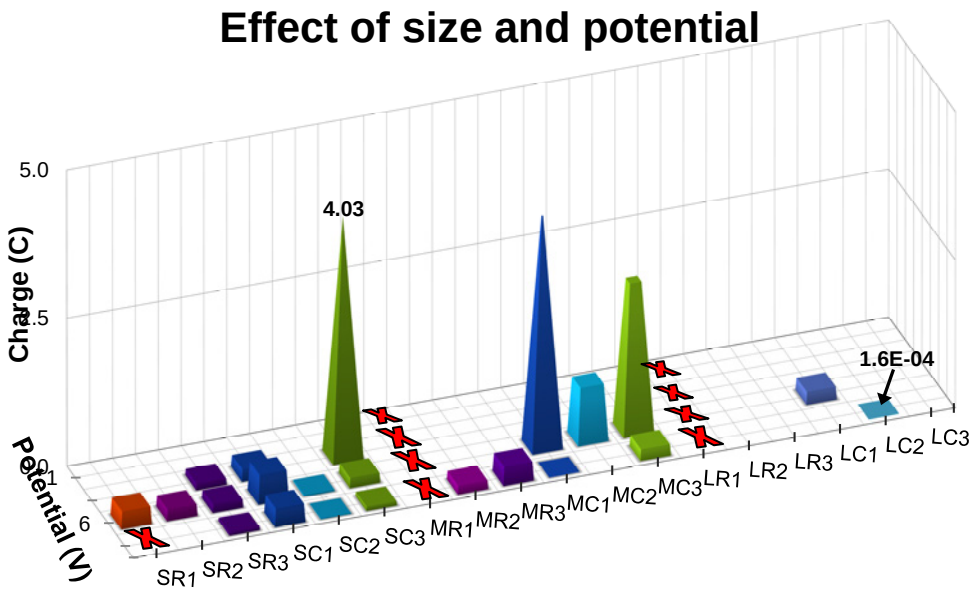

Figure 9.12: Plot showing the effect of size of component and potential on the ECM susceptibility on PCB represented by the total charge passed during dendrite formation and shorting. Values for minimum (LC2-18V) and maximum (SC3-3V) are shown in Coulombs.

At 1V potential no migration was observed for any circuits as this potential difference was too low for necessary electrochemical reactions. However, Lee et al [16] observed migration of pure tin at 1V bias voltage in 0.001wt % NaCl solution, indicating that migration at this potential is possible if contamination is present on the PCBA.

At 3V migration occurred on 3 out of the total 16 circuits (2 circuits were disabled due to current limitations). The migration occurred only on the "small" housings (0402) and of the 3 circuits on which migration was found, two of them were capacitor and one resistor circuits. For the 6V experiment, migration occurred on

10 of the total 16 circuits. All the small components showed migration, while no medium or large resistors showed migration. At 18V, migration was observed on 9 of the total 15 circuits. Again, migration was mainly on capacitors. The TFF values for the capacitors in Figure 9.13 can be regarded as the first component (out of the 10 in the circuit) that creates a short circuit due to migration. Even though the TFF in principle relies on 10 simultaneous experiments, some scatter is observed in the values when comparing housing sizes and potentials. However, a general trend is seen towards lower TFF values for higher potentials and smaller housings.

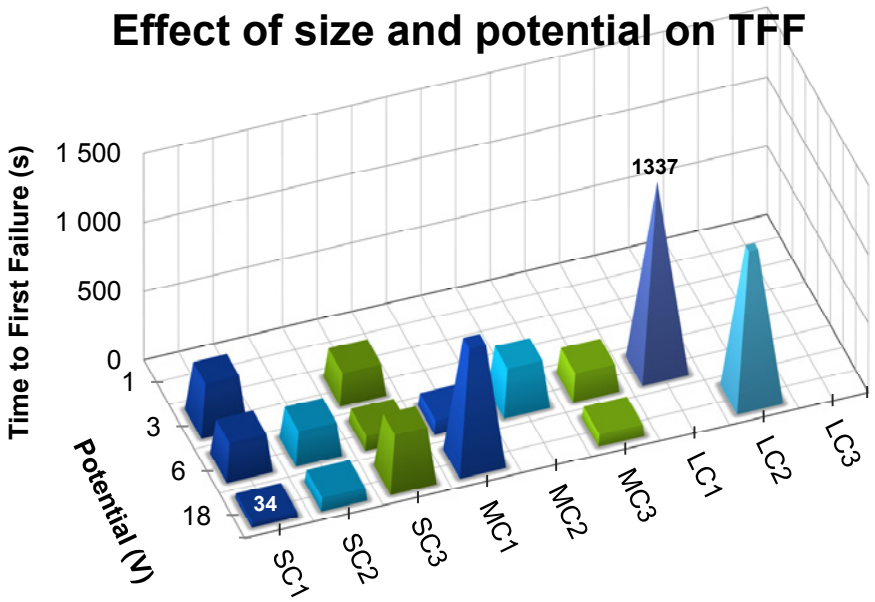

Figure 9.13: Plot showing the effect of size and potential on the time to first failure for capacitors on the PCB. Blank fields are circuits of components where no migration occurred. Values for minimum (SC1-18V) and maximum (LC1-6V) are shown in seconds.

Overall the increased potential in general has increased the probability of ECM at PCB level and more accumulated damage, while the dependency is also a function of the size of the component. Both effects are due to the change in the electric field as a function of the potential and component size, while the increased potential bias also increases the electrochemical reaction kinetics. It is expected that some of the non-migrated components might have shown severe corrosion without migration [9], which needs to be investigated in detail.

9.4.3 LEAD CONTAINING VS. LEAD FREE SOLDER ON TEST PCB

A comparison between lead containing and lead free soldered test PCBs was made at 6V potential bias with de-ionized WDs. The 6V bias was chosen based on the results presented in Section 9.4.2, where most migration was observed at this voltage.

Figure 9.14 presents the (a) charge and (b) TFF plots for the capacitors. Resistors showed similar results as observed in the previous section 9.4.2, where medium and large resistors did not migrate, and two of the three rows of small resistors migrated. Lead free soldered components are seen to have a little less tendency for ECM compared to the tin-lead soldered, and no migration was observed on two of the medium sized capacitor circuits. Results from a test on the open SIR pattern made of the reflow solder alloy using a droplet of 10µL DI water were included in the plots.

The migration of tin-lead is seen to conduct far more charge through the dendrites as compared to the SAC solder, though the SAC solder is seen to have a much shorter TFF than the Sn/Pb solder. However, in an overall comparison, the SAC solder seems to be slightly less prone to ECM than lead containing solder. The increase in soldering temperature for lead-free solders (see example in Figure 9.7) is therefore not found to increase the tendency for migration in these experiments.

The corrosion and ECM properties of tin-lead and lead free solders have been investigated in a number of studies, and an assessment of which solder alloy has the better corrosion performance seems to be case dependent. Zou and Hunt [17] investigated ECM of Sn-Pb and SAC solders contaminated with different flux types and at various flux concentrations using surface insulation resistance patterns, and found that dendrite formation occurs more readily with SAC alloy than with SnPb alloy due to silver migration. Additionally, solder flux contamination was found to be prime factor influencing ECM. Similarly, Yu et al. [18] found that same solder alloys had different times to failure in the presence of different solder flux types.

In another study by Yu et al [19] , Sn-Pb and lead free solder alloys were studied by water droplet testing in DI water, and it was concluded that though all solder

alloys migrated, Sn-Ag and Sn-Ag-Cu solders are more reliable than Pb bearing solders. Li et al. [20] studied the corrosion behaviour of Sn-Pb and lead free solders in 3.5wt.% NaCl solutions, and found that lead free solders had better corrosion properties due to lower passivation current density, lower corrosion current density after the breakdown of the passivation film and a more stable passivation film on the surface.

As an overall remark to these studies, the migration behaviour of both the Sn-Pb and SAC solders is seen to be extremely dependant on the cleanliness of the PCBA surface, and on the nature of any eventual contaminants that might be present.

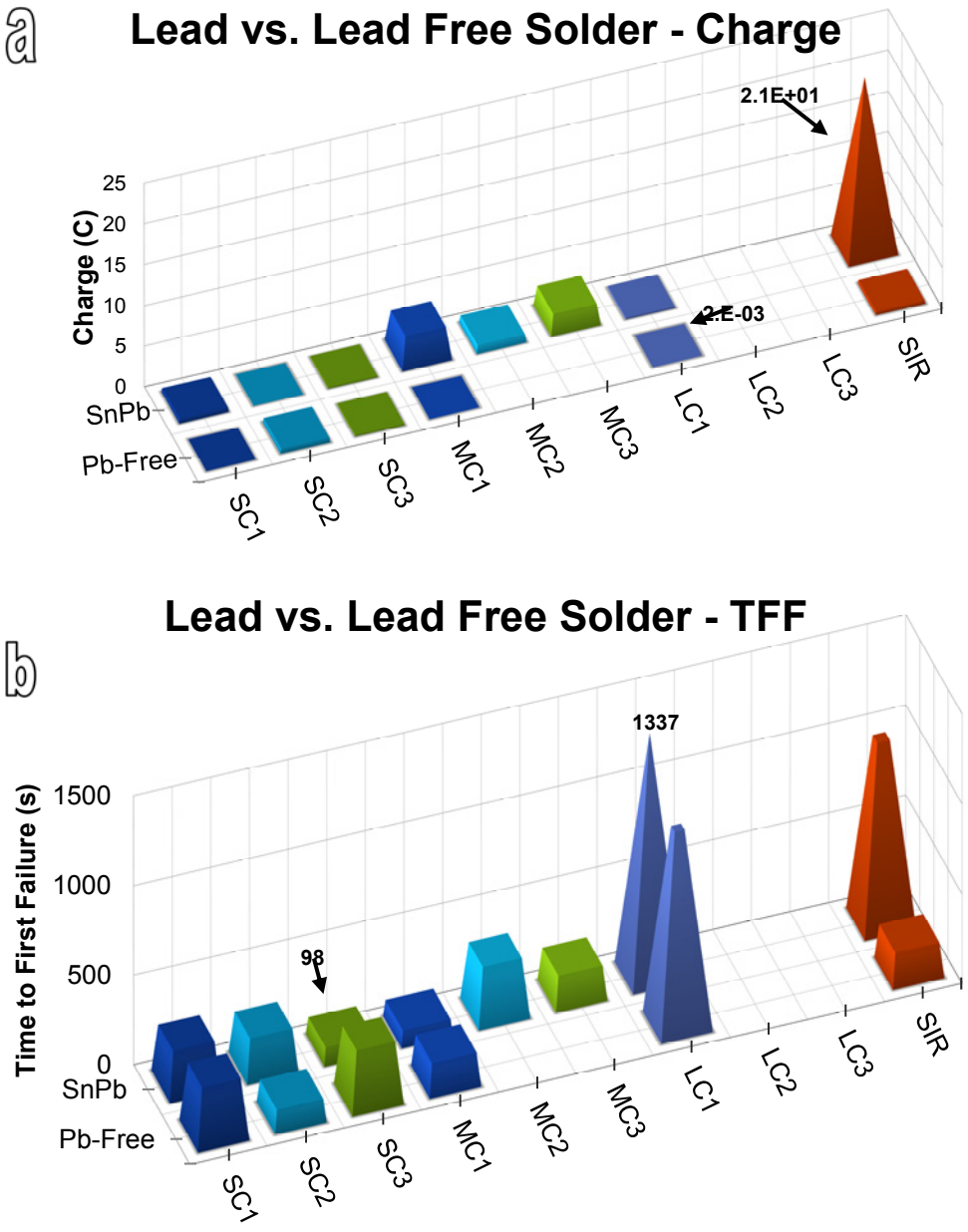

Figure 9.14: Comparison of plots for ECM of capacitors on the test PCB soldered with (a) lead containing and (b) lead free solder.

9.4.4 EFFECT OF HUMAN HANDLING (FINGER PRINTS) ON ECM

Contamination due to human handling is often found on PCBAs due to the lack of proper care or not using gloves for handling. Skin Surface Film Liquid (SSFL) that is transferred to the electronic device by human handling is hygroscopic and can absorb humidity easily to form a condensed layer of electrolyte. Presence of SSFL also provides conducting ions to the solution such as chlorides. SSFL have been studied extensively in relation to dissolution of metals that are kept in contact with the skin and a large variety of artificial SSFL solutions have been proposed. A review of Stefanie and Harvey [21] summarizes the work on artificial SSFL solutions and lists 45 different compositions that have been developed. A list of 61 different components that exist in real SSFL is given and the concentrations are found to vary from one person to the other, with age, physical activity etc.

In the present investigation, effect of handing of the PCB by bare hands was investigated using 5 test persons (TP) of varying age and geographic origin on lead free test PCB. During experiments with the test PCB, it was found that if the SIR pattern with reflow solder surface finish is touched while under a potential bias, a current increase was observed which differed greatly from one person to the other. The SIR pattern can therefore be used as a simple measure of the “fingerprint conductivity” for each TP. These conductivities are presented in Figure 9.15 below and show a difference by two orders of magnitude between the least and most conductive fingerprints. Fingerprints from TP1, TP2 and TP5 are seen to have low conductivity, while TP3 and TP4 had high conductivity.

ECM experiments were done at a low potential bias of 3V and using SAC soldered test PCBs in order to have a basis where as little migration occur as possible.

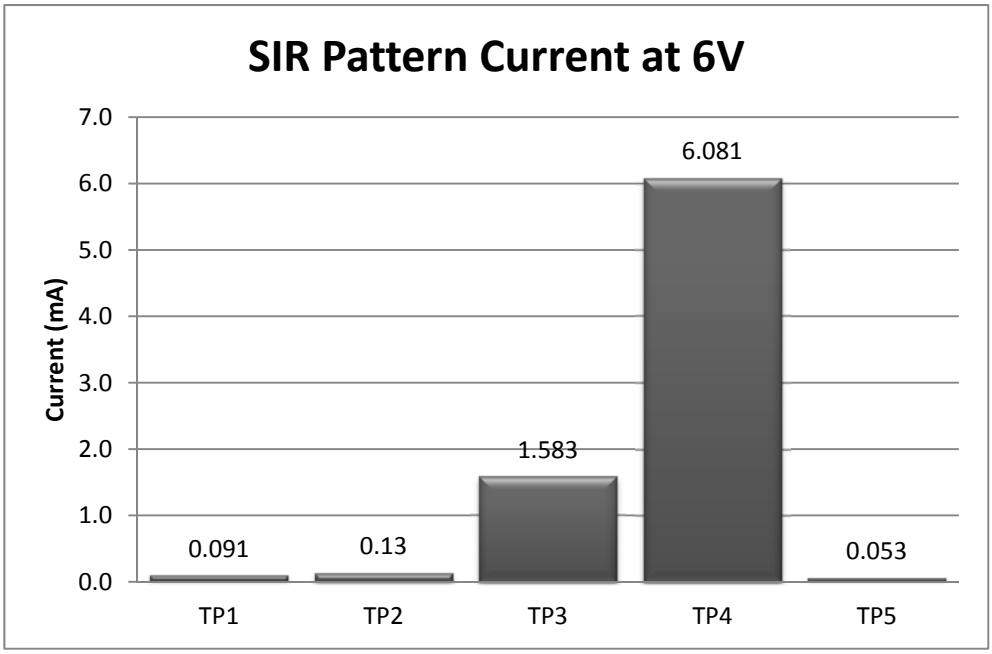

Figure 9.15: "Fingerprint" conductivity for the 5 test persons by placing the finger on the SIR pattern of the test PCB under 6V bias.

The charge and TFF plots are presented in Figure 9.16 a and b respectively. For reference, a clean 3V experiment is included in the diagrams. The fingerprint contaminations from all TPs are seen to significantly promote ECM. All circuits are seen to migrate, except some of the large components for TP3 and TP5. The TTF values for TP4, which had the highest conductivity of the fingerprints is also seen to have highest values for the charge and lowest values for the TFF. Especially on the medium and large components, the TFF values for TP4 are much lower than for other TPs showing that the SSFL from TP4 is more aggressive than others. More than the variation in susceptibility of finger prints, which is difficult to characterize due to the complexity in composition, results clearly shows the danger of bare handling of PCB on corrosion reliability. However, the variation in reactivity of finger prints found by this method correlates directly with the overall wetness of the test person's hand marking.

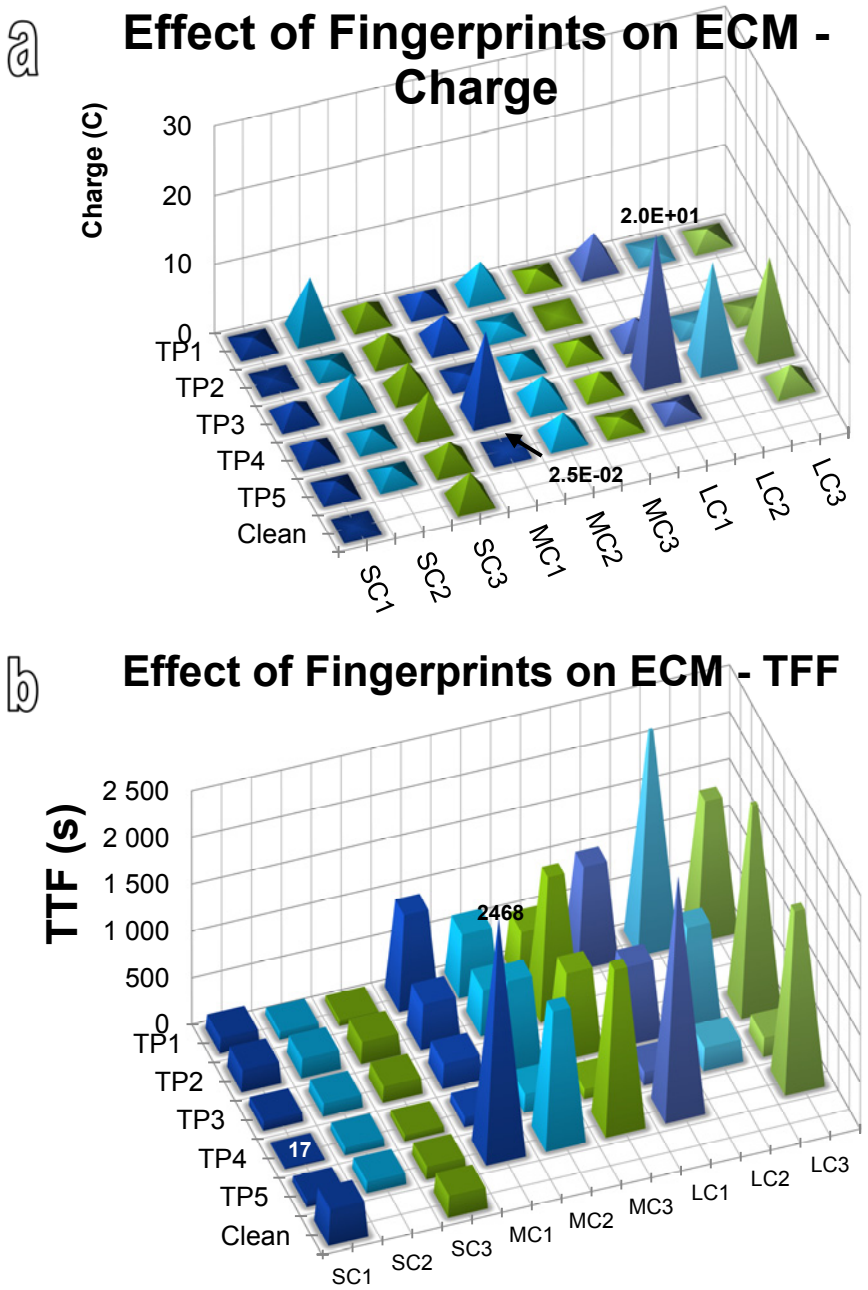

Figure 9.16: a) Charge and b) TFF plots showing the effect of fingerprints from 5 different test persons (TP) on migration. Minimum and maximum values are shown in both diagrams.

9.5 CONCLUSIONS

1. A new test PCB set up was designed and developed with necessary instrumentation for measuring the resulting current in multiple channels against an applied potential without interruption of voltage. This ensures no altering of the electrochemical processes on the test PCB during testing.
2. Electrochemical migration is found to occur on many components on both as received boards and boards that have been thoroughly cleaned using IPA. The tendency for ECM for various cleaning was “as received”>DI water rinse>IPA 2hrs>IPA ½hrs.
3. Components housings are commonly named by the area they occupy on a PCB, but the height of the component terminals in relation to the amount of solder paste and the dimensions of the solder pad are found to have an influence on the migration properties of the components.
4. The comparison between Sn/Pb and SAC soldered test PCBs showed that lead free boards had a slightly decreased tendency for migration, though testing directly on the solder alloys of the SIR patterns showed a much lower time to first failure for the lead free boards.
5. In the presence of human fingerprints, almost all components migrated. Differences were observed in the effect of fingerprints from different test persons, though all fingerprints were found to significantly increase the risk of migration. The results presented provide enough basis for a clear recommendation to avoid handling of electronics with bare hands as far as possible.

ACKNOWLEDGEMENTS

Current research has been conducted as part of the CELCORR consortium. Authors would like to acknowledge the Danish Ministry of Science, Technology and Innovation for the funding, project partners Danfoss A/S, Grundfos A/S, Vestas A/S and PRI-DANA Elektronik A/S, Danish Technological Institute and IPU for their commitment and help. Kathrine Bjørneboe from the Danish Technological Institute, Tåstrup, Denmark is acknowledged for SEM work. Danfoss Drives A/S in Gråsten, Denmark is greatly acknowledged for their participation of the CELCORR test PCB setup used in this work.

REFERENCES

[1] IPC-TR-476A, Electrochemical Migration: Electrically Induced Failures in Printed Wiring Assemblies, Northbrook, IL, USA, IPC, Institute for Interconnecting and Packaging Electronic Circuits, 1997.

[2] J.H. Lau, C.P. Wong, N.C. Lee, Electronics manufacturing: with lead-free, halogen-free, and conductive-adhesive materials, McGraw-Hill Professional, 2003.

[3] T. Takemoto, R.M. Latanision, T.W. Eagar, A. Matsunawa, Electrochemical migration tests of solder alloys in pure water, Corrosion Science. 39 (1997) 1415-1430.

[4] R. Williams, J. Banner, I. Knowles, M. Dube, M. Natishan, M. Pecht, An investigation of 'cannot duplicate'failures, Quality and Reliability Engineering International. 14 (1998) 331–337.

[5] D.A. Thomas, K. Ayers, M. Pecht, The"trouble not identified"phenomenon in automotive electronics, Microelectronics Reliability. 42 (2002) 641–651.

[6] D. Minzari, M.S. Jellesen, P. Møller, P. Wahlberg, R. Ambat, Electrochemical migration on electronic chip resistors in chloride environments, IEEE Transactions on Device and Materials Reliability. 9 (2009) 392–402.

[7] M.A. Johnsen, Effect of contamination on electrochemical migration, M. Sc. thesis, Technical University of Denmark, 2009.

[8] R. Ambat, M.S. Jellesen, D. Minzari, U. Rathinavelu, M.A. Johnsen, P. Westermann, Solder flux residues and electrochemical migration failures of electronic devices, in: Proceedings of Eurocorr 2009, Nice, 2009.

[9] D. Minzari, M.S. Jellesen, P. Møller, R. Ambat, On the Electrochemical Migration Mechanism of Tin in Electronics, To Be Submitted to Journal of the Electrochemical Society. (2010).

[10] S. Gobom, The hydrolysis of the tin (II) ion, Acta Chem. Scand. 30 (1976) 745–750.

[11] R.S. Tobias, Studies on the Hydrolysis of Metal Ions, Acta Chem. Scand. 12 (1958).

[12] IPC-9201, Surface Insulation Resistance Handbook, Northbrook, IL, USA, IPC, Institute for Interconnecting and Packaging Electronic Circuits, 1996.

[13] B.N. Ellis, On Insulation Resistance, Circuit World. 21 (1995) 5–11.

[14] D. Minzari, F.G. Grumsen, M.S. Jellesen, P. Møller, R. Ambat, Electrochemical Migration of Tin in Electronics and Microstructure of the Dendrites, Submitted to Corrosion Science. (2010).

[15] PERFAG-Gruppen, PERFAG-Specifications: 2E, Copenhagen, DK, Nyt Teknisk Forlag, 1997.

[16] S. Lee, M. Jung, H. Lee, T. Kang, Y. Joo, Effect of Bias Voltage on the Electrochemical Migration Behaviors of Sn and Pb, IEEE Trans. Device Mater. Relib. 9 (2009) 483-488.

[17] L. Zou, C. Hunt, Susceptibility of Lead-Free Systems to Electrochemical Migration, Middlesex, UK, National Physical Laboratory, 2007.

[18] D.Q. Yu, W. Jillek, E. Schmitt, Electrochemical migration of lead free solder joints, Journal of Materials Science: Materials in Electronics. 17 (2006) 229–241.

[19] D.Q. Yu, W. Jillek, E. Schmitt, Electrochemical migration of Sn-Pb and lead free solder alloys under distilled water, Journal of Materials Science: Materials in Electronics. 17 (2006) 219–227.

[20] D. Li, P.P. Conway, C. Liu, Corrosion characterization of tin-lead and lead free solders in 3.5 wt.% NaCl solution, Corrosion Science. 50 (2008) 995-1004.

[21] A.B. Stefaniak, C.J. Harvey, Dissolution of materials in artificial skin surface film liquids, Toxicology in Vitro. 20 (2006) 1265–1283.

10 PAPER 6: MORPHOLOGICAL STUDY OF SILVER CORROSION IN HIGHLY AGGRESSIVE SULFUR ENVIRONMENTS

Daniel Minzari[9], Morten S. Jellesen, Per Møller, Rajan Ambat

Department of Mechanical Engineering, Technical University of Denmark, DK 2800 Kgs. Lyngby, Denmark

ABSTRACT

A silicone coated power module with silver conducting lines, manufactured using Hybrid Thick Film technique, showed severe corrosion on all silver surfaces after prolonged use as part of an electronic device in a pig farm environment, where sulfur containing corrosive gasses are known to exist in high amounts. Permeation of sulfur containing species and humidity through the silicone coating to the interface has resulted in three corrosion types namely: uniform corrosion, conductive anodic filament type of Ag_2S growth, and silver migration with subsequent formation of sulfur compounds. Detailed morphological investigation of new and corroded power modules was carried out, and possible theoretical explanation for various corrosion mechanisms has been attempted.

KEYWORDS

Silver corrosion, Coatings, Sulfur, Dendrite, Failure, AC corrosion

ABBREVIATIONS

HTF:	Hybrid Thick Film
SHE:	Standard Hydrogen Electrode
SEM:	Scanning Electron Microscope
FEG-SEM:	Field Emission Gun Scanning Electron Microscope
FIB:	Focused Ion Beam
CAF:	Conductive Anodic Filament
IC:	Integrated Circuit

[9] Corresponding Author: Daniel Minzari, phone: +45 4525 2118, Fax: +45 4593 6213, email: dm@mek.dtu.dk

10.1 INTRODUCTION:

The use of electronic devices is continuously growing, as new markets are opened, price is reduced and device sophistication is increased. During the past decade, electronic devices have become a consumer item that is expected to be used anywhere in our everyday life, rather than a luxury item that is well taken care of and stored in a secure place.

Industries are receiving the benefits of the modern functionalities that electronic devices provides, and in the farming industries as an example, electronic devices are used for monitoring the food consumption of live-stock, monitoring air quality and temperature, regulation of ventilation etc.. However, the aggressive environment that often exists at industrial sites introduces reliability challenges to the manufacturers of the electronic components and to the materials usage. In the farming industries alone, the corrosive gases that the electronic device is exposed to will vary according to the animals held, the number of animals, on the ventilation, and even on the type of food that the animals are fed [1] . Apart from the corrosive gasses, geographical factors such as temperature and humidity will also influence the corrosion reliability of the electronic device.

Pig farms are known to produce large quantities of odors and aerial pollutants [1-9]. Particulate matter consisting of swine skin cells, feces, feed, bacteria, and fungi [9], and the presence of a wide variety of organic and inorganic gases including corrosive gases such as ammonia, sulfur dioxide, and hydrogen sulfide [6], and organic compounds such as amines and mercaptans could have a severe impact on the reliability of electronic devices. However, the use of electronics in pig farming and in general in the farming sector is increasing; therefore environmental reliability is a big concern. Though this paper takes focuses on a market failure from a pigs farm environment, silver sulfide corrosion has been reported in a number of highly polluted environments, including [10] rubber manufacturing, sewage/waste-water treatment plants, vehicle exhaust fumes (exit / entrance ramps), petroleum refineries, coal-generation power plants, paper mills, landfills, large-scale farms, automotive, swamps.

This paper presents the morphological analysis of silver corrosion found on a failed power module. The power module has been a part of the electronic device used in a pig farm in Denmark. The power module consists of a ceramic Hybrid Thick Film (HTF) substrate where conducting lines, various contact pads and some resistors are made by screen printing of thick-films that are sintered, and surface mount components are subsequently added using reflow soldering. Conducting lines and contact pads on this module are made of silver. Results presented in this paper describe some of the possible modes of corrosion on the silver surfaces on the HTF substrate during service in a pig farm environment. Morphological investigations were carried out using SEM, FEG-SEM, and FIB.

10.2 COMPONENT INVESTIGATED AND TECHNIQUES:

Figure 10.1 shows the partial view of the power module (before use) with the silicone coating (Semicosil 926). The power module is attached onto a nickel coated copper base plate, surrounded by a plastic frame with leads for external connections to a printed circuit board assembly and covered with a conformal coating consisting of a soft silicone gel.

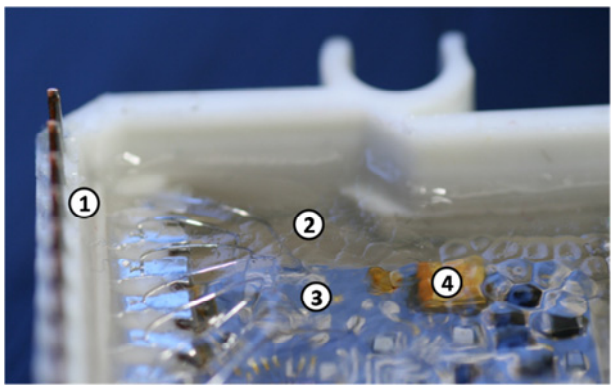

Figure 10.1: Top view of part of the power module investigated. The module is encapsulated by a white plastic frame with leads for external connections (1) and coated by approx. 10 mm silicone conformal coating (2). The ceramic substrate with thick film silver contact pads and conducting lines (3) along with surface mount components (4) can be observed through the coating.

For observing the surface of the HTF substrate under optical microscope and SEM, it was necessary to remove the silicone coating. Therefore, prior to the microscopic investigation, silicone gel was removed on a new power module and the corroded

one. For removing the conformal coating, the power module was immersed in a silicone remover (Dana lim siliconefjerner 911, Dana Lim A/S, Denmark) solution overnight and the process was repeated five times to get a substrate relatively free from the coating. The silver surfaces on the unused and corroded PCBA were intact after removal of the silicone coating. Small parts of silicone coating still remained on the surface, but it did not interfere with the subsequent analysis.

Surface morphology investigation of the new and failed HTF substrates was carried out using Optical Microscopy, SEM (JEOL 5900), EDS (Oxford Link ISIS), and FIB-SEM (Zeiss 1540EsB).

10.3 RESULTS:

Figure 10.2 shows comparison of the same area of the HTF substrate on a new and failed power module after removal of the silicone coating. All the silver lines are bright and clear on the unused module, but they have turned black in the case of the failed HTF substrate.

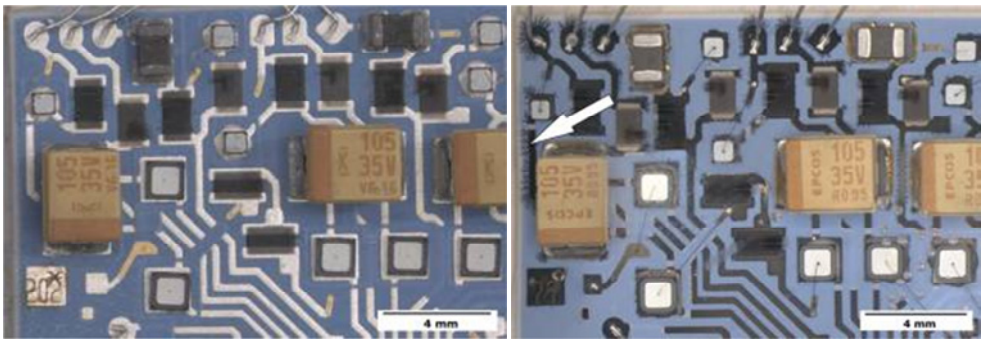

Figure 10.2: Part of power module investigated in this work: (a) unused module, and (b) failed module after use in pig farm environments. Dendritic growth is seen at localized areas, especially near edges of the HTF substrate, as indicated by arrow in (b).

Corrosion observed on the HTF substrate was uniform indicating that the permeation of gas was uniform through the silicone coating unlike a localized ingress of gas due to damage in the film. Small dendritic arms of the corrosion product can be seen protruding out from the conductive lines at several localized places, mainly, but not only, around the edges of the substrate (example indicated by arrow on Figure 10.2b).

10.3.1 MATERIAL MAKE-UP OF NEW AND FAILED MODULES:

Figure 10.3a gives a high magnification view of the various types of contact points on the HTF substrate. Figure 10.3b shows magnified SEM picture of one of these contact areas and locations where EDS analysis was carried out (Table 10.1). Comparing with the EDS analysis given in Table 10.1, it can be seen that the bright regions are made of silver, whereas the attached 200 µm thick wire is aluminium. The EDS analysis also shows some amount of silicon suspected to be from the remains of the silicone coating. Other parts of the power module had an Integrated Circuit (IC) and gold wires were used for connecting the IC to other contact points on the HTF substrate (Figure 10.3).

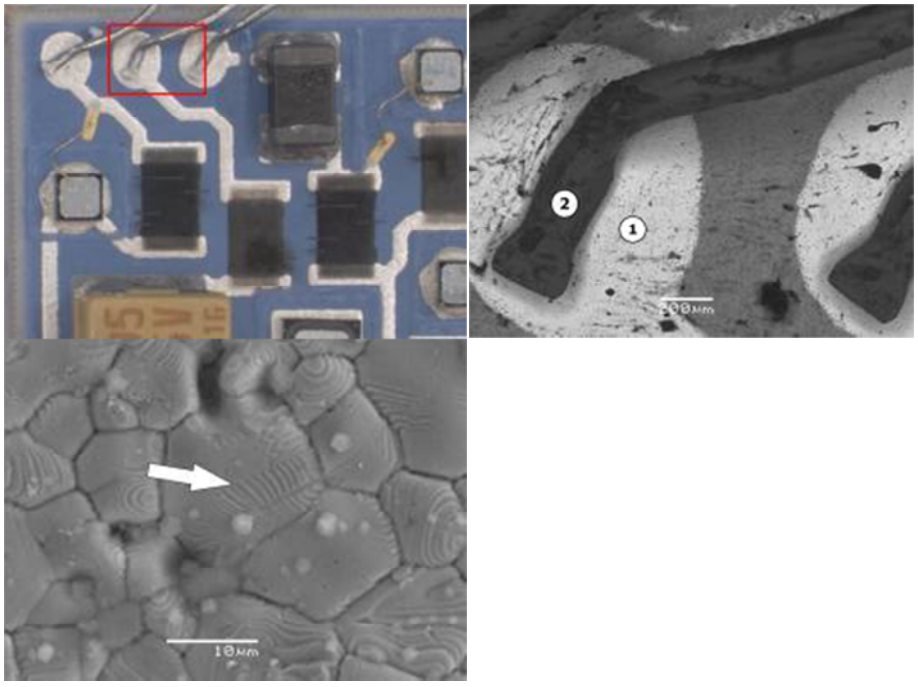

Figure 10.3: Magnified views of the power module HTF substrate: (a) optical picture, (b) SEM image of contact area (BE mode), (c) magnified view of Ag layer (SE mode). Areas marked by 1 and 2 on image (b) are places of acquisition of EDS presented in Table 10.1.

Table 10.1:EDS analysis of Ag conductor and Al connector wire in wt.%.

Spectrum	Al	Si	Ag
1	0	4	96
2	85	15	0

High magnification picture of the silver coating in Figure 10.3 (c) shows clear signs of grain structure with some large defects such as cavities. Particle like features on the surface are remains of the silicone gel. Average grain size of the coating was approximately 15 µm. Clear signs of features due to twinning/deformation bands or crystal faceting can also be seen in most of the grains (marked by arrow), possibly due to stresses in the silver coating induced by the ultrasonic bonding process of the Al wire or from the solidification of the silver thick film during the sintering process.

Due to the large difference in standard potentials of the three basic materials found on this HTF substrate namely Au, Al, and Ag, galvanic corrosion is a clear possibility where highest level of corrosion is expected for Al followed by Ag, while Au acts as an efficient cathode. However, applied potential bias on the HTF is also an important factor together with the potential waveform (AC or DC), which could alter the situation. From an electrochemical potential point of view aluminum has a standard potential $E_{0,Al}$=-1.66V vs. SHE would act as anode if galvanically coupled to silver ($E_{0,Ag}$=0.8V vs. SHE) or Au ($E_{0,Au}$=1.5V vs. SHE) which would act as cathode materials. Consequently, between silver and gold, silver becomes the anode. A possible problem would be the corrosion and possibly de-bonding of the aluminum wire. However, no aluminum corrosion was observed at the Al-Ag interfaces, indicating that the concentration of water in the conformal coating was too low for excessive Al corrosion to occur.

At some places, gold wires are used for connection, and at these sites, a gold layer is deposited on the silver conducting lines, probably to lessen galvanic corrosion at the contact point (see Figure 10.4). At the corroded sample, the silver corrosion near the gold did not seem to appear any worse than generally observed on the

HTF substrate, though discoloring of some of the gold wires was observed. Detail of this is given in later section of this paper.

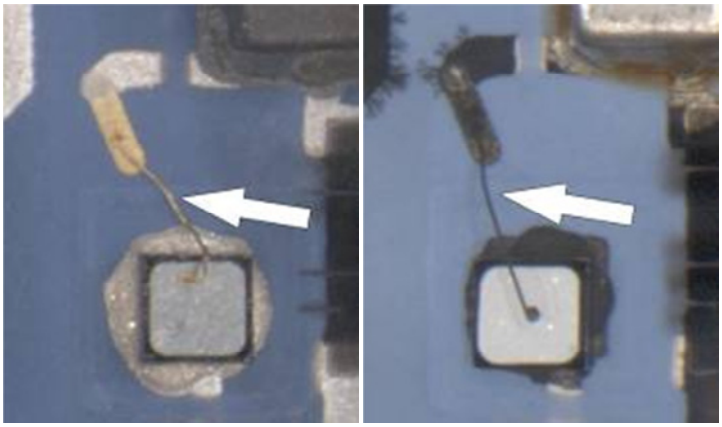

Figure 10.4: Discoloring of gold wire on HTF substrate after exposure to pig farm environment. (a) image from new HTF substrate and (b) image from same position on failed HTF substrate.

10.3.2 3.2 DETAILED SURFACE MORPHOLOGY OF CORRODED HTF SUBSTRATE

Figure 10.5 shows a set of magnified digital photographs of the failed HTF substrate showing dendrite formation at the edges of the silver conducting lines.

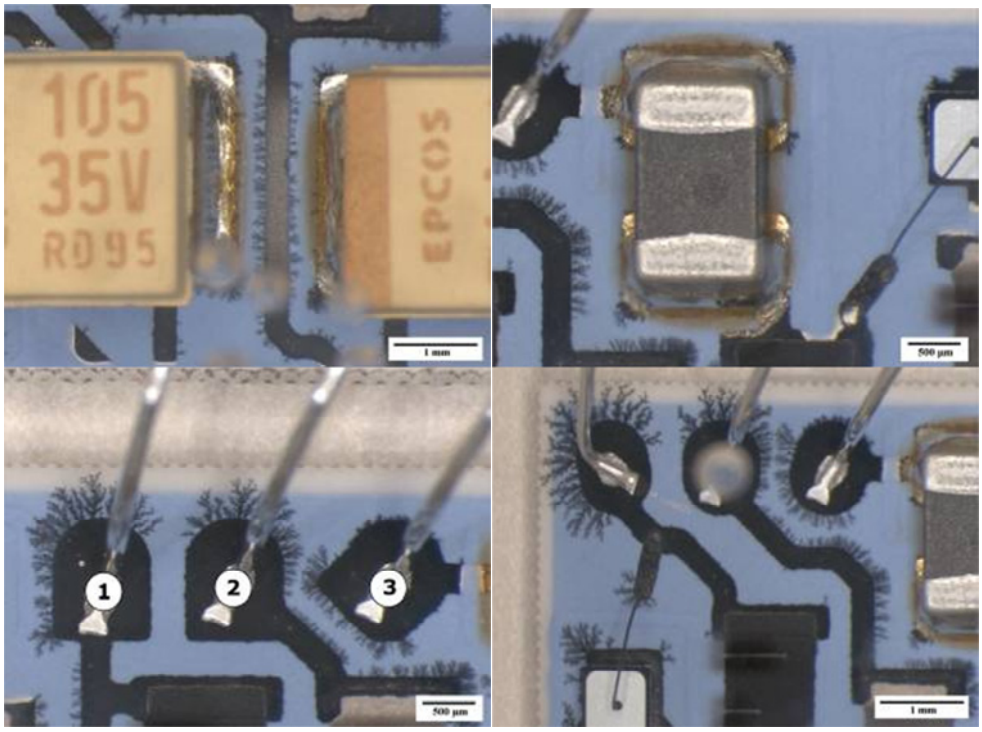

Figure 10.5: Microscopy images of dendritic growth on conductor pattern. Images were taken prior to removal of silicone coating and bubbles in the coating are seen as blurred areas on images a) and d).

While silver sulfide corrosion was observed at all silver surfaces on the HTF substrate, dendrite formation was localized mainly, but not only, at the edges of patterns on the HTF substrate. At some places, the dendrites are seen to grow from one side, while at other places they are seen to grow from both sides. This indicates that the dendrite growth might be driven by the electric fields, though no clear relation to the effect of the polarity of the field to the growth direction could be established.

At no place were the dendrites seen to bridge conducting lines, though leakage currents between the conducting lines are expected to have increased significantly due to the decreased distance and semi-conducting nature of many silver corrosion products. In Figure 10.5(c), three contact pads have been numbered 1, 2 and 3. During the device use, a 430 V AC potential is either applied to pads 1 and 3 or to pads 2 and 3. This further suggests that the dendrite growth is aided by the electric field, since no dendrites are growing between pad 1 and pad 2 where no potential

bias exist, and dendrites are seen between pad 2 and 3 where a potential bias exist. The HTF substrate is placed on a grounded metal base-plate, and this could explain the dendrite growth along the edges of the HTF substrate, since an electric field could exist between conductors and the base-plate, such as the dendrite growth from pads 1 and 2 towards the edge of the HTF substrate. Pad 3 is grounded, which explains why no dendrite growth is observed between this pad and the edge of the HTF substrate. On the contact pads seen on Figure 10.5(d), the same trend is seen as in Figure 10.5(c) and the potential bias applied here is same as described for Figure 10.5(c). Dendrite formation due to creep corrosion has been observed in numerous field failures [11-14] in the presence of highly aggressive gasses. Contrary to the present case, the phenomenon has commonly been observed on copper and silver without the influence of an electric field. However, the highly localized formation of the dendrites at several points where a high AC field exist strongly suggests that the dendrite growth is influenced by the electric field. Little research has been done on AC corrosion in electronics, and no relevant literature has been found regarding the influence of an AC potential on a silver sulfide formation. A possible mechanism for the dendrite formation is proposed in the discussion in section 4.

Figure 10.6 (b-f) shows magnified SEM picture of the dendrites shown in Figure 10.6(a) (indicated by the square).

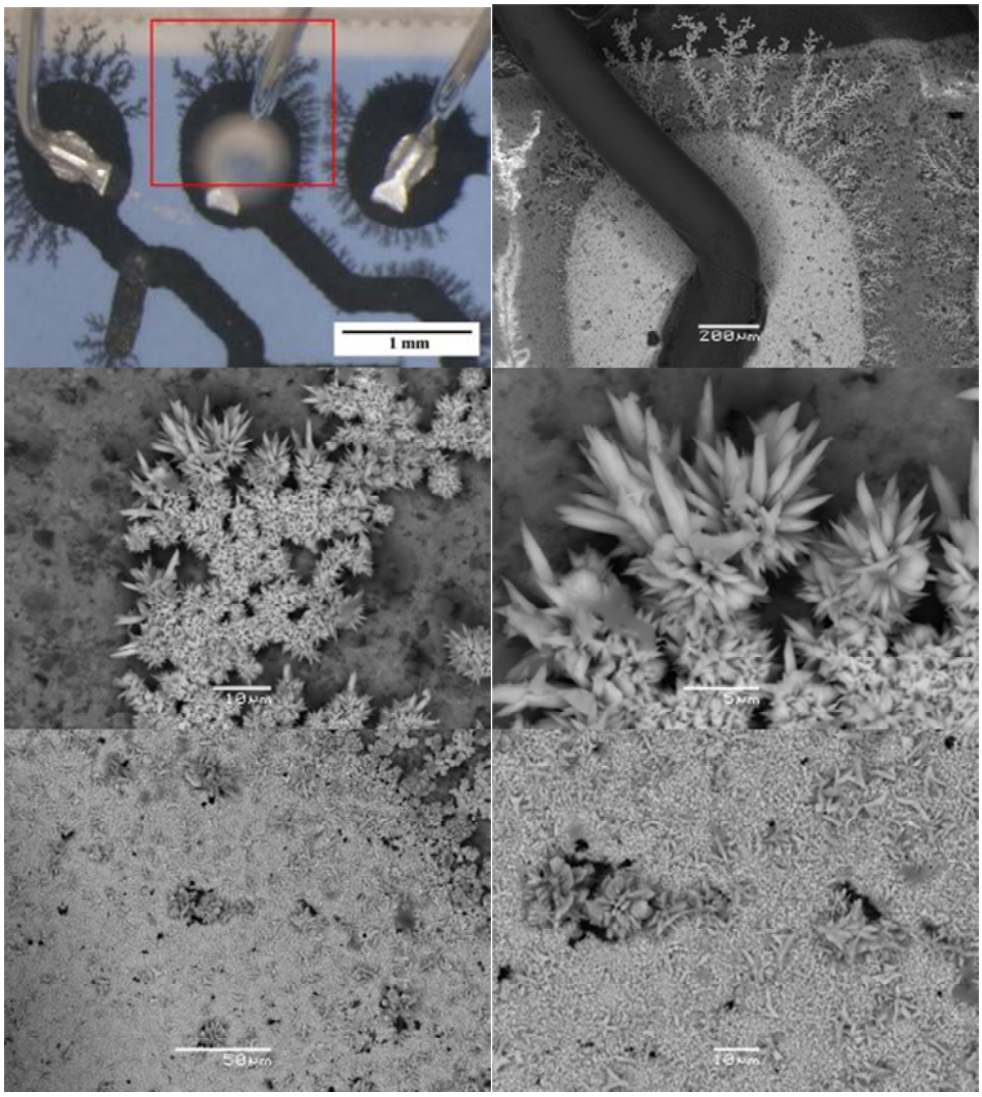

Figure 10.6: SEM images (BEC mode) of dendrite at various magnifications. Red square on the top LOM image shows the origin of the SEM images.

Figure 10.6 (b-d) shows the dendrite structure and morphology, while (e-f) show the surface of the contact pad. Flower-like silver sulfide growth with discontinuous blocks was generally observed on all silver surfaces (such as observed in Figure 10.6f), though dendrites only grew from edges of some conducting lines.

In order to investigate the internal structure of the dendritic branches, a FIB section was performed as presented in Figure 10.7. Places for acquisition of EDS analysis are shown on Figure 10.7 c and results in atomic per cent are presented in Table 10.2.

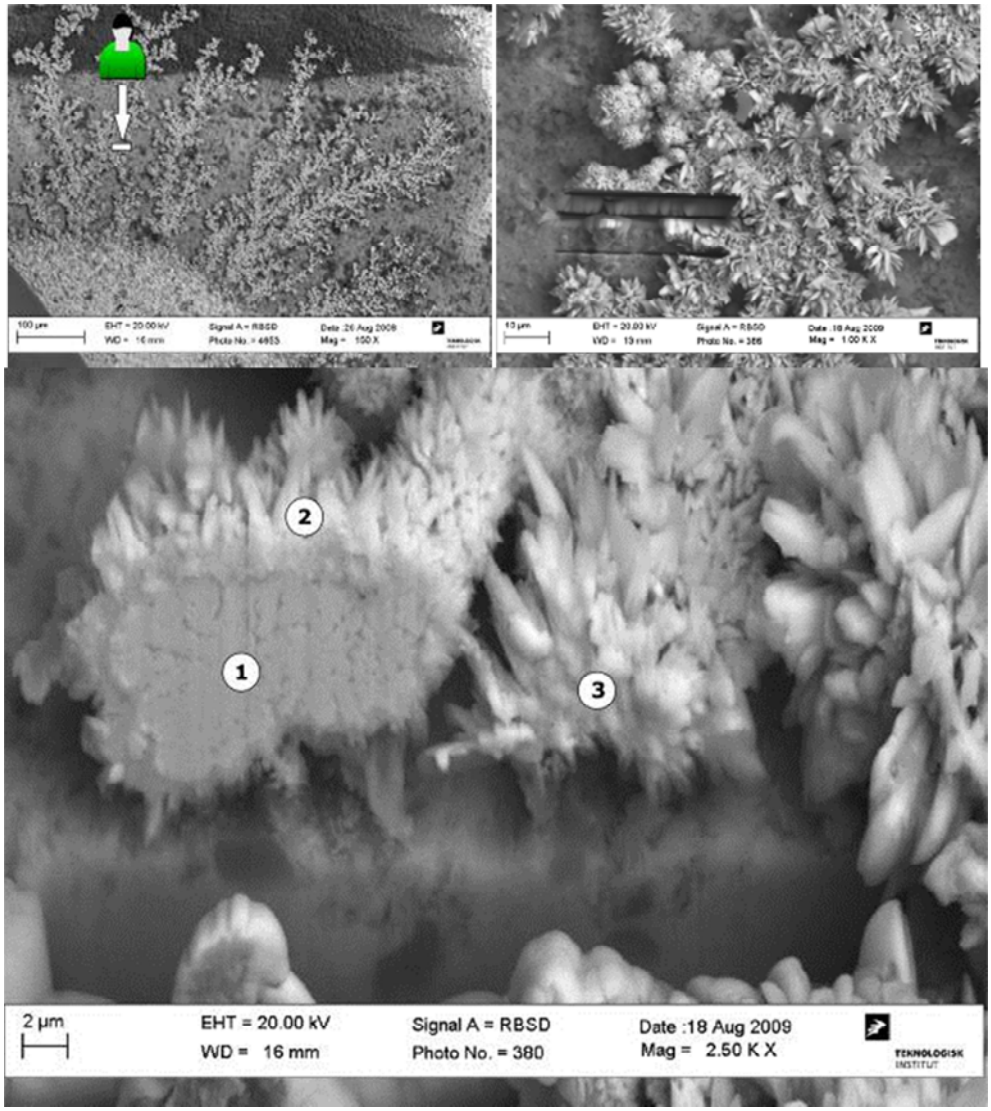

Figure 10.7: FIB cross section of dendritic branch. Image (a) shows where the cross sections was performed (the human figure and arrow illustrate the direction of view on images b and c). Image b show a top view of the FIB cross section, while image c gives a BE mode view of the dendritic branch.

The dendritic branch is seen to consist of various amounts of silver, sulfur and oxygen, indicating the presence of mixed corrosion products. No unambiguous conclusions on the nature of the corrosion products can be made from the elemental ratios of the EDS measurements, but the products are most likely to consist of silver sulfide, silver oxide, or silver sulfate (see discussion in section 10.4). Metallic silver was not observed in the dendritic structures at the site where the FIB milling was performed, suggesting that the dendrite growth is not an electrochemical migration type as conventionally seen under a DC bias. Al and Si signals are believed to be background signal from ceramic substrate and remnants of silicone coating.

Table 10.2: EDS analysis of FIB cross section as labeled in Figure 10.7 c. Content is given in at. %

Spectrum	O	Al	Si	S	Ag
1	51.27	7.75	5.67	2.49	32.82
2	14.23	2.62	3.00	29.22	50.93
3	42.12	4.69	3.79	10.58	38.82

Figure 10.8 shows the effect of the what is thought to be the high energy sites (such as twinning, deformation bands or crystal faceting described earlier, Figure 10.3c) on the formation of silver sulfide. Due to residual stresses at these sites, initiation of the silver sulfide corrosion is favorable and preferentially grown over these sites. Similar feature was observed on all silver conducting lines on the entire HTF substrate. Though sulfidation was seen to be favorable at the high energy sites, all silver surfaces was found to be corroded, and no exposed metallic silver was observed on the entire surface.

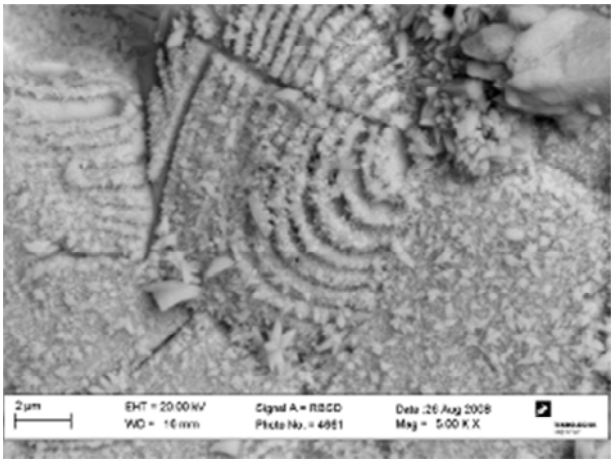

Figure 10.8: Preferential growth of silver sulfide at high energy sites on silver surface.

10.3.3 3.3 CREEP CORROSION OF SILVER ON AU WIRES:

Figure 10.9 shows part of the failed PCBA where an integrated circuit (IC) is placed. Gold wires are used for connecting this IC to other parts of the HTF substrate. It is clear from Figure 10.9 that some of these wires appear to have a golden color, while others are black (See red box in Figure 10.9 (a) and (1) and (2) in Figure 10.9 (b)).

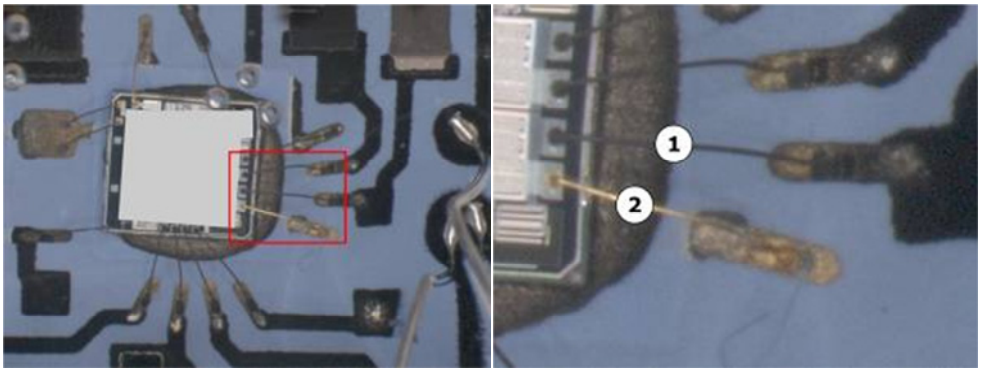

Figure 10.9: Discoloring of Au wire connectors around IC. (a) Overview image and (b) large magnification image.

EDS analysis results presented in Table *10.3* show the presence of high amounts of silver and sulfur on wire 1, while wire 2 consist of only gold. Since only 4 wt.% gold is detected on wire 1, this suggests that the deposited layer is rather thick as the probe depth of the EDS analysis is approx. 1 µm.

Table 10.3: EDS analysis of Au wire connectors that are discolored (Wire 1) and not discolored (wire 2). Content is given in wt. %

Spectrum	S	Ag	Au
Wire 1	12.9	82.9	4.2
Wire 2	0.00	0.00	100.0

For a more detailed analysis of the deposited layer, FIB SEM was performed on the gold wires. Figure 10.10a present the FIB cross sections of gold wire that was not discolored (Wire labeled 2 on Figure 10.9b). The slightly rough surface topography is due to sample preparation where a thin gold layer was sputtered on to the wires in order to ensure surface conductivity from the specimen to the sample holder. The wire was found to consist only of gold, and no deposits could be observed on the surface. The discolored wire however (Wire 1 on Figure 10.9b) is seen to have a relatively thick layer of ~1µm deposited to the surface (see Figure 10.10b and c). Figure 10.10d presents an image in backscatter mode, where difference in the atomic weight of the elements reflects as a change in the intensity of the image. Light materials therefore appear darker than heavy materials. It is seen, that the deposited layer is non-uniform, and that heavier (brighter) particles exist in the coating. EDS analysis was performed at two spots, as indicated by labels 1 and 2 in Figure 10.10d at the bright and dark areas respectively and results are presented in Table 10.4. It should be noted, however, that when doing EDS analysis on a spot, ~90% of the x-ray signal will be generated from a volume having approx. 1 µm diameter from the spot. Since the size of the whole deposit is ~1µm the EDS results therefore include more than the particle itself. This explains why gold is found in the spectra. However, spectrum 1 is seen to consist only of silver, while sulfur and trace of oxygen is found at the dark area presented in spectrum 2.

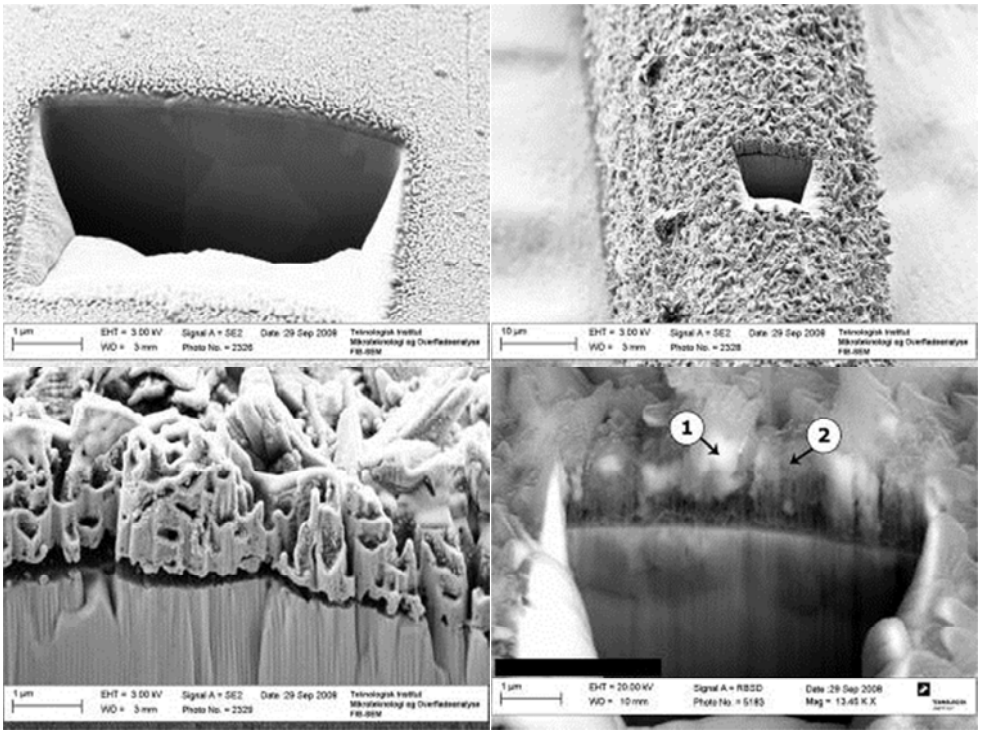

Figure 10.10: FIB Cross section of (a) gold colored wire (wire 2 in Figure 10.9b); (b) and (c) FIB section of deposited silver sulfide on gold wire (wire 1 in Figure 10.9b); (d) BEC mode image of silver sulfide layer (Numbers (1) and (2) indicate the places of EDS acquisition given in Table 10.4).

Table 10.4: EDS analysis of bright and dark areas in silver sulfide layers (wire 2). Content is given in wt. %

Spectrum	S	O	Ag	Au
1	0.00	0.00	77.5	22.5
2	11.3	0.8	68.8	19.1

10.4 DISCUSSION:

Silver is a rather noble metal having a standard potential of E_0= 0.8V vs. SHE. Generally silver has good corrosion properties and excellent electrical conductivity. These properties make it a very attractive material for electronics. However, it is well known that silver will corrode in environments containing chloride or sulfide

forming chlorargyrite (AgCl) or acanthite (Ag_2S) respectively, and that the high solubility of silver ions makes the material prone to electrochemical migration in both condensing and non-condensing environments [15]. For such reasons, use of silver in electronic applications could have dramatic reliability issues if the environment for which the electronic device is to be used contains aggressive corrosive gases.

In general, silver corrosion in the present failure investigation can be divided into the following categories:

1. Uniform silver sulfide corrosion
2. Dendritic growth of silver sulfide
3. Deposition of silver corrosion products on gold wires (Creep corrosion).

Uniform sulfide corrosion of silver surfaces is a well-studied phenomenon, and excellent information is this mechanism is found in the work of Graedel [16]. Silver will readily form silver sulfide by the reaction

$$2Ag + HS^- \rightarrow Ag_2S + ½H_2(g) \quad (1)$$

This reaction is not dependent on the presence of water, and therefore only requires that H_2S can diffuse through the silicone coating in the present case. However, the presence of water and nitrate is known to dramatically increase the speed of reaction (1) [17,18], contrary to [19]. Robb [20] investigated the permeabilities for various gasses in dimethyl-silicone rubber. Gasses such as H_2O, H_2S, NO_2, NH_3, and SO_2, which exist in high amounts in the pigs farm environment, are all found to have rather high permeabilities in silicone. It should be noticed that even though silicone is excellent as a barrier for liquid water, water vapor from humid air will still have a very high diffusion through silicone. A silicone coating can therefore be regarded as a low-pass filter when placed in a humid environment, smoothing out the sudden variations in the humidity of the air, but if a rather high average humidity is present over time, some amount of H_2O could be expected to be available at the surface of a coated HTF substrate. However, as observed in Section 3.1, the water uptake of the coating was seen to be insufficient for galvanic

corrosion of the Al wires to occur, indicating that the amount of absorbed water in the coating must have been relatively low. The corrosion of the silver surfaces must therefore be attributed more to the presence of sulfur containing gasses, than to the presence of water.

A composite reaction diagram for the silver sulfide corrosion has been proposed by Graedel [16], and a similar model is presented in Figure 10.11 where only species that are relevant to the present investigation is used based on the observations from the failure analysis. The formation of silver sulfide or silver sulfate can either occur by direct adsorption of HS^- or SO_4^{2-} on the silver surface, or by dissolution of Ag^+ in the presence of water and subsequent reaction with dissolved HS^- or SO_4^{2-}.

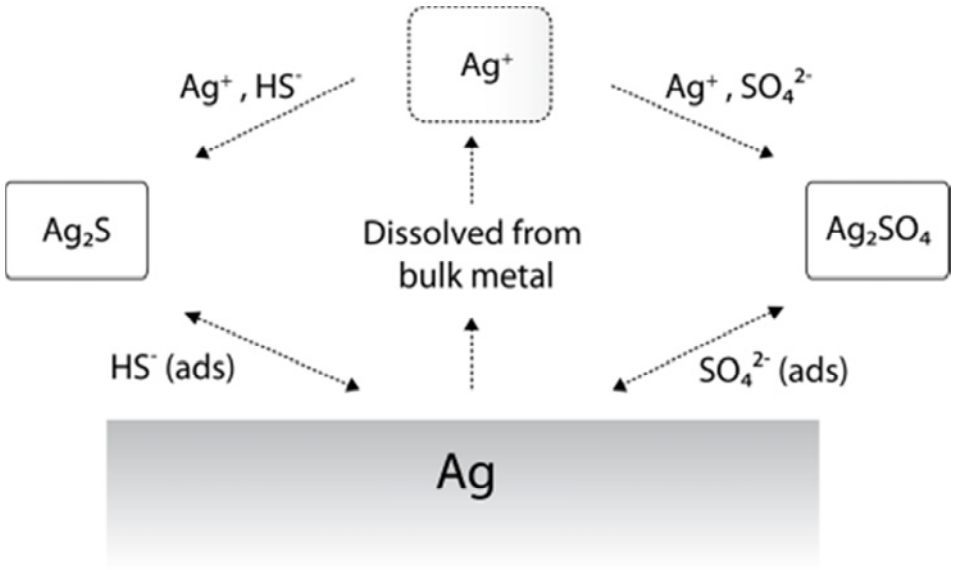

Figure 10.11: Composite reaction diagram for silver corrosion reactions.

Figure 10.8 also shows the microstructure of the silver coating influence sulfide corrosion. Preferential growth of Ag_2S along the special features might be due to the high activity of these regions.

In order to understand the dendritic growth observed in Figure 10.5, Pourbaix diagrams have been calculated for the Ag-Cl-N-S-H2O system at 25°C using Outokumpu HSC Chemistry 5.11 software (see Figure 10.12 where diagrams for silver and sulfur are presented). Concentrations of the species are estimated from

the typical content of the gasses in the pig farm environment and their permeabilities in silicone. Based on the observations made in the failure analysis, where no chloride was found at any place in the corrosion products, the amount of chloride is set to a rather low value. Though included in the calculations, chloride and nitrogen species are not found to be of relevance in the prominent reactions found in the diagrams, in good agreement with the EDS observations. Varying [S] by three orders of magnitude gave only minor changes to the diagram, where the Ag_2S region is expanded towards higher pH values, and the stability of the Ag^+ changes to $AgSO_4^-$ with increasing [S].

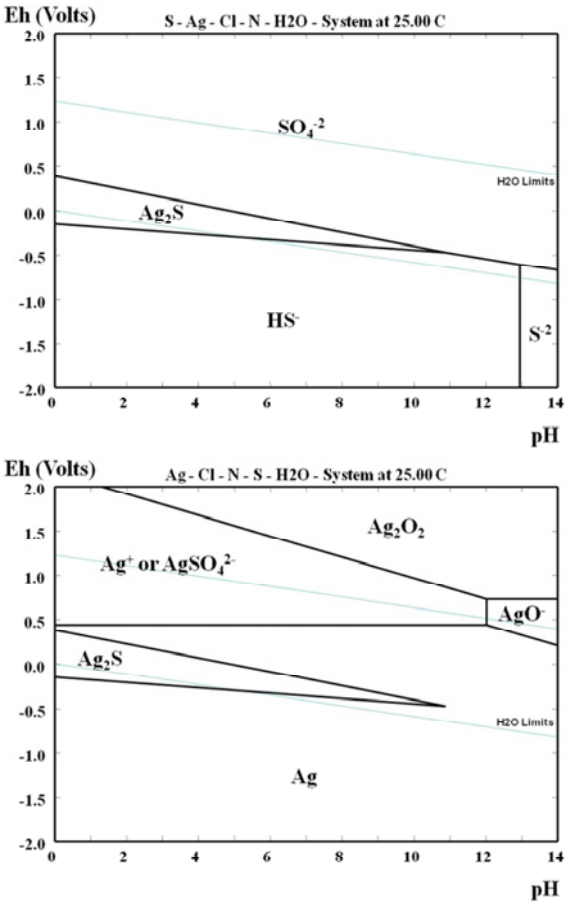

Figure 10.12: Pourbaix diagrams for the Ag-Cl-N-S-H_2O system at 25°C. (a): Ag diagram and (b): S diagram. Concentrations used are Ag (1 µM), Cl (1µM), N (100µM) and S (100 µM), which is based on a rough estimation of existing concentrations in the coating.

The Ag_2S dendrite formation at local sites are believed to be due to local ingress of water at the interface between the coating and the HTF substrate, where silver is dissolved into Ag^+ during the anodic sweep of the AC bias, and then reacts with HS^- or SO_2^{4-} to form Ag_2S or Ag_2SO_4 (see reaction diagram in Figure 10.11 and Pourbaix diagram for silver in Figure 10.12). The dendritic growth towards the grounded base plate clearly indicates that a conductive electrolyte might have been present at the coating- HTF substrate interface.

If the Ag_2S dendrites bridge the gap between conductors, it can result in electric short similar to Conductive Anodic Filament (CAF) growth [21-24] due to the semi-conducting nature of Ag_2S. Kulkarni et al. [25] reported a band gap value of 0.7 – 0.9 eV for Ag_2S and a resistivity of ~4 x 10^2 Ωcm for 3.3 µm thick film, while a metallic silver film of similar thickness has a resistivity of 0.56 x 10^{-5} Ωcm. Due to the same reason, a higher leakage current between conducting lines can be expected as the dendrites protrudes out from the conductors from both sides reducing the distance of separation. The growth direction could also be due to easier diffusion path of gasses at the interface between the conformal coating and the HTF substrate, though this does not explain the localization of the dendrites.

The FIB cross sections in Figure 10.10 shows a heterogeneous deposit at the gold wire, where the bright particles in the deposit could be metallic silver, while the dark areas are corrosion products. The presence of both silver and oxygen as detected by EDS indicate that the products are most likely silver sulfide and possibly small amounts of silver oxide or silver sulfate. It was noted that in general, only gold wires that are connected to the large silver parts are black colored, while gold wires that are soldered to small silver pads were not discolored. This suggests that the transport of corrosion products has occurred along the metal-coating interface, in a manner similar to the creep corrosion reported by [11-14]. Creep corrosion has previously been observed when galvanic coupling between Cu and Ag occurs in the presence of high humidity and high sulfur containing gasses. The process is sensitive to the surrounding surface on which the corrosion product creeps, and is believed to be controlled by mass transfer of the corrosion products. Contrary to

the case of Cu-Ag coupling, silver here is acting as anode material when coupled to gold.

Another explanation for the mechanism could be due to SO_4^{2-} ingress through the coating, where silver ions produced by galvanic coupling of the silver surface to the noble gold, thereby forming Ag^+ and $AgSO_4^-$ ions. Silver and silver sulfate ions are then precipitated as Ag_2SO_4 or Ag_2S on the wire. The mechanism is sketched in Figure 10.11. Discoloring of gold wires attached to large silver surfaces was found to be more severe than for wires attached to small silver surfaces, indicating that the uniform corrosion of the silver surfaces produces enough silver ions that deposit on the gold wires.

10.5 CONCLUSIONS:

1. Severe sulfide corrosion of silver surfaces was observed on a HTF substrate after exposure to the pig farm environment due to permeation of corrosive gasses through the silicone coating.

2. Three types of corrosion features were observed namely: Uniform distribution of silver sulfide, dendritic growth, and creep corrosion of silver on gold wires.

3. Formation of sulfur containing corrosion products with Ag might be attributed to the permeation of gases such as H_2S and SO_2 through the conformal coating, while the dendritic growth was assisted by the AC potential bias.

4. Failure of this power module shows the combined effect of various factors such as the use of materials with different electrochemical activity, effect of aggressive environment, and failure of a conformal coating to act as a barrier for outside environment.

ACKNOWLEDGEMENTS

Current research has been conducted as part of the CELCORR consortium. Authors would like to acknowledge the Danish Ministry of Science, Technology and Innovation for the funding, project partners Danfoss A/S, Grundfos A/S, Vestas A/S and PRI-DANA Elektronik A/S, Danish Technological Institute and IPU for their

commitment and help. Kathrine Bjørneboe from the Danish Technological Institute is greatly acknowledged for FIB-SEM work.

REFERENCES:

[1] L.D. Jacobson, A.J. Heber, S.J. Hoff, Y. Zhang, D.B. Beasley, J.A. Koziel, and B.P. Hetchler, "Aerial Pollutants Emissions from Confined Animal Buildings", Proceedings Workshop on Agricultural Air Quality: State of Science. Bolger Conference Center, Potomac, Maryland, 2006, pp. 775-784.

[2] A.J. Heber, J.Q. Ni, B.L. Haymore, R.K. Duggirala, and K.M. Keener, "Air quality and emission measurement methodology at swine finishing buildings," Transactions of the ASAE, vol. 44, 2001, pp. 1765-1778.

[3] B. Amon, V. Kryvoruchko, M. Fröhlich, T. Amon, A. Pöllinger, I. Mösenbacher, and A. Hausleitner, "Ammonia and greenhouse gas emissions from a straw flow system for fattening pigs: Housing and manure storage," Livestock Science, vol. 112, 2007, pp. 199-207.

[4] L. Loyon, F. Beline, F. Guiziou, P. Peu, S. Picard, and P. Saint Cast, "Assessment and comparison of annual gaseous emissions of three biological treatments of pig slurry with a storage–spreading system," Proceedings of The Workshop on Agricultural Air Quality: State of Science, 2006, pp. 5–8.

[5] T.T. Lim, A.J. Heber, J.Q. Ni, A.L. Sutton, and D.T. Kelly, "Characteristics and emission rates of odor from commercial swine nurseries," Transactions of the ASAE, vol. 44, 2001, pp. 1275-1282.

[6] L. Cai, J.A. Koziel, Y.C. Lo, and S.J. Hoff, "Characterization of volatile organic compounds and odorants associated with swine barn particulate matter using solid-phase microextraction and gas chromatography–mass spectrometry–olfactometry," Journal of Chromatography A, vol. 1102, 2006, pp. 60-72.

[7] G. Gustafsson, "Factors affecting the Release and Concentration of Dust in Pig Houses," Journal of Agricultural Engineering Research, vol. 74, 1999, pp. 379-390.

[8] P. Kai and A.B. Vinstrup, "Lugt fra husdyrbrug," Grøn Viden, Husdyrbrug, vol. 42, 2005, pp16-20

[9] S.J. Hoff, D.S. Bundy, M.A. Huebner, B.C. Zelle, L. D. Jacobson, A.J. Heber, J.Q. Ni, Y. Zhang, J.A. Koziel, D.B. Beasley, "Emissions of Ammonia, Hydrogen Sulfide, and Odor Before, During and After Slurry Removal from a Deep-Pit Swine Finisher", Journal of Air & Waste Management Association.Vol. 56, 2006, pp. 581-590.

[10] C. Hillman, J. Arnold, S. Binfield, and J. Seppi, "Silver and Sulfur: Case Studies, Physics, and Possible Solutions," SMTA International Conference, 2007.

[11] R. Schueller, D. Inc, and T. Austin, "Creep Corrosion on Lead-free Printed Circuit Boards in High Sulfur Environments," SMTA News and Journal of Surface Mount Technology, vol. 21, 2008, p. 21.

[12] Y. Zhou and M. Pecht, "Investigation on Mechanism of Creep Corrosion of Immersion Silver Finished Printed Circuit Board by Clay Tests."

[13] P. Zhao, M. Pecht, S. Kang, and S. Park, "Assessment of Ni/Pd/Au-Pd and Ni/Pd/Au-Ag Pre-Plated Leadframe Packages Subject to Electrochemical Migration and Mixed Flowing Gas Tests," IEEE Transactions on Components and Packaging Technologies, vol. 29, 2006, p. 818.

[14] P. Zhao and M. Pecht, "Mixed flowing gas studies of creep corrosion on plastic encapsulated microcircuit packages with noble metal pre-plated leadframes," IEEE Transactions on Device and Materials Reliability, vol. 5, 2005, pp. 268–276.

[15] S. J. Krumbein. “Metallic Electromigration Phenomena” IEEE Transactions on Components, Hybrids and Manufacturing Technology,vol. 11, No. 1, March 1988, pp 5-15
[16] T.E. Graedel, “Corrosion Mechanisms for Silver Exposed to the Atmosphere,” Journal of The Electrochemical Society, vol. 139, 1992, pp. 1963-1970.
[17] T. Graedel, J. Franey, G. Gualtieri, G. Kammlott, and D. Malm, “On the mechanism of silver and copper sulfidation by atmospheric H2S and OCS,” Corrosion Science, vol. 25, 1985, pp. 1163-1180.
[18] L. Volpe and P. Peterson, “The atmospheric sulfidation of silver in a tubular corrosion reactor,” Corrosion Science, vol. 29, 1989, pp. 1179-1187, 1189-1196.
[19] D.W. Rice, P. Peterson, E.B. Rigby, P.B.P. Phipps, R.J. Cappell, and R. Tremoureux, “Atmospheric Corrosion of Copper and Silver,” Journal of The Electrochemical Society, vol. 128, 1981, p. 275
[20] W.L. Robb, “Thin silicone membranes - Their Permeation Properties and Some Applications,” Annals of the New York Academy of Sciences, vol. 146, Jan. 1968, pp. 119.
[21] K. Rogers, C. Hillman, M. Pecht, and S. Nachbor, “Conductive filament formation failure in a printed circuit board,” Circuit World, vol. 25, 1999, pp. 6–8.
[22] G. Kohman, H. Hermance, and G. Downes, "Silver Migration in Electrical Insulation," The Bell System Technial Journal, 1955, pp1115.
[23] D. Lando, J. Mitchell, and T. Welsher, "Conductive Anodic Filament in Reinforced Polymeric Dielectrics: Formation and Prevention," *Proceedings of the Seventeenth International Reliability Physics Symposium*, 1979, pp. 51-63.
[24] M. Pecht, B. Wu and D. Jennings, "Conductive Filament Formation in Printed Wiring Boards," *Thirteenth IEEE/CHMT International Electronics Manufacturing Technology Symposium*, 1992, pp. 74-79.
[25] A.B. Kulkarni, M.D. Uplane, and C.D. Lokhande, “Preparation of silver sulphide from chemically deposited silver films,” Materials Chemistry & Physics, vol. 41, 1995, pp. 75–78.

11 Overall Discussion

As the appended papers in this thesis are highly interrelated, an overall discussion of the results in the various papers will be a repetition, and the paper on the migration mechanism (chapter 8) provides an overall summary. Therefore, the discussion in this chapter is limited to a broad-perspective analysis of the work done in the current thesis.

11.1 Component vs. PCB and Device Level Testing of ECM

Electrochemical migration of tin at component level was seen to be highly influenced by the local pH changes, and even for similar experiments, the rapid development in the pH boundaries was seen to differ from one experiment to the other. However, general trends from the effect of various parameters could clearly be differentiated, e.g. presence of halides and human handling were seen to highly promote formation of tin dendrites. As the ECM testing was expanded to the PCB level, external parameters such as surface finish, solder materials, and component height plays a significant role on ECM. However, such parameters would be difficult to identify, unless a thorough understanding of the migration behaviour of the base materials was present. For device level testing, due to the complexity of electronic devices, additional parameters such as e.g. housing design, heat capacity of heavy components and structures, active and passive cooling etc. provides an additional dimension to corrosion testing of electronics.

As electronic production shifts to lead-free soldering processes, the increased process temperature can locally reach as high as ~270°C, which could introduce surface contamination from degassing of corrosive species from the flame retardants of the PCB laminate. Suppliers of the PCB laminate materials may make changes to the chemistry of the laminates which is not communicated to the customers for commercial reasons, and such changes could have severe impact on the reliability of the electronic device. The same applies for solder flux chemistries, where a great deal of secrecy exists from manufacturers regarding the addition of e.g. surfactants and other chemicals to the flux. In order for device level testing to be useful, it is therefore essential that thorough and well established

testing procedures for the various materials and chemicals associated with the electronic device are used, where individual parameters from the various materials and chemistries involved are understood. Many of the standardized corrosion reliability test methods for electronics are not really formulated with clear understanding of the involved factors. This limits the ability of the test methods to predict and identify the actual field failures, although the prediction using accelerated tests even in highly standardized tests is in itself a difficult task.

In general, it is easy to make an electronic device fail. The difficult task from a reliability point of view is to simulate and predict market failures. In order to do so, a fundamental understanding on the corrosion mechanisms is of vital importance. The hope is that the findings in the present work have directed the understanding in such way, in relation to electrochemical migration of tin and tin alloys.

Many manufacturers assume that the application of a conformal coating will solve any issues related to corrosion. However, as the severe case presented in the appended paper on silver sulphide corrosion (paper 6) showed, a conformal coating is only to be regarded as a temporary barrier, and if a severe environment exists, corrosion will still occur, and mostly at increased speed/rate due to occlusion of the environment. The conformal coating can be regarded as a low-pass filter, where rapid changes to the humidity or concentrations of corrosive gasses are filtered away, but if a high average value of e.g. humidity is present over a prolonged period, diffusion though the coating will allow corrosion to occur. Any hygroscopic contaminants that might be present under the conformal coating would provide an osmotic pressure, thereby increasing water diffusion over the coating with possible blister formation.

11.2 Outlook and Suggestions for Future Work

1. The mechanisms influencing ECM proposed in the present work open for further work on prevention strategies against ECM. Though the present work has focused mainly on ECM of tin, similar mechanistic understanding could be developed on other metals based on the thermodynamic stability, and this also

opens up the possibility of functionalizing the conformal coatings, development of ECM inhibitors or other preventive strategies based on such mechanisms.

2. A more detailed fundamental investigation on ECM is being attempted based on in-situ observation of dendrite formation in high resolution SEM using a micro-chip corrosion cell with electron transparent window. This opens up the possibility of taking up the mechanistic understanding of the ECM to higher level.

3. During the present doctoral thesis, a setup was developed for ECM testing in humid, non-condensing environment and in the presence of gases. The setup was constructed in a manner, so that the temperature could be controlled with less than 0.5°C precision, and so that no thermal gradients existed in the setup. Preliminary experiments using this set up on ECM in non-condensing environment did not show any migration, but a detailed investigation on the ECM for various metals in non-condensing humidity and mechanistic aspects are needed.

4. Change into lead-free solder brings up several challenges due to the higher temperature used for soldering and more aggressive flux systems in some cases. The effect of lead-free soldering and aspects of corrosion reliability is needed, which includes understanding of the thermal profile and flux decomposition, any effect on laminate due to higher temperature, adhesion of solder mask etc.

5. Building the link between single component to PCBA level, and to device level failures is important and a difficult task to achieve. A related aspect is the standardized corrosion reliability test methods, which also need to be modified as per the new realities and understanding.

6. Work in this thesis is focused only on the ECM and silver sulphide corrosion. There are many other serious corrosion issues such as galvanic corrosion, fretting corrosion etc. for which a deeper understanding should be developed for a holistic view on electronic corrosion.

12 Overall Conclusions

1. The electrochemical migration of tin was found to be highly dependent on the thermodynamic stability of tin species formed at various pH domains of the micro-volume condensed droplets. A highly alkaline environment is produced at the cathode and acidic environment at the anode, and these domains rapidly interact with each other and are influenced by convection from gas evolution at the electrodes and ion migration.
2. The electrode material, inter-electrode distance, droplet volume, surface roughness of the electrodes, potential bias, and nature of the electrolyte are key factors influencing the migration properties, and unless these interrelated parameters are simulated in a manner that relates to the practical conditions, misleading results can be obtained.
3. Determined by the stability of tin species in the micro-volume of environment in which the migration is taking place, three different types of behaviour could be expected with increased dissolution of tin: (i) formation of a metallic dendrite, (ii) metallic dendrite mixed with hydroxides, and (iii) only hydroxide precipitate, but no dendrites. The structure and conductivity of the dendrite is highly dependent on the growth conditions, such as electric field, pH and concentration of tin species that can be deposited.
4. The tin dendrites produced by ECM were found to consist of metallic tin having sections of single crystalline orientation. Electron diffraction patterns were indexed to metallic tin and high magnification images of the main branch of the dendrite showed highly ordered crystalline lattice. Defects in the crystalline structure were found along the main dendritic branch, probably due to rearrangement of the dendritic structure during the growth stage. An oxide layer was found to surround the metallic tin core at local areas along the growth direction, which attributed to unstable growth during the electrochemical migration stage.
5. A hierarchal approach towards ECM testing must be made, in order to isolate the parameters originating from materials, chemicals and processing. In the

current work, this was obtained by dividing ECM testing into component, PCB, and device level testing.

6. Conformal coatings were found to provide protection from rapid changes to the environment surrounding an electronic device, but prolonged exposure to a severe environment can lead to corrosion failures, some times more severe due to the possibility of occlusion of environment.
7. Corrosive gasses containing sulphur were found to diffuse through a silicone coating to induce heavy silver sulphide corrosion of all silver surfaces, possibly aided by the presence of low concentrations of water, AC potential bias, and presence of other metals such as gold.
8. Reaction between silver and sulphur containing gases led to the formation of silver sulphide dendrites and the growth direction was influenced by the high voltage AC field.
9. Creep corrosion of silver on gold surfaces was observed to occur at the interface between a hybrid circuit and a silicone conformal coating, and possible chemical reactions leading to the silver sulphide creep were suggested.

APPENDIX A

CELCORR TESTPCB SPECIFICATIONS

Specifications for PCB manufacturer:

BOARD	
Type of board	Double sided with PT-holes
Board size	168 x 112.4 mm.
Material	FR4-In accordance to IPC-4101/21 and Tg. min. 135° C.
Thickness of board	1.6 mm
Material CTI value	>=175
Material Classed UL	94V-0
UL approved operation temp	>=105 deg. C.
Thickness of final copper	35.0 µm.
FINISH	
Solderresist layer	BOTH
type	LIQUID FILM
colour	GREEN
Machining of contour	ROUTING or PUNCHING
PLEASE NOTE	300pcs. HOT AIR LEVELING 200pcs. LEAD FREE HOT AIR LEVELING min. 2µm

DESIGN NOTES	
Smallest used conductor width	0.15 mm
Smallest used insulation spacing	0.35 mm
General soldermask clearance	0.10 mm
Via soldermask clearance	0.00 mm
Smallest used component hole diameter	0.90 mm
Via drill/annular ring	0.6/1.0 mm
Smallest used width of annular rings	0.20 mm

REMARKS

The PERFAG 2 (latest issue) norm for production of rigid PC-boards applies. The PCB is intended for SURFACE MOUNTED TECHNOLOGY. Requirements to warp and twist according to PERFAG paragraph 13.2.B . Pattern positioning tolerances according to PERFAG paragraph 2.10 .
The PCB shall be free from dust which appear during the production process. It is not allowed to make repairs on any layer except on soldermasks.

HEATING PROFILE FOR SN-PB SOLDERED TESTPCB.

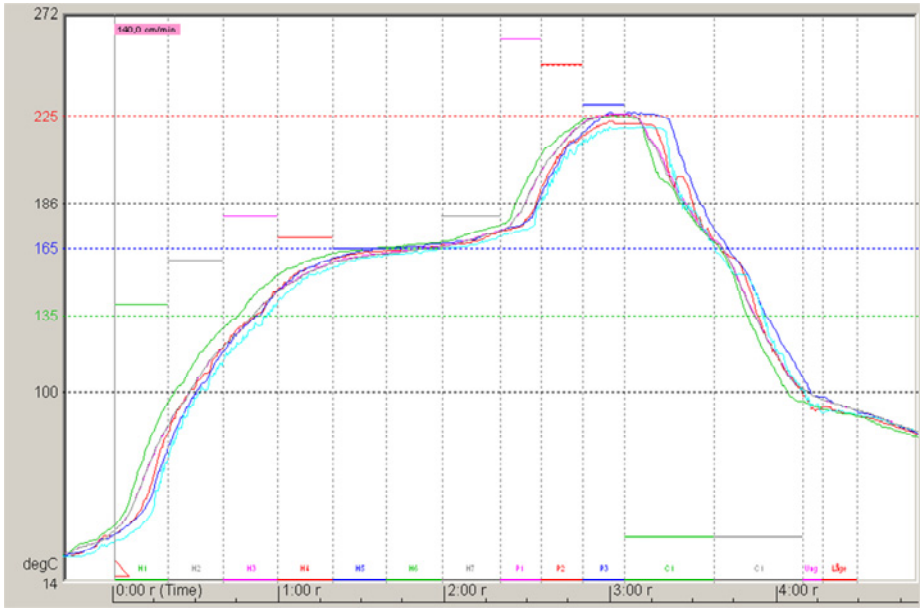

HEATING PROFILE FOR LEAD FREE SOLDERED TESTPCB.

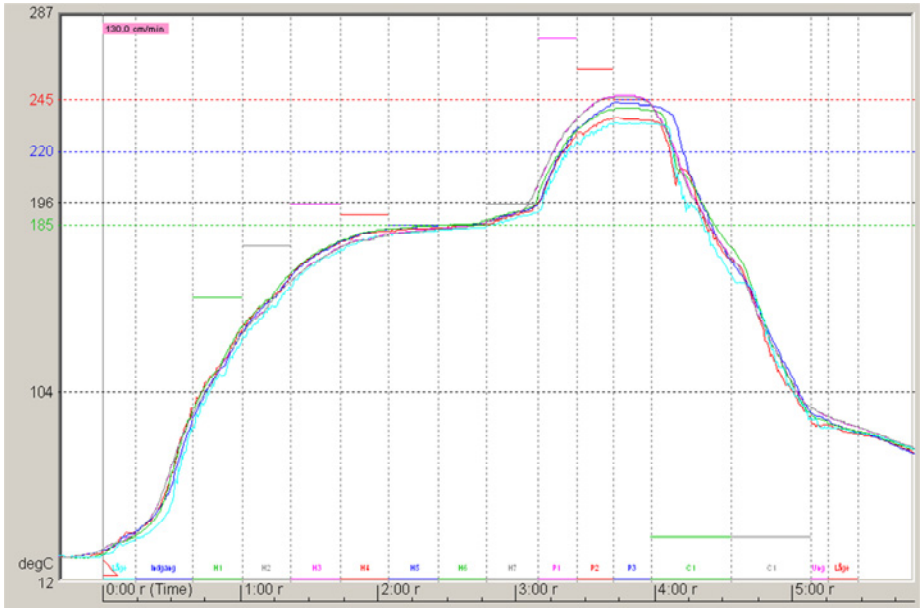

TESTPCB COMPONENT DETAILS

House	CH	Resistance / Capacitance	Power Rating (W)	MAX Potential due to Power rating (V)	Rated Voltage (V)	$U_{70\ mA}$ (V)
	1	1000 Ω	0.063	8	50	**7**
0402	2	10000 Ω	0.063	**25**	50	70
	3	100000 Ω	0.0625	79	**50**	700
	4	100 Ω	0.10	3	50	**0.7**
0603	5	100000 Ω	0.063	79	**75**	700
	6	1000000 Ω	0.063	251	**75**	7000
	7	68 Ω	0.1	3	150	**0.5**
0805	8	330000 Ω	0.125	203	**150**	2310
	9	1000000 Ω	0.125	354	**150**	7000
	10	SIR	-	-	-	-
	11	1000 p F				
0402	12	1000 p F				
	13	1000 p F				
	14	47 p F				
0603	15	1 n F				
	16	100 n F				
	17	22 p F				
0805	18	1 n F				
	19	100 n F				
	20	SIR	-	-	-	-

The highlighted values show the maximum DC potential that can be biased on each channel on the CELCORR TestPCB, which is determined either due to power rating, rated voltage or the maximum allowed current to avoid out of range measurement of the DMM and destruction of switch relay (U_{70mA} values).

TEST PCB BLOCK DIAGRAM